Understanding functional mechanisms of genetic susceptibility to mycobacterial infection

Ali M. Alisaac

Department of Medicine

University of Cambridge

This dissertation is submitted for the degree of

Doctor of Philosophy

Darwin College 2017

Abstract

Title: Understanding functional mechanisms of genetic susceptibility to mycobacterial infection

Name: Ali M. Alisaac

Tuberculosis remains a major public health problem and one of the leading causes of death worldwide. Human genetic factors determine susceptibility to *M. tuberculosis (M. tb)* infection and predispose to clinical TB. Genome-wide association studies (GWAS) aim to discover human genes associated with susceptibility to TB. Recently, a GWAS conducted by our lab identified a new TB-associated gene *ASAP1* that encodes an Arf GTPase-activating protein (GAP). ASAP1 is known to be involved in regulation of actin and membrane remodeling.

My Ph.D. included three projects. In my first project, I used RNAi and CRISPR-Cas9 technologies to study the role of ASAP1 in dendritic cells and macrophages, cells that play critical roles during mycobacterial infection. I demonstrated that in these cells ASAP1 is essential for migration and phagocytosis of mycobacteria. I characterized proteins that ASAP1 interacts with during mycobacterial infection. Finally, I found that the ASAP1-mediated pathway regulates expression of a large number of the immune response genes. These findings emphasize the important role of ASAP1 in mycobacterial infection and explain its involvement in TB pathogenesis.

In my second project, I was involved in a large study conducted by our laboratory that characterized transcriptional responses to *M. tb* infection in macrophages from a cohort of 144 healthy subjects. We used RNA-Seq to study transcriptomes of the infected and non-infected macrophages and identified differentially expressed genes. We also genotyped DNA polymorphisms of these subjects and studied the association between genetic variants and levels of gene expression, which allows us to identify expression quantitative trait loci (eQTLs), i.e., DNA polymorphism that affect gene expression. In particular, we identified an

eQTL located in the *TLR10-TLR1-TLR6* gene cluster. In non-infected macrophages, a group of polymorphisms in this region was associated in *cis* with the level of expression of *TLR1*, but not of the other two TLR genes. In *M. tb*-infected macrophages the same polymorphisms were associated in *trans* with levels of expression of 37 genes. This network includes essential immune response proteins, including multiple cytokines and chemokines. The discovery of this TLR1-driven network will help to better understand mechanisms of macrophage responses to mycobacterial infection.

Our study also identified a DNA polymorphism located upstream of the *ARHGAP27* gene, regulating its expression in infected and non-infected macrophages. In our GWAS this polymorphism was associated with TB risk, which implicated ARHGAP27 in TB pathogenesis. The ARHGAP27 protein is a Rho-GAP involved in the endocytic pathway. In my third project, I used CRISPR technology to establish the ARHGAP27-knockout macrophage cell model and characterized the function of ARHGAP27, showing that it is involved in cell migration and phagocytosis of mycobacteria. Taken together, my studies highlighted functional mechanisms implicating TB-associated GAP proteins ASAP1 and ARHGAP27 in mycobacterial infection and TB pathogenesis.

I would like to dedicate this thesis to my lovely wife Tagreed Alisaac, my children Renaad, Mohammed, and Ajeebah, and my loving parents, borthers, and sisters for their love and support during my Ph.D. study.

Declaration

I hereby declare that except where specific reference is made to the work of others, the contents of this dissertation are original and have not been submitted in whole or in part for consideration for any other degree or qualification in this, or any other University. This dissertation is the result of my own work and includes nothing which is the outcome of work done in collaboration, except where specifically indicated in the text. This dissertation contains less than 65,000 words including appendices, bibliography, footnotes, tables and equations and has less than 150 figures.

Ali M. Alisaac

2017

Acknowledgments

I would like to acknowledge and thank colleagues who have supported and helped me during my Ph.D. First and foremost, I would like to express my great gratitude to my supervisor Dr. Sergey Nejentsev for giving me the opportunity to be one of his students, his support, and guidance throughout my research projects.

I would also like to thank Mrs. Mailis Maes, Ms. Emma Goss, and Mr. James Curtis who worked with me as a team and for their help and suggestions. I would like to express my sincerest thanks to Dr. Davide Eletto for introducing me to cloning and helping me with CRISPR-Cas9 genome editing. I would express thanks to Dr. Olivier Papapietro for his comments and help for protein interaction analysis. I would like to thank Dr. Changxin Wu who trained me on tissue culture. My sincere thanks also go to Dr. Delphine Cuchet-Lourenco for being my mentor at the beginning of my P.hD and her help with confocal microscopy experiments.

Finally, I would express a deep sense of gratitude to my family, especially to my wife, who has always supported, encouraged, and stood by me through all the good and bad times.

Contents

List of Figures

List of Tables

Abbreviation

Abbreviation	Full names
ADA	Adenosine deaminase
AP	Antarctic Phosphatase
Arf	ADP-ribosylation factor
BAL	Bronchoalveolar lavage
BCG	*Mycobacterium bovis-Bacillus Calmette–Guérin*
BCS	Bathocuproindisulfonic acid disodium salt
Cas9	CRSPIR-associated protein 9
CDR	Circular dorsal ruffle
CEBPD	CCAAT/Enhancer Binding Protein Delta
CFU	Colony-forming unit
CR	Complement receptor
CRISPR	Clustered regularly interspaced palindromic repeat
crRNA	CRISPR RNA
DC	Dendritic cell
DC-SIGN	Dendritic cell-specific intercellular adhesion molecule(ICAM)-3-grabbing non-integrin
DSB	Double-strand break
ECM	Extracellular matrix
EDTA	Ethylenediaminetetraacetic acid
eQTL	Expression quantitative trait locus
EtBr	Ethidium bromide
FACS	Fluorescence-activated cell sorting
FAK	Focal adhesion kinase
FBS	Fetal bovine serum
FcγR	Fc gamma receptor
FDR	False Discovery Rate
GAP	GTPase-activating protein
GM-CSF	Granulocyte-macrophage colony-stimulating factor
GO	Gene Ontology
GWAS	Genome-wide association study
HDR	Homology-directed repair
HIV	Human immunodeficiency virus
icl	Isocitrate lysate

IFN-γ	Interferon-γ
IL-4	Interleukin 4
IL-6	Interleukin 6
indels	Insertion of deletion
KEGG	Kyoto Encyclopedia of Genes and Genomes
LAM	Lipoarabinomannan
LM	Lipomannan
LPF	Low power field
M. tb	*Mycobacterium tuberculosis*
ManLAM	Mannose-capped lipoarabinamannan
MARCO	Macrophage receptor with collagenous structure
MCP-1	Monocyte chemoattractant protein 1
M-CSF	Macrophage colony-stimulating factor
MDM	Monocyte-derived macrophages
MDR	Multidrug-resistant
MFI	Mena fluorescence intensity
MGC	Multinucleated giant cell
MOI	Multiplicity of infection
MR	Mannose receptor
MSMD	Mendelian susceptibility to mycobacterial disease
MTBC	M. tuberculosis complex
NdkA	Nucleoside diphosphate kinase
NHEJ	Non-homologous end joining
NO	Nitric oxide
Nramp1	Natural resistance-associated macrophages protein 1
PAMP	Pathogen-associated molecular patterns
PBMC	Peripheral blood mononuclear cell
PBS	Phosphate-Buffered Saline
PDL	Poly-D-Lysine
PI	Propidium iodide
PID	Primary immunodeficiency
PIK3AP1	Phosphoinositide-3-kinase adaptor protein 1
PIM	Phosphatidylinositol mannoside
PIP2	Phosphatidylinositol 4,5-bisphosphate
PIP3	Phosphatidylinositol 3,4,5-trisphosphate
PMA	Phorbol 12-myristate 13-acetate
PP2	Tyrosine kinase inhibitor
PPARD	Peroxisome proliferator-activated receptor delta
PPRE	PPAR response element
PRR	Pattern recognition receptor
PSM	Peptide-spectrum match
PtpA	Tyrosine phosphatase
PTX3	Pentraxin 3, long
qRT-PCR	Quantitative reverse transcription PCR

qRT-PCR	Quantitative Reverse transcription polymerase chain reaction
RBC	Red blood cell
ROI	Reactive oxygen intermediates
RXR	Retinoid X receptor
SCID	Severe combined immunodeficiency disease
sgRNA	Single guide RNA
siRNA	Small interfering RNA
SNP	Single nucleotide polymorphism
SR	Scavenger receptor
T7E1	T7 endonuclease I
TLR	Toll-like receptor
TNFα	Tumor necrosis factor alpha
transRNA	Trans-activating crRNA
TSS	Transcription start site
v-ATPase	a vesicular proton-ATPase
ZC3H12A	Zinc finger CCCH-type containing 12A
ZENs	Zinc-finger nuclease
α-TG	α-thioglycerol

Chapter 1 Introduction

1.1 Microbiology

Mycobacteria are strictly aerobic, non-spore-forming, non-motile long rods. Most species are slow-growing organisms that multiply every 8 to 24 hours. Mycobacteria cell wall consists of mycolic acid, which is a long chain cross-linked fatty acid, and a variety of unique lipids, such as lipoarabinomannan (LAM), trehalose dimycolate and phthiocerol dimycocerosate, which anchor noncovalently with the cell membrane and appear to play a central role in the virulence of *M. tb* (Meena and Rajni, 2010). Lipids, polysaccharides, and peptides together create a waxy cell surface that makes mycobacteria strongly hydrophobic and leads to their acid-fast staining characteristic (Harvey, 2008).

Mycobacteria are Gram-positive bacilli that belong to *Actinomycetes* and include numerous distinct species. These species differ in their virulence, ranging from non-pathogenic *M. smegmatis* to the human pathogen, *M. tuberculosis* (*M. tb*). *M. tb* is a member of *M. tuberculosis* complex (MTBC) including different strains, for example, the human pathogen *M. africanum* and the animal pathogen *M. bovis* (Galagan, 2014). Mycobacteria are commonly transmitted via inhalation of aerosol droplets or ingestion of pathogens. Mycobacteria can infect diverse types of cells, such as alveolar macrophages in lungs infected with *M. tb* or intestinal macrophages in intestines infected with *Mycobacterium avium* subspecies *paratuberculosis* (Valentin-Weigand and Goethe, 1999; Killick *et al.*, 2013). Although *M. tb* can multiply and

survive within different phagocytic cells, it prefers alveolar macrophages as its favorite niche (Gillespie, 2006). *M. tb* is able to infect different parts of the human body, including bones, meninges, and lymph nodes, but it infects predominantly the lungs, causing pulmonary tuberculosis, which accounts for 80% of all cases (O'Garra *et al.*, 2013).

M. tb can remain dormant within host cells for years causing no harm to the host and retaining its ability to be resuscitated and return to a stage of metabolic and replicative activity. The bacterium can escape and avoid the activated immune system of the host by realigning its central metabolism, terminate replication, and thereby transform into a stage of dormancy or latency to assure survival. Mutation in isocitrate lysate (*icl*) gene, encoding for an enzyme essential for the metabolism of fatty acids, did not affect *M. tb* growth during the acute phase of infection. In contrast, disruption of *icl* led to the failure of *M. tb* to maintain chronic infection in the lung of immunocompetent mice in the persistent phase of infection (McKinney *et al.*, 2000). Conventional TB drugs that target processes necessary for bacterial growth and division tend to be less active against slow- and nonreplicating-bacteria (so-called dormant *M. tb*). Dormancy could be one explanation for the prolonged time required to eradicate the TB infection (Parrish, Dick and Bishai, 1998).

1.2 Prevalence

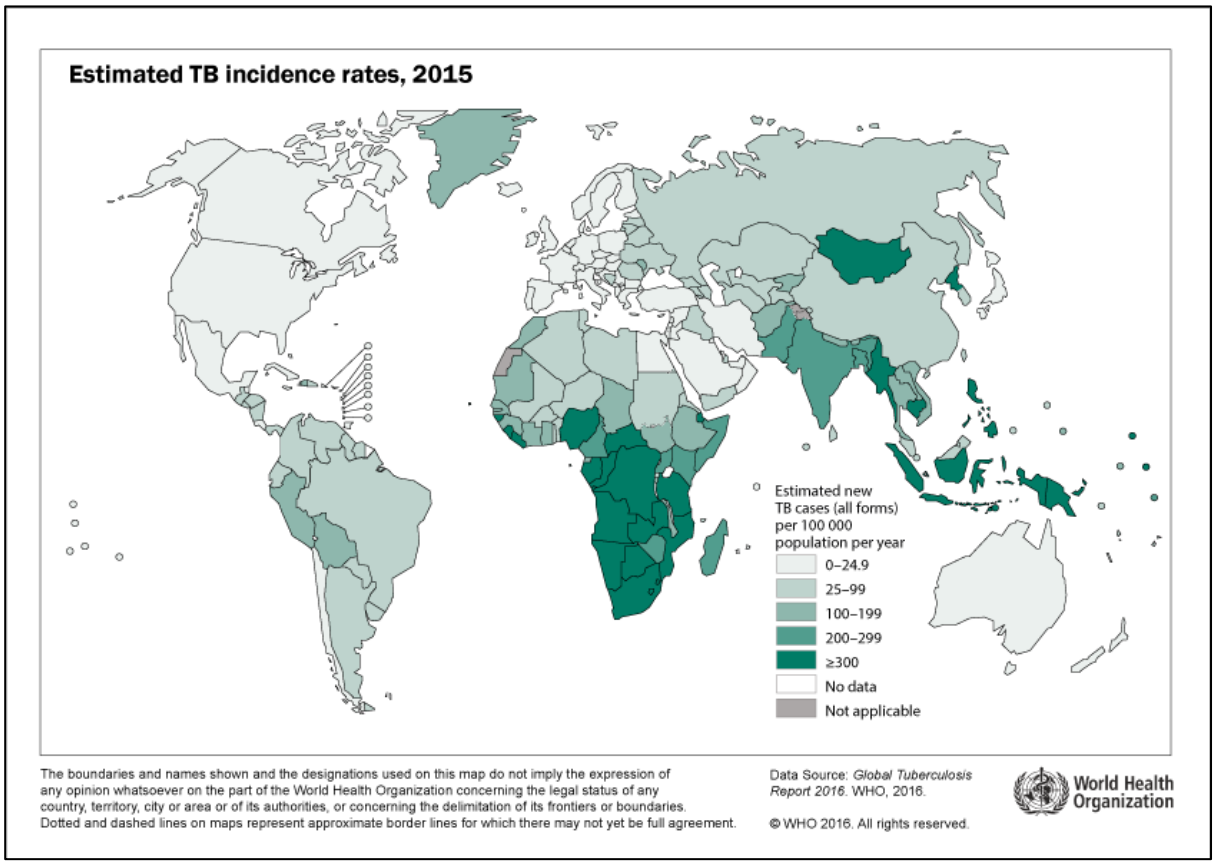

Figure 1.2-1:Estimated TB incidence rates, 2015 (WHO, 2016)**.**

Despite the tremendous progress in *M. tb* research since its first identification in 1882 by Robert Koch and the availability of anti-tuberculosis drugs, tuberculosis remains one of the leading causes of death worldwide and a major health problem. It has been estimated that one-third of the human population is infected with *M. tb* and remains asymptomatic, which is known as latent TB. However, 10% of the infected population progress to develop active tuberculosis (Ernst, 2012; O'Garra *et al.*, 2013). In 2015, 10.4 million people developed active tuberculosis worldwide with 1.4 million deaths (**Figure 1.2-1**) (WHO, 2016).

1.3 Treatment and drug resistance

The typical tuberculosis antibiotic course requires nearly 6 to 9 months and a combination of multiple drugs (isoniazid, ethambutol, rifampin, etc.) to prevent acquired resistance. The resistance can be prompted by inappropriate drug regimens and poor adherence to medications (Shenoi and Friedland, 2009; Zumla *et al.*, 2013). The effective treatment of active TB requires early diagnosis, analysis of the HIV status, and antibiotic susceptibility screening (Zumla *et al.*, 2013).

The TB-related deaths decreased dramatically in Western Europe and the United States between 1900 to 1980. Since much of this decline was before the availability of anti-tuberculosis drugs, it was thought that the improved live conditions contributed to the decline of TB cases. However, progress in most high-burden countries has been slower. Currently, the worldwide decline rate in incidence is only about 1.5% per year (Pai *et al.*, 2016).

The emergence of drug resistance has become a significant concern. Shortly after the introduction of streptomycin as the first anti-tuberculosis drug in 1945, *M. tb* strains appeared that developed resistance to it (Shenoi and Friedland, 2009). Multidrug-resistant *M. tb* (MDR-TB) is defined as the bacterium that is resistant to isoniazid and rifampin. Globally in 2016, 4.1% of new cases and 19% of previously treated cases are estimated to have MDR-TB (WHO, 2017). In addition, different countries have witnessed the emergence of the extensively drug-resistant (XDR) and totally drug-resistant *M. tb* strains (Zumla *et al.*, 2013). The spreading of MDR-TB is an increasing public health threat and compound the problems with tuberculosis treatment. MDR-TB cases are expensive and difficult to treat, taking into account the challenges that might be encountered throughout the prolonged treatment course, such as drug toxicity, side

effects, and pharmacokinetics interactions (Zumla *et al.*, 2013). Re-treatment of MDR-TB cases is common (Ellner, 2012). However, sometimes they are incurable.

The global TB burden is exacerbated by co-infection MDR-TB and human immunodeficiency virus (HIV). HIV is a highly effectual risk factor that accelerates the natural history of TB disease leading to TB reactivation. More than 70% of HIV/TB coinfected cases are living in sub-Saharan Africa. TB is the leading killer of HIV-positive individuals (Martinson, Hoffmann and Chaisson, 2011; Ellner, 2012).

1.4 Vaccine

Currently, the only approved vaccine against tuberculosis is the century-old bacillus Calmette-Guerin (BCG), a live attenuated vaccine. It has been administered to newborns in most of the areas endemic for TB. Since its introduction in 1920, BCG stocks have been maintained independently for decades. As a result, different BCG substrains exhibiting distinct genotypic and phenotypic heterogeneity have emerged (Behr, 2002). More importantly, the efficiency of the current BCG vaccine is still questionable. Meta-analysis studies suggested that the BCG vaccine protects from severe extrapulmonary TB in children, such as tuberculous meningitis and miliary TB, by an average of 50% (Brewer, 2000; Roy *et al.*, 2014). In clinical trials, the overall capacity of BCG vaccine to protect from TB in adolescents and adults varied from 0 to 80% (Colditz *et al.*, 1994), and its protection wanes over time (Sterne, Rodrigues and Guedes, 1998).

The reasons behind the variability in the efficacy of the BCG vaccine are not completely understood, but some explanations have been proposed. The previous exposure to non-tuberculous mycobacteria might interfere with the host immune response to BCG vaccine. Another possibility is that there might be differences or mutations in the BCG vaccine sub-

strains (Skeiky and Sadoff, 2006). Some other factors including the length of exposure time to tuberculosis, variation in the virulence of *M. tb*, the route of administration, age of vaccinated individuals (Skeiky and Sadoff, 2006), genetic variations of vaccinees, and nutritional differences among them have been attributed to the change of BCG vaccine efficacy (Fine, 1995).

The other concern about the BCG vaccine is its safety in countries in which the prevalence of HIV infection is high (Behr, 2002). In addition, live BCG can cause severe clinical disease in children with inborn errors of immunity referred as BCG-osis (Fortin *et al.*, 2007).

The first attempt to develop the vaccine was in the late 19th century by Robert Koch himself who used heat-killed bacilli (Tyagi, Nangpal and Satchidanandam, 2011). More effort has recently been focused on the development of subunit vaccines and recombinant BCG and DNA based vaccines (Tyagi, Nangpal and Satchidanandam, 2011; Zumla *et al.*, 2013), which should overcome the shortcomings of the BCG vaccine and have higher efficacy.

1.5 Pathogenesis of TB

M. tb is transmitted between people via the inhalation of droplets containing the pathogen (**Figure 1.5-1a**). Once in the lung, the pathogen encounters alveolar macrophages that patrol lung surfaces. It is believed that *M. tb* is internalized through phagocytosis by alveolar macrophages and dendritic cells (DCs). The internalization is mediated by pattern recognition receptors (PRRs) on phagocytes that distinguish highly conserved pathogen-associated molecular patterns (PAMPs), including Toll-like receptors (TLRs) and mannose receptor (MR), as well as Fcγ receptor (FcγR), complement receptors (CRs), and scavenger receptors (SRs) (Pieters, 2008; O'Garra *et al.*, 2013). It is likely that the recognition and internalization of

mycobacteria occur through cooperation of multiple receptors. Phagocytosis via distinct receptors influences the survival of *M. tb* intracellularly, depending on the signaling pathways triggered downstream of each receptor (Schäfer *et al.*, 2009). However, it is still elusive how mycobacteria exploit the selection of distinct receptors for its survival as a pathogenic strategy.

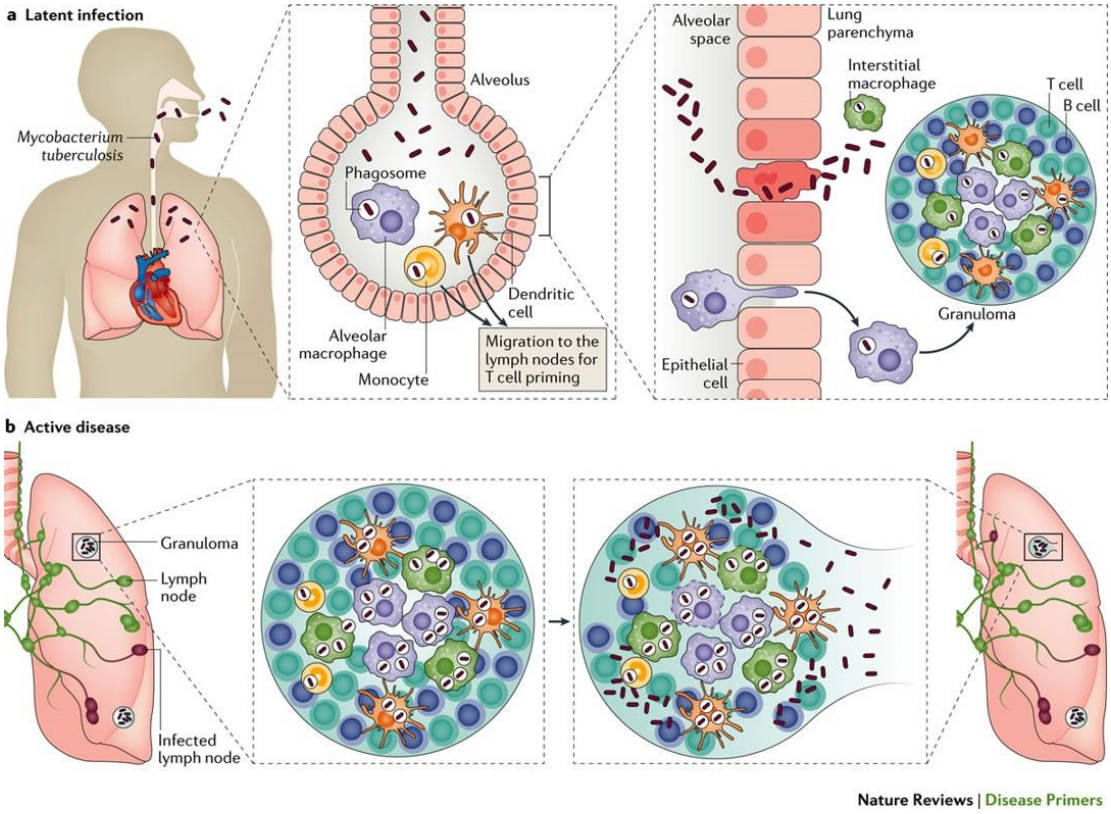

Figure 1.5-1*: Mycobacterium tuberculosis* infection

(**a**) Inhaled *M. tb* establishes infection in alveolar macrophages (AMs). Neutrophils and DCs can be infected too. *M. tb* infection leads to cell death. Dying cells containing *M. tb* are taken up by lung resident DCs and newly recruited macrophages. DCs infected with *M. tb* migrate to draining lymph nodes and stimulate naïve T cells. Antigen-specific T cells, then, are recruited to the lung and activate macrophages and other immune cells to establish granuloma in which *M. tb* is kept in check. Ninety percent of infected individuals have latent infection, whilst ~10% develop active TB. (**b**) During active disease, *M. tb* is released from granulomas into the airways. Individuals with active TB are infectious and disseminate *M. tb* when they cough (Pai *et al.*, 2016).

Members of the Toll-like receptor (TLR) family that are present on macrophages and dendritic cells recognize and bind to mycobacterial ligands. For example, TLR2 is believed to interact with lipoproteins, peptidoglycan, and glycolipids such as Lipoarabinomannan (LAM), Lipomannan (LM), and Phosphatidylinositol mannoside (PIM). This interaction stimulates the production of pro-inflammatory cytokines such as Interleukin 1 beta (IL-1β), Interferon-gamma

(IFN-γ), and tumor necrosis factor alpha (TNF-α) through the activation of NF-κB and MAPK signaling pathways (Ishikawa, Mori and Yamasaki, 2016).

The MR is primarily expressed on macrophages and DCs and recognize the mycobacterial mannose-capped lipoarabinomannan (ManLAM). Indeed, this receptor is considered to be the primary receptor for the phagocytosis of *M. tb* (Schäfer *et al.*, 2009). The interaction between MR on macrophages and ManLAM of *M. tb* during phagocytosis has been shown to deliver bacilli into a phagosomal compartment that has limited fusion with lysosomes, resulting in the survival of the pathogen (Kang *et al.*, 2005).

DC-SIGN (dendritic cell-specific intercellular adhesion molecule (ICAM)-3-grabbing non-integrin) is a C-type lectin receptor present mainly on DCs. It plays a key role as a phagocytic receptor of *M. tb* (Schäfer *et al.*, 2009). The binding of DC-SIGN receptor on DCs to ManLAM of *M. tb* leads to the internalization of the bacilli into DCs and the impairment of DCs maturation, which may facilitate the survival of the pathogen (Geijtenbeek *et al.*, 2002).

Complement receptors (CRs) are opsonic receptors that are expressed on the surface of phagocytes. Opsonization of *M. tb* with complement component (C3) facilitates the macrophage phagocytosis via the binding of bacilli to CR1, CR3, and CR4. The phagocytosis of *M. tb* via CRs seems to be advantageous to the pathogen. Indeed, the interaction between CR3 and *M. tb* does not lead to activation of NOX2-dependent respiratory burst or even the induction of inflammatory responses (Hossain and Norazmi, 2013; Hmama *et al.*, 2015).

FCγ receptors (FCγRs), other opsonic receptors on the surface of phagocytes, bind to immunoglobulin G-coated pathogens and deliver it into a phagolysosomal compartment (Hmama *et al.*, 2015). FCγRs seem to be less important for mycobacterial infection.

M. tb-infected phagocytes undergo cell death and signal to activate other uninfected phagocytes, such as monocytes and DCs. DCs containing *M. tb* migrate to draining lymph nodes to prime the T cell responses. Infection of DCs by *M. tb* impairs antigen presentation and migration, resulting in delayed adaptive immune responses (Urdahl, Shafiani and Ernst, 2011). The activation of adaptive immunity of T cells are required for the maintenance of the mature granuloma but are not essential for early granuloma formation (O'Garra *et al.*, 2013). In granuloma, the infected macrophages keep the pathogen in check and aggregate in the center. Macrophages in granuloma undergo further transformations leading to the formation of foamy macrophages, epithelioid macrophages, or fusion of cell membrane of many macrophages forming multinucleated giant cells (MGCs) (Ramakrishnan, 2012).

IFN-γ and TNF-α contribute to the immunity to tuberculosis. The effective interaction between T cells and macrophages is important to arrest the pathogen inside granuloma. IFN-γ has a well-established productive role in the restriction of *M. tb* infection. T cell-secreted-IFN-γ activates macrophages leading to the induction of its antimycobacterial mechanisms. IFN-γ-activated macrophages produce NADPH oxidase complex (NOX2) and inducible nitric side synthase (iNOS), generating reactive oxygen species (ROS) and reactive nitrogen species (RNS), respectively. Under the acidic condition, NOX2 and iNOS are recruited to produce reactive oxygen and reactive nitrogen intermediates that exert bactericidal activities on a broad range of molecules such as nucleic acids, proteins, microbial membrane lipid, and carbohydrates (Ehrt and Schnappinger, 2009; Awuh and Flo, 2016). Infection with mycobacteria or stimulation with its components promote macrophages and other immune cells to produce TNF-α, which is essential for granuloma formation and maintenance (Philips and Ernst, 2012). TNF-α blockage

in patients with Crohn's disease and rheumatoid arthritis leads to reactivation of tuberculosis in those who were latently infected (Keane *et al.*, 2001).

Thus, the granuloma is considered as a balance between the pathogen and the host immunity. Attenuation of the host immune system leads to bacterial proliferation and caseating granulomas that fail to contain the infection. *M. tb* eventually erodes into the airway leading to the progression from latent to active TB (**Figure 1.5-1b**).

1.6 Molecular mechanisms of host-pathogen interaction

Despite the efficaciousness of the host immune system to arrest the pathogen, it is often insufficient to completely eliminate it. *M. tb* has adopted several mechanisms to circumvent host immune responses and to manipulate the infected phagocytes to its own advantage (Ernst, 2012; Gupta *et al.*, 2012). *M. tb* alters the trafficking of the mycobacterial phagosome to avoid the killing and the degradation in the mature phagolysosome (Ernst, 2012; Gupta *et al.*, 2012; Podinovskaia *et al.*, 2013). It has been known that mycobacterial phagosome retains the early endosomal marker (Rab5) and fails to recruit late endosomal/lysosomal marker (Rab7), preventing the phagosome-lysosome fusion. Another lysosomal marker is a vesicular proton-ATPase pump (v-ATPase), and its absence leads to the lack of phagosome acidification (Russell, 2001; Gupta *et al.*, 2012; Philips and Ernst, 2012). The prolonged retention of Rab5 may be caused by the secretion of two *M. tb* effector proteins PtpA, a tyrosine phosphatase, and nucleoside diphosphate kinase (NdkA). It has been reported that PtpA dephosphorylates Vps33B, a host protein involved in the regulation of membrane fusion in the endocytic pathway (Bach *et al.*, 2008). NdkA acts as GTPase-activating protein (GAP). NdkA probably catalyzes the conversion of GTP-bound-Rab5 and Rab7 to inactive forms of GDP-bound-Rab5 and Rab7,

leading ultimately to the blockage of phagolysosome fusion and the increased mycobacterial survival (Sun *et al.*, 2010).

Moreover, *M. tb* uses the type VII secretion system (ESX-1), which is absent in the attenuated *M. bovis* BCG, to induce necrosis of the infected host cells and recruit additional macrophages (Ernst, 2012). The ESX-1 secretion system mediates the cell-to-cell dissemination and also helps the bacterium to escape the phagosome and to multiply inside the cytosol (Philips and Ernst, 2012). *M. tb* also has adapted mechanisms to inhibit the apoptosis in the infected host cells. Such inhibition leads to the survival of the infected phagocytes and a higher bacterial burden within a given cell before cell death (Ernst, 2012). *M. tb* prefers necrosis of the host cells over the apoptosis. The latter is regarded as an additional mechanism to trigger the host protective immunity via cross-presentation pathway (Philips and Ernst, 2012)

1.7 Genetic susceptibility to tuberculosis

The reasons behind the fact that only less than 10% of *M. tb*-infected individuals develop the clinical disease of tuberculosis are still largely unidentified (Möller and Hoal, 2010). Although there are few recognizable risk factors such as alcohol abuse, AIDS, chemotherapy, or immunosuppressive drugs, these factors are only encountered in the minority of the cases. The rest of active TB cases are attributed to genetic and environmental factors (Bellamy, 1998). Accumulating lines of evidence, such as case observations, twin studies, and animal model studies, have indicated that differential susceptibility to TB is modulated by host genetic factors (Möller and Hoal, 2010; Stein and Western, 2012).

1.7.1 Lübeck disaster

The variations in susceptibility to tuberculosis were noted in a tragic Lübeck accident in Germany in 1926. During vaccination program, 251 neonates were unintentionally immunized with a virulent live *M. tb* strain instead of BCG. Of these newborns, 173 showed clinical manifestations of TB but overcame the infection; 77 babies died. Indeed, those infants demonstrated a varied range of resistance to virulent *M. tb*. The babies who cleared the infection perhaps had stronger immune response compared to those who succumbed to the infection. Therefore, the different clinical outcomes observed in Lübeck disaster emphasizes the idea that the genetically controlled immune system may influence the progression of TB infection (Meyer and Thye, 2014; Fox, Orlova and Schurr, 2016).

1.7.2 Mendelian susceptibility to mycobacterial disease (MSMD)

Rare patients with primary immunodeficiencies (PIDs) who suffer from Mendelian susceptibility to mycobacterial disease (MSMD) provide additional evidence of the importance of genetic factors. MSMD patients manifest severe clinical symptoms when exposed to BCG and environmental mycobacteria (EM) as well as *M. tb*. Some affected patients also suffered severe infection caused by *Salmonella*. Notably, BCG-osis, caused by BCG, and EM disease were usually diagnosed in relatives, indicating Mendelian inheritance (Fortin *et al.*, 2007; Boisson-Dupuis *et al.*, 2015). Since the identification of the first MSMD mutation in the IFN-γR1 gene in 1996, a total of 9 genes has been identified to be implicated in MSMD (Newport *et al.*, 1996). MSMD genes are: *IL12p40,* encodes a subunit of interleukin 12; *IL12Rβ1,* Interleukin 12 Receptor Subunit Beta 1; *IFN-γR1,* encodes the ligand-binding chain (alpha); *IFN-γR2,* encodes the non-ligand-binding beta chain; *IRF8,* is a transcription factor of the interferon (IFN) regulatory factor (IRF) family; *STAT1,* Signal Transducer And Activator Of Transcription 1;

JAK1, Janus kinase 1; *NEMO,* encodes the regulatory subunit of the inhibitor of kappaB kinase (IKK) complex; *ISG15,* ISG15 Ubiquitin-Like Modifier, and *CYBB,* Cytochrome b beta chain,. Mendelian mutations in these genes are associated with infections caused BCG or EM (Ottenhoff *et al.*, 2002; Möller and Hoal, 2010). Interestingly, these mutations impair the production of or the response to IFN-γ, either directly or indirectly, highlighting that the IFN-γ pathway is crucial for the restriction of mycobacterial infection (Ottenhoff *et al.*, 2002; Fortin *et al.*, 2007).

1.7.3 Twin studies

Further evidence emphasizing the significance of hereditary factors in the etiology of TB comes from twin studies. Generally, homozygous twins showed TB concordance rates twice as high as those observed in dizygotic twins, which indicates the importance of the host genetic components in the susceptibility to TB (Bellamy, 1998; Stein and Western, 2012). One example is the results obtained by Diehl and Von Verschuer in a survey, which was considered statistically representative. The study material included 205 pairs. Results showed that concordance rates of tuberculosis are 25% in dizygotic and 65% in monozygotic twins. The study concluded that this difference was due to the genetic components rather than the environmental factors (Kallmann and Reisner, 1942; Jepson, 1998; Schurr, 2011). Comstock reanalyzed data from the Prophit survey with more sophisticated statistical tools trying to eliminate variables other than zygosity. He found that the higher concordance rate observed among monozygotic twins compared to dizygotic twins indicated that genetic determinants are paramount in the development of TB (Comstock, 1978).

Another study included 282 healthy twin pairs from The Gambia aged between 12 and 83 years conducted to evaluate the role of the genetic component in the regulation of immune

responses to *M. tb* and *M. bovis* BCG antigens. The results suggested that genetic factors, in part, regulate the cellular immune responses to *M. bovis* 65 kDa proteins and to *M. tb* secreted proteins (Jepson *et al.*, 2001). Collectively, genetic components are major determinants in the development of TB. This evidence has led researchers to use new and different approaches to identify causative genes.

1.7.4 Animal models

While most of these studies support the notion that the variation of the susceptibility to tuberculosis is controlled by heritable factors, it is a complex process to identify genes that underpin the difference in multifactorial traits, such as susceptibility to tuberculosis. Early studies focused on animal models attempting to understand the mechanisms of susceptibility to TB. It is worth mentioning the work of Lurie who continued to breed rabbits leading to the development of two distinct families based on their susceptibility to pulmonary tuberculosis: resistant and susceptible. Upon infecting these rabbits with *M. tb,* the resistant rabbits showed pulmonary tuberculosis similar to that observed in immunocompetent patients, whereas the susceptible rabbits exhibited disseminated form of the disease that displayed in immunocompromised patients. Lurie concluded that variations in susceptibility to the disease were genetically mediated (Lurie, Abramson and Heppleston, 1952; Bellamy, 1998).

Inbred mice exhibited variation in susceptibility to BCG and other intracellular pathogens, such as atypical mycobacteria, *Salmonella*, and *Leishmania*. Positional cloning was used to identify the causative gene that was named *Nramp1* (Natural resistance-associated macrophage protein-1, now referred to as *Slc11a1*), containing a point mutation in codon 169 changing amino acid from glycine to aspartic acid (Vidal *et al.*, 1993; Bellamy, 1998).

Another study in inbred mice showed hypersensitivity to *M. tb* by rapid death after infection due to increased *M. tb* replication inside macrophages. The responsible gene, *Ipr1,* was identified by positional cloning (Pan *et al.*, 2005). The closest human homolog of *Ipr1* is the SP110 protein, a transcription factor regulated by IFNs (Bloch *et al.*, 2000).

1.7.5 Genome-wide association studies

Family-based linkage and candidate gene association studies were widely used to identify genes that affect susceptibility to tuberculosis in humans (Möller and Hoal, 2010). Linkage studies were used to scan the whole genome to identify any gene that exerts a substantial effect. However, this approach failed to detect genetic regions containing minor or moderate disease susceptibility loci due to the fact that it has relatively low statistical power (Newport and Levin, 1999). Despite a considerable number of candidate gene association studies, no gene showed a consistent association with TB across these studies.

GWAS (genome-wide association study) is a powerful approach to investigate the genetic determinants of complex diseases. It was complicated and time-consuming prior to the completion of human genome sequence and the International HapMap project. The progress that has been made after 2005 in the development of SNP chips or arrays that detect most common variation in the genome allows GWAS to scan hundreds of thousands and even millions of single nucleotide polymorphisms (SNPs) across the entire genome in thousands of individuals. The GWAS overcame the disadvantages of family-based genome-wide linkage studies in which hereditary pattern is related to few hundreds of genomic markers, and the sample size is generally smaller (Manolio *et al.*, 2009; Möller and Hoal, 2010; Ricaño-Ponce and Wijmenga, 2013).

GWASes have led to the discovery of a significant number of genomic loci that are associated with complex trait and diseases, including TB. Most GWAS loci contain SNPs that reside within intergenic or intronic regions, perhaps interfering with regulation of gene expression. Moreover, disease-associated genetic variants are usually in linkage disequilibrium (LD) with each other; therefore, it is still the main challenge to precisely pinpoint the causal variant and the gene influenced by it. This slows our understanding of how such SNPs perturb the biology of the genome, cells, and eventually affect the phenotype of the disease (Edwards *et al.*, 2013).

Several GWAS have been published thus far in TB. Thye et al. published the first GWAS consisting in total of 2,237 TB cases and 3,122 unaffected controls from Ghana and The Gambia. This combined analysis reported a significant association with one locus mapped to chromosome 18q11.2 with an overall $P = 6.8 \times 10^{-9}$ (Thye *et al.*, 2010), thus reaching the genome-wide significance threshold of $P \leq 5 \times 10^{-8}$ (Ricaño-Ponce and Wijmenga, 2013). Later, imputation of data provided by the 1000 Genome Project into the same dataset of Ghanaian TB patients and controls led to the identification of a new tuberculosis susceptibility locus on chromosome 11p13 with genome-wide significance ($P = 2.63 \times 10^{-9}$). The SNP that showed strong association with TB susceptibility was located in the intergenic region downstream of the *WT1* gene, encoding Wilms tumor 1 (Thye *et al.*, 2012). However, TB-associated genes in these loci and the biological mechanisms underpinning these associations remain unknown.

Our lab performed a large TB GWAS in TB patients and controls from Russia (Curtis *et al.*, 2015). We used Affymetrix Genome-Wide Human SNP Array 6.0 to genotype 5,530 HIV-negative pulmonary TB patients and 5,607 healthy controls. This GWAS identified a locus on chromosome 8q24 that contains seven TB-associated SNPs within introns of the *ASAP1* gene

(rs1017281, rs10956514, rs1469288, rs17285138, rs2033059, rs4733781, and rs12680942). The top signal in the discovery set was at rs2033059 with a *P* value of 1.1×10^{-8}. Seven *ASAP1* SNPs that were most strongly associated with TB were then genotyped in additional 1,085 TB patients and 2,865 controls for replication. In the combined analysis of more than 15,000 subjects in both the discovery and replication sample groups, these SNPs showed convincing evidence of association with TB; the most significant association was at rs4733781 ($P = 2.6 \times 10^{-11}$) (**Figure 1.7-1**).

The next major challenge lies in moving from associated SNPs to finding the strongest candidate causal variant and then identifying the affected gene. First, we tried to dissect which of the polymorphisms is the functional variant underlying the observed association with TB risk in our GWAS. We applied a Bayesian approach, to calculate a posterior probability of causality for SNPs across all loci identified. This analysis was done by Dr. Yang Luo at the Wellcome Trust Sanger Institute. As a result of this refinement, four out of seven (rs10956514, rs1469288, rs2033059, and rs4733781) were likely to be causal SNPs in our GWAS with a posterior probability > 5%. The highest posterior probability was 43.6%, indicating the limit of genetic resolution in our Russian data set. However, this genetic association did not provide us with direct information about the underlying mechanism implicating ASAP1 in TB pathogenesis.

Finally, our GWAS found evidence of TB association at the 11p13 locus (rs2057178, *P* = 0.00068) that was previously identified in African populations (Thye *et al.*, 2012) and replicated in the admixed South African Colored population (Chimusa *et al.*, 2014). There was, however, no replication for other TB-susceptibility-associated loci that have been reported

Pinpointing the causal variant is still a challenge because many genetic variants in LD are typically associated with the same phenotype. Another reason is that the phenotype could be driven by a combination of variants and not only by the lead SNP (Vasquez *et al.*, 2016). Finally, the majority of the hit signals are located in the noncoding sequence making it difficult to define the biological mechanism (Farh *et al.*, 2015). Therefore, the next step is to explore the mechanism involved the gene of interest in the observed traits. Genetic manipulation techniques such as siRNA knockdown and CRISPR-Cas9-mediated perturbations in cellular models or organisms should be considered. Given that determining the putative variant is still tricky and most of the disease-associated SNPs confer only modest effects, achieving the overall reduction of expression of the target gene by knockdown or introducing a loss-of-function mutation can overcome these challenges and maximize the biological impact on the gene of interest in appropriate models (Edwards *et al.*, 2013).

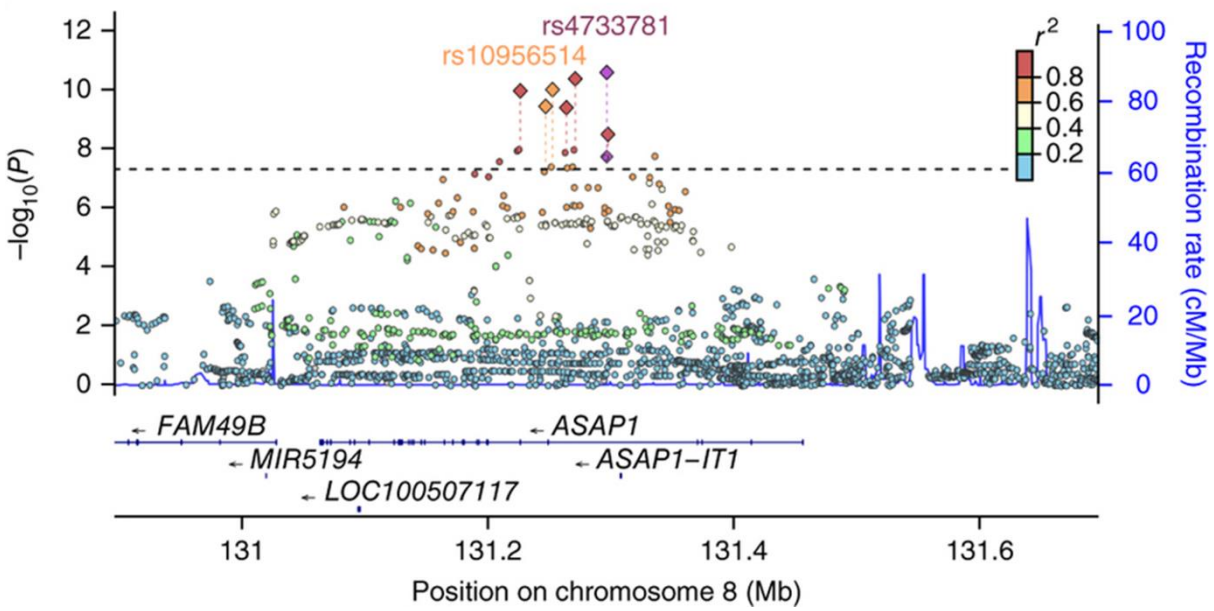

Figure 1.7-1: Regional plot showing SNPs in the *ASAP1* gene region.

Single nucleotide polymorphisms (SNPs) are colored based on their r^2 with the labeled hit SNP, rs4733781, which has the smallest *P* value in the region. Circles show *P* values obtained in GWAS in set1; diamonds show *P* values found in the follow-up study of seven SNPs in sets 1 and 2 combined (Curtis *et al.*, 2015).

1.7.5.1 ASAP1 and its role in podosomes and invadopodia

The *ASAP1* gene encodes the ASAP1 protein (also known as AMAP1, DDEF1, DEF1, PAG2, Shag1, KIAA1249, and Centaurin 2 beta), an Arf (ADP-ribosylation factor) GAP (GTPase-activating protein). It contains the BAR, PH, ArfGAP, Ankyrin repeat, Proline-rich, D/ELPPKP repeat, and SH3 domains. Members of the Arf-GAP family regulate the hydrolysis of GTP bound to the Arf proteins (Shiba and Randazzo, 2011). Arfs are members of the Ras superfamily. Arfs and their Arf-GAPs play fundamental roles in regulating membrane trafficking and remodeling of actin cytoskeleton (Inoue and Randazzo, 2007). The ASAP1 protein interacts with a variety of cytoskeleton regulatory proteins, such as Src family, focal adhesion kinase

(FAK) family, and cortactin as well as phosphoinositides. ASAP1 is found in focal adhesions, circular dorsal ruffles (CDRs), invadopodia, and podosomes (Inoue *et al.*, 2008). In fibroblasts, the association between ASAP1 and focal adhesion is driven by the interaction between SH3 domain and FAK (Randazzo *et al.*, 2000; Inoue *et al.*, 2008). High level of ASAP1 blocked the cell spreading and formation of membrane ruffles (Randazzo *et al.*, 2000; Liu *et al.*, 2002).

Highly invasive cancer cells have been found to express elevated levels of ASAP1. The siRNA-mediated suppression of ASAP1 expression inhibited the invasive activities (Onodera *et al.*, 2005). In transformed fibroblasts, ASAP1 has been found in invadopodia and podosomes, which are actin-based structures that form close contacts with extracellular matrix (ECM) and are able to degrade its components (Linder, 2009). Podosomes are spot-like actin-rich structures that are formed in motile cells of the myeloid lineage such as macrophages, monocytes, DCs, osteoclasts, and megakaryocytes as well as nonmyeloid cells such as endothelial cells and smooth muscle cells (Schachtner *et al.*, 2013). Invadopodia are similar structures found in cancer cells (Linder, 2009). They play pivotal roles in extracellular matrix degradation, cell migration, and in pathological invasive processes such as metastasis (Linder, 2009).

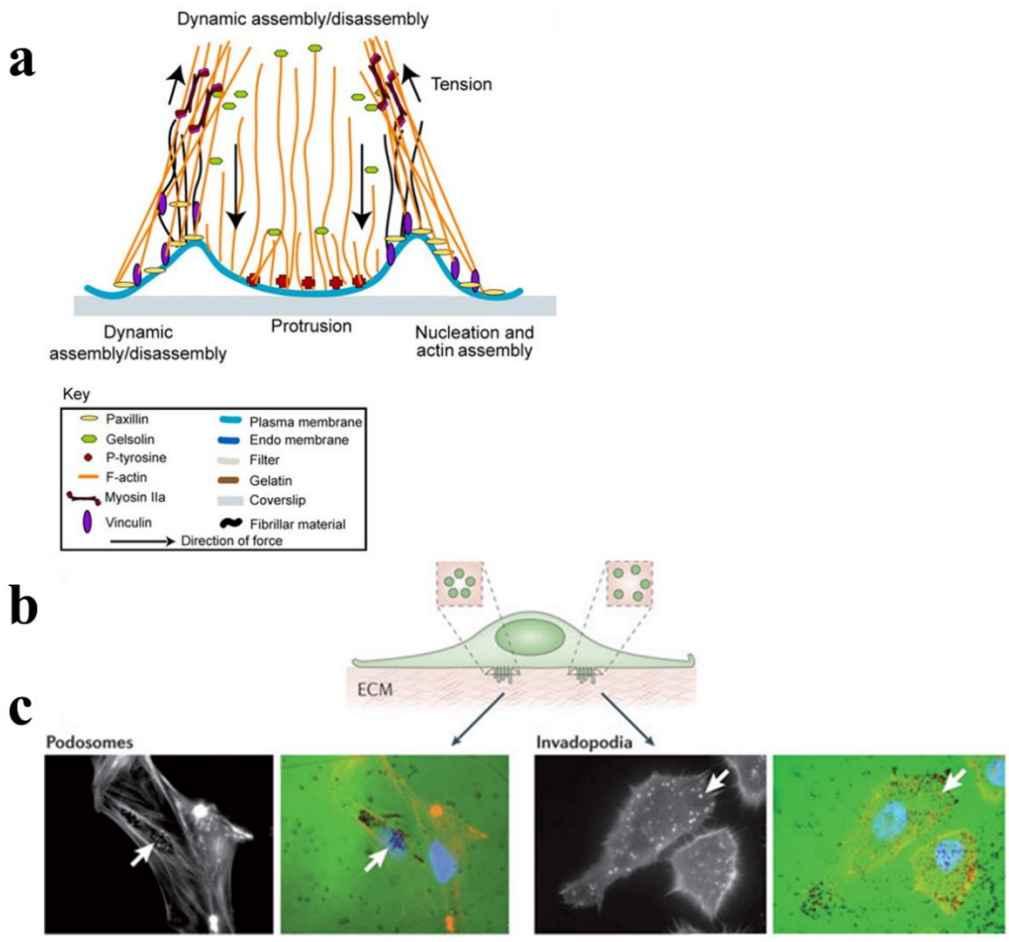

Figure 1.7-2: Podosomes and Invadopodia structures

(**a**) Schematic diagram shows the arrangement of proteins in a single podosome. Paxillin (yellow) and vinculin (violet) at sites of integrin binding, forming the ring structure. The interaction with the inner side of the ring structure provides an interaction domain for actin filaments, stabilizing the crosslinking, generating force, puckering membranes. Centrally, in the developing protrusions, actin core is formed via phosphotyrosine signaling and phosphorylation at the actin-binding proteins, leading to mechanical tension, then to degradation of the substrate. Adapted from (Gawden-Bone *et al.*, 2010). (**b**) schematic diagram shows the extended protrusions below the podosomes. (**c**) Representative examples of a cell containing podosome (left) and a cell containing Invadopodia (right) showing the colocalization between F-actin puncta (red dots) and matrix degradation (black region) as indicated by white arrows. Adapted from (Murphy and Courtneidge, 2011).

Structurally, podosomes are characterized by the presence of actin-rich core and surrounding ring region containing common adhesion proteins such as paxillin, vinculin, talin,

and focal adhesion kinase FAK. (**Figure 1.7-2**). Podosome formation may be induced by different stimuli such as phorbol ester treatment or engagement of integrins with substrates. These triggers may act mainly via activation of Src. The activation of Src induces phosphorylation of interacting proteins and substrate, leading to the podosomes formation. The interacting partners include WASP, integrins, FAK, paxillin, cortactin, and ASAP1 (Bharti *et al.*, 2007; Schachtner *et al.*, 2013). Unlike paxillin, vinculin is not enriched in invadopodia, so it can be used as a marker to distinguish between podosomes and invadopodia (Linder, 2009). Podosomes and invadopodia are collectively termed invadosomes (Murphy and Courtneidge, 2011). The phenotype switch from resting cells to migratory one is characterized by the disassembly of focal adhesion and the initiation of invadosome formation at the contact sites with ECM (Murphy and Courtneidge, 2011).

1.7.5.2 Potential role of ASAP1 in mycobacteria phagocytosis

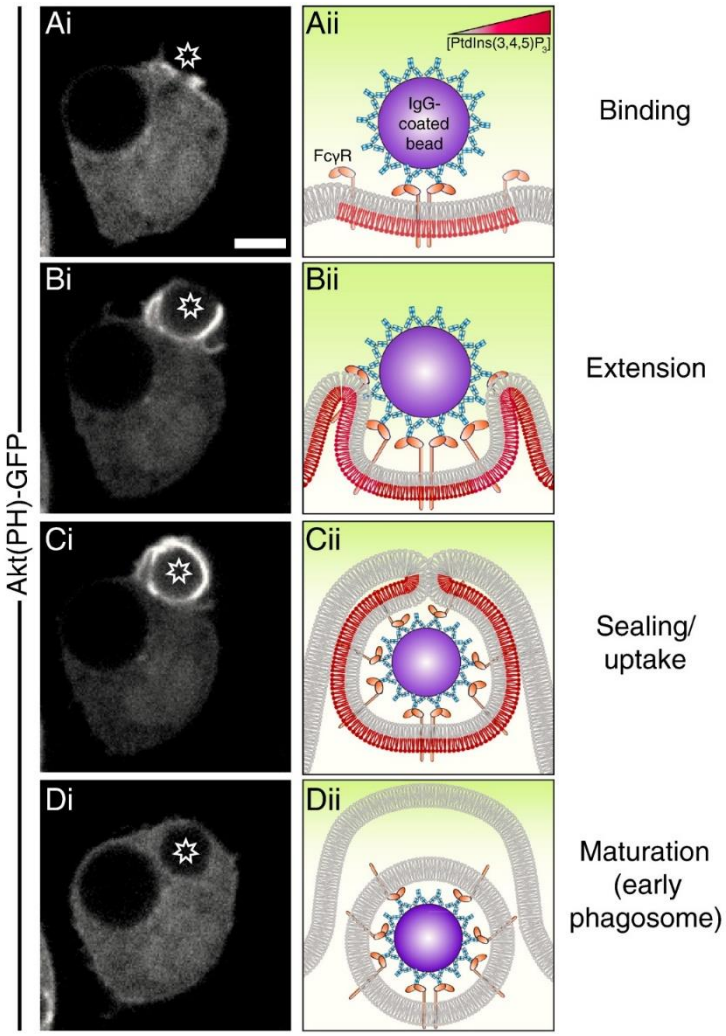

Figure 1.7-3: Stages of phagocytosis process.

(**A**) Particles binding site. (**B**) Phagocytic cup formation and signaling. (**C**) Particle engulfment (**D**) Early formed phagosome. (Left) Time-lapse confocal microscopy in RAW 264.7 shows the spatiotemporal appearance of phosphatidylinositol 3,4,5-trisphosphate (PIP_3). The PIP_3 increases at the particle binding site in the membrane of the phagocytic cup. Its presence is associated with the disappearance of phosphatidylinositol 4,5-bisphosphate (PIP_2) and persists until the scission occurs (Levin, Grinstein and Schlam, 2014).

Phagocytosis is defined as the cellular internalization of large particles (> 0.5 µm) in a receptor-mediated manner (Flannagan, Jaumouillé and Grinstein, 2012). Macrophages, neutrophils, and DCs are professional phagocytes. They play vital roles in host innate immunity

by operating fundamental tasks such as immune surveillance and clearance of pathogens (Levin, Grinstein and Schlam, 2014), and DCs activate the adaptive immune responses by presenting antigens to lymphoid cells (Botelho and Grinstein, 2011).

Phagocytosis can generally be divided into three different stages: recognition of target antigen via surface receptors, enrichment of receptors underneath the secured particles accompanied with early signaling, and phagosome closure driven by actin reorganization (**Figure 1.7-3**) (Jaumouillé and Grinstein, 2011). Once the extracellular particles adhere to a specific cell surface receptor, such as FcγRs, CRs, SRs, and TLRs, they trigger the phagocytes to form a phagosome, which is a plasma membrane-bound vacuole. Later, a fully formed phagosome undergoes maturation and fusion with lysosomes. Phagocytosis is a complex process that is orchestrated by actin cytoskeletal rearrangement and membrane remodeling. FcγR-mediated phagocytosis by far is the best-characterized system (Botelho and Grinstein, 2011; Levin, Grinstein and Schlam, 2014).

Rac and Cdc42, Rho family proteins, which are activated by tyrosine phosphorylation, are instrumental regulators of actin polymerization and rearrangement during the growing pseudopod extensions that wrap around IgG-coated particles (Botelho and Grinstein, 2011). GTP-bound Cdc42 was observed at the tip of the growing extensions, while GTP-bound Rac1 peaked at the time of pseudopod fusion. In their GTP-locked forms, they interact with downstream effectors (e.g., WASP), which stimulate the actin-nucleating activity of the Arp2/3 complex. That provides a central point of an actin polymer network (Niedergang and Chavrier, 2005).

In addition to the Rho family proteins, phosphoinositides regulate the highly dynamic nature of the actin cytoskeleton assembly and disassembly during phagocytosis. For example,

phosphatidylinositol 4,5-bisphosphate (PIP_2) accumulates in the leading edges of the phagocytic cup in F-actin-rich region. It, however, diminishes in the base of the phagocytic cup during phagosome closure (Botelho and Grinstein, 2011; Egami, Fukuda and Araki, 2011; Levin, Grinstein and Schlam, 2014). The product of phosphoinositide 3-kinase, phosphatidylinositol 3,4,5-trisphosphate (PIP_3) plays important roles in other phases of phagocytosis. Its spatial and temporal dynamic appearance during phagocytosis is associated with the PIP_2 disappearance from the phagocytic cup (**Figure 1.7-3**) (Levin, Grinstein and Schlam, 2014). PIP_3 is abundantly found in the inner membrane of the phagocytic cup and is essential for the completion of the phagosome sealing and actin depolymerization (Egami, Fukuda and Araki, 2011; Levin, Grinstein and Schlam, 2014).

Unlike FcγR-mediated phagocytosis, in CR3-mediated phagocytosis, the internalized particle sinks into the phagocyte without growing pseudopods and with minimal cell membrane disturbance and does not usually result in an inflammatory response or oxidative burst (May and Machesky, 2001).

As an alternative to phagocytosis, cells can internalize bacteria and particles by macropinocytosis. It is a distinctive endocytic pathway that allows the formation of large vesicles independent of any receptors. Macropinocytosis can be a spontaneous process or can be induced by growth factors (Swanson, 2008; Kerr and Teasdale, 2009; Levin, Grinstein and Schlam, 2014). Some viruses and bacteria (Swanson, 2008; Levin, Grinstein and Schlam, 2014), including mycobacteria (García-Pérez, Mondragón-Flores and Luna-Herrera, 2003; García-Pérez *et al.*, 2008) can force their entry by stimulating cell-surface ruffling and macropinocytosis.

ASAP1 may be involved in regulation of phagocytosis and macropinocytosis. ASAP1 contains the BAR domain, which senses membrane curvature (Nie and Randazzo, 2006).

ASAP1 interacts with Arf1 and Arf5 and, to a lesser extent, with Arf6 (Randazzo et al., 2000). It has been found to reduce the Arf1 GTP levels and to increase the Arf6 GTP levels (Inoue and Randazzo, 2007). Arfs have been associated with membrane trafficking and actin cytoskeleton rearrangements. Arf6 predominantly localizes to the plasma membrane and regulates trafficking process at the cell surface such as endocytosis, exocytosis (D'Souza-Schorey and Chavrier, 2006), and FcγR-mediated phagocytosis (Niedergang et al., 2003). It was shown that the intracellular pathogen, *Salmonella*, was able to manipulate the WAVE regulatory complex (WRC) by activating Arf1 and Arf6, which facilitated ruffling and engulfment (Humphreys et al., 2012, 2013). Recently, the role of ASAP1 in Arf1-dependent *Salmonella* invasion has been demonstrated (Davidson *et al.*, 2015). Thus, it seems plausible that ASAP1 may be involved in the phagocytosis of mycobacteria with a similar mechanism.

The actin cytoskeleton remodeling during phagocytosis is orchestrated by phosphoinositides that regulate the location and activity of actin-binding proteins (Levin et al., 2014). The interaction between the PH domain of ASAP1 and PIP_2 is known to modulate cytoskeletal remodeling during cell spreading and membrane growing ruffles induced by PDGF (Randazzo et al., 2000). It is also possible that ASAP1 may regulate the interaction between Arfs and plasma membrane during the formation of the phagocytic cup.

.

1.7.6 Molecular function of GTPases, GTPase-Activating Proteins (GAPs) and Guanine nucleotide Exchange Factors (GEFs)

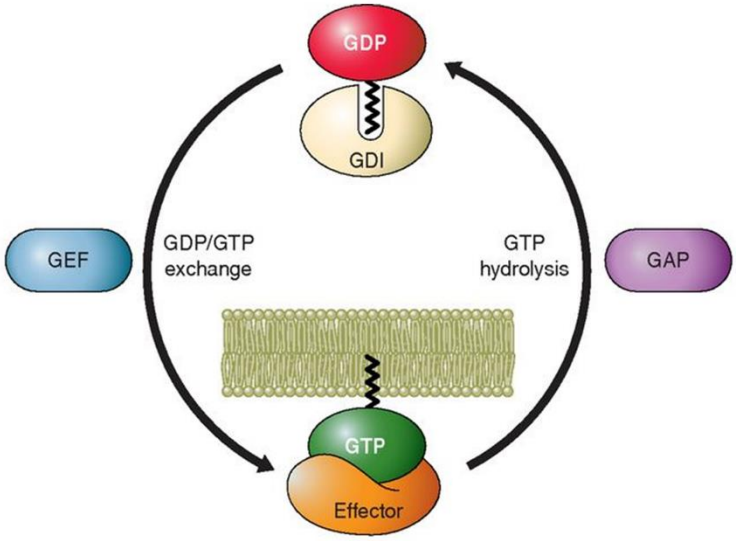

Figure 1.7-4: The GTPases molecular cycle.

The small GTPases cycle between their active form (GTP-bound) and inactive form (GDP) with help hand of Guanine nucleotide exchange factors (GEFs) and GTPase-activating proteins (GAPs). GEFs (blue) activate GTPases by facilitating the dissociation of GDP (red). GAPs (Violet) inactivate GTPases by inducing the hydrolysis of GTP to GDP. Each small GTPase subfamily is tightly controlled by specific GEF and GAP subfamilies. Adapted from (Cherfils and Zeghouf, 2013).

Dynamic remodeling of the actin cytoskeleton is essential for a diverse range of essential cellular processes such as adhesion, migration, cytokinesis, endocytosis, and phagocytosis (Santy and Casanova, 2002). The Arf and Rho among others subfamilies belong to the small GTPases of the Ras superfamily, which is important for regulating membrane trafficking and reorganization of the actin cytoskeleton. In general, GTPases serve as molecular switches cycling between inactive (bound to GDP) and active (bound to GTP) forms. The cycling

between the two conformations is mediated by two types of proteins. Guanine nucleotide exchange factors (GEFs) facilitate the exchange of GDP to GTP. In contrast, GTPase activating proteins (GAPs) inactivate GTPases by promoting the hydrolysis of GTP binding proteins (**Figure 1.7-4**) (Bar-Sagi and Hall, 2000). GAPs regulate the activity of both Rho and Arf GTPases. (Santy and Casanova, 2002).

1.7.7 Genetic regulation of gene expression in *M. tb*-infected macrophages.

Recently, it has become clear that individuals show genetically determined variation in their transcript abundance, which can be analyzed and studied by genetic tools as any other quantitative trait, such as height or body weight. The advancement in technology, such as the use of microarrays and high-throughput sequencing, enables the measurement of gene expression from thousands of genes in a significant number of individuals. Then one can find DNA variants that regulate the abundance of transcripts in a target cell or organism. These have been termed expression quantitative trait loci (eQTLs). Several studies have uncovered eQTLs' effects on gene expression. eQTLs can regulate gene expressions locally (typically within 1Mb region, likely *cis-acting*) (**Figure 1.7-5a**); they are known to be enriched around transcription start sites (TSS). Unlike *cis-acting*, *trans-acting* eQTL influences gene expression remotely and may be located on a different chromosome. (**Figure 1.7-5b**) (Cheung and Spielman, 2009; Cookson *et al.*, 2009).

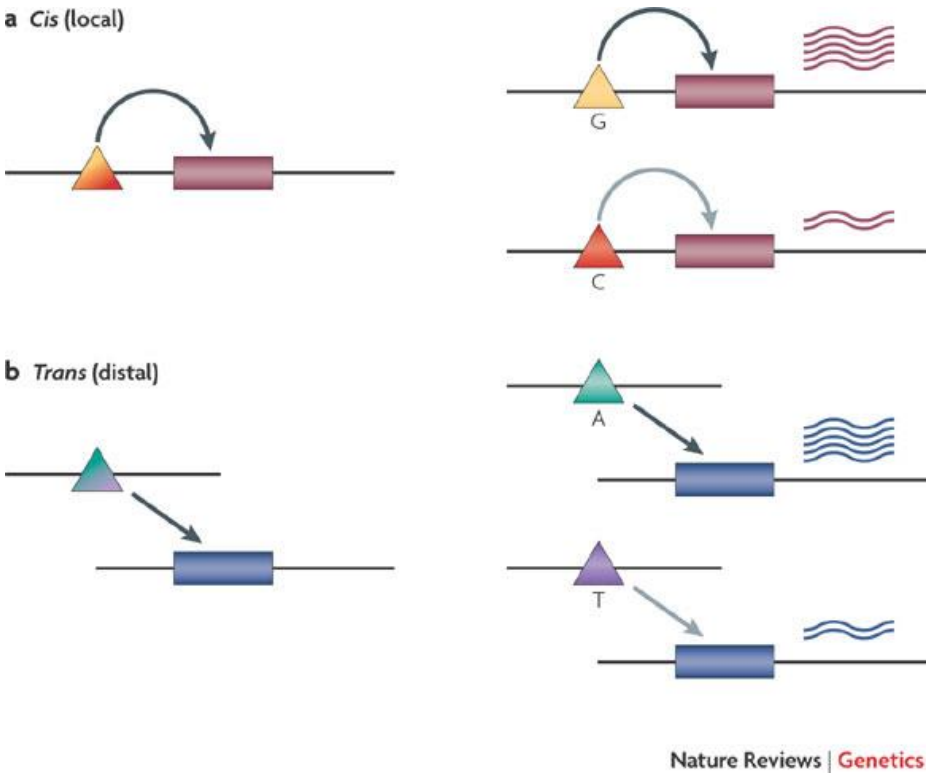

Figure 1.7-5: Schematic diagram showing the effect of cis and trans-acting DNA variants on gene expression.

(Left) **(a)** *cis* **(b)** *trans-acting* variants influence the level of gene expression. (Right) the gene expression level is affected by different alleles. Individuals with the G variant at the cis-acting element and individual with the A variant at the trans-acting element show a higher gene expression level compared to people with C and T alleles, respectively (Cheung and Spielman, 2009)

Previously, data of gene expression were obtained by microarrays, which in principle use one or few probes to measure gene expression of thousands of genes. Studies that used this tool to measure variations in gene expression shed light on mechanisms of action of loci associated with various diseases (Pickrell *et al.*, 2010). Currently, microarrays are still used for gene expression profiling and can be affordable for many research laboratories (Zhao *et al.*, 2014). However, microarrays have some drawbacks. They have less sensitivity for genes that are either expressed at low levels or at very high levels due to their small dynamic range. The microarray

is limited and only detects the known transcripts (Wang, Gerstein and Snyder, 2009). The advances in sequencing termed "RNA-Seq" overcome the shortcomings of microarrays. In principle, RNA-Seq takes advantage of the poly (A) tail to generate a library of cDNA fragments with adapters ligated to one end or both ends (Wang, Gerstein and Snyder, 2009), which are then sequenced using highly parallel sequencing. Sequence reads are then aligned to a genome and represent the abundance of various transcripts. Unlike microarrays, RNA-Seq produces very low background noise so that sequenced reads can be mapped to distinct regions of the genome. This high-throughput technology has a high dynamic range since it does not have an upper limit of quantification. The RNA-Seq is becoming widely preferable to microarrays for whole transcriptome profiling (Zhao *et al.*, 2014). The increased accuracy and sensitivity of RNA-Seq enable studies to use unbiased quantification of expression level for the entire length of a transcript without the need for probes or primers (Wang, Gerstein and Snyder, 2009; Pickrell *et al.*, 2010). It also helps to identify novel transcripts and isoforms, alternative splice sites, and allele-specific expression (Pickrell *et al.*, 2010; Zhao *et al.*, 2014). Therefore, this high-throughput approach has improved and facilitated studies of gene expression (Pickrell *et al.*, 2010).

Several studies have been conducted to evaluate the natural variation of gene expression in human cells or population. For example, Molony *et al.* performed analysis of gene expression in immortalized B cell lines. They used linkage analysis for expression phenotypes. The analysis identified numerous transcriptional regulatory loci, without previous knowledge of the regulatory mechanism. This study and similar studies for variation in gene expression in cells, tissues or diseases at a baseline level of expression were regarded as a proof of principle of the genome-wide eQTL (Morley *et al.*, 2004). To date, many studies have been published

interrogating different immune cells and have identified cell-specific eQTL. However, many eQTL studies used PBMC that are easily accessible cells. This approach may underestimate the effect of DNA variant from specific cell subtypes that only represents small proportion of total cell counts (Fairfax and Knight, 2014).

Many of the identified regulatory variants that affect gene expression were associated with various human diseases or traits in GWAS. Therefore, the identification of eQTL has significant biomedical interest. Variation in gene expression shapes the severity of immune responses and genes associated with immune-mediated diseases exhibit higher heritability for expression, which reflects the selective pressure of infectious disease (Fairfax and Knight, 2014). Fairfax *et al*. investigated the effect of immune stimuli on eQTLs monocytes; this work highlighted the effects of *cis*-acting and *trans*-acting regulatory elements that were associated with gene expression and were peculiar to the activation of innate immunity. In this study, monocytes from 432 European individuals were exposed to different stimuli, IFN-γ or LPS. They then mapped eQTLs. The majority of *cis*-eQTLs observed interfered with gene expression only after cell stimulation (response eQTL [*cis*-reQTL]); their effects were also dependent on the duration of the exposure time (Fairfax *et al.*, 2014). Similarly, the study by Lee et al. characterized transcriptional responses to LPS, influenza virus, and IFN-β in DC-derived monocytes from different ethnic groups. They revealed that the majority of *cis*-QTLs identified were also described as context-specific *cis*-reQTLs (Lee *et al.*, 2014) .

Equally important, aforementioned Lee et al. and Fairfax et al. studies also described *trans*-reQTLs that drive the expression of sets of downstream genes. For example, *IRF7* is affected by *cis*-QTL in DCs stimulated with LPS, IFN-β, and influenza. The same DNA variant acts as *trans*-reQTL for sets of genes in response to influenza infection (Lee *et al.*, 2014; Pacis,

Nédélec and Barreiro, 2014; Albert and Kruglyak, 2015). Another *cis*-eQTL was found after LPS treatment for 2 hours to be associated with *IFNB1* expression. The same SNP proceeded to act as *trans*-reQTL for a set of 17 genes, many of which were early interferon response genes, including *IRF7* (Fairfax *et al.*, 2014; Pacis, Nédélec and Barreiro, 2014).

Recently, a genome-wide study of gene expression was conducted to interrogate transcriptomic response to *M. tb* in monocyte-derived DCs from 65 healthy donors. As a result, 198 response eQTLs were identified to be attributed to the variations in individual immune responses to *M. tb* infection in DCs. Upon integration of this data with previously published GWAS, the identified response eQTLs were strongly implicated as genetic determinants of tuberculosis susceptibility (Barreiro *et al.*, 2012).

Intriguingly, these three eQTL-mapping studies have shown that immune re-QTLs were enriched for DNA variants associated with infectious diseases and immunity identified by GWAS. Therefore, combining results obtained for studies of eQTL response to different treatments and GWAS data may lead to the identification of new variants associated with immune-mediated diseases that would have been underlooked by GWAS alone (Pacis, Nédélec and Barreiro, 2014).

However, a study with efficient samples sizes and using RNA-seq, which provides more accurate measurement of gene expression, potentially can provide more power to reveal genes, influencing biological processes that underlie complex diseases such as tuberculosis. During my Ph.D. project, our laboratory was conducting a genome-wide study of gene expression in *M. tb*-infected and non-infected monocyte-derived macrophages (MDMs) in order to investigate the regulatory mechanisms that underpin susceptibility to tuberculosis.

1.7.7.1 Characterizing the function of novel TB-associated proteins using RNAi and CRISPR-Cas9 technologies

To characterize the function of the newly identified TB-associated proteins, ASAP1 and ARHGAP27, I used RNA interference (RNAi) and CRISPR-Cas9 technologies. These allowed me to deplete specific genes in cellular models and then study their functional performance during mycobacterial infection. Here I briefly describe these technologies.

1.7.7.1.1 RNAi technology

The discovery of RNAi in *Caenorhabditis elegans* has revolutionized the way scientist study gene expression. The small interfering RNA (siRNA) is one of the RNAi pathways, which involves exogenous synthetic or viral inducer of RNAi (Wilson and Doudna, 2013). Briefly, long-strand RNA is processed endogenously in the cytoplasm by Dicer, leading to the formation of 21 nucleotide-long siRNA. The siRNA also can be introduced into cells exogenously. The siRNA hybridizes with the sequence of target mRNAs. This interaction eventually leads to the degradation of the target mRNAs through biochemical complex termed RNA-induced silencing complex (RISC) (Unniyampurath, Pilankatta and Krishnan, 2016).

1.7.7.1.2 CRISPR-Cas9

CRISPR (clustered regularly interspaced palindromic repeat) technology outperforms other genome editing systems, such as zinc-finger nuclease (ZENs) and transcription activating-like effector nucleases (TALENs), owing to its simplicity and ease of use (Chira *et al.*, 2017). In 1987, a Japanese group was first to describe repetitive elements as short regularly spaced repeats in *Escherichia coli* (Ishino *et al.*, 1987). Later, CRISPRs were identified in different bacteria and archaea. In 2005, a putative link between CRISPR and prokaryotic immunity resulted from the

observation that many spacer sequences derive from bacteriophages and plasmids (Mojica *et al.*, 2005). At the beginning of January 2013, three independent scientific groups empirically showed that the CRISPR-Cas9 is an efficient tool to engineer bacterial and mammalian genomes (Cong *et al.*, 2013; Jiang *et al.*, 2013; Mali *et al.*, 2013). It took a few more months for the CRISPR-Cas9 (CRISPR-associated protein 9) genome editing technology to revolutionize the entire genome editing field for DNA editing as well as mammalian gene editing (Unniyampurath, Pilankatta and Krishnan, 2016).

The CRISPR-Cas9 system is a microbial adaptive immune system. Three main types –(I - III), based on Cas genes, have been identified. Thanks to its simplicity, the type II, derived from *Streptococcus pyogenes*, has been extensively used for genome editing in eukaryotes, including mammalians (Unniyampurath, Pilankatta and Krishnan, 2016). The CRISPR-Cas9 type II is composed of the Cas9 nuclease and chimeric single guide RNA (sgRNA), which is a combination of a CRISPR RNA (crRNA) and a trans-activating crRNA (*trans*RNA). sgRNA binds to Cas9 nuclease and guides it to a complementary target sequence. The target sequence is always associated with a protospacer-adjacent motif (PAM) containing a 5'NGG sequence. Cas9 can be directed to any genomic locus of interest in close proximity to PAM by changing the 20-nt guide sequence within the sgRNA. At the target sequence, Cas9 creates a double-strand break (DSB), which induces the non-homologous end joining (NHEJ) or homology-directed repair (HDR). NHEJ results in small random insertion or deletion (indels) at the DSB site usually generates gene knockout. HDR can be applied in the presence of a donor DNA template to create a gain of function (knock-in) by replacing the desired sequence at the DSB (Wang, La Russa and Qi, 2016; Chira *et al.*, 2017)

Several online tools have been available to aid in designing sgRNAs. These tool use developed algorithms to optimize designing sgRNAs by maximizing the on-target activity and reducing potential unwanted "off-target" effects (Wang, La Russa and Qi, 2016; Chira *et al.*, 2017). It is common to design sgRNA targeting early exons in coding sequences to ensure the disruption of the targeted translated protein as much as possible by frameshift mutations (Wang, La Russa and Qi, 2016).

The RNAi and CRISPR-Cas9 based technologies have their own advantages and disadvantages. For example, in primary cells, CRISPR-Cas9 is difficult to use for knocking out a gene because of the time required for genome editing. On the other hand, RNAi technology is quick and efficient to suppress transiently posttranscriptional gene expression on a pool of primary cells. Unlike siRNA, CRISPR-Cas9 is preferable for generating individual clones with a stably knocked out gene in the genome. Both RNAi and CRISPR-Cas9 can be utilized as tools to assess genes functions and their participation in disease phenotypes.

1.8 Aim and objectives

In my Ph.D., I focus on three projects. In Project 1 I investigate the role of the ASAP1 protein in TB, following results of our large GWAS that discovered DNA polymorphisms in the *ASAP1* gene associated with susceptibility to TB. I used a range of molecular biology techniques to investigate *ASAP1* involvement in susceptibility to TB in cellular models of mycobacterial infection, including primary macrophages and dendritic cells as well as macrophage-like cell line THP-1.

In project 2, I participated in a large analysis of gene expression in *M. tb*-infected macrophages done by our lab. I contributed to this project by isolating monocytes from blood samples, deriving MDMs, infecting MDMs with mycobacteria, and extracting RNA from MDMs, as well as analyzing the newly identified genes. This work led to the discovery of a TLR1-regulated transcriptional network, and my aim was to characterize this gene network together with other lab members. Project 2 also identified a strong cis-eQTL in the *ARHGAP27* gene associated with TB. Therefore, in Project 3 I focused on studying the functional role of *ARHGAP27* in macrophages infected with mycobacteria. I used CRISPR-Cas9-edited ARHGAP27-knockout THP-1 macrophage cell line to characterize mechanisms implicating ARHGAP27 in TB.

Chapter 2 Materials and Methods

2.1 Mycobacteria preparation

M. tb virulent strain (H37Rv) or *Mycobacterium bovis* BCG (mCherry or DsRed2 expressing strains) was cultured on Lowenstein-Jensen medium (VWR Chemicals) for three to four weeks. Alternatively, mycobacteria were grown in 7H9 medium (BD) supplemented with 10% of OADC (BD) and Tween-80 (0.5 ml/L) (Sigma-Aldrich), to reduce clumping. Grown colonies were harvested and washed in Phosphate-Buffered Saline (PBS). Bacteria were pelleted at (3700 x G) for 20 minutes to remove large clumps. The pellet was vortexed with 3-5 glass beads five times for 10-15 seconds each. Then, the pellet was suspended into 50 ml of PBS and spun at low speed (230 x G) for 2 minutes to sediment large clumps. For BCG, the bacterial suspension was also passed through by 25-gauge needles 30 times then, the supernatant was then pelleted at high speed (3700 x G) for 20 minutes and resuspended in 7H9 medium in addition to 20% glycerol. Aliquots of 500 µl each were stored at -80 ºC for later experiments (Bosedasgupta and Pieters, 2014).

2.2 Cell lines

Hela cells were cultured in Dulbecco's modified Eagle's medium (Gibco) supplemented with 10% heat-inactivated FBS and 1% Penicillin-Streptomycin (Gibco). THP-1, a monocyte-like cell line, was maintained in RPMI-1640 (Life technologies) with 10%

heat-inactivated FBS containing Penicillin/Streptomycin (100 µg/ml and 100 U). THP-1 cell line was differentiated into macrophages at a density of 1×10^6 cells/ml by the exposure to 50ng/ml phorbol 12-myristate 13-acetate (PMA) for 48 hours and left for extra 24 hours resting in medium without PMA.

2.3 Ethics

A signed written consent was obtained from each participant. Blood from healthy volunteers obtained from Cambridge Bioresources or unscreened blood from Cambridge Blood Donor Centre (NHS Blood and Transplant) was studied with approval from the National Research Ethics Committee, (Cambridgeshire, REC, 10/H0304/71).

2.4 Cell preparation and infection

Peripheral blood mononuclear cells (PBMC) from healthy volunteers or from leukocyte cones were obtained by centrifugation with a gradient of Ficoll-Paque Plus (GE Healthcare). Briefly, around 50 ml of donor blood was centrifuged at (860 G) for 23 minutes at room temperature (BOYUM, 1964). Then, a magnetic cell separator (MACS) and magnetic CD14 MicroBeads (Miltenyi, UK Cat. No 130-050-201) were used to purify $CD14^+$ monocytes from the buffy coat by the CD14 positive selection (Miltenyi *et al.*, 1990). For monocyte-derived macrophages (MDM), isolated monocytes were plated in 24-well plates at 1×10^6 cells/well for 6 days in RPMI-1640 (Life technologies) containing gentamicin (100 µg/ml), 10% heat-inactivated fetal bovine serum (FBS), and 50 ng/ml macrophage colony-stimulating factor (M-CSF) (Miltenyi, UK) (Jaguin *et al.*, 2013). For, monocyte-derived

dendritic cells, monocytes were cultured for 6 days in RPMI-1640 containing gentamicin (5ug/ml), 5% heat-inactivated FBS, GM-CSF (50U/ml, Milteny, UK), and IL-4 (1,000 U/ml, R&D Systems). Culture media were changed on day 3 to feed the cells with the same supplements (Chapuis *et al.*, 1997). The remaining PBMC were stored at -80 ºC for DNA extraction.

Prior to infection, an aliquot of *M. tb* H37Rv or BCG bacteria were incubated overnight at 37 ºC to revive the microorganism. MDMs were incubated with antibiotic-free RPMI-1640 supplemented heat-inactivated FBS for 2 to 4 hours before infection. Cells were infected with mycobacteria to achieve a multiplicity of infection (MOI) of 4 bacteria per cell (4:1) and incubated at 37 ºC plus 5% CO_2 for 24 hours; 10% glycerol-PBS was used as a negative control to non-infected MDMs.

2.5 RNA extraction

The infected and non-infected MDMs were lysed after 24 hours post-infection, and total RNA was then extracted using the RNeasy mini kit with some modifications (Qiagen cat No 74106). Briefly, the medium was removed, and 350 µl of buffer RLT was added to the monolayer. To kill mycobacteria, we added 850 µl of 100% ethanol to the lysate, providing 70% final concentration of ethanol, for 10 minutes (CDC, 2008)**.** Then, 70% ethanol was diluted in 850 µl of buffer RLT and 350 µl RNase free water to achieve the recommended concentrations for RNeasy spin column of 35% ethanol and 50% buffer RLT. The rest of the RNA extraction was carried out as per manufacturer's manual. The total RNA concentration and purity were evaluated using spectrophotometry by NanoDrop 1000 (Thermo Fisher). One

µl of RNA sample was enough to calculate A260/230 and A260/280 ratios in order to assess the presence of contaminants. As a result, RNA samples with required quality (i.e., 230/260 ratio of 0.70) and quantity (i.e., 500 ng to 750 ng per library) were used for library preparation.

2.6 qRT-PCR

The *ASAP1* and *ARHGAP27* mRNA expression were analyzed using two-step qRT-PCR. Total RNA was isolated using Isolate RNA Mini Kit (Bioline UK). The concentration of 200 ng was used to generate the first-strand cDNA using Thermo Scientific Maxima Reverse Transcriptase (Thermo Scientific, UK). Then, 2µl of 1:5 diluted first-stand was used for qPCR using KAPA SYBR FAST Universal qPCR kit (Kapa Biosystems, UK) and primers for *ASAP1*, *ARHGAP27*, housekeeping genes β2 microglobulin, and *HPRT*. ΔC_t was analyzed in triplicate to provide *ASAP1* and *ARHGAP27* mRNA expression levels relative to the mRNA of a housekeeping gene.

Table 2.6-1: Quantitative PCR primers

ASAP1	Forward	CCAAATGTGCAGTCCAGAGA
	Reverse	GCCTGGCAGTCATAAATGGT
β2 microglobulin	Forward	GATGAGTATGCCTGCCGTGTG
	Reverse	CAATCCAAATGCGGCATCT
ARHGAP27	Forward	ACTCCCGAGACGGACTACC
	Reverse	CCCACTGCTCCTGAGTGAAG
HPRT	Forward	TGCTCGAGATGTGATGAAGG
	Reverse	TCCCCTGTTGACTGGTCATT

2.7 Immunofluorescence for confocal microscopy

Differentiated DCs or macrophages were plated on glass coverslips coated with fibronectin in a 24 well plate and incubated at 37º C and 5% CO_2 for 4 hours. Cells then were fixed with 4% PFA for 10 min at room temperature. Coverslips were washed three times with PBS and permeabilized with 0.1% Triton X-100 for 15 min. Cells were washed three times with PBST and blocked with 1% BSA in PBST for 60 min. Coverslips were incubated with anti-ASAP1 mouse antibody (Santa Cruze Biotechnology) and anti-Viculin rabbit antibody (Invitrogen) for 60 min in a humidified chamber for 60 min at room temperature. Primary antibodies were decanted, and coverslips were washed three times. Cells were

immunostained with secondary antibodies (Alexa Fluor 488-conjugated donkey anti-mouse IgG, Molecular Probes), Alexa Fluor 633-conjugated goat anti-rabbit IgG (Molecular Probes), and Alexa Flour 568-conjugated phalloidin (actin). After washing, coverslips were mounted using ProLong Gold Antifade Mountant with DAPI and visualized using Leica SP5 confocal microscopy.

2.8 DNA extraction and genotyping

PBMC from healthy donors were used to extract genomic DNA using DNA extraction kit (Qiagen Cat 51104) as per manufacturer's instruction. Briefly, Proteinase K was added to the bottom of microcentrifuge tube, followed by donor's PBMC. Lysis buffer and vortexing were applied to achieve efficient lysis. Samples then were incubated for 10 min at 56 °C, followed by the addition of an equal volume of 96-100% ethanol. Samples were then transferred to QIAamp Mini spin column for washing. Eluted genomic DNA was concentrated using Vacu Prep. DNA was quantified using Qubit and normalized to 100 ng/µl or 200 ng/µl. Genomic DNA samples were stored in matrix boxes at -80 ºC before being sent to the Department of Pathology at the University of Cambridge for genotyping. Genotyping was done using Illumina Human OmniExpressExome v1.2 BeadChips arrays containing 964,193 markers.

2.9 Microarray sample preparation

Briefly, the high-quality RNAs as of A_{260}/A_{280} ratio ranging from 1.7 to 2.1 were used to generate cDNA. After treating the total RNA with the RiboMinus™ Human/Mouse

Transcriptome Isolation Kit (Invitrogen) to deplete most of the ribosomal RNA, one microgram of treated RNA was used for the double amplification procedure as per manufacturer's instructions to obtain hybridization targets using the GeneChip® WT cDNA Synthesis and Amplification Kit (Affymetrix, Ltd, UK). The sense oriented single-stranded DNA of hybridization targets then were fragmented, and ends were labeled by using the GeneChip® WT Terminal Labeling Kit (Affymetrix, Ltd, UK). The fragmented and labeled DNA was hybridized to GeneChip® Human Gene 1.0 ST Array (Affymetrix, Ltd, UK).

2.10 Library preparation

Briefly, Qubit® RNA HS Assay Kit (Life technologies) and Bioanalyzer were used to evaluate the quantity and quality of the total RNA, respectively. TruSeq RNA Sample Preparation Kit was used to convert total RNA into libraries of double-stranded cDNA for high-throughput sequencing as per manufacturer's recommendations. The mRNAs were purified from the total RNA by using poly-T oligo-attached magnetic beads. The purified RNAs, subsequently, were fragmented by using divalent cations under elevated temperature to denature the mRNA and allow the binding of the magnetic beads. Random hexamers and SuperScript II were used to synthesize the first strand of cDNA. Then DNA polymerase I and RNase H were used to synthesize the second strand. AMPure XP beads were used to separate the double strands blunt-ended cDNA produced by exonuclease/polymerase activities. After adenylation of 3' end of DNA fragments, sequencing adaptors were ligated to prepare for hybridization. The products with ligated adapters were amplified using PCR primer cocktails. The final cDNA library quantification was carried out by qPCR with Illumina primers that

are specific to adaptors. Sequencing was done on Illumina HiSeq 2000 machines using single-end 50 nucleotide reads.

2.11 Bioinformatics analysis of the transcriptome data and eQTLs in macrophages

Bioinformatics analysis was done by Drs Kitty Lo and Vincent Plagnol at UCL. Briefly, genotype imputation was performed using minimac (July 2013 release) and the build hg19 of the human genome (1.000 Genome phase 1, release v3, EUR panel.).

Topat-2.0.13 was used without duplicate exclusion to align single-end reads from FASTQ files against the build hg19 of the human reference genome. Mapped reads were then counted using dexseq_count.py script provided as part of the DEXSeq package. Counts were then combined across all exons to generate gene counts. These gene counts were normalized across samples by computing the size factors, as implemented in the DESeq2 package (package version 1.10.1, R version 3.2.2). This generated normalized expression values (across samples) for each combination of gene and samples. These estimates were then combined with the genotype data using the R package MatixEQTL version 2.1.1 for eQTL analysis. To minimize storage requirement and facilitate processing, we stored the genotype data using the raw format, as implemented in the R package snpStats version 1.2. the MatrixEQTL analysis generated an eQTL P-value for each combination of variant and gene. We retained all P-values more significant than 10^{-4} for subsequent analyses. Principal component analysis was performed based on the normalized gene count data.

2.12 Bioinformatics analysis of the transcriptome data in THP-1 cells

I used Galaxy bioinformatics tools to perform RNA-Seq analysis (Sloggett, Goonasekera and Afgan, 2013). Briefly, HISAT2 (Galaxy Version 2.0.5.2) was applied to align single-end reads from FASTQ raw data files against the build hg19 of the human reference genome from iGenomes. FASTQ Groomer (Galaxy Version 1.0.4) was used to verify and convert FASTQ files to the standard format that is compatible with Galaxy downstream processing. Gene expression levels were then counted by quantifying raw mapped reads using intersection-nonempty counting mode of HTSeq-count (Galaxy Version 0.6.1galaxy3). Differential expression analysis was performed using DESeq2, which uses, as the reference distribution, the negative binormal distribution and its normalization approaches (Conesa *et al.*, 2016).

2.13 siRNA transfection

Purified $CD14^+$ monocytes were transfected at 7.5×10^5 cells/well on day 0 and day 3, using Hiperfect (Qiagen) with a mixture of three siRNA targeting *ASAP1* (life technologies, HSS147202, HSS147203, HSS181756) in order to suppress the endogenous ASAP1 expression in macrophages or DCs. AllStars negative control siRNA (Qiagen Cat no 1027281) was used as scrambled siRNA (control negative, si-Ctrl). Hiperfect alone was used with non-transfected control. The Hela cell line was seeded in 24-well plates at a density of 6 X 10^4 cells per well. Seeded cells were then transfected with siRNA-ASASP1 or control siRNA for 48 to 72 hours. THP-1 cells were seeded at a density of 5 X 10^5 per well in 24-

well plate and differentiated with PMA for 24 hours. PMA-differentiated THP-1cells were transfected with siRNA-ASAP1 or si-Ctrl for 24 to 72 hours. The depletion efficiency was evaluated by western blot using anti-ASAP1 antibody (ab11011, Abcam; 1:1000) and ImageJ software for quantification.

2.14 Lentiviral particles production

Lenti-X 293T Cells (Clontech, # 632180) were trypsinized prior to transfection. Transfection was performed using Lipofectamine 2000 as manufacturer's instructions. In brief, two solutions were prepared. The first solution was comprised of 13.5 µl of Lipofectamine 2000 and Optimem medium (reduced serum medium) to a final volume of 500 µl and incubated at room temperature for 5 mins. The second solution contained 1.4 µg of the packaging vector plasmid, psPAX2 (Addgene 12260), 1 µg of the envelope plasmid, pCMV-VSV-G (Addgene 8454), and 2 µg of transfer vector in a final volume of 500 µl of Optimem medium and incubated at room temperature for 5 mins. The two-prepared solution was pooled and incubated for 20 min at room temperature. Two ml of DMEM antibiotic-free media was added to 60 mm Poly-D-Lysine (PDL) coated petri-dish. The mixed DNA complex solution was added to the PDL coated dish, and the plate was swirled gently. Then, 3 million of trypsinized Lenti-X 293T cells were seeded onto the DNA complex and incubated overnight at 37 ºC. After 24 hours, transfection media was replenished with a fresh DMEM antibiotic-free medium. Then, the virus-containing supernatant was harvested 48 hours post-transfection and centrifuged at 1000G for 5 min. The supernatant was passed through 0.45 µm filtered. Polybrene, then, was added to the virus at a concentration of 8 µg/ml to be used for transduction.

2.15 Engineering Cas9-expressing stable cell lines

LentiCas9-Blast vector (Addgene 52962) was used to generate cell lines stably expressing Cas9 (**Figure 3.1-9a**) (Sanjana, Shalem and Zhang, 2014). Lentiviral particles were produced using Lenti-X 293T Cells. THP-1 cells were seeded at 5 X 10^4 cells/ml and then transduced with viral particles. Two days post-transduction, the bulk cultures were subjected to blasticidin selection with a concentration of 5 µg/ml for 5-7 days. Cells were subjected to limiting dilution and plated in 96 cell plates to obtain single clones stably expressing Cas9. If cells do not tolerate growth at low cell density, the growth medium was supplemented with antioxidants at a final concentration of 1 mM sodium pyruvate (Gibco), 50 µM α-thioglycerol (α-TG, Sigma), and 20 nM bathocuproindisulfonic acid disodium salt (BCS, Sigma) (Brielmeier *et al.*, 1998). After approximately 3-4 weeks of clonal expansion, cells were lysed with RIPA buffer for protein. Clones were screened for Cas9 expression level with anti-FLAG antibody (clone = M2, Sigma-Aldrich) (**Figure 3.1-9b**). A single clone was used to generate CRSPIR-Cas9 knockout cell lines.

2.16 CRISPR-Cas9-mediated gene knockout.

There are several online tools that help in designing sgRNAs. I used the Zhang's tool at http://crispr.mit.edu) to design sgRNAs that target the ASAP1 and ARHGAP27 genes (Table **2.16-1**). Although the online tool filter sgRNAs based on an algorithm to reduce off-target effects, there were few criteria considered during the selection of sgRNAs. First, the overall on-target quality score for sgRNA was more than 70. Second, the off-target score was less than 1.5 with 4 mismatches (**Figure 3.1-10**). Third, since the sgRNA expression is U6

promoter-driven, G was added as the first nucleotide for effective expression if no target sequence were found where G is 20 bp upstream of PAM sequence (Ran *et al.*, 2013). Last, corresponding overhangs were included in the designed oligos as shown in (Table **2.16-1**). LentiGuide-Puro (Addgene 52963) (**Figure 3.1-9a**) was digested using BsmBI enzyme (NEB R0580S) at 55 ºC overnight. (**Figure 3.1-11**) showed BsmBI-digested vector and a filler with a size of ~8000 bp and 2000 bp, respectively, as previously described (Sanjana, Shalem and Zhang, 2014). Linearized vector was dephosphorylated using Antarctic phosphatase (AP) (NEB M0289S) at 37 ºC for 1 hour. Dephosphorylated vector was loaded on an agarose gel; band corresponding to the linearized plasmid with size around 8 kb (**Figure 3.1-11**) was excised and purified using QIAquick Gel Extraction Kit (Qiagen). Unphosphorylated oligos targeting either ASAP1 or ARHGAP27 were phosphorylated, annealed, and ligated to linearized vector at 37 ºC for 1 hour followed by 5 min at 95 ºC, then ramping from 95 ºC to 25 ºC at 5 ºC/min. Constructed vector was sequenced with hU6-F primer (GAGGGCCTATTTCCCATGATT) to verify the success of cloning and the presence of targeting oligos. Constructed vector was used to produce viral particles. The Cas9-expressing cells were transduced with LentiGuide-Puro. Two days post-transduction, the bulk cultures were subjected to puromycin selection with a concentration of 3 µg/ml for 5-7 days. Cells were subjected to limiting dilution and plated in 96 well plates to obtain single cell clones of the genome-edited knockouts. Single cell clones were expanded for 3-4 weeks.

Table 2.16-1: sgRNA oligonucleotides (oligo).

ASAP1 exon 5 guide#3	Top Oligo	CACCgagtcgagacaaccccgacct
	Bottom Oligo	AAACaggtcggggttgtctcgactC
	Guide sequence	AGTCGAGACAACCCCGACCT**TGG**
ASAP1 exon 5 guide#7	Top Oligo	CACCgcacaagttcttgataagtt
	Bottom Oligo	AAACaacttatcaagaacttgtgc
	Guide sequence	GCACAAGTTCTTGATAAGTT**TGG**
ARHGAP27 exon 3 guide#1	Top Oligo	CACCgcgactcggggtagtccgtct
	Bottom Oligo	AAACagacggactaccccgagtcgC
	Guide sequence	CGACTCGGGGTAGTCCGTCT**CGG**
ARHGAP27 exon 3 guide#6	Top Oligo	CACCgaggaggactattctcccgt
	Bottom Oligo	AAACacgggagaatagtcctcctc
	Guide sequence	GAGGAGGACTATTCTCCCGT**GGG**
ASAP1 exon 30 guide#1	Top Oligo	CACCgctgcgttttgctagtcagac
	Bottom Oligo	AAACgtctgactagcaaaacgcagC
	Guide sequence	CTGCGTTTTGCTAGTCAGAC**AGG**
ASAP1 exon 30 guide#4	Top Oligo	CACCgtcagacaggatatgaacaa
	Bottom Oligo	AAACttgttcatatcctgtctgac
	Guide sequence	GTCAGACAGGATATGAACAA**AGG**
ARHGAP27 exon17 guide#2	Top Oligo	CACCgagatgtccgcgcactgctgc
	Bottom Oligo	AAACgcagcagtgcgcggacatctC
	Guide sequence	AGATGTCCGCGCACTGCTGC**AGG**
ARHGAP27 exon17 guide#13	Top Oligo	CACCgtcacaggccagcagtcagtg
	Bottom Oligo	AAACcactgactgctggcctgtgaC
	Guide sequence	TCACAGGCCAGCAGTCAGTG**CGG**

2.17 T7 endonuclease 1 assay

Genomic DNA was extracted from Cas9-edited cells using QuickExtract solution (Epicentre) according to the manufacturer's protocol. Typically, 10 µl or 50 µl of the solution was used for 96-well or 24-well plate. The extracted DNA was incubated at 65º C for 15 min then at 98º C for 10 min. PCR was performed in 20 µl reaction using GoTaq polymerase (Promega) with primers spanning the sgRNA genomic target sites. The thermocycler parameters were 1 cycle of 2 min at 95° C, followed by no more than 35 cycles of 20 sec at 95° C, 20 sec at 52° C to 60° C (primer-dependent temperature, **Table 2.17-1**), and 1 min/kb at 72°C, and finishing with 1 cycle of 5 min at 72° C.

Table 2.17-1: PCR primers.

Name	Complete sequence	TM
ARHGAP27 exon3 FW	TCCCACAGACCTAAGGACCA	55.76°C
ARHGAP27 exon3 Rv	TGTGGGGAGAGGAATGGTCA	56.43°C
ASAP1 exon5 Fw	TGTACTCCTAACCTAACCTTTGGG	55.32°C
ASAP1 exon5 Rv	TGGAAGTTACCTAGGACTAAAAAGC	54.35°C

The T7 assay was performed to assess the efficiency of Cas9-mediated genome editing for a specific sgRNA. Briefly, 13 µL of unpurified PCR products were denatured and reannealed using pre-programmed thermocycler with the following parameters; 95° C for 10 min, ramping from 95º to 85º C at 2 C/sec, ramping from 85º C to 25º C at 0.3 C/sec. The PCR heteroduplexes were incubated with 2 units of mismatch-sensitive T7 endonuclease I (T7E1) (NEB # M0302S) at 37º C for 1 hour. The enzymatic activity of endonuclease was halted by using 1µl of 0.25 Ethylenediaminetetraacetic acid (EDTA). T7E1 digestion

products were separated on 2-3% agarose gel and visualized with Ethidium bromide (EtBr) or SYBR safe staining (Invitrogen).

Amplicons predicted to have indel mutations due to the CRISPR-Cas9 targeting were purified using Qiagen's PCR purification kit (Qiagen). The purified PCR products were sent to GATC Biotech company for Sanger sequencing to confirm the genomic mutations.

2.18 Western blotting

Cells were washed twice with ice-cold PBS. RIPA buffer (Sigma-Aldrich) and protease inhibitor cocktail (Sigma-Aldrich) were added to each sample to extract proteins. Samples were kept on ice for 20 min, then centrifuged at 12,000G for 10 min at 4º C. Total protein concentration was estimated by Pierce™ BCA Protein Assay Kit (ThermoScientific). Laemmli Sample Buffer (Bio-Rad), was added to cell lysates and incubated at 95° C for 10 min. Lysates were loaded and electrophoresed in a %10 TGX fast Cast acrylamide gel (Bio-Rad) at 150 V for 60-70 min. Proteins were transblotted onto nitrocellulose membranes using Trans-Blot Turbo Transfer System (Bio-Rad). Membranes were blocked with 5% milk (PBST; PBS and 0.1% Tween-20) for 30 min at room temperature. Membranes were incubated with primary antibodies, rabbit antibody to ASAP1 (ab11011, Abcam; diluted 1: 1,000) or mouse antibody to Actin (Clone AC-15, A5451, Sigma-Aldrich; 1: 10,000) overnight at 4ºC. After washing in PBS, membranes were incubated with 1: 2,000 horseradish peroxidase (HRP) conjugated anti-rabbit secondary antibody and 1:1,1000 HRP-conjugated anti-mouse secondary antibody for 1 hour at room temperature. Membranes were incubated with Amersham ECL Western Blotting Detection Reagent (GE Healthcare); signal

emitted by chemiluminescence reaction was detected with subsequent exposure of the membranes to Fuji Medical X-ray film (Fujifilm) and then developed using Compact X4 (XOgraph).

2.19 Bacterial enumeration

THP-1 WT, THP-1 ASAP1-knockout (KO), or THP-1 ARHGAP27-KO cells were differentiated in RPMI-1640 supplemented with 10% FBS and 50 ng/ml of PMA for 3 days followed by resting in medium without PMA for 24 hours. Monolayers were infected with mycobacteria with MOI of ~1-2 for mycobacterial survival assay or MOI of ~10 for phagocytosis assay. Infection was carried out in duplicate in 96-well plates and traced at different time points ranging from 1 hour to several days.

For mycobacterial survival assay, media was discarded at the end of each time point. Then, infected cells were immediately lysed with 50 µl of 0.06% SDS for 10 min at room temperature, as previously described (Kumar *et al.*, 2010). For phagocytosis assay, before lysing the cells with 50 µl of 0.06% SDS, mycobacteria-infected cells were first washed thrice with PBS to remove the excessive number of extracellular bacteria.

Duplicated wells were combined and serially diluted in 7H9 medium. Then, lysate dilutions were plated on 7H10 supplemented with OADC; in the case of *M. tb*, 0.5% glycerol was also supplemented. Square plates (12 X 12) were used for plating to reduce the number of plates used. Each concentration of serial dilutions was spotted in duplicate and allowed to air-dry. Plates were then incubated at 37º C. Grown colonies were enumerated with 2-3 weeks of incubation (Kumar *et al.*, 2010).

2.20 Phagocytosis in MDMs

Aliquots of the mCherry-expressing BCG from-80 ºC were defrosted and incubated at 37 ºC overnight. Prior to infection, MDMs treated with *ASAP1*-siRNA pool, treated with control siRNA, or treated only with Hiprefect were scrapped using policeman scraper. Trypan blue (Life technologies) was used to estimate the proportion of dead cells and to normalize cell count. Consequently, 1×10^5 MDMs of each condition were seeded on a sterile coverslip in PRMI-1640 supplemented with 10% heat-inactivated FBS, and 50 ng/ml M-CSF without antibiotics before infection and allow to attach for 2-3 hours. The monolayer, then, was infected with 65 µl of BCG-mCherry (~MOI of 10) for 1 hour or/and 2 hours. Infected cells were washed three times with ice-cold PBS to remove extracellular bacteria, and fixed in 4% paraformaldehyde. Coverslips were stained with TB stain kit ZN (BD), containing carbolfuchsin (primary stain), decolorizer, and methylene blue (secondary stain). Coverslips were mounted on slides using nail polish and pictured using EVOS®XL Core Imaging System (1000x). Phagocytosis was estimated by randomly counting between 100 and 300 macrophages per coverslip. Percentage of phagocytosis was determined by counting cells that were infected with at least one bacillus divided by total cells counted. Phagocytic index was calculated using this equation: (percentage of macrophages containing bacilli × mean number of intracellular bacteria per infected cell) (Bonilla *et al.*, 2013).

2.21 Viability test

The CellTiter 96 AQueous One Solution Reagent (Promega) is a colorimetric method, containing solutions of a novel tetrazolium compound (MTS) and an electron coupling

reagent (phenazine methosulfate; PMS). The MTS tetrazolium compound is converted by metabolically active cells producing NADPH or NADH into a colored formazan product. The CellTiter 96 was used to evaluate cell viability in mycobacteria-infected THP-1 cells as manufacturer's protocol. In 96-well plate, THP-1 (wild-type or knockout) was differentiated and plated at a density of 5 X 10^4 per well. PMA-differentiated THP-1 cells were infected in duplicate. Cell viability was rated at different time points every 24 hours from day 1-4, considering 24 hours post-infection as day 0. Culture medium was replenished with 20 µl of CellTiter 96 solution premixed with 100 µl of fresh media to each well in 96-well assay plate. The plate was incubated at 37º C for 1 hour. The absorbance at 490 nm was then recorded using a 96-well plate reader (Bio-Rad). The percentage of cell death was calculated by comparison of cell viability in infected at various times points to that in non-infected cells at day 0.

2.22 Transwell migration assay

Transwell migration assay was performed by using Thincert cell culture insert with a pore diameter of 8 µm (Greiner Bio-One) in 24-well plates. PMA differentiated THP-1 cells were incubated with accutase (Gibco) at 37º C for 30 min to detach adherent cells. Detached cells were counted with trypan blue. A total of 10^5 cells resuspended in 200µl RPMI-1640 with 10% FBS media were placed in the upper chamber of the insert and allowed to equilibrate for 1 hour. The lower compartment was then refilled with 500 µl RPMI 1640 with 10% FBS media supplemented with 100-200 ng/ml of monocyte chemoattractant protein 1 (MCP-1) to induce migration. Cells were allowed to migrate for 24 hours. Cell attached to the top of the insert filter were removed with cotton swabs. Cells adherent to the underside of the

insert filter were fixed with 4% PFA and stained with Hoechst (Invitrogen). Migratory cells were then calculated in 3-5 random fields using epifluorescent microscopy with a 20x lens. An average number of migratory cells per field in the ASAP1KO or THP-1 ARHGAP27-KO THP-1 cells was compared to those of the WT THP-1 cells.

2.23 Dunn chemotaxis chamber

The siRNA-treated DCs were seeded on coverslips coated with 0.025 mg/ml fibronectin (Sigma) and incubated at 37 °C for 4 hours in their RPMI-1640 supplemented with 5% FBS without GM-CSF or IL-4. Similarly, differentiated THP-1 knockouts or control cells were detached using accutase and seeded on coverslips treated with 0.025 mg/ml fibronectin and incubated overnight at 37 °C in 10% FBS RPMI-1640 medium. Coverslips were then inverted onto Dunn chambers containing GM-CSF (100 U/ml) or MCP-1 (200ng/ml) as chemoattractants for DCs or THP-1 cells, respectively. Time-lapse clips were recorded with an interval of 4 min for a minimum of 2 hours at 37° C in the chamber of Leica SPE with a 10x objective. Cells were tracked using the manual track plugin of ImageJ (Schindelin *et al.*, 2012), and velocity was calculated using the chemotaxis and migration plugin within ImageJ.

2.24 Matrix degradation assay

Coverslips were coated with 0.2 mg/ml FITC-coupled gelatin (Molecular Probes) for 30 min protected from light and subsequently blocked using the complete medium. Cells were seeded on the coverslips and incubated at 37 °C ranging from 4 to 24 hours and fixed

with 4% PFA. The cells were labeled with Alexa Fluor 568–coupled phalloidin (Molecular Probes) and mounted in antifade with DAPI (Molecular Probes). Images were obtained by using a Leica SP5 confocal microscope. The images were processed using ImageJ. Cell number was determined by using high-intensity threshold for DAPI positive signal. Matrix degradation was quantified by measuring the area where the FITC-labeled gelatin signal was below the threshold as previously described (Götz and Jessberger, 2013).

2.25 Podosome turnover assay

DCs were seeded on fibronectin-coated coverslips and starved in serum-free medium for 1 hour. Starved cells were treated with either DMSO or tyrosine kinase inhibitor (PP2) at a final concentration of 25µm in serum-free medium for 1 hour. Treated cells were washed and incubated with RPMI-1640 medium supplemented with 5% FBS for times indicated. Coverslips were fixed and immunostained for F-actin, labeling podosome core, with Alexa-labeled phalloidin and HCS CellMask green stain, labeling cytoplasm, (Invitrogen) for 30 min (Cervero, Panzer and Linder, 2013).

2.26 Flow cytometry

Differentiated THP-1 cells were infected with BCG expressing DsRed2 at different MOIs. After infection, cells were detached using accutase and vortexed vigorously to separate cell aggregates. Cells were fixed with 4% PFA for 10 min and permeabilized with 0.1% Triton X-100 for 15 min. After blocking with 3% BSA/PBS for 1 hour, cells incubated with primary antibody anti-*M. tb* (ab 905) suspended in 3% BSA/PBS for 30 min at 4 ºC.

Cells were washed 3 times by centrifugation at 400 g for 5 min and resuspended in ice-cold PBS. Alex-Flour 488-conjugated secondary antibody was resuspended in 3% BSA/PBS and used to visualize BCG. Infected cells with BCG were quantified using flow cytometry with BD Fortessa2 machine and FACS Diva software. The data were analyzed with the FlowJo software.

2.27 Automated microscopy assay for phagocytosis

Differentiated cells were plated at a density of 4 x 10^5 per well in 24-well plate, infected with BCG expressing DsRed2 at MOI of 10, and incubated at 37 ºC for 4 hours. Cells were washed 4-5 times with PBS to remove extracellular BCG, fixed, and stained for nuclei with Hoechst. Images were obtained using a quantitative, high-throughput, imager called the Cellomics ArrayScan XTI automated fluorescence microscope (ThermoFischer) with 20x magnification Zeiss objective. The fluorescent signal was detected in two channels with LED excitation light source. Hoechst fluorochrome (nucleus) was detected in channel 1 with a LED excitation source of 386 nm with 23 nm band and emission detected with a 420 - 460 nm filter. The intracellular DsRed2 signal was detected on channel 2 with a LED excitation source of 560 nm with 25 nm bandpass and emission detected with 584-645 nm filter. Image analysis was performed with HCS Studio software version 6.6.0 (ThermoFischer). Spot Detector BioApplication algorithm was utilized to detect bacteria aggregations within cells. This algorithm, as part of HCS Studio software, is providing generic spot identification and analysis of any intracellular punctate objects. The Spot Detector protocol was optimized for this particular experiment.

2.28 Generic technique for gene tagging

A549 stably expressing Cas9 were cotransfected with a universal plasmid (pMA-universal *tai1l* vector, generously provided by Dr. Bürckstümmer) and lentiGuide-Puro harboring sgRNA targeting C-terminus of *ASAP1* or *ARHGAP27*. Transfection was performed using Lipofectamine 2000 as previously described in (**section 2.14**). A concentration of 0.5 µg of each plasmid was mixed in a final volume of 500 µl of Optimem and used for transfection. Then, 4 hours post-transfection, media was removed and replenished with fresh medium for overnight. One day post-infection, a pulse of puromycin selection at a concentration of 3 µg/ml was applied to enrich for cells with fused proteins for 2 days. After a week, cells were expanded for clonal isolation for 2-3 weeks. A single clone was tested with fluorescent microscopy and PCR with primers binding to the insert and the flanking genomic DNA.

2.29 Rapid immunoprecipitation mass spectrometry of endogenous protein (RIME)

RIME is a mass spectrometry (MS)-based method that facilitates the study of interactomes in a rapid and robust manner. RIME was performed as previously described (Mohammed *et al.*, 2013, 2016). In brief, differentiated ASAP1-KO or WT THP-1 cells (total of 2 X 10^7 per condition) were infected with DsRed2-expressing BCG or left uninfected in 10% FBS RPMI-1640 antibiotic-free medium for 4 hours. The medium was then discarded, replenished with medium containing 1% formaldehyde (Invitrogen), and then crosslinked for 9 min. A final concentration of 0.1 M of Glycine was used to quench crosslinking. The cells

were washed twice with ice-cold PBS and harvested in PBS. The protein was extracted initially by resuspending the pellet in 300 µl of RIBA buffer for 10 min at 4° C. Then, cells were sonicated in a water bath sonicator using a 30-s on/off cycle for 10 min (Diagenode Bioruptor). Lysates were centrifuged at 4º C for 10 min at 12,000 G to purify the debris. The supernatant was then incubated with 12 µg of ASAP1 antibody overnight at 4 º C. Then, 40 µl of magnetic beads (Dynal) was added to immunoprecipitate complexes and incubated on a rotor at 4º C for 1 hour. The beads were washed ten times in 500 µl of RIPA buffer and twice in 100 mM ammonium hydrogen carbonate (AMBIC) solution. For the second AMBIC wash, the beads were transferred to new tubes and stored at -80º C. Samples were submitted to the biochemistry department at the University of Cambridge to perform mass spectrometry. The software Cytoscape (version 3.4.0) and its plugin, ClueGO (Bindea *et al.*, 2009), were used to group annotate ASAP1 interactomes based on the Gene Ontology (GO) and Kyoto Encyclopedia of Genes and Genomes (KEGG) databases. In the annotation module network, GO terms were represented as nodes that were linked based on a predefined kappa score level (>0.4).

2.30 Statistics

Data are presented as mean ± SEM unless otherwise stated and were analyzed with the Prism software (GraphPad) by two-tailed Student's t-test. A p-value below 0.05 was considered significant.

Chapter 3 Results

3.1 GWAS discovered *ASAP1* as a novel gene implicated in TB susceptibility

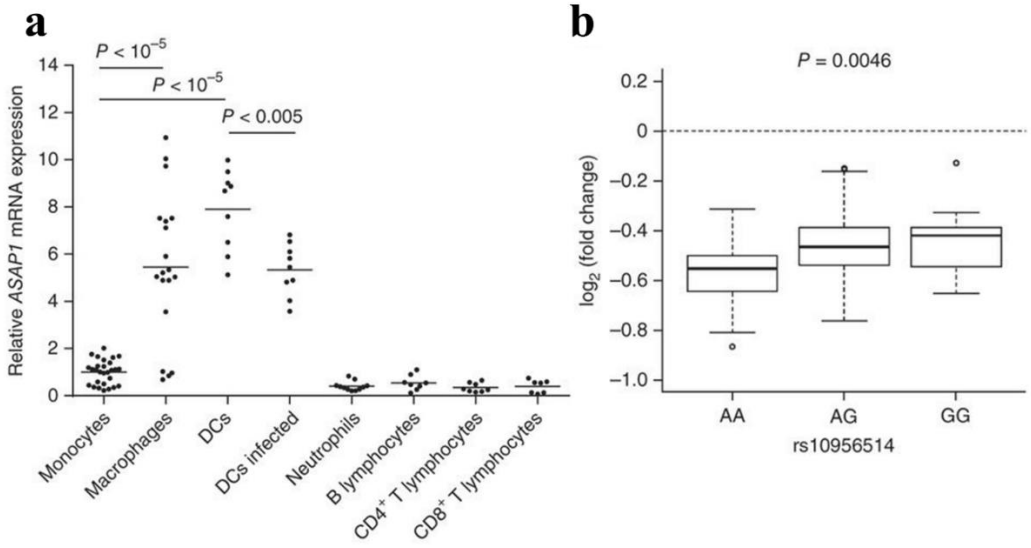

Figure 3.1-1: *ASAP1* expression level in peripheral blood leukocytes (lymphocytes and myeloid cells).

(**a**) The qRT-PCR graph shows relative *ASAP1* mRNA expression in leukocytes relative to expression in monocytes, each measured in triplicate. *P* values were calculated by two-tailed Student *t*-test.(**b**) Box-whisker plot shows a reduced level of *ASAP1* mRNA expression (log2 fold change, y-axis) in *M. tb* infected DCs from 65 individuals as a function of rs10956514 genotypes; AA (23), AG (30), and GG (12) (Curtis *et al.*, 2015). Box-whisker plot middle line presents median; whiskers indicate 1.5 interquartile range from the first and third quartiles. Data are obtained from a previous study (Barreiro *et al.*, 2012). Reported *P* values were determined by 2df test.

Functions of *ASAP1* in immune cells, in particular, DCs and macrophages have not been investigated previously. To study it, we initially extracted PBMC from 8 healthy donors

and then sequentially isolated different immune cells including monocytes, B cells, $CD4^+$ T cells, and $CD8^+$ T cells. Neutrophils were isolated from polymorphonuclear cell sediment and red blood cells (RBCs). We also derived macrophages and dendritic cells from these peripheral blood monocytes. In addition, we infected DC with BCG to study gene expression level in the infected cells. Thereafter, total RNA was extracted from these cells using a commercial kit.

Two steps quantitative reverse transcription polymerase chain reaction (qRT-PCR) was used to characterize levels of *ASAP1* mRNA expression in primary immune cells from healthy volunteers. In this experiment, I worked together with Dr. Changxin Wu in the lab. We found that B lymphocytes, T lymphocytes ($CD4^+$ and $CD8^+$), neutrophils, and monocytes exhibited relatively low levels of *ASAP1* mRNA expression. Nevertheless, monocyte-derived macrophages and monocyte-derived DCs expressed increased levels of *ASAP1* mRNA compared with that of monocytes (**Figure 3.1-1a**). Importantly, when DCs were infected with BCG, the infection led to the reduced expression levels of *ASAP1* compared to non-infected DCs, which is consistent with the previous observation in DCs infected with *M. tb* (**Figure 3.1-1b**).

Another potential approach used to identify functional mechanisms of GWAS signals was GWAS-eQTL link. It is well-recognized that GWAS signals for common diseases are enriched with eQTLs in a tissue-specific manner (Edwards *et al.*, 2013) or stimulus-dependent manner (Fairfax *et al.*, 2014), implicating the variant and the tissue in the disease mechanism. Therefore, we integrated our GWAS data with the previous eQTL data that was kindly provided by L. Barreiro (University of Montreal) (Barreiro *et al.*, 2012). Barreiro and his colleagues used microarrays to study genome-wide expression in monocyte-derived DCs

from 65 Caucasian volunteers. They infected cells with *M. tb* or left them non-infected for 18 hours. Illumina HT-12 expression array was used to study their gene expression (Barreiro *et al.*, 2012). We used Barreiro's raw data for our analysis. We investigated whether any of the newly identified TB-associated SNPs has effects on *ASAP1* expression in DC from the 65 individuals who were previously studied (Barreiro *et al.*, 2012). Consistent with our results (**Figure 3.1-1a**), DCs infected with *M. tb* expressed significantly lower *ASAP1* mRNA levels compared to non-infected DCs with $\log_2$ fold change = -0.49 and $P_{corrected}$ =2.9 x 10^{-18} (**Figure 3.1-1b**) (Barreiro *et al.*, 2012). We then quantified allele-specific expression for rs1096514 and rs473378 that had been already genotyped for the 65 subjects (Barreiro *et al.*, 2012). We found an association between SNP rs10956514 and *ASAP1* mRNA expression levels in non-infected DCs with P = 4.6 x 10^{-3}. In addition, it showed association with the extent of reduction of *ASAP1* expression in DCs upon infection with *M. tb* with P = 4.6 x 10^{-3} (**Figure 3.1-1b**). AA homozygotes, associated with a higher predisposition to TB in our GWAS, showed a more significant reduction of *ASAP1* expression level after *M. tb* infection compared to GG homozygotes, which showed association with lower TB risk. When we investigated other SNPs associated with TB, we found that these SNPs exhibited a weaker association with the *ASAP1* mRNA levels of expression in *M. tb* infected DCs than that observed with rs10956514 (**Figure 3.1-1b**).

The absence of significant association of rs4733781, which was the top signal in our GWAS study (Curtis *et al.*, 2015), with the level of *ASAP1* expression highlights the impact of differences in linkage disequilibrium (LD) between human populations. For example, in the Russian dataset, the r^2 between rs4733781 and rs10956514 was 0.8 while it was only 0.62 in the non-Russian Caucasian dataset of 65 subjects (Barreiro *et al.*, 2012; Curtis *et al.*,

2015). Overall, the GWAS-eQTL analysis indicated that either rs10956514 or other polymorphisms co-inherited with it might be responsible for regulating *ASAP1* mRNA expression level in *M. tb*-infected DCs. To conclude, given this evidence, rs10956514 is a strong candidate for a causative variant contributing to the predisposition to TB that functions as a genetic regulator for *ASAP1* expression in DCs.

3.1.1 ASAP1 is found in podosome structures in myeloid cells.

Given the increased *ASAP1* mRNA level of expression in macrophages and DCs (**Figure 3.1-1b**) and their essential roles in innate immunity, we decided to interrogate the role of ASAP1 proteins in primary DCs and macrophages (MDMs and macrophage-like THP-1 cells).

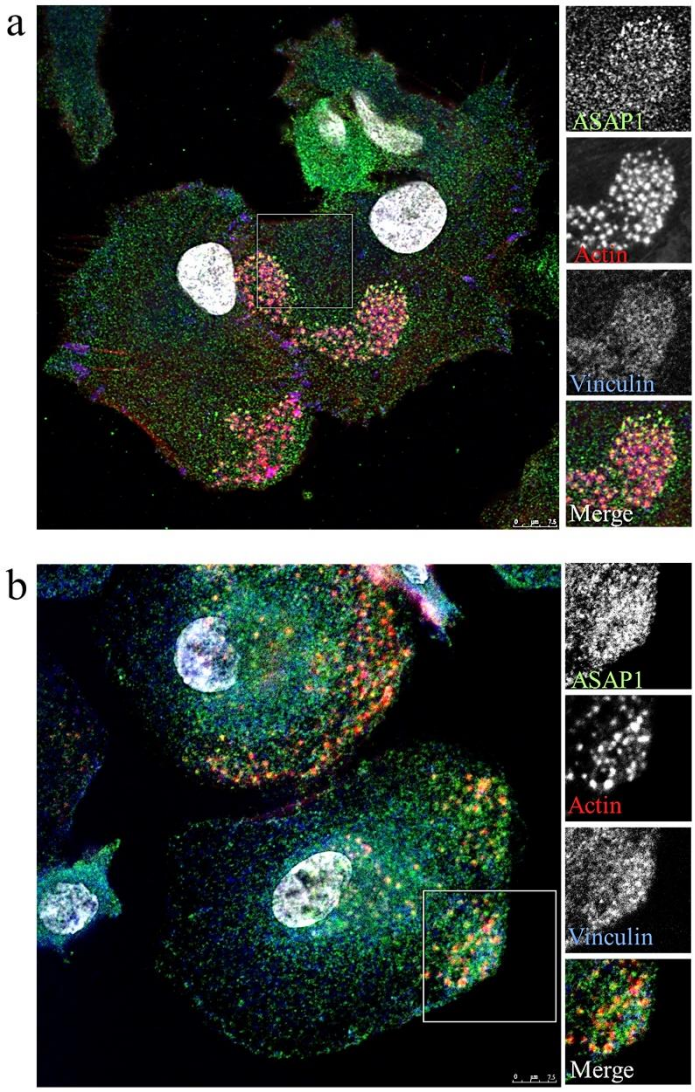

Figure 3.1-2:ASAP1 is associated with podosomes in dendritic cells and macrophages.

(a) CD14+ monocytes were differentiated to DCs with granulocyte-macrophage-colony-stimulating factor (GM-CSF) and interleukin (IL)-4 for 6 days and seeded on fibronectin for 4 hours. **(b)** CD14+ monocytes were differentiated to MDMs on coverslips with macrophage colony-stimulating factor (M-CSF) for 6 days. (**a** and **b**) Cells were labeled with ASAP1 (green), actin (Phalloidin-red) and vinculin (blue). Box indicates enlarged, greyscale pictures on the right. Scale bar represents 7.5µm.

Initially, we studied the cellular localization of ASAP1 in primary DCs and macrophages. In these experiments, I worked together with Dr. Delphine Cuchet-Lourenco in the lab. Isolated primary $CD14^+$ monocytes were differentiated *in vitro* for 6 days either with GM-CSF plus IL-4 towards DCs or with M-CSF towards macrophages. In both DCs (**Figure 3.1-2a**) and macrophages (**Figure 3.1-2b**), the confocal microscopy demonstrated that ASAP1 was exclusively localized in the cytoplasm. Moreover, in DCs and to a lesser extent in macrophages, ASAP1 colocalized partly with highly dynamic actin structures containing vinculin. These structures are known as podosomes in normal cells and invadopodia in cancer cell lines. (Schachtner *et al.*, 2013). Podosomes are known to be involved in the modulation of migration and other specialized functions such as transmigration through cell and matrix barriers (Schachtner *et al.*, 2013).

3.1.2 Validation of siRNA targeting *ASAP1*

To investigate whether the reduction of *ASAP1* expression in DCs or in macrophages has any impact on cell functions, we initially used RNAi technology to reduce the overall ASAP1 protein level in cellular models.

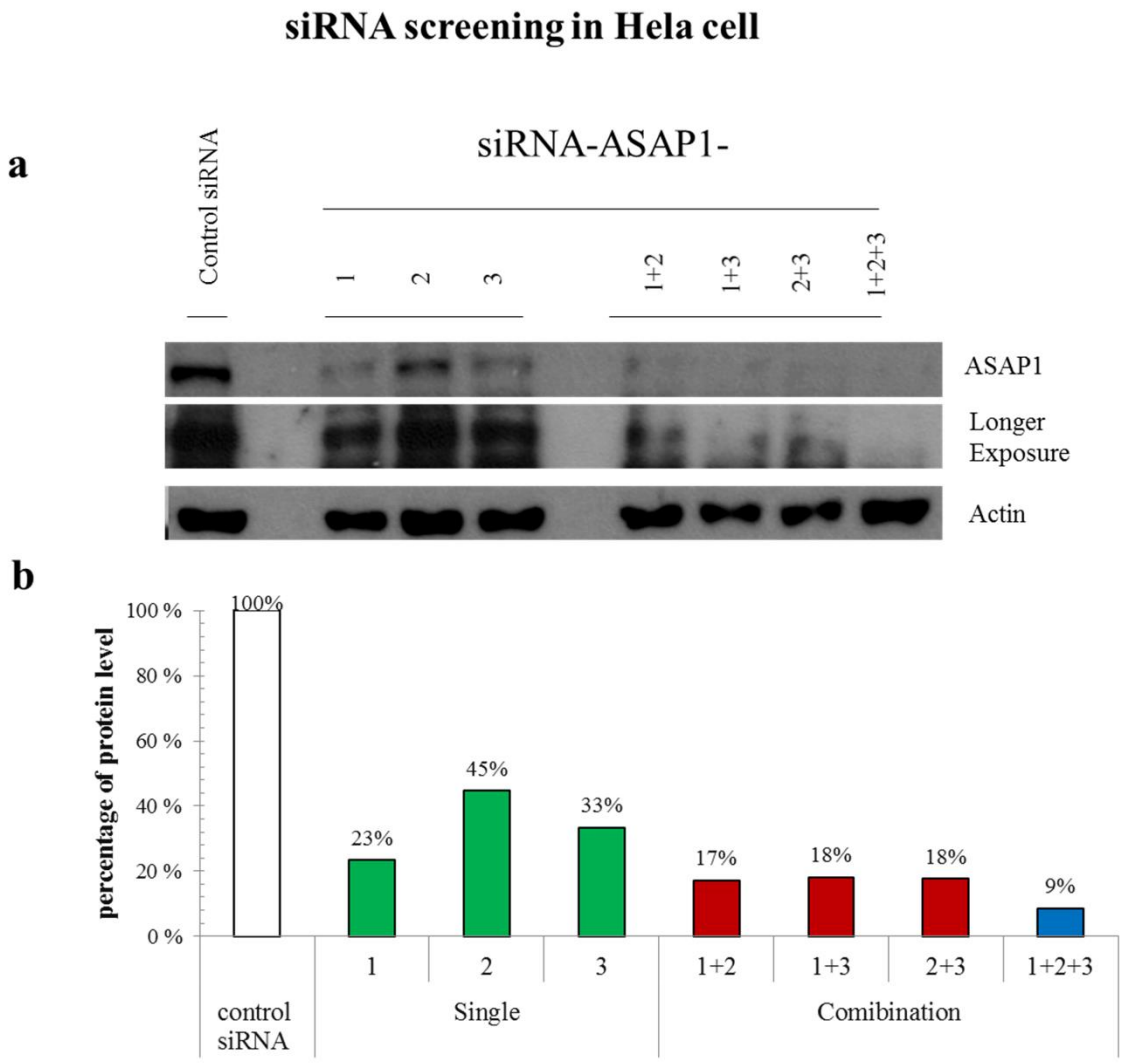

Figure 3.1-3: siRNA targeting ASAP1 screening in Hela cell line.

(a) Immunoblot for the screening of siRNAs targeting *ASAP1* that were transfected as singles or in a combination of 2 or pool of 3. siRNAs ASAP1-1 (HSS147202), ASAP1-2 (HSS147203), and ASAP1-3 (HSS181756) were tested. Control cells were transfected with a scrambled siRNA (si-Ctrl). Samples were collected 48 hours post-transfection and loaded on a 10% acrylamide gel. The membrane was incubated using anti-ASAP1 and anti-Actin antibodies. **(b)** Densitometry analysis of ASAP1 expression level in siRNA ASAP1 transfected samples in relation to the level in si-Ctrl transfected cells. The blot presented in (**a)** was used to do densitometry analysis of ASAP1 bands. Image J software was used, and the results are shown as a percentage of the quantity obtained relative to control siRNA.

Initially, I screened 3 commercially available small interfering RNAs (siRNAs) targeting *ASAP1* (siRNAs ASAP1-1, ASAP1-2, and ASAP1-3) to evaluate their efficiency in knockdown of the ASAP1 protein expression using the easy transfectable Hela cell line. Seeded Hela cells were transfected with si-Ctrl or with ASAP1 siRNAs as singles or in combinations of 2 or all 3 together as a pool. Forty-eight hours post-transfection, cells were lysed, and proteins were extracted. Expression levels of ASAP1 in each condition were studied by western blotting (**Figure 3.1-3a**). Densitometric analysis showed that the transfection of all 3 siRNAs together achieved the best depletion with approximately 90% reduction of the ASAP1 protein compared with cells transfected with the control siRNA (**Figure 3.1-3b**). Thereafter, the 3 siRNAs were used as a pool to suppress ASAP1 expression in different cell types.

3.1.3 Matrix degradation capacity of myeloid cells is affected by the ASAP1 reduction

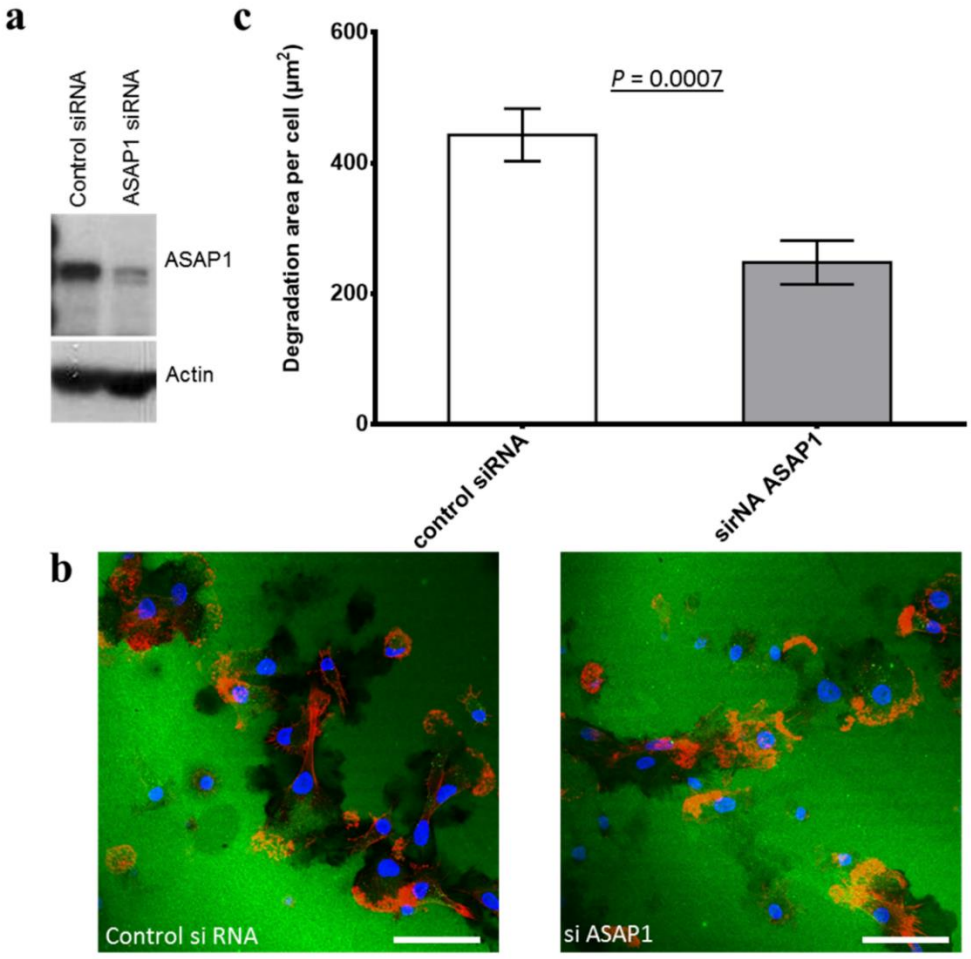

Figure 3.1-4: Degradation of gelatin matrix is affected by the ASAP1 knockdown in DCs.

CD14+ monocytes were treated with siRNA , differentiated with granulocyte-macrophage-colony-stimulating factor (GM-CSF) and interleukin (IL)-4 for 6 days, and then seeded on FITC-conjugated gelatin (green) for 4 hours. **(a)** Cell lysates were additionally collected for western blot and probed with anti-ASAP1 and anti-Actin. **(b)** The cells were labeled with actin (Phalloidin-red) and DAPI (blue). Scale bar represents 50µm. **(c)** Graph represents quantification of matrix area degraded per cell for three independent experiments (~400 cells). Data are averages, and error bars are mean ± s.e.m. T-test.

To evaluate the role of the reduced ASAP1 expression in matrix degradation by myeloid cells, we isolated monocytes from healthy donors and differentiated them to either DCs or macrophages. Monocytes underwent two rounds of transfection with three siRNAs on day 0 and another round on day 3 to efficiently decrease ASAP1 expression (**Figure 3.1-4a**). After the course of transfection and differentiation, DCs were plated on coverslips coated with FITC-coupled gelatin matrix for 4 hours and stained for nuclei and F-actin. Knockdown of ASAP1 (**Figure 3.1-4a**) in DCs led to a significant decrease in degradation of gelatin matrix (**Figure 3.1-4b**). Quantitative analysis of the degraded area of gelatin matrix indicated that the mean of degraded area per cell (248 μm^2) was significantly less than that of control cells (443 μm^2, $P = 0.0007$, **Figure 3.1-4c**). Similarly, ASAP1-depleted MDMs showed a significantly reduced ability to degrade matrix (mean of 577 μm^2 degraded area per cell, $P = 0.0004$) compared with control cells (1036 μm^2) (**Figure 3.1-5a-c**). Thus, both innate immune cells, DCs, and macrophages, demonstrated markedly impaired capacity to degrade gelatin matrix after ASAP1 depletion.

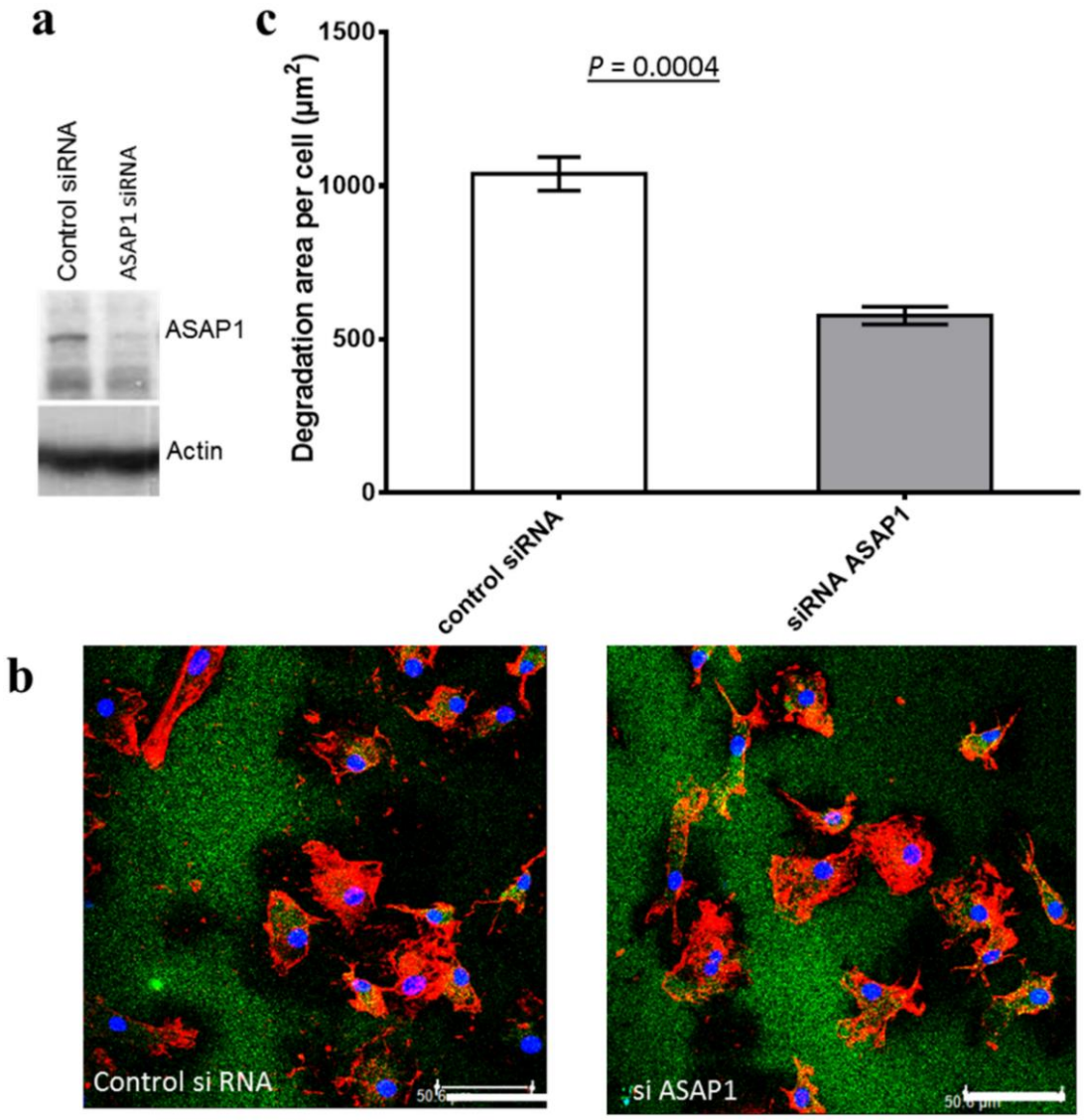

Figure 3.1-5: Efficient matrix degradation by Macrophages requires ASAP1.

CD14+ monocytes were treated with siRNA, differentiated with macrophage-colony-stimulating factor (M-CSF) for 7 days, and then seeded on FITC-conjugated gelatin (green) for 4 hours. (**a**) Cell lysates were additionally collected for western blot and probed with anti-ASAP1 and anti-Actin. (**b**) The cells were labeled with actin (Phalloidin-red) and DAPI (blue). Scale bar represents 50µm. (**c**) Matrix-remodeling podosome activity was determined by the area of gelatin degradation per cells (~900 cells). Data are averages, and error bars are mean ± s.e.m from three independent experiments.

3.1.4 Podosome turnover is altered by the reduction of ASAP1 in DCs.

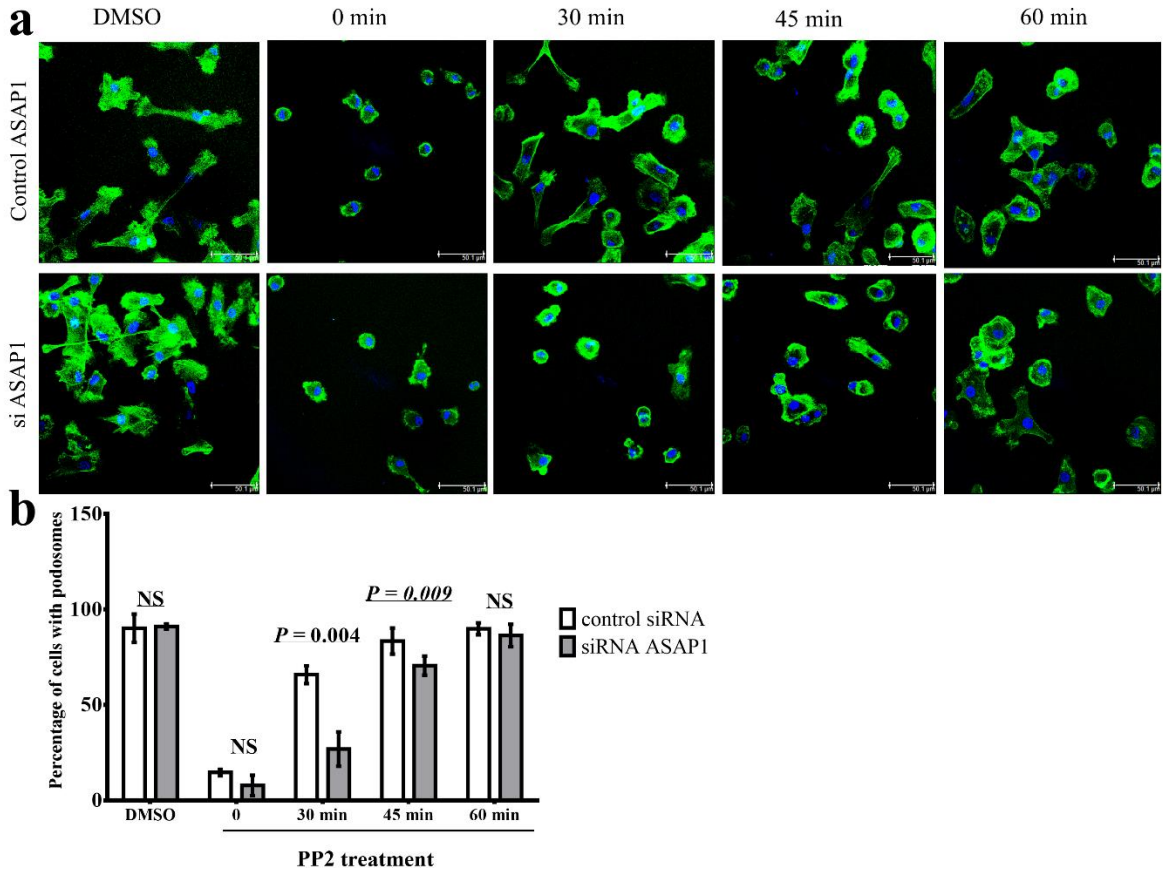

Figure 3.1-6: Podosome turnover is affected by the ASAP1 reduction.

(a) DCs were plated on fibronectin-coated coverslips and treated with DMSO as control and the PP2 tyrosine kinase inhibitor. Cells were fixed and stained for F-actin (green) and nuclei (blue). **(b)** Quantitative analysis shows an average number of cells containing podosomes in three independent experiments; at least 100 cells were counted per condition in each experiment. Error bars, ±SD. Significant *P* values were estimated by two-tailed t.test. Scale bars, 50 µm not significant (NS).

Since the localization of ASAP1 to podosome core was more pronounced in DCs (**Figure 3.1-2a**) compared with that in macrophages, we investigated podosome turnover in DCs. We isolated $CD14^+$ cells from PBMCs using positive selection with magnetic beads, transfected them with ASAP1 siRNAs or control siRNA, differentiated to DCs for 6 days and

plated on fibronectin-coated coverslips. The ASAP1 depleted DCs and control cells were starved of serum and then treated with DMSO as control or tyrosine kinase inhibitor (PP2) to disassemble podosomes. After 1 hour, treatment with PP2 resulted in a significant disappearance of podosomes. When treated with PP2, few cells formed podosomes (15 % of the cells in control DCs and 8% of the cells in ASAP1-depleted DCs formed podosomes) (**Figure 3.1-6a** and **b**). Thereafter, treated cells were allowed to recover in the PP2-free medium for 10, 30, 45 or 60 minutes to reform podosomes. Cells were fixed and stained for F-actin for labeling podosome core using phalloidin antibody and cytoplasm using HCS CellMask stain. For the clarity of the images, the HCS CellMask channel was deleted. Confocal microscopy and quantification analyses showed that among the ASAP1-depleted DCs, there were considerably fewer cells containing podosomes after 30 min compared to control cells (P = 0.004). The number of podosomes was still significantly reduced after 45 min (P = 0.009). Longer recovery led to the reappearance of podosomes in the ASAP1-depleted DCs and control cells, which was comparable to that observed in DMSO-treated cells (**Figure 3.1-6a** and **b**). Although the knockdown of ASAP1 expression affected podosome turnover, it did not cause disruption of the existing podosomes in DCs and/or in MDMs.

3.1.5 DCs migration is impaired by ASAP1 reduction.

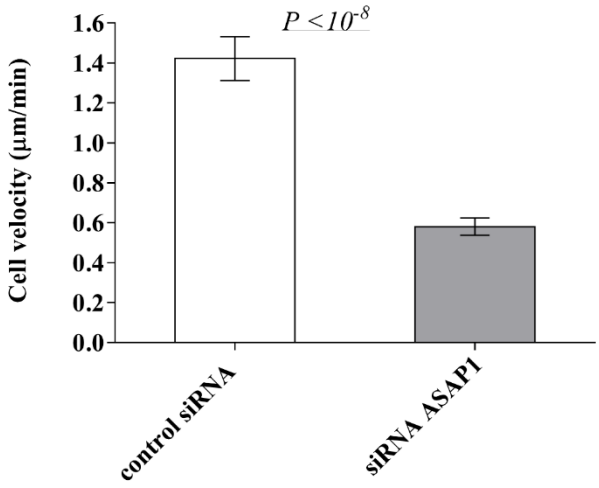

Figure 3.1-7: Migration velocity of DCs in the absence of ASAP1.

CD14+ monocytes were differentiated with GM-CSF and IL-4 for 6 days, treated with siRNA as indicated and seeded on fibronectin-coated coverslips for 4 hours. Coverslips were then inverted onto Dunn chambers containing 100U/ml GM-CSF and imaged every 4 mins for 2 hours. Cells were tracked using Manual tracking plugin of ImageJ and velocity was calculated. Graph represents three independent experiments with ~ 20 cells track/experiment. Error bars, mean ± s.e.m. Two-tailed Student's t-test was used, *P* value 2.8 x 10^{-10}.

We then examined whether ASAP1 plays a role in myeloid cell migration. Monocytes were transfected with the ASAP1 siRNA or scrambled siRNA and derived to DCs or MDMs. Cells were plated on fibronectin-treated coverslips and allowed to attach. Coverslips were inverted onto Dunn chambers containing medium supplemented with GM-CSF as chemoattractant. Cell motility was recorded using inverted microscopy up to 4 hours with an interval of 2 to 4 min. Results showed that MDMs did not show any sign of motility toward the chemoattractant (GM-CSF) even if MDMs were treated with control siRNA. On the other hand, DCs migrated to the chemoattractant. The mean velocity of DCs treated with the ASAP1 siRNA was significantly reduced (0.6 µm/min) compared to control cells (1.4 µm/min, $P < 10^{-8}$, **Figure 3.1-7**).

3.1.6 Study of the ASAP1 role in internalization of mycobacteria in human primary macrophages

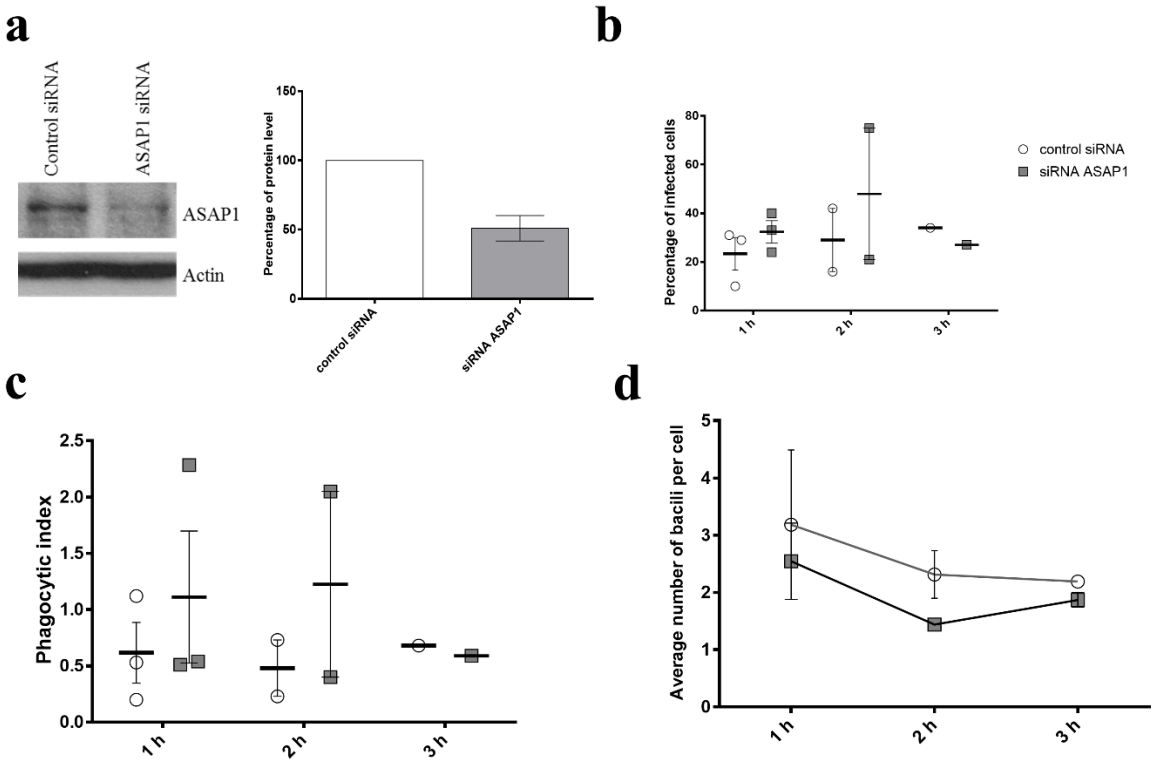

Figure 3.1-8: The effect of ASAP1 depletion on macrophage phagocytosis of BCG.

(**a**) (Left) Western blot of lysates probed with ASAP1 antibody and actin to assess the efficiency of knockdown. (Right) densitometry of semiquantitative analysis of control siRNA (white) and ASAP1-depleted MDMs (gray) showed the percentage of protein level for three independent experiments. Error bars, mean ± SD. imageJ software was used to quantify protein bands. (**b**) MDMs were treated with control siRNA or siRNA ASAP1 and infected with BCG at MOI of 10. Cells were stained with Zn stain, and the percentage of phagocytosis was calculated. (**c**) Phagocytic index was calculated by multiplying the percentage of infected cells and mean of the intracellular pathogen. (**d**) an average of bacilli per infected cell was shown in control cells (white) and in ASAP1-depleted cells (gray).

Then, I investigated whether the reduction of ASAP1 protein in macrophages affects phagocytosis of mycobacteria. Monocytes were extracted from healthy volunteer's blood or

leukocyte cones from NHS blood & transplant, derived to MDMs in the presence of M-CSF for 6 days, and then infected with BCG at MOI of 10. The efficiency of knockdown was assessed by western blotting and densitometry analysis. The knockdown efficiency varied, ranging from 39% to 58% in three independent experiments as shown (right panel, **Figure 3.1-8a**). Phagocytosis of the ASAP1-depleted MDMs or control MDMs was monitored for 1, 2, 3 hours. Cells were fixed and stained using Ziehl-Neelsen (Zn) staining. The percentage of infected cells (**Figure 3.1-8b)**, as well as the number of bacteria per cell (**Figure 3.1-8d**), were quantified using light microscopy. Then, the phagocytic index was calculated by multiplying the percentage of infected cells by the mean of intracellular bacilli (**Figure 3.1-8c**). As shown in (**Figure 3.1-8b-d**), internalization of BCG by MDM at 1 and 2 hours post-infection was slightly lower in the ASAP1-depleted MDMs compared to control MDMs but was not statistically significant. However, there was a considerable variation between experiments. Due to the limited cell number, phagocytosis at 3 hours post-infection was assessed in the ASAP1-depleted MDMs only once and showed no clear difference to the control cells. Thus, the results were not conclusive and did not unequivocally show the role of ASAP1 in phagocytosis of mycobacteria by macrophages. It is possible that differences between experiments, e.g., insufficient level of ASAP1 depletion, contributed to this variable results. Moreover, primary cells from different donors have inter-individual genetic and physiological differences, which may have influenced the outcome of experiments.

Therefore, a more stable cell model was needed for further experiments. As an alternative to MDMs, human myeloid cell line THP-1 can be studied. I used 50 ng/ml of PMA to differentiate THP-1 to macrophage-like cells. Then, I tried to deplete ASAP1 by using siRNA transfection. However, this method was inefficient to knock down ASAP1 in

this cell model (data not shown). Therefore, I decided to apply CRISPR-Cas9 technology to generate stable ASAP1-knockout THP-1 cell lines that would facilitate the analysis of phagocytosis and other experiments.

3.1.7 Using CRISPR-Cas9 to knock out ASAP1 in THP-1 cells

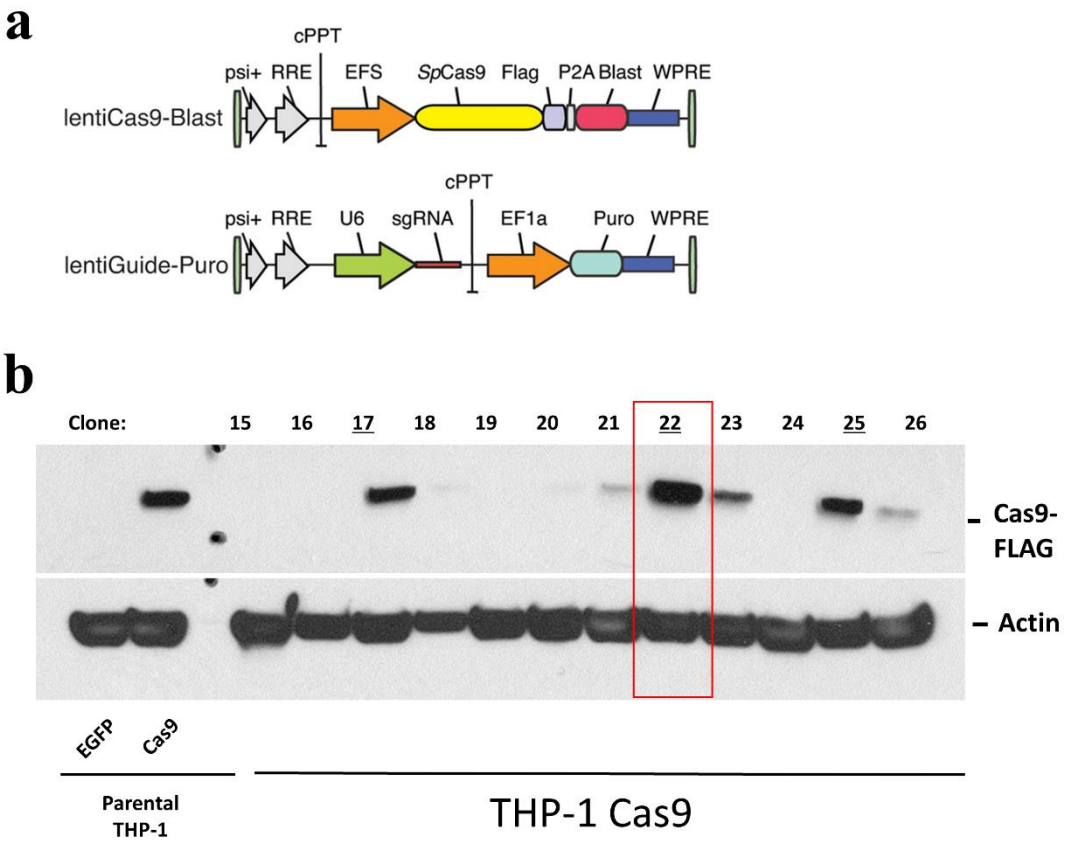

Figure 3.1-9: Generating stably Cas9-expressing cell lines.

(**a**) Schematic diagram for CRISPR lentiviral vectors. LentiCas9-Blast vector expresses *S. pyogenes* Cas9 (SpCas9). LentiGuide-Puro expresses U6-driven sgRNA under the control of U6 promoter. psi+, Psi packaging signal; RRE, Rev response element; cPPT, central polypurine tract; EFS, elongation factor 1α short promoter; WPRE, post-transcriptional regulatory element; Flag, Flag octapeptide tag; Puro, puromycin selection marker; P2A, 2A self-cleaving peptide; Blast, blasticidin selection marker; EF1a, elongation factor 1a promoter adopted from (Sanjana, Shalem and Zhang, 2014). (**b**) Immunoblotting for screening for THP-1 stably expressing Cas9 protein. Clones indicated by numbers on the top of the blot. Anti-Flag antibody used to detect clones that express Cas9 protein. Actin is used as input. THP-1 expressing EGFP with no expression of Cas9 was used as negative control. Parental THP-1-Cas9 (bulk culture) was used as positive control.

At first, I used reagents commercially designed and validated by the company Horizon. THP-1 cells were electroporated with the GFP-Cas9-expressing plasmid harboring sgRNA targeting *ASAP1*. Two days post-transfection, cells were stained for viability with Propidium iodide (PI). Fluorescence-activated cell sorting (FACS) was used to sort GFP positive and PI negative cells as singles into 96-well plates. Cells were expanded for few weeks. Unfortunately, few cells were able to grow after cell sorting. This can be explained in part by the toxicity of nucleofection and using a large plasmid expressing both Cas9 and GFP.

To overcome the limitation in the previous attempt in generating knockout cell lines, I used the CRISPR-Cas9 system introduced by Zhang's lab at the Broad Institute. The system was designed as two separate lentiviral vectors to increase the viral titer and the transduction efficiency (**Figure 3.1-9a**) (Sanjana, Shalem and Zhang, 2014). In this project, I worked with Dr. Davide Eletto, a postdoc in our lab. First, I generated several cell lines that stably express Cas9, including THP-1, U937, Hela, and A549. For illustration, THP-1 cells were transduced with the lentiCas9-Blast vector (**Figure 3.1-9a**) for 48 hours. The transduced cells were subjected to blasticidin selection for 5-7 days. After antibiotic selection, THP-1 cells were diluted to a density of 5 cells/ml, and 100 µl was dispensed into 96-well plates to obtain a single cell per well. Single cells were expanded for 3-4 weeks in a medium supplemented with antioxidants at a final concentration of 1 mM sodium pyruvate, 50 µM α-thioglycerol (α-TG), and 20 nM bathocuproindisulfonic acid disodium salt (BCS). The mixture of the protective antioxidants helped cells that are sensitive to growth at low cell density, such as THP-1, to tolerate the induction of apoptosis under low cell density (Brielmeier *et al.*, 1998). Cell clones were then screened for the Cas9 protein expression by western blotting. The

expressed Cas9 was tagged with Flag, so I used anti-Flag antibodies (**Figure 3.1-9b**). An isolated clone stably expressing Cas9 was amplified and used to generate knockout cell lines.

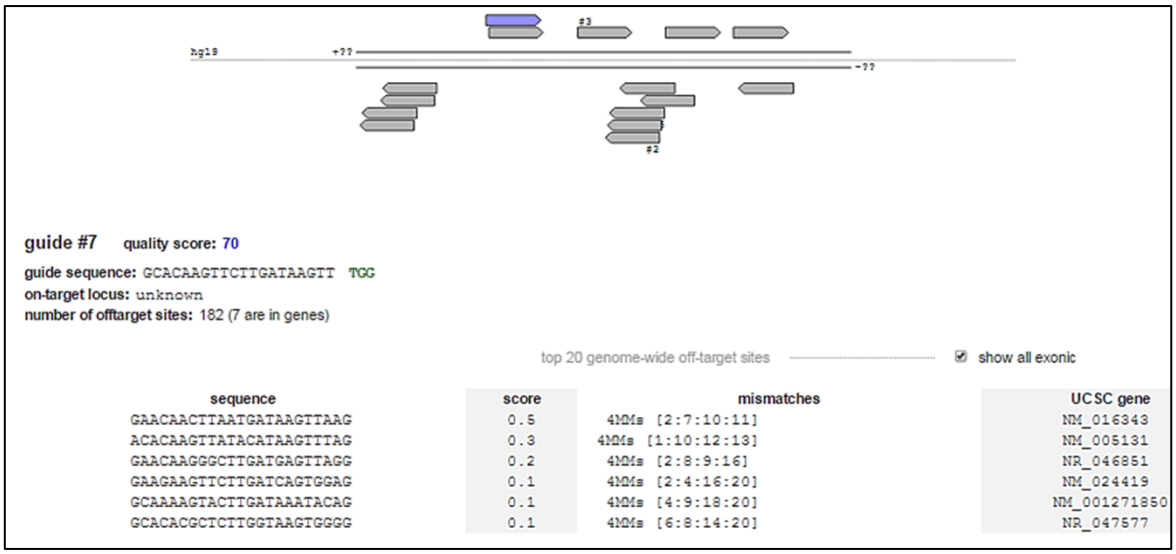

Figure 3.1-10: Zhang's online tool to design sgRNA targeting ASAP1 exon 5.

Figure shows that the guide#7 has an on-target score of 70. The number of off-target sites are 182, including only 7 that are located in exons. It also shows where mismatches are located.

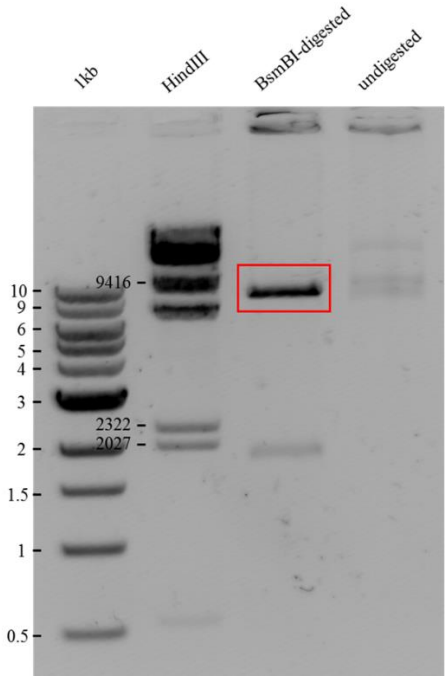

Figure 3.1-11: Agarose gel electrophoresis of BsmBI digested LentiGuide-Puro vector.

Gel shows the product of the linearized vector around 8 kb (red box). Lane1: 1kb ladder marker; lane2 HindIII ladder marker; lane3: digested plasmid; lane4; uncut vector.

Having clonal Cas9-expressing cell lines facilitates the screening of the newly designed sgRNAs. To disrupt protein expression, it is preferable to choose first few exons in the coding sequence to be targeted by CRISPR-Cas9 because this should lead to an early termination of the translation (Wang, La Russa and Qi, 2016). Target sequences were used as inputs for the online tools to design sgRNAs targeting *ASAP1* (**Figure 3.1-10**). Two sgRNAs targeting *ASAP1* exon 5 (ENST00000518721.5), a common exon in most of the ASAP1 transcripts, were chosen from lists of candidates (**Table 2.16-1**). These two sgRNAs have acceptable on-target activity score (> 50) and few off-targets sequences. Oligos containing guide sequences were cloned into the BsmBI-linearized lentiGuide-Puro vector (**Figure**

3.1-11), containing the programmable chimeric sgRNA. Prior to generating THP-1 cell knockout, I validated selected sgRNAs for their efficiency in the Hela cells that also stably expressing Cas9. Hela cells were transduced with the lentiGuide-Puro vectors encoding ASAP1 sgRNAs. Two days post-transduction, puromycin selection was applied to enrich for the edited cells. The pool of genomic DNA was extracted from the bulk culture. Genomic DNA was amplified using primers spanning the genomic region containing the target site, *ASAP1* exon 5. The PCR products were denatured and reannealed in a thermal cycler to create heteroduplex pairs. These products were incubated with the T7E1 nuclease, which recognizes and cleaves mismatched heteroduplexes. The T7E1 enzyme was able to cleave PCR products, resulting in shorter bands on an agarose gel as shown in (right panel, **Figure 3.1-12**).

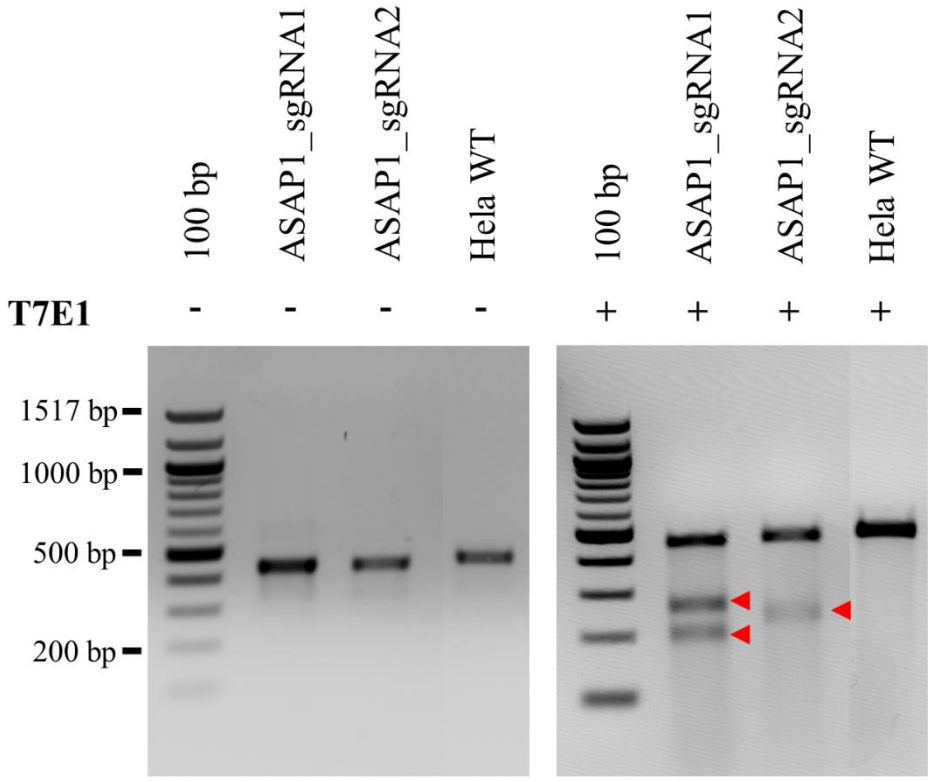

Figure 3.1-12: T7E1 assay validates the efficiency of sgRNAs targeting ASAP1.

PCR products flanking exon 5 of *ASAP1* were amplified from DNA extracted from a pool of CRISPR-Cas9 edited cells transduced with lentiGuide-Puro vectors encoding ASAP1 sgRNAs. Heteroduplex products were subjected to T7E1 nuclease to cleave mismatch products with mutations. The cleaved PCR products were visualized using 2% of agarose gel before T7E1 treatment (left) or after T7E1 treatment (right). Cleaved bands were not observed in PCR amplicons that were not incubated with the T7E1 enzyme or unedited Hela cell line. Cleaved bands displayed after the T7E1 treatment in transduced cells are indicated by red arrows.

The functional sgRNAs targeting exon 5 of *ASAP1* as suggested by the T7E1 assay were used to generate clonal ASAP1-knockout THP-1 cell lines. Cas9-expressing THP-1cells were transduced with the lentiGuide-Puro vectors encoding *ASAP1* sgRNA1 or sgRNA2. Two days post-transduction, cells were exposed to puromycin selection for 5 days. Individual cells were obtained by limiting dilution and plated in 96-well plates in medium supplemented

with antioxidants and expanded for 3-5 weeks. Single-cell clones were screened for the mutations in the ASAP1 gene using T7E1assay as shown in (**Figure 3.1-13a**). Clones showed cleaved bands after incubation with the T7E1 enzyme or different migration speed on an agarose gel (labeled with red) were selected for further confirmatory analyses. For example, clone #10 showed a substantial shift in the migration of the PCR product compared to other clones on the agarose gel, indicating the presence of a large insertion. All potential THP-1 ASAP1 knockout (ASAP1-KO) clones were probed for ASAP1 protein expression by western blotting. Two clones were selected, clone A (ASAP1 sgRNA 1) and clone B (ASAP1 sgRNA 2). Both clones showed complete absence of the ASAP1 protein expression compared with the unedited control when probed with a polyclonal antibody against ASAP1 (**Figure 3.1-13c**). Both clones were sequenced using Sanger sequencing. Clone A showed a homozygous insertion of ~ 250 nucleotides (**Figure 3.1-13b** and **S 1**) while clone B displays complex biallelic loss-of-function mutations.

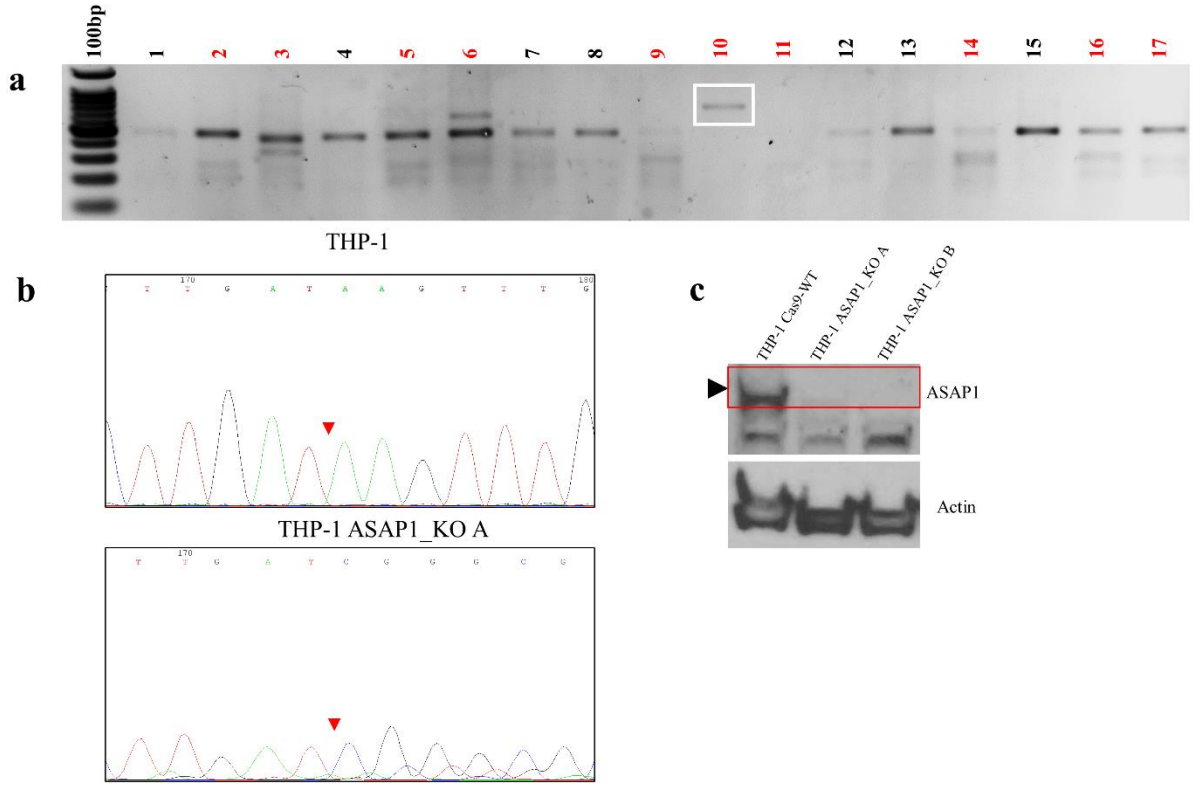

Figure 3.1-13: Generation and validation of THP-1 ASAP1 knockout (KO) cell lines.

(**a**) The T7E1 assay shows PCR amplicons from individual clones as indicated by numbers on the top. Single-cell clones that produced PCR product sensitive to the T7E1 enzyme are indicated by (red), and those where T7E1-treated PCR product did not differ from the expected size are labeled with (black). The single-cell clone (10, clone A) in white rectangle migrated slower than other clones, indicating a large insertion. (**b**) Sanger sequencing of clone A showed an insertion around 250 nucleotides. Arrows showed the site of insertion (**c**) THP-1 lysates of the THP-1 Cas9 WT cells and the ASAP1-KO single-cell clones (sgRNA1, clone A and sgRNA2, clone B), probed with ASAP1 antibody and Actin antibody as a loading control.

3.1.8 ASAP1-KO THP-1 cells show impaired macrophage migration

I studied the role of ASAP1 in macrophage migration using as a model, the THP-1 macrophage-like cell line, in which ASAP1 was knocked out. I used the transwell migration assay. Boyden introduced the transwell assay to study the chemotactic responses of

leukocytes (Boyden, 1962). This experiment uses two medium-containing chambers separated by a porous membrane through which cells migrate. Membranes are available with different pore diameters ranging from 3 to 12 μm. The membrane pore size is decided by the size of the cells to be assayed. Technically, cells are plated in tissue culture medium in the upper compartment (insert) and allowed to migrate in vertical direction through the permeable membrane toward the medium supplemented with a chemoattractant in the lower chamber (**Figure 3.1-14a**).

First, it is essential that the optimal chemoattractant concentration is used. Macrophages and monocytes are known to migrate towards chemokine MCP-1. To determine the MCP-1 concentration that induces macrophages migration, I differentiated THP-1 cells to macrophage-like phenotype using PMA for three days followed by resting in medium without PMA for 24 hours. Cells were then detached using accutase and counted using trypan blue. The top of each insert (pore 8 μm) was seeded with a total of 1 x 10^5 differentiated cells, while the lower compartment was filled with 500 μl of culture medium with increasing concentrations of MCP-1 (100 – 600 ng/ml). Cells were incubated at 37 ºC under 5% CO_2 and allowed to migrate for 24 hours. Inserts were washed, and cells in the topside of the inserts were removed using cotton swabs. Filters were fixed and stained. All images were acquired using inverted microscopy. The average of cell number per field of those cells migrated and attached to the underside of the filters were quantified using ImageJ software. As expected, this assay depends on gradient concentration. When the MCP-1 concentration was low or very high, few cells migrated because, in the latter case, MCP-1 concentrations in two chambers reached equilibrium. Cell migration peaked after 24 hours with MCP-1

concentrations of 200 and 300ng/ml (**Figure 3.1-14b**). As a result, 200 ng/ml of MCP-1 was chosen as an ideal concentration for the induction of macrophage migration.

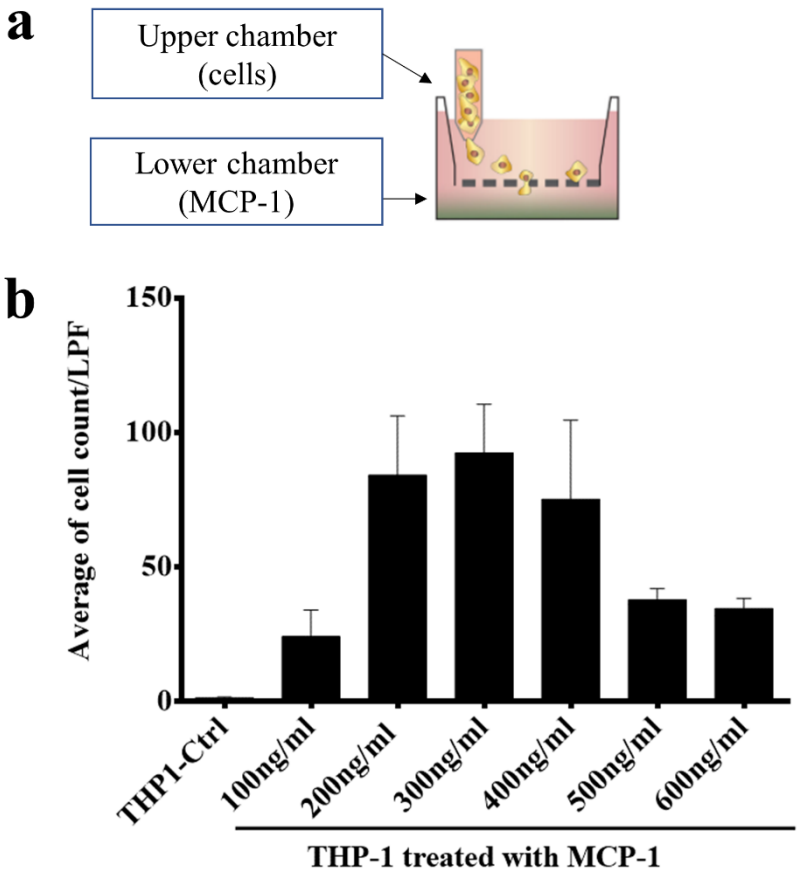

Figure 3.1-14: Optimal concentration of MCP-1 to induce macrophage migration.

(a) A diagram of the transwell apparatus used to measure cell migration. Differentiated THP-1 cells were added to the upper chamber of a Transwell and allowed to migrate for 24 hours towards 100, 200, 300, 400, 500, and 600 ng/ml MCP-1 in the lower chamber adapted from (Katt *et al.*, 2016). **(b)** Data are displayed as an average number of cells per field that migrated to the underside of the insert filter. Data show the mean of cell number per field in 5 fields. Error bar, mean ± s.e.m.

Then, the parental wild-type THP-1 cells or THP-1 ASAP1-KO clone A were differentiated to macrophages by PMA. Cells were placed in the upper compartment of a 24-

transwell apparatus and allowed to migrate towards the lower chamber containing the chemokine MCP-1 at a concentration of 200 ng/ml. Cells were fixed and stained. The number of migratory cells in the lower chamber was counted by microscopy, and the results were expressed as an average cell number per low power field (LPF). Upon stimulation of the cells by MCP-1, the average number of migratory cells per field were significantly smaller among THP-1 lacking ASAP1 than those among the wild-type THP-1 (P = 0.004, **Figure 3.1-15a** and **b**). Results indicated that ASAP1 knockout resulted in a considerable decrease in the migration of THP-1 cells towards the chemokine MCP-1.

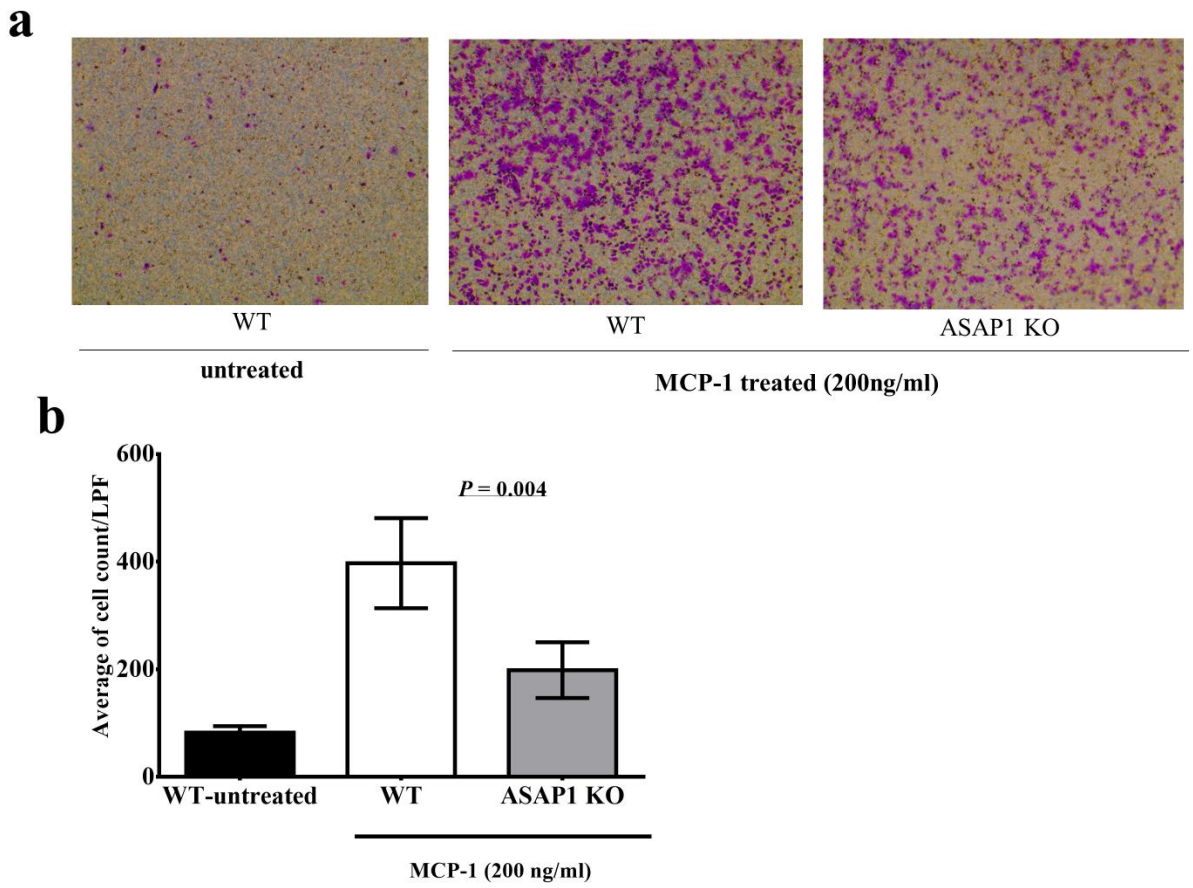

Figure 3.1-15: Transwell migration assay of the ASAP1-knockout THP-1 cells (clone A).

(a) Representative images of the THP-1 cell transwell migration. The lower chamber of transwell apparatus was filled with tissue culture medium as a negative control for WT THP-1 or tissue culture medium supplemented with the chemokines MCP-1, respectively. Migratory cells in the underside of the porous membrane were stained with crystal violet, pictures of the migrated cells (purple stained) were taken using a microscope with a 20x objective. **(b)** Quantification of cells migrating towards lower chamber was quantified using ImageJ software and expressed as the average of cell number per LPF from three independent experiments (average of 3-5 field per experiment). Error bar, mean ± s.e.m. Two-tailed Student's t-test was used.

Although the transwell migration assay indicated that the ASAP1-knockout cells exhibited impairment in migration compared to the wild-type THP-1 cells, the data should be interpreted with caution. The transwell assay is most commonly used to examine cell

migration due to its relative simplicity. However, there are some drawbacks. The optimal time point of the assay has to be determined for each cell type. The short-lasting chemokine gradient between the two compartments may reach equilibrium before the assay comes to a halt. Moreover, the cells on the topside of the membrane are removed by cotton swabs before staining, which frequently appears to be difficult, leading to variable success (Kramer *et al.*, 2013).

Therefore, I decided to confirm impaired migration of the ASAP1-knockout cells using a different assay. I studied chemotaxis of these cells in the Dunn chamber, measuring cell velocity. Initially, I ran a pilot experiment to ensure that THP-1 cell migration is induced by MCP-1 in the Dunn chamber assay. A total of 2 x 10^5 wild-type PMA-differentiated THP-1 cells were placed on fibronectin-treated coverslips and allowed to attach overnight. Coverslips were inverted onto Dunn chambers containing medium as a negative control (untreated) or medium plus 200 ng/ml of MCP-1 as a chemoattractant. Cell motility was recorded at 4 min intervals for up to 5 hours using inverted microscopy. The recorded videos then were analyzed by Manual tracking plugin of ImageJ software (Schindelin et al. 2012), and velocity was calculated. Analysis of tracks acquired by time-lapse imaging of multiple cells indicated that 200 ng/ml of MCP-1 induced migration (P = 0.0075, **Figure 3.1-16a**).

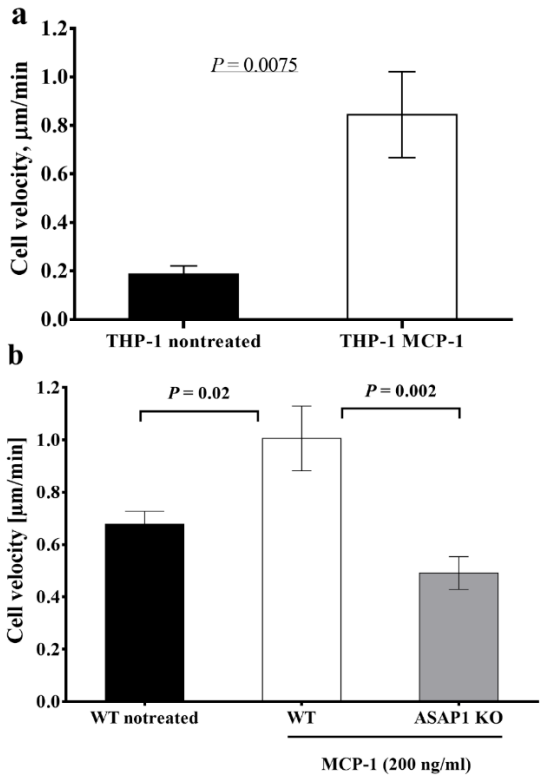

Figure 3.1-16: Velocity of the THP-1 macrophages migrating towards MCP-1.

(a) Differentiated THP-1 cells were seeded on the fibronectin-coated coverslips for 24 hours. Coverslips were then inverted onto Dunn chambers containing 200 ng/ml and imaged every 4 min for up to 5 hours. Cells were tracked using Manual tracking plugin of ImageJ and velocity was calculated. The graph represents one experiment with 10 cells tracked. Error bars, mean ± s.e.m. Two-tailed Student's t-test was used. **(b)** Differentiated WT THP-1 cells and ASAP1-KO THP-1 cells were studied as in (a). The graph represents one experiment with ~ 20 cells tracked. Error bars, mean ± s.e.m. Two-tailed Student's t-test was used.

To confirm the impact of the ASAP1 knockout on macrophage migration, I studied the wild-type and the ASAP1-KO THP-1 cells using the Dunn chamber assay. All cells were differentiated, plated on fibronectin-coated glass coverslips, and incubated overnight. Cells were inverted onto Dunn chambers containing either complete growth medium for control or medium containing MCP-1 to induce migration. Time-lapse live cell imaging was employed using confocal microscopy over 5 hours. Images were acquired at 4 min interval with a 10x

objective. A total of 20 cells were tracked using Manual tracking plugin of ImageJ software. Upon stimulation of MCP-1, the mean velocity of the ASAP1-KO THP-1 cell migration on fibronectin-coated glass appeared to be lower than that of the wild-type THP-1 cells, 0.49 ± 0.27 μm/min (±s.e.m) versus 1.005 ± 0.55 μm/min , respectively (**Figure 3.1-16b**). Thus, migration of THP-1 cells and its velocity were significantly impaired when cells lacked ASAP1.

3.1.9 ASAP1 is involved in matrix degradation by macrophages

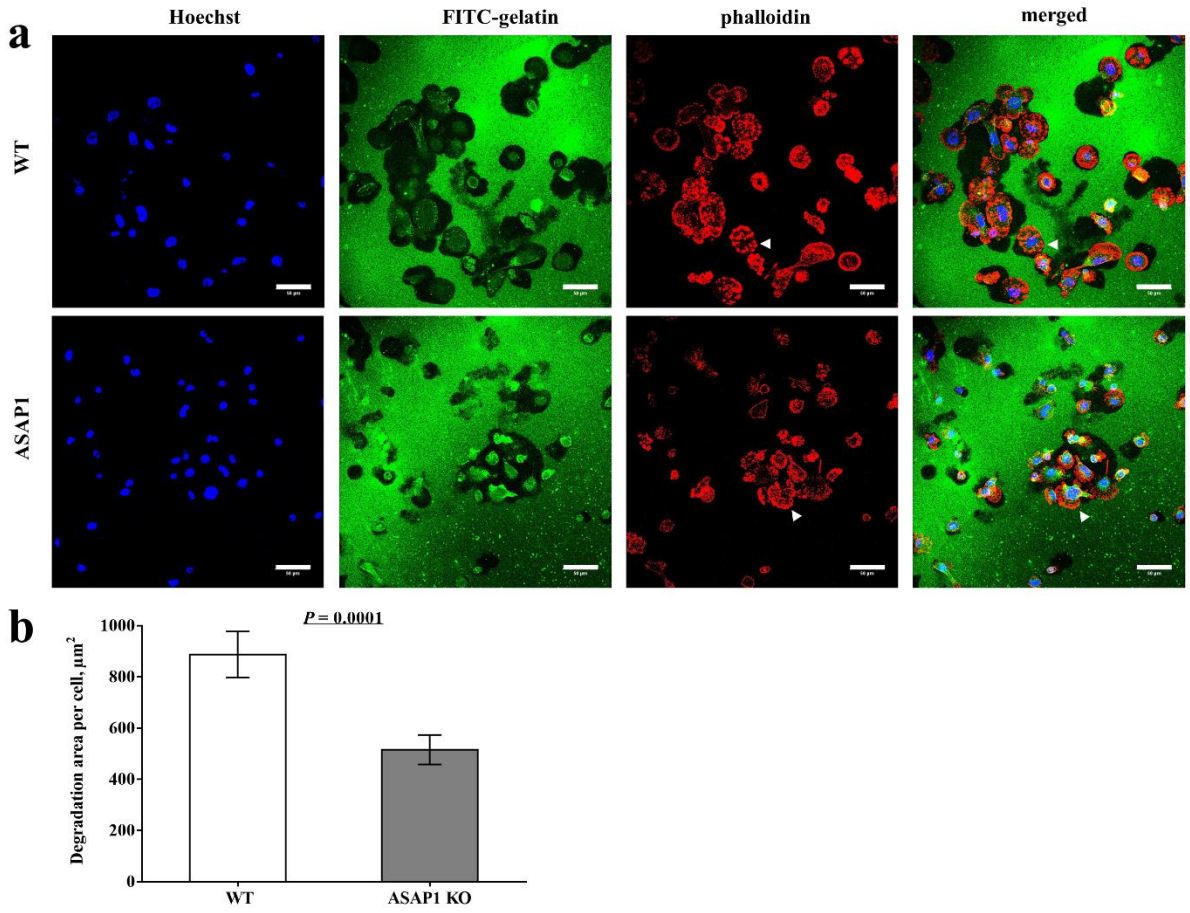

Figure 3.1-17: Matrix degradation by the ASAP1-KO THP-1 cells is impaired.

Confocal immunofluorescence microscopy analysis of the gelatin matrix degradation by the WT THP-1 cells and the ASAP1-KO THP-1 cells. Cells were differentiated with PMA for 3 days and plated on the FITC-conjugated gelatin (green) for 24 hours (5 x 10^5). (**a**) The cells were stained using Phalloidin for actin (red) and Hoechst for the nucleus (blue). Dark regions in the fluorescent gelatin layer (green) indicate matrix degradation; white arrowheads indicate invadosomes. The pictures were obtained with a confocal laser scanning microscope and are representative of three independent experiments. Scale bar, 50µm. (**b**) Graph represents quantification of matrix area degraded per cell (~450 cells were analyzed per condition). Data indicate means ± s.e.m from three independent experiments. Two-tailed Student's t-test was used.

Invadosome is a collective term that describes podosomes and invadopodia. The maturation process of these structures involves secretion of pericellular specialized proteases that mediate extracellular matrix degradation (Murphy and Courtneidge, 2011). We previously found that the ASAP1-depleted monocyte-derived dendritic cells and macrophages exhibited a noticeable defect in the degradation of extracellular matrix (Chapter 3.1.3). To test a possible role for ASAP1 to affect matrix degradation capacity in THP-1 macrophages, I performed the gelatin matrix degradation assay using ASAP1-KO THP-1 cells. Wild-type and ASAP1-KO THP-1 were differentiated with PMA for 72 hours followed by removing PMA and replenishing with fresh medium for 24 hours. Differentiated cells were detached using accutase, quantified, and plated on the fluorescent-gelatin-coated glass coverslips for 24 hours (total of 5 x 10^4 per genotype). Glass coverslips were fixed and stained for F-actin, an obligate component of invadosome (Murphy and Courtneidge, 2011), using phalloidin and for nuclei using the Hoechst dye. Gelatin matrix was visualized and photographed using a confocal microscope with an oil immersion 40x objective. The ASAP1-KO THP-1 cells showed diminished matrix degradation, compared to the parental THP-1 cells (**Figure 3.1-17a**). Quantitative analysis demonstrated that the mean of degraded area per cell in the ASA1-KO THP-1 was considerably decreased (516.1 ± 206.3 μm^2) compared to control THP-1 cell (887.7 ± 297.1 μm^2 (±s.e.m), *P* value = 0.0001, **Figure 3.1-17b**). Consistent with our previous data in primary cells, the ASAP1-KO THP-1 cells showed little or no difference in the formation of invadopodia (indicated by arrowheads) or F-actin content as compared with the wild-type THP-1 cells (**Figure 3.1-17a**). Therefore, the function of ASAP1 is dispensable for the formation of invadosomes. However, these findings confirmed

an important role of ASAP1 in their function, which resulted in impaired matrix degradation in the absence of ASAP1.

3.1.10 Intracellular bacterial growth in the ASAP1-KO THP-1 macrophages

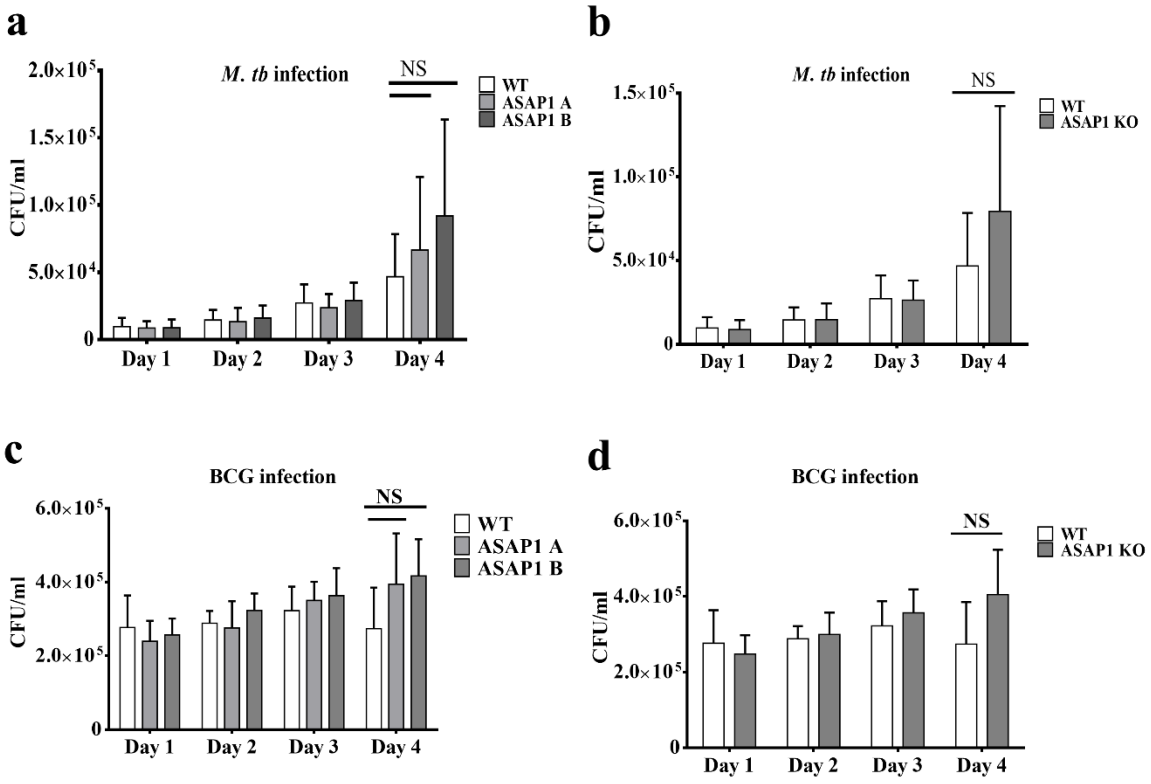

Figure 3.1-18: Intracellular mycobacterial growth in THP-1 macrophages lacking ASAP1.

PMA differentiated wild-type THP-1 (white) and two THP-1 ASAP1-KO clones (clone A, gray and clone B, dark gray) were infected with *M. tb* or BCG at MOI of ~2 and monitored for 96 h. (**a**) Results of the CFU assay in the ASAP1-KO clones A and B and the WT THP-1 cells at days 1, 2, 3, and 4 post-infection with M. tb (H37Rv). (**b**) Results of the CFU assay shown in (a) but with the ASAP1-KO clones A and B combined. (**c**) Results of the CFU assay in the ASAP1-KO clones A and B and the WT THP-1 cells at days 1, 2, 3, and 4 post-infection with BCG. (**d**) Results of the CFU assay shown in (c) but with the ASAP1-KO clones A and B combined. Data indicate means ± SD from three independent experiments. Two-tailed Student's t-test was performed; NS - not significant.

It is well established that ASAP1 is involved in membrane trafficking and actin remodeling, which may affect phagosome structure and trafficking. Does this ASAP1

function affect the intracellular expansion of mycobacteria? To evaluate the role of ASAP1 in controlling mycobacterial growth, I used a colony-forming unit (CFU) assay to quantify live intracellular bacteria. The wild-type and the ASA1-KO THP-1 cells lines (including clones A and B) were differentiated with PMA for 72 hours and seeded in duplicate in 96-well plates at a density of 5 x 10^4 per well. The tissue culture medium was discarded and replenished with antibiotic-free medium without PMA for 24 hours. Cell monolayers were then infected with virulent *M. tb* (H37Rv) or BCG at MOI of 2 and monitored for 96 hours. Infected cells were lysed daily to measure viable intracellular bacteria. Duplicates of cell lysates were combined and serially diluted in 7H9 medium. Each dilution was plated on square plates in duplicates and incubated at 37 ºC for 2-3 weeks when colonies were counted. I found that *M. tb* (**Figure 3.1-18a**) and BCG (**Figure 3.1-18b**) could grow intracellularly within THP-1 cells lacking ASAP1 similarly to the wild-type THP-1 cells. To increase the statistical power, CFU results obtained from individual ASAP1-KO clones were combined and analyzed together. Combined CFU results also showed that there was no difference in bacterial burden between the wild-type cells and ASAP1-KO THP-1 cells at least up to 4 days post infection with *M. tb* (**Figure 3.1-18c**) and BCG (**Figure 3.1-18d**). A slight increase in bacterial load at day 4 after infection with *M. tb* or BCG was found, although it was not significant. Nevertheless, I decided to study mycobacterial infection at later time points. I evaluated intracellular bacterial growth for 10 days at an interval of 2 days using the same approach. The data demonstrated considerable variation and inconsistent results between clones lacking ASAP1 after 4 days of infection (**S 2a-c**). The variation was also observed between wild-type duplicates**.** However, combined statistical analysis for both clones showed no significant difference between the wild-type and the ASAP1-KO THP-1 cells. Thus, these experiments

demonstrated that ASAP1 does not affect the intracellular growth of *M. tb* and BCG in macrophages.

3.1.11 ASAP1 has no effect on the viability of cells infected with mycobacteria

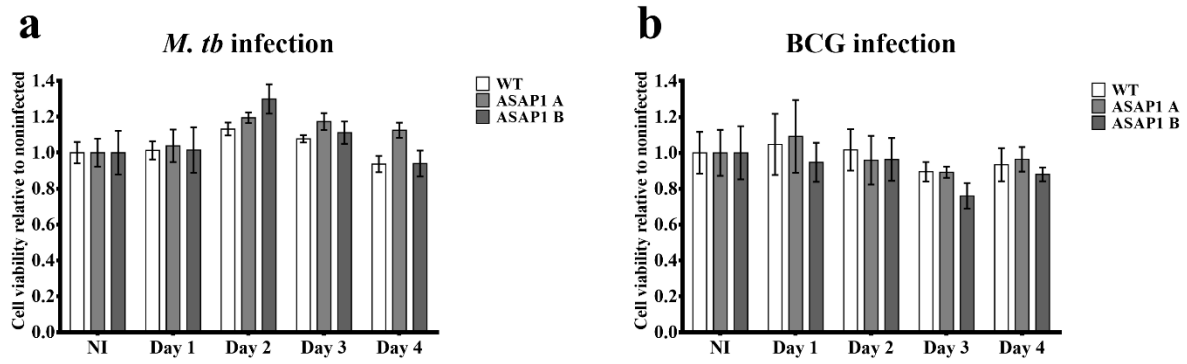

Figure 3.1-19: Evaluation of the mycobacteria-induced cytotoxicity in the wild-type and ASAP1-KO THP-1 cells.

The wild-type THP-1 cells (white) and the ASAP1-KO clones (clone A, gray; clone B, dark gray) were infected with (**a**) *M. tb* or (**b**) BCG and monitored for 4 days. Cell viability was determined by CellTiter 96 One Solution Reagent. Data were expressed as a relative ratio to non-infected cells. Experiments were averages of three replicates. Data indicate means ± s.e.m from three independent experiments performed in duplicates. Two-tailed Student's t-test was used.

To study the effect of ASAP1 on cell viability in the context of mycobacterial infection, I used CellTiter 96 AQueous One Solution Cell Proliferation Assay (MTS), which estimates the metabolic activity of the viable cells. The wild-type and the ASAP1-KO cells (including clone A and clone B) were differentiated and seeded in duplicates in 96-well plates at a density of 5 x 10^4 per well. Differentiated cells were then infected with virulent *M. tb* or BCG at MOI of ~ 2 and monitored for 96 hours. Infection medium was removed and replenished with fresh medium containing 20 µl of CellTiter 96 AQueous One Solution Reagent and incubated at 37ºC for 1 hour. The absorbance was recorded using plate reader.

Results showed that the ratio of viable ASAP1-KO cells infected with *M. tb* (**Figure 3.1-19a**) or BCG (**Figure 3.1-19b**) was comparable to that of the wild-type cells. Therefore, cell viability upon mycobacterial infection was not affected by the absence of ASAP1.

3.1.12 Studying the role of ASAP1 in mycobacteria phagocytosis in THP-1 cells

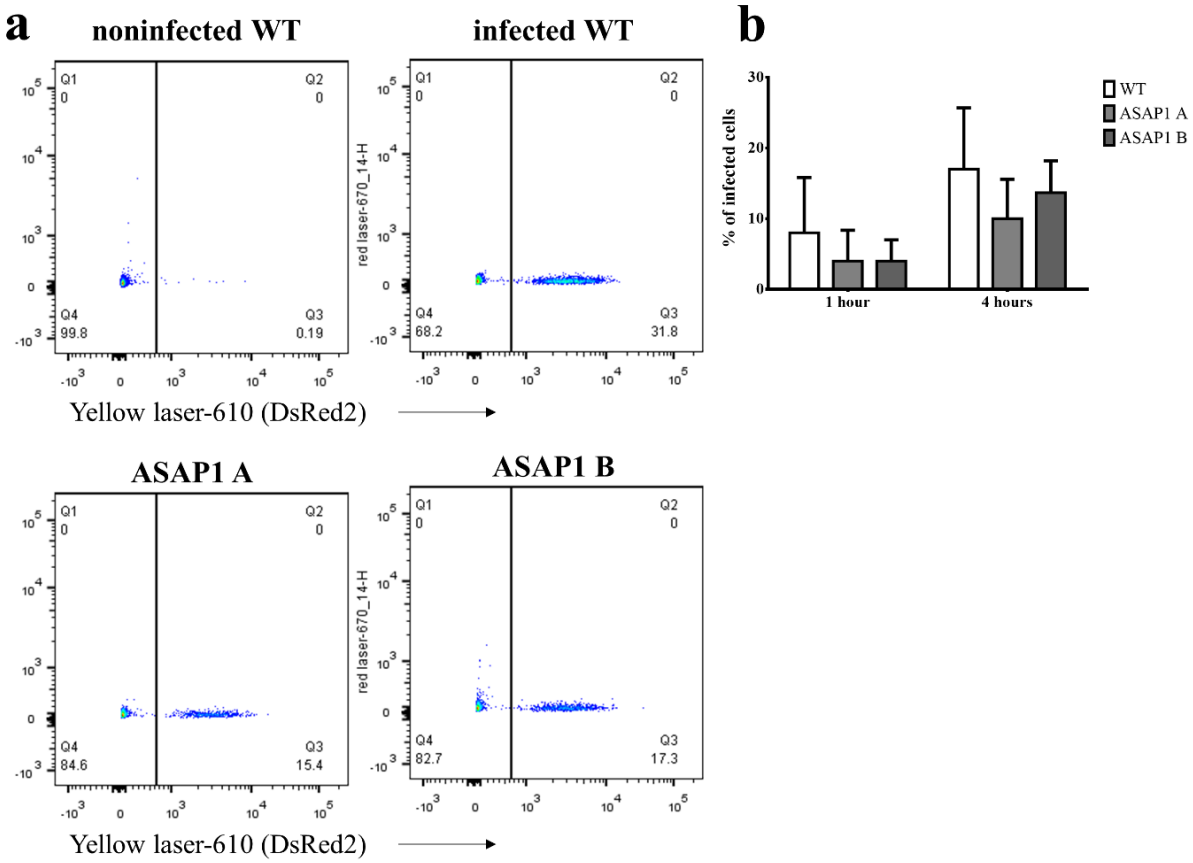

Figure 3.1-20: Assessment of phagocytosis of mycobacteria by the wild-type and ASAP1-KO THP-1 cells using flow cytometry.

Differentiated wild-type THP-1 and ASAP1–KO THP-1 cells (including clones A and B) were infected with the DsRed2-expressing BCG at MOI of 10 for 1 and 4 hours. Phagocytosis was assessed using flow cytometry. Representative images of flow cytometry for non-infected and BCG-infected THP-1 cells at 4 hours post-infection are shown. DsRed2-expressing BCG was detected using a yellow laser (610 nm). (**b**) Graph represents data as means ± SD from three independent experiments. Two-tailed Student's t-test was used.

Previous evidence has shown that *Salmonella* hijacks non-phagocytic cells and forces its entry using an ASAP1-dependent mechanism. The *Salmonella* effectors (SopE, SptP, and SopB) manipulate macropinocytosis machinery, implicating ASAP1 in an Arf1-dependent manner (Humphreys *et al.*, 2012; Davidson *et al.*, 2015). Previously, I studied the ASAP1 role in phagocytosis of mycobacteria in primary macrophages treated with the ASAP1 siRNAs. The results of those experiments were not conclusive largely due to inconsistent depletion of the ASAP1 expression between experiments. Now, I used stable ASAP1-KO cell lines to assess phagocytosis. Also, now I applied different methods (flow cytometry, CFU, high-throughput imaging system) thus avoiding labor-intensive and time-consuming techniques, such as manual quantification using an inverted confocal microscope.

To evaluate the effect of the ASAP1 deficiency on the phagocytosis of mycobacteria by macrophages, I examined the uptake of mycobacteria at early time points (up to 4 hours). Differentiated wild-type and ASAP1-KO THP-1 cells were infected with DsRed2-expressing BCG strain at MOI of 10. Infected cells were treated with accutase and fixed with 4% PFA. Thereafter, the uptake of fluorescent mycobacteria was analyzed using flow cytometry. The ASAP1-KO cells showed reduced phagocytosis of BCG at 1 and 4 hours post-infection, but it was not statistically significant compared to the wild-type THP-1 cells (**Figure 3.1-20**a and **b**), possibly due to a large variation between the experiments (**Figure 3.1-20b**). I hypothesized that the FACS assay did not allow enough precision to detect small differences in phagocytosis that may exist between these cells.

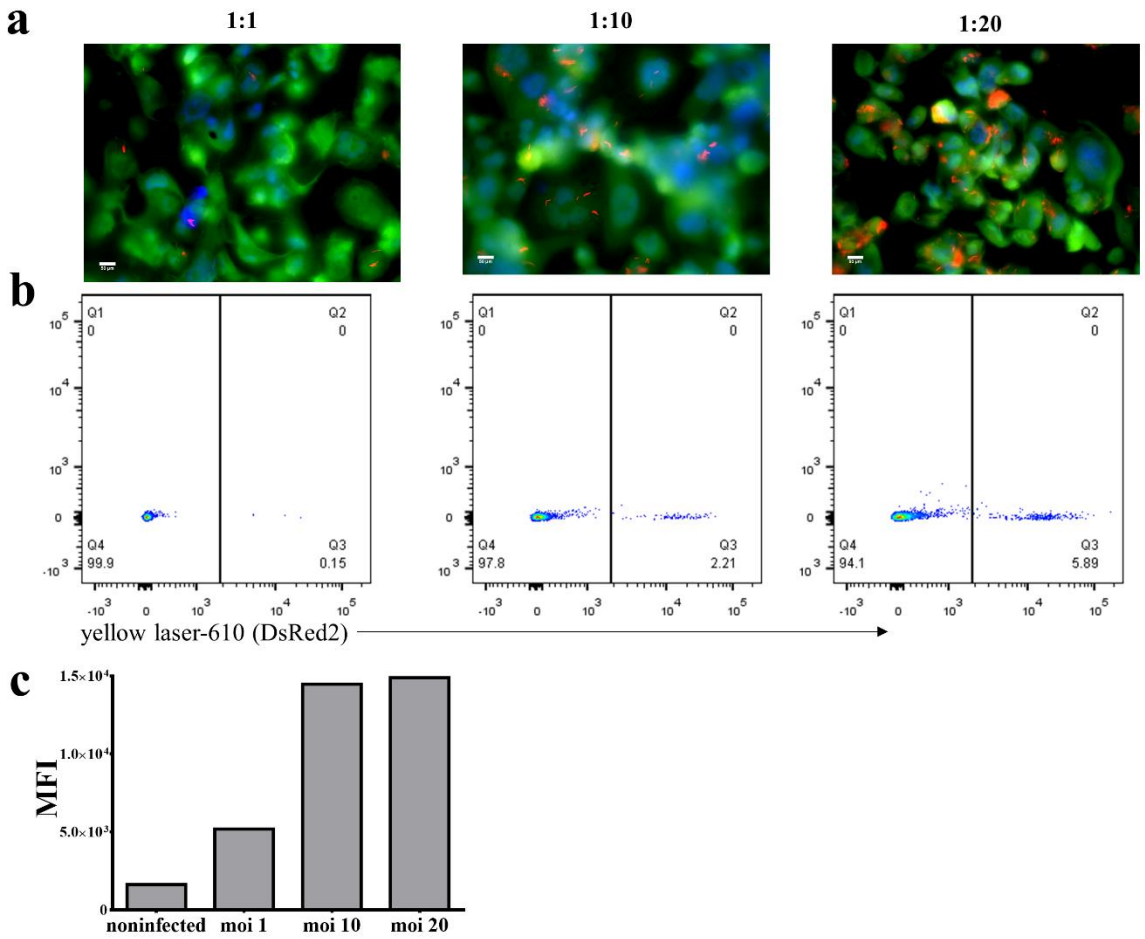

Figure 3.1-21: Testing flow cytometry as a method to detect THP-1 cells infected with BCG expressing DsRed2.

Differentiated THP-1 were infected with BCG-DsRed2 at MOIs of 1, 10, and 20 for 24 hours. (**a**) Representative images of THP-1 cells infected with different MOIs. Cells were stained with HCS CellMask green stain and DAPI. Images were obtained using fluorescent microscopy with a 90x objective (x900). Scale bar, 50 µm. (b) Flow cytometry data shows the percentage of infected cells using yellow laser channel. (**c**) Flow cytometry graph shows the mean fluorescence intensity (MFI) in cells infected with BCG expressing DsRed2 or non-infected cells.

To investigate the limitation of flow cytometry in capturing dim signals emitted by BCG in the THP-1 infected cells, I analyzed cells infected with DsRed2-BCG strain at different MOIs (MOI = 1, 10, and 20) for 24 hours using both fluorescent microscopy and flow cytometry. It is well established in our lab that at this time point 20% of cells are infected when MOI=1 is used, and more than 90% of cells are infected with MOI=10. Infected cells were fixed and stained with HCS CellMask green stain for the cytoplasm and with DAPI for the nuclei. Representative images of fluorescent microscopy revealed that MOI=1 achieved low BCG infection (left panel), while MOI=10 showed that most of the cells were infected with few bacilli (middle panel). When MOI=20 was used, most of the cells were highly infected (right panel, **Figure 3.1-21a**). However, when similar conditions were used in the flow cytometry assay, the microscopy results did not correlate with flow cytometric results (**Figure 3.1-21b**). The flow cytometry results showed that when cells were infected at MOI= 20, only 6% of the cells were positive for DsRed2-BCG (**Figure 3.1-21b**). In addition, mean fluorescence intensity (MFI) was similar in cells infected with MOIs 10 and 20, indicating that cells infected with few bacilli were below the detection limit.

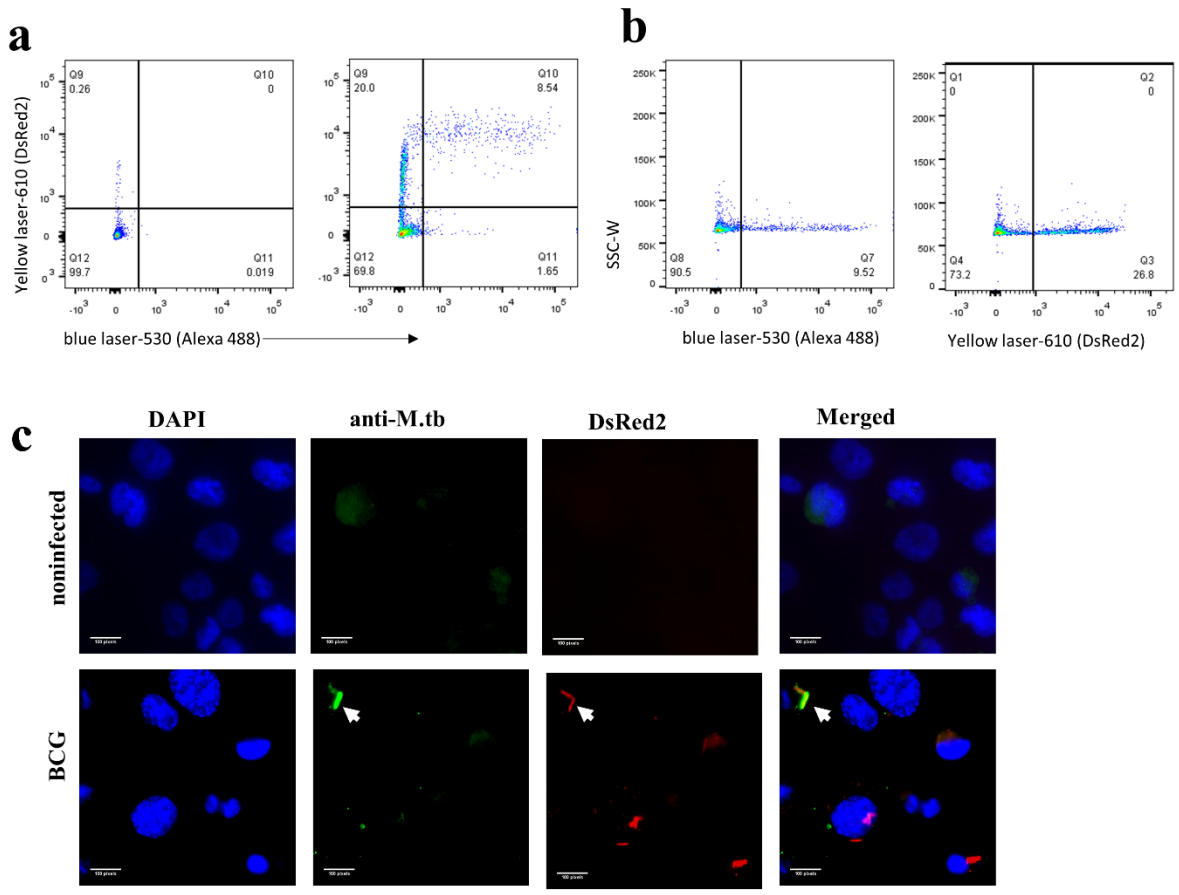

Figure 3.1-22: Testing the detection of THP-1 cells infected with BCG using anti- mycobacterial antibody.

Differentiated THP-1 were infected with BCG-DsRed2 at MOI=10 or left non-infected for 24 hours. Cells were fixed and stained with primary antibody (anti-*M. tb*) and secondary antibody (labeled with Alexa-Flour 488). (**a**) Representative images of dual-parameter dot plots show DsRed2 signal on y-axis and Alex488 signal on x-axis for non-infected THP-1 (left) or BCG-infected THP-1 cells (right). (**b**) Related to (**a**), flow cytometry shows Alexa Flour 488 signals (left) and DsRed2 signal (right) for THP-1 cells infected with BCG. (**c**) Cells infected with BCG expressing DsRed2 (red, bottom panel) or left non-infected (top panel) were fixed and stained with anti-*M. tb* (green) for mycobacteria and with DAPI for nuclei (blue). Images were obtained using fluorescent using a microscope with a 90x objective (x900). Arrowhead indicates co-staining. Scale bar, 50µm.

To enhance the detection of infected cells using flow cytometry, I used an antibody against mycobacteria to increase signal intensity and detect the infected cells. THP-1 cells were infected with BCG expressing DsRed2 at MOI of 10 overnight. Cells were harvested, fixed, and washed for flow cytometric analysis. Representative images of dual-parameter dot plots displayed that 8.5% of BCG-infected cells were positive for DsRed2 and Alexa Flour 488 signals (right panel, **Figure 3.1-22a**). Moreover, infected cells were 9.5% positive for Alexa Flour 488 and 27% positive for the DsRed2 signal (**Figure 3.1-22b**). Consistent with flow cytometric results, microscopic analysis for cells infected with BCG showed that most of the BCG bacilli expressing DsRed2 were not co-stained with the anti-mycobacterial antibody (Alexa Fluor 488, **Figure 3.1-22c**), potentially indicating that the antibody binds to mycobacterial epitopes that were altered during the fixation. Overall, cells infected with few BCG-DsRed2 bacilli were not detected by flow cytometry. In addition, an antibody against mycobacteria could not enhance the signal intensity and improve signal detection by flow cytometry.

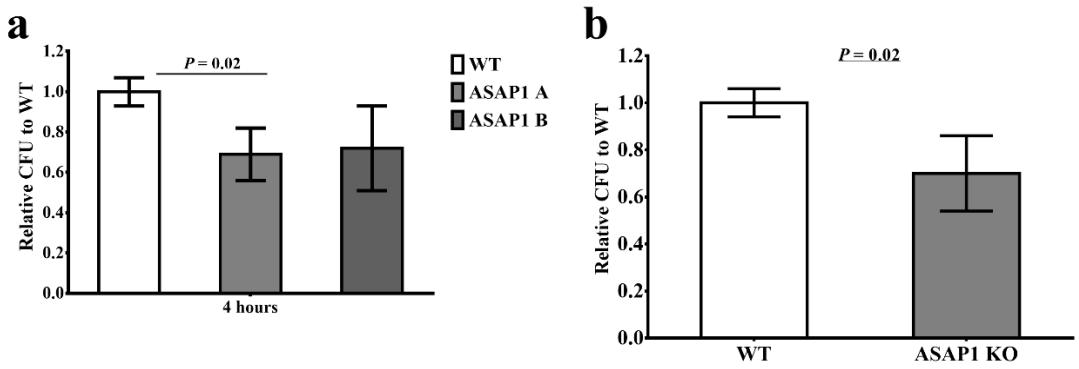

Figure 3.1-23: CFU assay for phagocytosis assessment in the ASAP1-KO cells infected with mycobacteria.

PMA differentiated THP-1 control cells and two THP-1 ASAP1-KO cell lines (clone A and clone B) were infected with BCG expressing DsRed2 at MOI of ~10. Cells were lysed and plated in duplicates for CFU count. Data were represented as CFU relative to THP-1 WT cells (**a**) Relative CFU count shows results for each individual clone. (**b**) Average results of ASAP1 lacking clones were combined. Data indicate mean ± SD from three independent results performed in duplicate. Two-tailed Student's t-test was used.

Given the above results, I decided to use the CFU assay to determine whether ASAP1 deficiency influences the engulfment of mycobacteria by macrophages. Differentiated wild-type THP-1 cells and the ASAP1-KO THP-1 cells (clones A and B) were plated in duplicates in 96-well plate at a density of 10^4 cell per well, infected with BCG at MOI of 10 and then incubated at 37 ºC. Four hours postinfection, the medium was removed, and cells were washed with PBS 4-5 times to remove extracellular bacilli. BCG-infected cells were lysed; the lysate from duplicate wells was combined, and then serially diluted in 7H9 broth. All dilutions were plated on 7H10 agar in duplicates and incubated at 37 ºC for 2-3 weeks. Then, colonies were counted. Relative to the wild-type THP-1 cells, the ASAP1-KO cells engulfed fewer BCG bacilli, but the difference was significant only for clone A (P = 0.02, **Figure 3.1-23a**). The combined analysis of the two ASAP1-KO clones indicated 30% ± 16% (±SD) reduction in the number of BCG CFU; this difference was statistically significant (P = 0.02, **Figure 3.1-23b**).

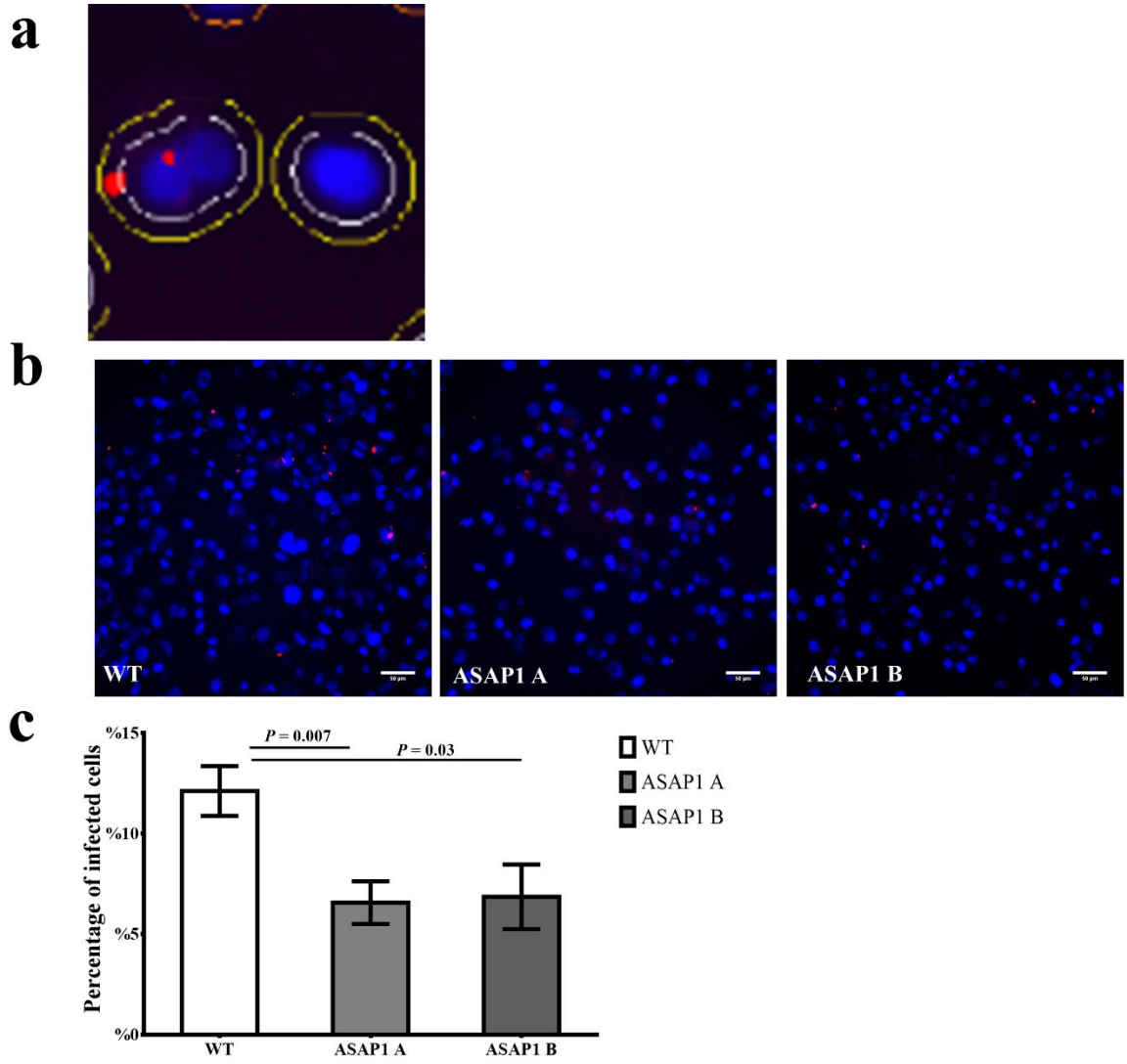

Figure 3.1-24: Analysis of phagocytosis of mycobacteria in the wild-type and ASAP1-KO THP-1 cells using automated fluorescence microscope.

Differentiated wild-type THP-1 and ASAP1-KO cells (clones A and B) were infected with the DsRed2-expressing BCG at MOI of 10 for 4 hours. Cells were fixed and stained for nuclei using Hoechst dye. Images were obtained using Thermo Fischer Scientific ArrayScan XTI automated fluorescence microscope with the 20x magnification Zeiss objective. (**a**) Representative image shows gate around the nucleus (white); another gate (yellow) highlights the extended area to be included in spot detection. (**b**) Representative images for the wild-type THP-1 and ASAP1-KO THP-1cells (clones A and B) infected with BCG expressing DsRed2, Scale bar, 50µm. (**c**) Data expressed as mean ± s.e.m from two experiments performed in biological replicates (n=6, 6000-9000 cells per line). Two-tailed Student's t-test was used.

To confirm the previous observation, I employed high-throughput imaging system to study the ASAP1 involvement in the macrophage engulfment of mycobacteria. The wild-type THP-1 and the ASAP1-KO THP1 clones were differentiated in triplicates and then infected with BCG expressing DsRed2 at MOI of 10. Four hours post-infection, cells were washed 4-5 times with PBS to remove extracellular bacilli, then fixed, and stained for nuclei with the Hoechst dye. Plates were scanned and photographed using Cellomics Arrayscan XTI automated fluorescence imager. Acquired images were analyzed to evaluate macrophages ingestion of BCG using Spot Detector, a built-in BioApplication. Briefly, individual cell nuclei were identified in the first channel by setting gates around each nucleus (white line **Figure 3.1-24a**). This step was followed by bacilli/spots identification in the second channel (DsRed2) by setting another measuring gate around the region of interest (yellow line **Figure 3.1-24a**). Protocol parameters were adjusted in order to set gates only around cellular objects excluding background noise and non-cellular objects. Spot identification threshold criteria were checked against negative and positive sample controls. The same protocol was used across all samples to ensure analysis consistency. A total of 6000 to 9000 cells per line was analyzed. The percent of cells with the BCG-DsRed2 aggregates among total analyzed cells was calculated. Representative images (**Figure 3.1-24b**) demonstrated that fewer BCG bacilli (red) were found in the ASAP1-KO THP-1 cells compared to the wild-type THP-1 cells. Quantitative analysis showed that the number of the ASAP-KO THP-1 cells containing BCG bacilli was markedly reduced with 6.6% and 6.9% infected cells in clones A and B, respectively, compared to 12% infected cell observed in wild-type THP-1 cells (**Figure 3.1-24c**). Collectively, these findings confirmed the above results indicating that the ability of

macrophages lacking ASAP1 to internalize mycobacteria was significantly impaired ($P < 0.02$, **Figure 3.1-24c**).

3.1.13 ASAP1 interactomes

To investigate further the role of the ASAP1 protein, I wanted to characterize protein complexes that ASAP1 is involved in inside non-infected macrophages and during mycobacterial infection. Several ASAP1-associated proteins were identified using the yeast two-hybrid approach, where ASAP1 and its partner had to be physically adjacent (Liu *et al.*, 2002; Inoue *et al.*, 2008; Shiba and Randazzo, 2011). However, this approach is limited to finding interactions between pairs of proteins rather than interactomes including multiple proteins (Mohammed and Carroll, 2013). Another technique commonly used for the identification of interacting proteins is mass spectrometry after tandem affinity purification (TAP) (Chen *et al.*, 2016). TAP involves cloning tags onto the gene of interest and forced expression of a fused protein. Despite its successes in the identification of novel partners, tags may alter the protein structure of the bait. Forced expression leads to the excessive levels of the protein and may cause ectopic intracellular localization. These factors may result in the identification of false interacting proteins, which limits the physiologic relevance of this approach (Mohammed and Carroll, 2013). Rapid immunoprecipitation mass spectrometry of endogenous protein (RIME) has been described as an alternative robust method to study interactomes of endogenous proteins. RIME combines protein cross-linking, immunoprecipitation, on-beads protein digestion and mass spectrometry.

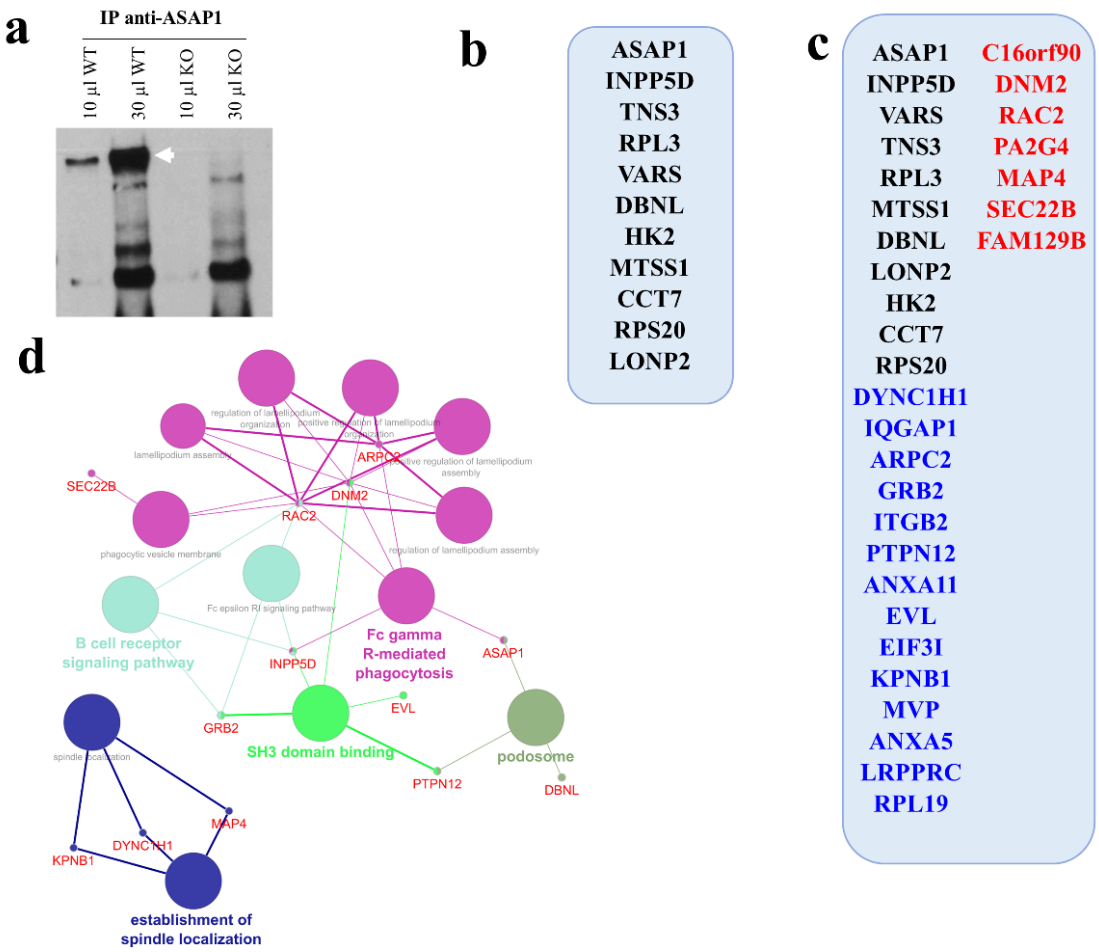

Figure 3.1-25: List of the ASAP1-associated proteins identified by RIME.

(**a**) Immunoprecipitations (IPs) were performed with 12 µg of ASAP1 antibody and Dynabeads. Western blotting shows that the ASAP1 protein (white arrowhead) with different loading lysates extracted from formaldehyde cross-linked is found in the wild-type THP-1 IP and absent in ASAP1-KO IP. (**b**) Stringent list of the ASAP1-associated protein partners in THP-1 cells. These proteins appeared in seven out of seven individual RIME experiments in the wild-type THP-1 cells and were not found in any of the three experiments in the ASAP1-KO THP-1 cells that were used as negative controls. (**c**) Relaxed list of the ASAP1-associated protein partners. These proteins appeared in at least five out of seven individual RIME experiments in the wild-type THP-1 cells and were not found in any of the three experiments in the ASAP1-KO THP-1 cells. Proteins appeared in seven replicates (black font), six replicates (blue font), and five replicates (red font). (**d**) ASAP1-associated proteins were annotated based on the GO and KEGG databases, and the relationships among these annotated terms were calculated and grouped using Cytoscape`s plugin (ClueGO) to create an annotation module network. The generated network represented the terms as nodes that were linked based on a predefined kappa score level (>0.4).

To identify the novel ASAP1-associated protein partners, I purified endogenous ASAP1 from 2 x 10^7 THP-1 cells, including the wild-type THP-1 cells and the ASAP1-KO cells used as a negative control. Briefly, THP-1 cells were differentiated using PMA. Untreated cells were cross-linked with formaldehyde, which fixed protein-protein interactions (Mohammed and Carroll, 2013). Cells were lysed, sonicated, and incubated with an antibody against ASAP1. Immunoprecipitations were performed using Dynabeads on lysates from the cross-linked cells; the resulting immunoprecipitates were analyzed by mass spectrometry (**Figure 3.1-25a**). For a stringent list of the ASAP1 interactors (**Figure 3.1-25b**), I considered the ASAP1-associated proteins that occurred in 7 out of seven independent replicates of the wild-type THP-1 cells and the peptide-spectrum match (PSM) more than 1. This list includes proteins with the strongest evidence for interaction with ASAP1. For a relaxed list of the ASAP1 interactors (**Figure 3.1-25c**), I considered proteins that appeared in at least 5 out of seven replicates. In both lists, any proteins found in any of three ASAP1-KO THP-1 cells were excluded, because such cells do not express ASAP1 and any putative interactors are false, probably resulting from a non-specific binding to the anti-ASAP1 antibody. This RIME experiment detected ASAP1, as expected (47 peptides giving 49% coverage), and characterized the ASAP1 interactome: 10 proteins and 31 proteins were identified in the stringent and relaxed lists, respectively. Proteins in the relaxed list of ASAP1 interactors were annotated using ClueGO plugin based on the Gene Ontology (GO) and Kyoto Encyclopedia of Genes and Genomes (KEGG) databases. The most significant enriched GO terms were related to phagocytic vesicles, receptor internalization, podosomes, and SH3 binding (**Figure 3.1-25d** and **Table 3.1-1**).

Most of the identified ASAP1-associated proteins act as regulators in cytoskeleton remodeling. PTP-PEST (PTPN12, Tyrosine-protein phosphatase non-receptor type 12) plays a role in cell cytoskeleton organization, by regulating focal adhesion disassembly required for cell migration (Angers-Loustau *et al.*, 1999). DNM2 (Dynamin2) has been shown to regulate actin reorganization (Pittis and Garcia, 1999). TNS3 (Tensin-3) seems to be involved in cell migration (Katz *et al.*, 2007). The DBNL (Drebrin-like protein) protein is involved in phagocytosis; its absence in PMN significantly reduced β2 integrin-mediated phagocytosis of *E. coli* and *Salmonella* (Schymeinsky *et al.*, 2009). MIM-B (MTSS1, Metastasis suppressor protein 1) is known to interact with RAC to modulate the formation of lamellipodia (Bompard *et al.*, 2005). The Arp2/3 complex, including ARPC2, promotes actin assembly in lamellipodia and may participate in lamellipodial protrusion (Welch *et al.*, 1997).

Some of the ASAP1 interacting proteins are involved in endocytic machinery. IQGAP1 (Ras GTPase-activating-like protein) regulates phagocytosis and cell migration (Brandt *et al.*, 2007). It also has been identified in the BCG-containing phagosomes (Lee *et al.*, 2010). ANXA11 (Annexin A11) is another protein that has been demonstrated to translocate predominantly to phagosomes upon particle ingestion in macrophage (Pittis and Garcia, 1999). SHIP-1 (INPP5D, Phosphatidylinositol 3,4,5-trisphosphate 5-phosphatase 1) has been shown to orchestrate the formation of leading edges and polarization required for chemotaxis (Nishio *et al.*, 2007) and plays a role in phagocytosis mediated by Fcγ receptors and complement receptor 3 (Nishio *et al.*, 2007). ASAP1 and SHIP-1 have been found to selectively bind to the SH3 domain of Tec tyrosine kinase (Tomlinson *et al.*, 2004). GRB2 (Growth factor receptor-bound protein 2) has been found to be involved in the endocytic pathway as a regulator of Rab5 (Martinu *et al.*, 2002).

Our results also found EVL (Ena/VASP-like protein) in ASAP1 interactome, that has been localized in focal adhesions and the leading edge of lamellipodia in fibroblasts (Lambrechts *et al.*, 2000) . It is also considered as a potential link between actin remodeling and spectrin-based skeleton (Bournier *et al.*, 2006).

In addition, proteins that are known to be involved in ATPase activity including LONP2 and DYNC1H1, (Poirier *et al.*, 2013; Pomatto, Raynes and Davies, 2016), and ribosomal proteins such as RPL3 and RPS20, were found to interact with ASAP1 in my RIME experiment.

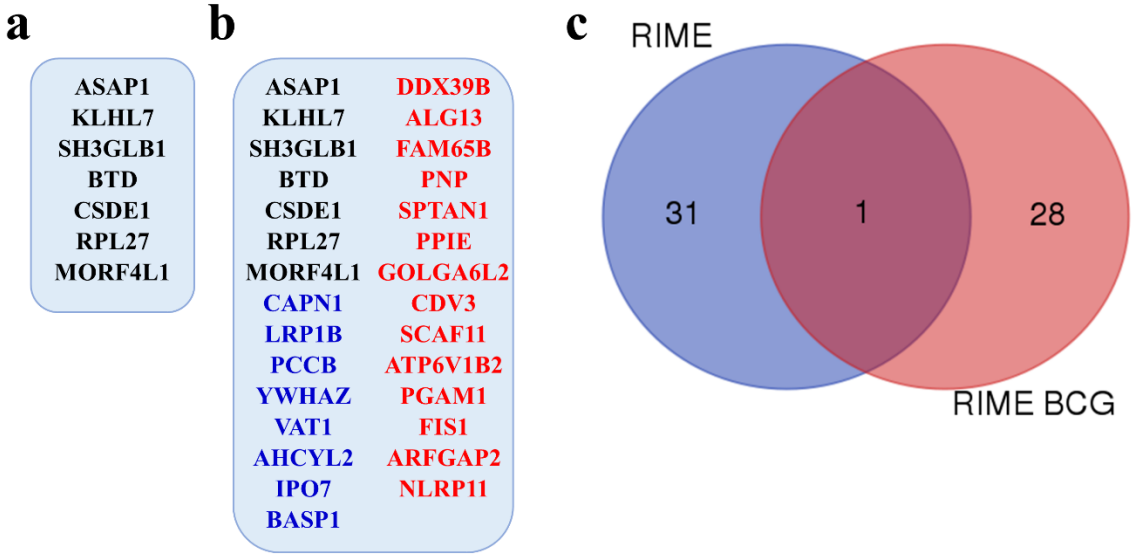

Figure 3.1-26: List of the ASAP1-interacting proteins identified by the RIME experiment in THP-1 cells following BCG infection.

THP-1 cells were differentiated and left non-infected or infected with BCG for 4 hours, crosslinked, and then ASAP1 RIME was conducted. (**a**) Stringent list of the ASAP1-associated proteins partners in THP-1 cells following BCG infection. These proteins appeared in seven out of seven individual RIME experiments in the wild-type THP-1 cells and were not found in any of the three experiments in the ASAP1-KO THP-1 cells that were used as negative controls (**b**) Relaxed list of the ASAP1-associated proteins partners in THP-1 cells following BCG infection. These proteins appeared in at least five out of seven individual RIME experiments in the wild-type THP-1 cells and were not found in any of the three experiments in the ASAP1-KO THP-1 cells. Proteins appeared in seven replicates (black font), six replicates (blue font), and five replicates (red font). (**c**) Venn diagram shows the overlap in the ASAP1-interacting proteins in non-infected and BCG-infected THP-1 cells.

To study how the ASAP1 interactome will change during mycobacteria infection, I then repeated this RIME experiment in THP-1 cells following 4 hours of BCG infection. Seven independent replicates were conducted. I only considered ASAP1-associated proteins with PSM more than 1. Again, as expected, ASAP1 itself was detected, which provided a

positive control. I applied similar criteria for that employed for analyzing ASAP1 RIME in non-infected cells. After BCG infection a total of 6 proteins appeared in the seven ASAP1 wild-type THP-1 samples and were not found in the three ASAP1-KO THP-1 samples (**Figure 3.1-26a**). Using the relaxed criteria resulted in the identification of a total of 28 ASAP1 interacting proteins (**Figure 3.1-26b**) that appeared in at least five replicates out of seven. Interestingly, the list of ASAP1 partners in non-infected THP-1 cells and after BCG infection did not overlap (**Figure 3.1-26c**), This is a fascinating finding suggesting that ASAP1 is involved in highly dynamic protein complexes that change their composition in response to BCG infection.

In BCG-infected cells, the majority of the ASAP1-interacting partners (e.g., GOLGA6L2, CDV3, KLHL7, and PCCB) have not been associated with ASAP1 or TB previously. Thus, my experiment revealed novel ASAP1 interactors that were induced by the infection. Interestingly, BASP1 is a known corepressor of the *WT1* protein (Wilms Tumor 1), a zinc finger transcription factor (Carpenter *et al.*, 2004). The *WT1* gene has been associated with TB risk in previous GWAS (Thye *et al.*, 2012; Chimusa *et al.*, 2014). Thus, my finding provided a biological mechanistic link between two TB-associated genes, *ASAP1* and *WT1*, that were discovered previously.

Several of the ASAP1-associated proteins have been implicated in endocytic machinery and actin remodeling, including ATP6V1B2 (ATPase H+ Transporting V1 Subunit B2). The vacuolar (H+)-ATPases (or V-ATPases) is a universal multisubunit (A-H) enzyme that regulates acidification of eukaryotic intracellular organelles such as lysosomes (Nishi and Forgac, 2002) and various mycobacterial components have been linked to the exclusion of V-ATPase leading to the inhibition of phagolysosomal maturation. For example,

mycobacterial protein PtpA binds directly to V-ATPase subunit H (Soldati and Neyrolles, 2012). YWHAZ (14-3-3 protein zeta/delta) belongs to the family of 14-3-3 proteins. It involves in regulating actin rearrangement. YWHAZ stimulates cell migration by regulating the formation of membrane ruffles (Chen et al.) and affects RAC1 activation (Goc *et al.*, 2012). Phosphorylated FAM65B binds to 14-3-3 family proteins and becomes more stable. FAM65B acts as RhoA inhibitor (Gao *et al.*, 2015). FAM65B involves cytoskeletal rearrangement, filopodia formation (Yoon *et al.*, 2007), and T cell migration via the inhibition of RhoA activity (Rougerie *et al.*, 2013). ARFGAP2 is a key component of the COP-I-coated vesicles and is necessary for proper vesicle formation (Frigerio *et al.*, 2007; Kartberg *et al.*, 2010).

The α-spectrin has newly proven to be involved in cell adhesion and spreading (Machnicka *et al.*, 2012). One of the ASAP1 interactors following BCG infection was SPTAN1, which encode for αII-spectrin subunit in non-erythrocytic cells. The αII-spectrin SH3 domain has been reported to participate with actin in cell adhesion and spreading via EVL protein (Bournier *et al.*, 2006). EVL was also found in our RIMEs as an ASAP1 partner in non-infected macrophages. The spectrin-based skeleton has been shown to be critical for the pathogenesis of enteric intracellular pathogens, including *S. typhimurium*, *Listeria monocytogenes* (Ruetz, Cornick and Guttman, 2011), and *Shigella flexneri* utilize (Ruetz, Lin and Guttman, 2012).

My results suggested that ASAP1 may also have additional undiscovered regulatory functions in cellular processes. For example, the ASAP1 interactome includes SH3GLB1 (Endophilin-B1), which has been demonstrated to be translocated to the mitochondria, and its reduction led to alternations of the mitochondrial distribution and morphology (Karbowski,

Jeong and Youle, 2004). FIS1 (Mitochondrial fission 1 protein) involves in mitochondrial fission, and its expression at the mitochondrial surface regulates mitochondrial morphology within the cell (Stojanovski *et al.*, 2004).

Collectively, this RIME experiment in non-infected cells or after BCG infection identified two distinct sets of the ASAP1-interacting proteins. Future experiments have to validate these ASAP1 interactors, starting with the co-immunoprecipitation experiments. They should also investigate in detail protein complexes that ASAP1 engage in during mycobacterial infection.

Table 3.1-1: Enriched GO terms describing ASAP1 interactome in non-infected THP-1 cells.

ID	GO Term	Bonferroni corrected P-value	Genes
GO:0004662	B cell receptor signaling pathway	3.43E-04	[GRB2, INPP5D, RAC2]
GO:0004664	Fc epsilon RI signaling pathway	4.52E-04	[GRB2, INPP5D, RAC2]
GO:0004666	Fc gamma R-mediated phagocytosis	3.23E-06	[ARPC2, ASAP1, DNM2, INPP5D, RAC2]
GO:0017124	SH3 domain binding	1.45E-05	[DNM2, EVL, GRB2, INPP5D, PTPN12]
GO:0030670	phagocytic vesicle membrane	2.02E-04	[DNM2, RAC2, SEC22B]
GO:0002102	podosome	1.36E-04	[ASAP1, DBNL, PTPN12]
GO:0051293	establishment of spindle localization	1.39E-04	[DYNC1H1, KPNB1, MAP4]
GO:0030032	lamellipodium assembly	5.52E-04	[ARPC2, DNM2, RAC2]
GO:0010592	positive regulation of lamellipodium assembly	4.62E-05	[ARPC2, DNM2, RAC2]
GO:1902745	positive regulation of lamellipodium organization	1.14E-04	[ARPC2, DNM2, RAC2]
GO:0010591	regulation of lamellipodium assembly	1.30E-04	[ARPC2, DNM2, RAC2]
GO:1902743	regulation of lamellipodium organization	2.04E-04	[ARPC2, DNM2, RAC2]

GO:0051653	spindle localization	1.45E-04	[DYNC1H1, KPNB1, MAP4]

3.1.14 ASAP1-mediated pathway regulates gene expression during mycobacterial infection

a

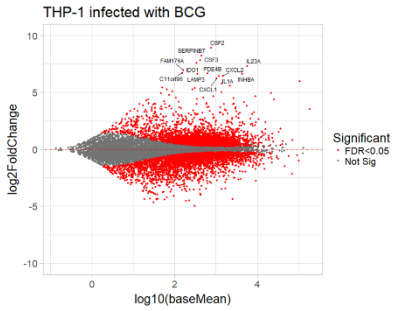

Gene	baseMean	log2FoldChange	padj
IL6	20.77165	4.278272	1.74E-13
IL23A	5803.718	7.30732	0
CCL2	13.61808	-1.20748	0.020919
CCL7	4.529716	-1.42899	0.047366
TLR1	845.9839	0.314568	0.080482
TLR2	10204.25	1.198591	3.84E-34
TLR4	426.2554	-2.51748	2.63E-31
ZC3H12A	3095.259	3.321053	1.1E-171
ADA	223.4419	-0.05716	0.851841
IL1B	188722.5	3.544675	3.8E-108
IRF7	748.5132	-0.83019	9.29E-08
CSF1	23423.61	1.370889	2.88E-27
IL1R1	397.715	-0.84336	3.53E-06
TGFB1	9065.803	-1.22243	6.09E-16
ATP6V1A	1973.618	0.996106	4.72E-19
DUSP14	1584.343	-0.48937	0.00288
CXCL10	24.06978	-2.03082	8.06E-06
CXCR7	620.8719	1.291174	6.95E-17
CXCR6	11.01842	0.844005	0.219639
CCL5	15792.67	1.765466	7.91E-25
CCL3	26081.85	4.349665	4.89E-80
CCL4	2681.079	4.508278	2.09E-84
CCR7	1394.539	5.007873	3.8E-110

b

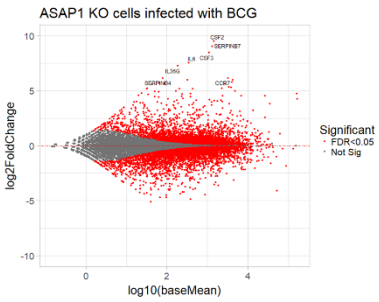

Gene	baseMean	log2FoldChange	padj
IL6	351.6356	7.529156	1.68E-84
IL23A	4277.798	5.965168	0
CCL2	6153.994	-0.11927	0.004209
CCL7	3652.658	-0.70407	2.45E-56
TLR1	697.515	0.044127	0.676873
TLR2	7439.305	0.668782	8.3E-121
TLR4	752.6236	-2.26271	3.8E-142
ZC3H12A	4138.793	2.808322	0
ADA	334.8873	0.245416	0.046927
IL1B	163001.5	4.746867	0
IRF7	1993.079	-0.70267	1.79E-45
CSF1	11798.77	0.925462	5.48E-42
IL1R1	1447.132	-1.84032	1.7E-203
TGFB1	8205.504	-1.23393	3.9E-244
ATP6V1A	1353.596	0.653159	1.21E-26
DUSP14	1970.234	-0.34529	6.46E-11
CXCL10	367.0744	-3.01714	6E-124
CXCR7	428.5438	0.814964	5.52E-15
CXCR6	12.5899	0.444847	0.452949
CCL5	26801.11	2.576879	0
CCL3	34990.07	3.813005	0
CCL4	3422.912	5.322867	0
CCR7	3261.604	6.137154	0

Figure 3.1-27: Differential expression analysis of THP-1 cells infected with BCG.

Differentially expressed genes were studied in the wild-type THP-1 cells and ASAP1-KO THP-1 cells infected with BCG at MOI of 10 for 24 hours. (**a**) MA-plot shows differentially expressed genes in control cells (top). The table shows altered expression of selected genes (bottom) (**b**) MA-plot shows differential gene expression in the ASAP1-KO THP-1 cells (top). The table shows altered expression of selected genes (bottom). Genes with FDR < 0.05 are labeled red and genes with FDR < 10^{-20} and absolute log 2-fold change greater than 6 are labeled with text.

PMA-differentiated THP-1 wild-type cells and ASAP1-KO THP-1 cells were infected with BCG at MOI of 10. Then, cells were incubated for 24 hours, and RNA was extracted. Three biological replicates were done. Then libraries for RNA-seq were prepared and

sequenced using Illumina HiSeq machines. For bioinformatics analysis, I used the Galaxy pipeline for RNA analysis. I aligned 50-nucleotide single-end reads against the human genome (hg19) using HISAT2. Mapped reads were quantified using HTSeq-count. Using DESeq2, I found 6,695 and 7,558 genes to be differentially expressed after mycobacteria infection in wild-type THP-1 cells (**Figure 3.1-27a)** and cells lacking ASAP1 (**Figure 3.1-27b)**, respectively (False Discovery Rate, FDR < 0.05). To validate these results, I checked some selected genes that are expected to change their levels of expression in macrophages after mycobacterial infection (e.g., genes for cytokines *IL-6, IL-1β*, and chemokines, including *CCL3* and *CCL4* **Figure 3.1-27a** and **b** bottom panels) (Tailleux *et al.*, 2008). These genes altered their expression significantly and following the same pattern in the wild-type and knockout cells. Next, I performed DESeq2 to analyze differential gene expressions after ASAP1 knockout in non-infected macrophages or after BCG infection for 24 hours by comparing the wild-type and the ASAP1-KO THP-1 cells.

There were 2,119 (**Figure 3.1-28a)** differentially expressed genes in non-infected THP-1 macrophages, and 3,112 genes (**Figure 3.1-28b**) in the BCG-infected THP-1 macrophages when comparing wild-type versus ASAP1-KO cells (FDR < 10^{-5}). Therefore, quite unexpectedly, the ASAP1-mediated pathway may be involved in the regulation of gene expression for a significant number of genes. An alternative explanation is that this large number of differentially expressed genes is an artifact. Thus, while making the clonal ASAP1 knockout line, THP-1 cells underwent transduction and limiting dilution, which took

approximately 2 months of tissue culture maintenance before obtaining a single-cell clone. This may have resulted in physiological changes between parental THP-1 and the ASAP1-KO THP-1 cell, leading to differential gene expression in plenty of genes. However, it has been reported that ASAP1 silencing resulted in an increase in production of proinflammatory cytokines in macrophages in response to a variety of stimuli including a series of TLR ligands as well as LPS (Haque *et al.*, 2011). Later, another study demonstrated that ASAP1 works as an inhibitory feedback regulating NF-κB pathway by preventing the association of IKKβ and NEMO (Tien *et al.*, 2015). In the analysis of the whole transcriptome, this may have led to differential expression of a large number of genes.

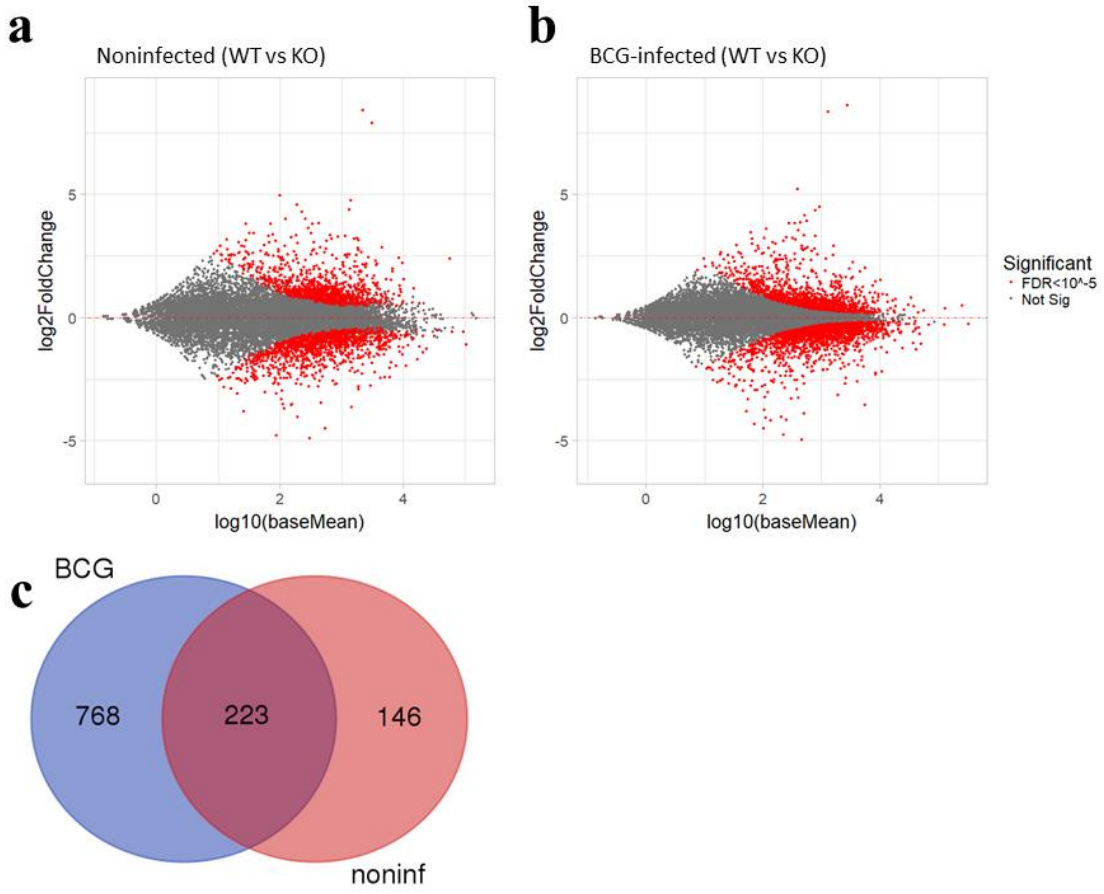

Figure 3.1-28: Analysis of differential gene expression in non-infected and BCG-infected ASAP1-KO THP-1 cells.

(**a**) MA-plot shows differentially expressed genes in non-infected macrophages comparing wild-type cells versus ASAP1 knockout cells. (**b**) MA-plot shows differentially expressed genes in macrophages comparing wild-type cells versus ASAP1-KO cells after BCG infection. Genes with FDR < 1 x 10^{-5} are labeled red. (**c**) Venn diagram shows genes differentially expressed (FDR < 1 x 10^{-20}) in non-infected cells and BCG-infected cells that used for GO and KEGG classification (*Draw Venn Diagram*, no date)

To learn about variation in gene expression due to ASAP1 knockout, I performed gene functional classification based on all GO categories and KEGG. This analysis allowed us to identify gene groups that change expression due to the ASAP1 knockout. Using stringent FDR < 1 x 10^{-20}, I found that a total of 369 genes were differentially expressed in

non-infected macrophages (including 146 genes unique to non-infected cells and 223 genes common to both non-infected and BCG-infected cells). This set of genes were enriched for GO categories related to type I interferon signaling pathway (e.g., *SP100*, *STAT1*, *STAT2*, and *ISG15*), positive regulation of cell migration (e.g., *FGR*, *PDGFA*, *BCAR1*, and *CCL7*), and positive regulation of NF-kappaB transcription factor activity (e.g., *TRAF1*, *MYD88*, *AIM2*, and *NLRP3*). Most of the genes were related to cellular components in the cytoplasm. Moreover, these genes were enriched for chemokine signaling pathway (e.g., *CXCL1*, *CCL2*, and *CXCL3*) and TNF signaling pathway (e.g., *LIF*, *TRAF1*, and *FOS*,) based on KEGG (**Table 3.1-2**).

There were a total of 768 genes whose expression levels changed exclusively after BCG infection in the ASAP1-KO cells. These genes were mostly involved in phagocytosis, intracellular infection, phagosome, and migration (**Table 3.1-3**, $P_{\text{corrected}} < 0.05$). For instance, differentially expressed genes contained in the GO classifications includes genes involved in phagocytosis (e.g., *CORO1C*, *CORO1A*, *CD14*, and *SLC11A1*), leukocyte migration (e.g., *ICAM1, F11R, ITGB2,* and *GRB2*), and integrin-mediated signalling pathway (e.g., *ITGA1*, *ITGA2*, *ITGA3*, *ITGA4*, and *ITGA7*). Coronin1, *CORO1A,* has been reported to be recruited to phagosome and inhibit phagosome maturation (Jayachandran *et al.*, 2007). Also, *SLC11A1* has been identified to be associated with susceptibility to BCG and other intracellular pathogens (Vidal *et al.*, 1993). Moreover, this subset of genes was enriched in KEGG for phagosome (e.g., *ATP6V0C*, *ATP6V1A*, *LAMP2*, and *CD36*), tuberculosis (e.g., *IL6*, *CEBPB*, and *TLR2*), and bacterial invasion of epithelial cells (e.g., *PIK3CB*, *ARPC4*, and *ACB*).

To be noted, this strategy of pairwise comparison may result in overestimating the difference between genotypes. However, GO and KEGG enrichment analysis in non-infected

THP-1 macrophages showed that ASAP1 is likely to be involved in regulating essential cellular responses. Differentially expressed genes in wild-type cells versus ASAP1-KO cells after infection were mainly involved in phagocytosis, phagosome functioning and cell migration suggesting that in the context of mycobacterial infection ASAP1-mediated pathway regulates these processes. My results are in agreement with our previous observation that ASAP1-KO THP-1 cells exhibited reduced migration and phagocytic activity.

Table 3.1-2: GO and KEGG enrichment analysis of differentially expressed genes in non-infected wild-type THP-1 macrophages and non-infected ASAP1-KO THP-1 macrophages

ID	Gene Ontology terms	Genes	Benjamini-corrected P-values
GO:0051607	defense response to virus	28	4.61E-14
GO:0060337	type I interferon signaling pathway	18	4.81E-12
GO:0009615	response to virus	20	3.65E-10
GO:0045071	negative regulation of viral genome replication	12	1.17E-07
GO:0006955	immune response	32	1.55E-07
GO:0006954	inflammatory response	29	8.83E-07
GO:0006935	chemotaxis	16	5.86E-06
GO:0070098	chemokine-mediated signaling pathway	12	3.73E-05
GO:0060333	interferon-gamma-mediated signaling pathway	11	3.06E-04
GO:0071222	cellular response to lipopolysaccharide	13	5.32E-04
GO:0034340	response to type I interferon	5	9.63E-04
GO:0007267	cell-cell signaling	18	2.39E-03
GO:0042127	regulation of cell proliferation	15	3.28E-03
GO:0001666	response to hypoxia	14	6.05E-03
GO:0007165	signal transduction	44	8.13E-03
GO:0051092	positive regulation of NF-kappaB transcription factor activity	12	9.15E-03
GO:0034097	response to cytokine	8	8.67E-03
GO:0030335	positive regulation of cell migration	14	9.43E-03
GO:0032496	response to lipopolysaccharide	13	1.19E-02
GO:0045087	innate immune response	22	1.54E-02
GO:0001525	angiogenesis	15	1.53E-02
GO:0016525	negative regulation of angiogenesis	8	2.07E-02
GO:0032480	negative regulation of type I interferon production	6	2.53E-02
GO:0060326	cell chemotaxis	8	2.54E-02
GO:0042493	response to drug	17	3.32E-02
GO:0035457	cellular response to interferon-alpha	4	4.65E-02
GO:0035456	response to interferon-beta	4	4.65E-02
GO:0005829	cytosol	111	1.25E-07
GO:0005615	extracellular space	54	4.07E-05
GO:0005764	lysosome	19	3.14E-05
GO:0070062	extracellular exosome	85	6.30E-04
GO:0005576	extracellular region	53	5.55E-03
GO:0005737	cytoplasm	131	7.70E-03
GO:0009897	external side of plasma membrane	13	3.16E-02

GO:0008009	chemokine activity	11	2.06E-05
GO:0001730	2'-5'-oligoadenylate synthetase activity	4	9.31E-03
GO:0008201	heparin binding	13	1.70E-02
GO:0005515	protein binding	208	2.12E-02

ID	KEGG pathways	Genes	Benjamini-corrected P-values
hsa05164	Influenza A	21	8.23E-06
hsa05168	Herpes simplex infection	21	9.60E-06
hsa04062	Chemokine signaling pathway	21	8.40E-06
hsa05162	Measles	15	7.09E-04
hsa04668	TNF signaling pathway	11	2.45E-02
hsa05133	Pertussis	9	3.26E-02
hsa05160	Hepatitis C	12	2.86E-02

Table 3.1-3: GO and KEGG enrichment analysis of differentially expressed genes in the wild-type and ASAP1-KO THP-1 macrophages infected with BCG

ID	Gene Ontology terms	Genes	Benjamini-corrected P-values
GO:0006954	inflammatory response	40	4.27E-04
GO:0007165	signal transduction	85	3.64E-04
GO:0006928	movement of cell or subcellular component	16	2.19E-03
GO:0050900	leukocyte migration	19	2.00E-03
GO:0002576	platelet degranulation	17	2.92E-03
GO:0006955	immune response	39	2.61E-03
GO:0071404	cellular response to low-density lipoprotein particle stimulus	6	6.08E-03
GO:0030036	actin cytoskeleton organization	18	9.73E-03
GO:0045669	positive regulation of osteoblast differentiation	12	1.04E-02
GO:0042102	positive regulation of T cell proliferation	12	1.04E-02
GO:0070527	platelet aggregation	10	1.13E-02
GO:0009615	response to virus	16	1.29E-02
GO:0007229	integrin-mediated signaling pathway	15	1.41E-02
GO:0031623	receptor internalization	10	1.30E-02
GO:0043123	positive regulation of I-kappaB kinase/NF-kappaB signaling	19	2.62E-02

GO:0006909	phagocytosis	10	2.77E-02
GO:0098609	cell-cell adhesion	26	2.86E-02
GO:0006915	apoptotic process	43	3.13E-02
GO:0071222	cellular response to lipopolysaccharide	15	3.95E-02
GO:0070062	extracellular exosome	221	6.12E-24
GO:0005925	focal adhesion	65	1.83E-20
GO:0016020	membrane	173	5.23E-18
GO:0005829	cytosol	215	3.07E-13
GO:0042470	melanosome	22	2.79E-08
GO:0045121	membrane raft	26	4.40E-05
GO:0009986	cell surface	47	5.12E-05
GO:0005911	cell-cell junction	23	6.50E-05
GO:0048471	perinuclear region of cytoplasm	50	1.40E-04
GO:0009897	external side of plasma membrane	25	1.68E-04
GO:0005737	cytoplasm	259	2.02E-04
GO:0030027	lamellipodium	21	1.91E-04
GO:0015629	actin cytoskeleton	25	1.95E-04
GO:0005789	endoplasmic reticulum membrane	62	1.88E-04
GO:0005886	plasma membrane	212	1.79E-04
GO:0001726	ruffle	15	3.17E-04
GO:0030670	phagocytic vesicle membrane	12	4.62E-04
GO:0005615	extracellular space	84	6.01E-04
GO:0005783	endoplasmic reticulum	58	6.25E-04
GO:0005913	cell-cell adherens junction	30	7.44E-04
GO:0000139	Golgi membrane	45	8.11E-04
GO:0001725	stress fiber	11	9.26E-04
GO:0043209	myelin sheath	18	2.13E-03
GO:0005765	lysosomal membrane	25	4.31E-03
GO:0001772	immunological synapse	8	6.00E-03
GO:0045177	apical part of cell	11	1.29E-02
GO:0005884	actin filament	10	1.74E-02
GO:0005794	Golgi apparatus	53	2.37E-02
GO:0005764	lysosome	20	2.56E-02
GO:0043025	neuronal cell body	25	2.50E-02
GO:0030426	growth cone	13	3.20E-02
GO:0002102	podosome	6	3.30E-02
GO:0005903	brush border	9	3.45E-02
GO:0031410	cytoplasmic vesicle	20	3.41E-02
GO:0044754	autolysosome	4	4.21E-02
GO:0043234	protein complex	29	4.70E-02

GO:0008305	integrin complex	6	4.89E-02
GO:0005515	protein binding	464	1.57E-15
GO:0051015	actin filament binding	19	2.68E-03
GO:0098641	cadherin binding involved in cell-cell adhesion	30	1.99E-03
GO:0019901	protein kinase binding	35	2.26E-03
GO:0005178	integrin binding	15	1.47E-02
GO:0031625	ubiquitin protein ligase binding	27	1.55E-02
GO:0019904	protein domain specific binding	21	3.76E-02

ID	KEGG pathways	Genes	Benjamini-corrected P-values
hsa04670	Leukocyte transendothelial migration	25	3.70E-06
hsa04145	Phagosome	27	2.18E-05
hsa04810	Regulation of actin cytoskeleton	31	9.10E-05
hsa04142	Lysosome	22	1.21E-04
hsa05323	Rheumatoid arthritis	18	2.09E-04
hsa04510	Focal adhesion	26	5.51E-03
hsa04666	Fc gamma R-mediated phagocytosis	15	5.75E-03
hsa05152	Tuberculosis	23	7.41E-03
hsa05100	Bacterial invasion of epithelial cells	14	7.65E-03
hsa05134	Legionellosis	11	1.47E-02
hsa05146	Amoebiasis	16	1.36E-02
hsa05144	Malaria	10	2.44E-02
hsa04514	Cell adhesion molecules (CAMs)	18	3.46E-02
hsa04380	Osteoclast differentiation	17	3.53E-02
hsa05110	Vibrio cholerae infection	10	3.45E-02

3.2 Genetic regulation of gene expression in macrophages

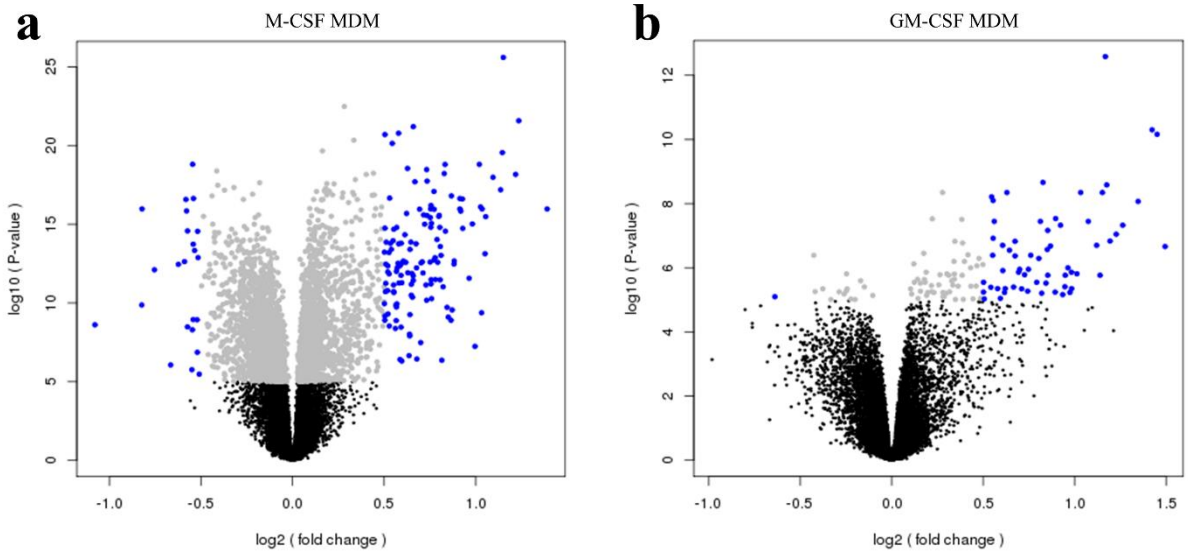

Figure 3.2-1: Volcano plots showing genes that were differentially expressed after mycobacterial infection in human macrophages differentiated from monocytes using either M-CSF or GM-CSF cytokines.

(**a**) Plot shows genes that were differentially expressed after infection of MDMs differentiated using M-CSF. (**b**) Plot shows genes that were differentially expressed after infection of MDMs differentiated using GM-CSF. The negative log10 P-values (y-axis) are plotted against log2 fold changes (x-axis). Black represents non-differentially expressed genes, while gray represents significantly differentially expressed upon BCG infection with *P* value $<10^{-5}$. Blue represent significantly differentially expressed genes with *P* value $<10^{-5}$ and log2 fold change > 0.5 or < -0.5.

Macrophages are the main host cells that provide a niche for the survival and replication of *M. tb*. They play instrumental roles in innate and acquired immunity by releasing cytokines, presenting antigen to lymphoid cells, and killing microbial pathogens. Macrophages can be differentiated from monocytes in various ways. In order to decide which MDM model would be more informative for the analysis of gene expression, we initially performed a pilot experiment comparing MDMs derived using M-CSF and GM-CSF (Verreck *et al.*, 2004). We used microarrays to evaluate gene expression in BCG-infected and non-infected MDMs from 33 healthy volunteers from the Cambridge BioResource cohort.

Dr. Y. Luo at the Wellcome Trust Sanger Institute performed the analysis. Upon mycobacterial infection, 149 genes significantly changed their expression in M-CSF MDMs and 60 genes in GM-CSF MDMs ($P < 10^{-5}$, **Figure 3.2-1a** and **Figure 3.2-1b**, respectively). Of these, 53 genes were consistently up- or down-regulated in both types of MDMs. As M-CSF MDMs responded stronger to mycobacterial infection, they were selected as a model for the genome-wide study of gene expression in *M. tb*-infected MDMs.

3.2.1 Study of gene expression in *M. tb*-infected monocyte-derived macrophages.

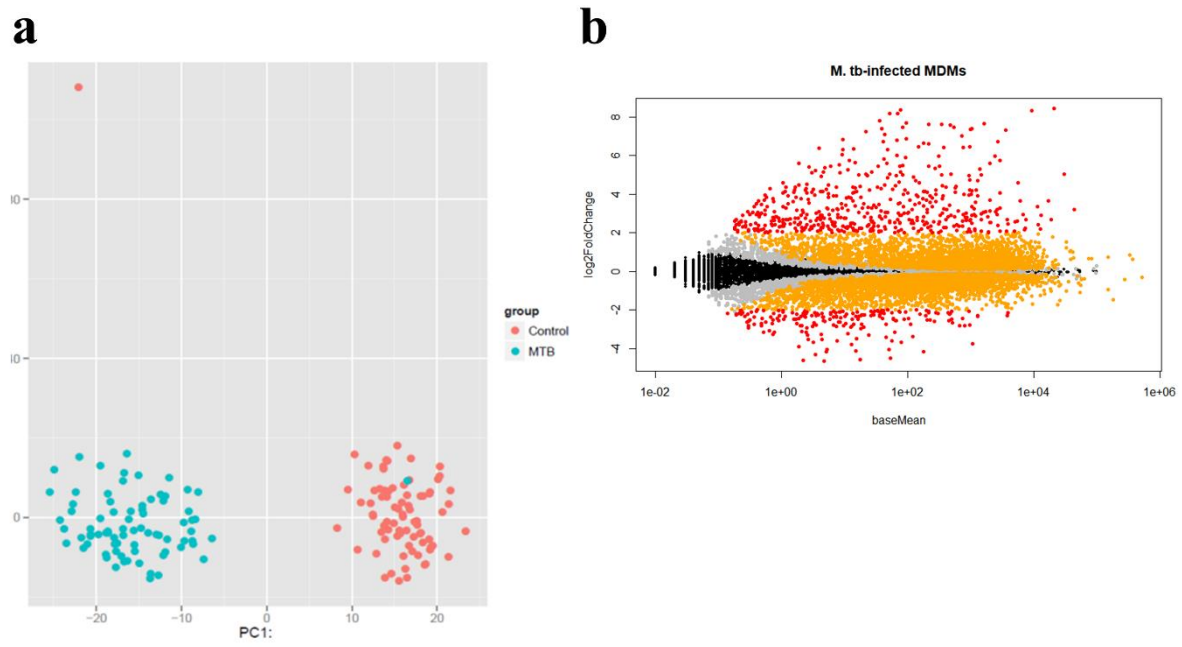

Figure 3.2-2: Gene expression in *M. tb*-infected versus non-infected macrophages.

Monocytes were differentiated to MDMs for 7 days and infected with *M. tb* for 24 hours. (**a**) Principal Component Analysis of transcriptome data plot shows two clusters of samples, *M. tb*-infected (blue) and non-infected macrophages (orange). (**b**) MA plot shows gene expression in *M. tb*-infected MDMs compared to uninfected MDMs. Differentially expressed genes are highlighted in gray, orange, and red (FDR < 0.5) and non-differentially expressed genes are presented by black dots (FDR > 0.05). Orange dots represent genes with FDR < 10^{-5} and red dots represent FDR < 10^{-5} and 2 log2 fold change.

We then studied blood from a cohort of 144 healthy volunteers obtained from the Cambridge BioResource. All participants recruited in this study were from Cambridgeshire. MDMs isolated from these donors were infected with *M. tb* with MOI of 4-5 or left uninfected for 24 hours. To study gene expression, we then lysed these cells, extracted RNA,

and prepared libraries for RNA-seq. Sequencing was done at the Cancer Research UK Cambridge Institute.

Bioinformatics analysis was done by Kitty Lo and Vincent Plagnol at the UCL Genetics Institute on 144 individuals of the cohort. First, performed principal component analysis (PCA) was done to evaluate the response of macrophages to *M. tb* infection. PCA showed a clear separation between *M. tb*-infected macrophages and non-infected macrophages, indicated by two clear clusters of samples; one subject was excluded from downstream analyses based on PCA results, as there was probably a sample swap (**Figure 3.2-2a**). In total, 8041 genes were found to be differentially expressed in mycobacteria-infected macrophages ($P < 1 \times 10^{-5}$) (**Figure 3.2-2b**).

To highlight the cellular and molecular functions of differentially induced genes in *M. tb*-macrophages, we performed functional annotations using DAVID for all GO categories and KEGG enrichment. Analysis of significantly up-regulated genes revealed significant enrichment of genes belonging to inflammatory response, response to cytokine, immune response, leukocyte migration, and *TNF*-signaling pathway ($P_{corrected} < 0.05$, **Table 3.2-2**). Conversely, negatively regulated genes showed few significant enrichment of GO annotations including metabolic pathways and metal ion binding ($P_{corrected} < 0.05$, **Table 3.2-3**).

3.2.2 Identification of regulatory variants

We next aimed to discover eQTLs in *M. tb*-infected and non-infected macrophages. To achieve that, we genotyped SNPs across the genome of each individual of these healthy volunteers and studied the association between gene expression obtained from their infected

or non-infected macrophages and genotypes at all SNPs. After mapping eQTLs separately in infected and non-infected macrophages, we found that expression of 4,182 and 3,551 genes was regulated by eQTLs in non-infected and infected macrophages, respectively (FDR < 0.05).

We then studied whether the strong *cis*-eQTLs ($P < 10^{-10}$) identified in our macrophage study were associated with TB in previous GWASes. We found that previously reported TB-associated SNPs on chromosomes 8, 11, and 18 were not eQTLs in our macrophage study. The lack of significant effect of these SNPs on gene expression in macrophages may be due to the low statistical power resulted from analyzing small sample size (144 samples). It is also possible that such variants exert their effects in a cell-specific manner. For example, we found that TB-associated variant on chromosome 8 identified in our GWAS was associated with the level of the *ASAP1* gene expression in DCs. Different eQTL effects in various cell types can be caused by differential binding of transcription factors that regulate gene expression in a tissue-specific manner. Thus, it is essential to study different relevant cells and tissues in order to discover true effects of eQTLs.

3.2.2.1 Identification of the cis-eQTL in the *TLR1* gene and its *trans*-eQTL network

We then set to investigate other eQTLs in the macrophage data. We noticed that in non-infected macrophages a group of polymorphisms located in the *TLR10-TLR1-TLR6* gene cluster on chromosome 4 was associated with the level of expression of *TLR1*, but not of the other two TLR genes, making it a *cis*-eQTL for *TLR1*. Multiple polymorphisms in this region

are associated with *TLR1* expression. These polymorphisms are in strong linkage disequilibrium with each other, making it difficult to establish the causative variant.

Importantly, the same group of polymorphisms in the *TLR1* gene has been reported to be associated with TB risk (Hart and Tapping, 2012; Schurz *et al.*, 2015), and they also showed evidence of association with TB risk in our GWAS (Curtis *et al.*, 2015), although did not reach the genome-wide significance level. For example, SNP rs73236618 is located between *TLR1* and *TLR10* genes. Its major allele is associated with the increased risk of TB (OR=1.13, P = 0.0025), and the same allele is associated with lower level of *TLR1* expression in macrophages ($P = 1.7 \times 10^{-9}$). Therefore, the lower level of *TLR1* expression induces a weaker immune response in macrophages, and that increases TB risk. While we found an association between these polymorphisms and the level of *TLR1* transcript, others have seen that the same polymorphisms are associated with the level of TLR1 protein on the surface of monocytes (Wurfel *et al.*, 2008).

M. tb is known to activate Toll-like receptors. In particular, it has triacylated lipoproteins LpqH, LprA, LprG, PhoS1 that bind to TLR1/TLR2 heterodimers, which induces downstream signaling. The crystal structure of the TLR1/TLR2 dimer binding to its ligand, a synthetic triacylated lipopeptide Pam3CSK4, was resolved ten years ago (Jin *et al.*, 2007). Mycobacterial cell wall glycolipids, including lipoarabinomannan (LAM), lipomannan (LM), and phosphatidylinositol mannoside (PIM), are another class of TLR1/TLR2 agonists. These lipoproteins and glycolipids vary in their potency to induce downstream responses (Harding and Boom, 2010).

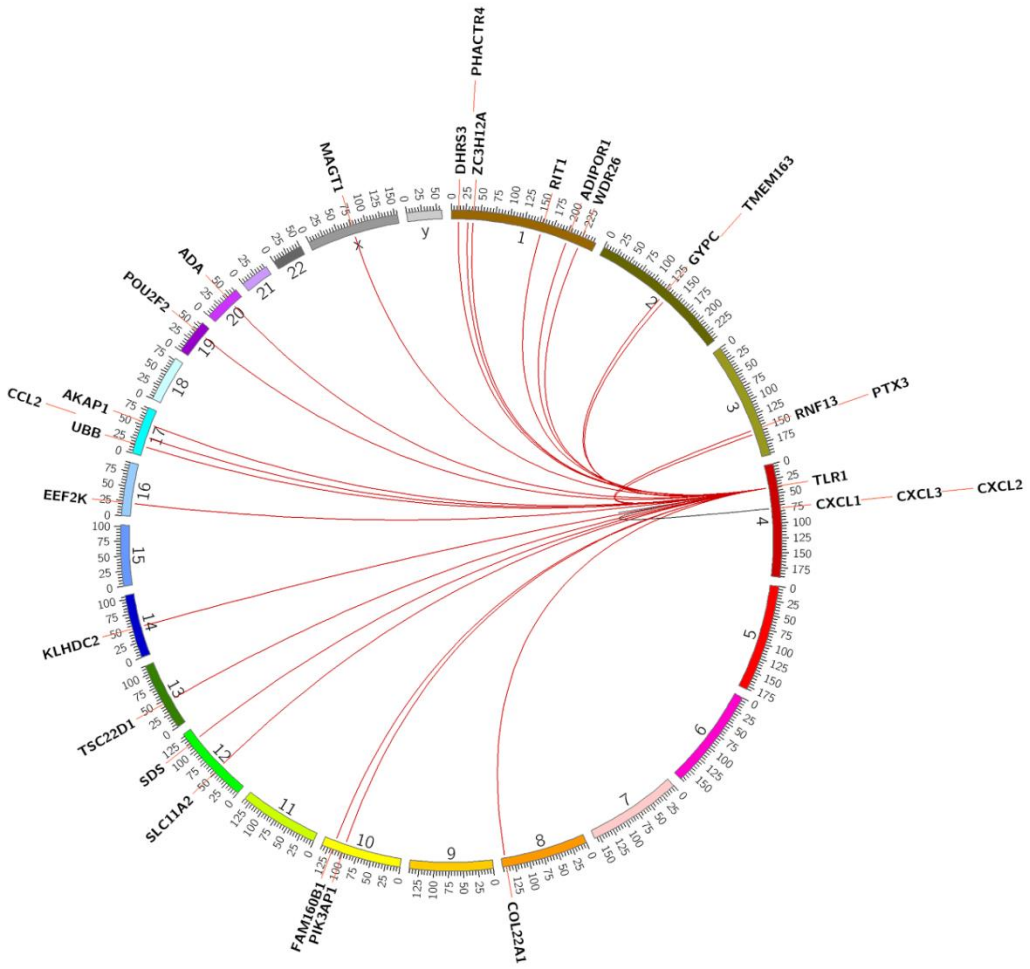

Figure 3.2-3: Circular plot illustrating the genomic location of eQTLs for rs17616434 in MDMs.

From outside to inside: chromosome number; relative distance along chromosome. Red lines indicate genes regulated in *trans*, which are potential TLR1 targets.

We also found that the same group of polymorphisms was associated with levels of expression of 37 genes located in different parts of the genome in *M. tb*-infected macrophages, making it a *trans*-eQTL that influence expression levels for all these genes in (**Table 3.2-1**). For example, rs17616434 acted as *trans*-eQTL and affected the level of expression of 27 genes (**Figure 3.2-3**).

Table 3.2-1: Transcription network regulated by the *trans*-eQTL in the TLR1 gene.

Gene	baseMean expression	log2FC after *M. tb* infection	chromosome
ADA	628.32	1.62	20
ADIPOR1	4604.33	0.25	1
CCL7	349.30	4.44	17
CCL2	5973.63	3.66	17
CEBPD	408.73	-0.50	8
COL22A1	115.02	1.72	8
CXCL5	9084.83	8.35	4
CXCL1	1037.65	7.39	4
CXCL3	1368.77	5.31	4
CXCL2	843.01	2.63	4
DHRS3	917.92	-0.85	1
DSE	1465.59	2.09	6
EEF2K	693.87	0.58	16
FAM160B1	552.93	-0.04	10
GALM	1448.56	-1.01	2
GGA2	2488.45	-0.57	16
GYPC	788.17	0.28	2
IL6	214.87	7.61	7
KLHDC2	548.20	-0.69	14
LYN	4974.41	1.83	8
OLIG1	30.12	1.58	21
PIK3AP1	9843.93	0.98	10
POU2F2	194.69	1.82	19
PPARD	2077.71	0.99	6
PTX3	78.11	-0.05	3
RIT1	1593.01	0.51	1
RNF13	7214.68	-0.12	3
SDS	3165.01	-0.62	12
SLC11A2	2733.98	0.88	12
TBL2	439.46	-0.06	7
TMEM163	279.92	-0.38	2
TMED3	1192.54	-0.22	15
TSC22D1	1713.46	0.69	13
WDR26	3448.30	0.29	1
ZC3H12A	759.62	2.93	1
MAGI1	0.20	-0.41	3

Functional annotation analysis revealed that this *TLR1*-driven network was significantly enriched for genes involved in inflammatory response, chemokine signaling pathway, and intracellular infections salmonellosis and legionellosis ($P_{corrected} < 0.01$ and 0.03, respectively, **Table 3.2-2**).

There is a recognizable group of genes in our *TLR1*-regulated network that encodes chemokines and cytokines including (*CCL2, CCL7, CXCL1, CXCL2, CXCL3,* and *IL6*). *CCL2* has been reported to be elevated in blood obtained from pulmonary tuberculosis patients (Lin *et al.*, 1998). *CCL2* and *CCL7* attract monocytes and macrophages while *CXCL1, CXCL2*, and *CXCL3* recruit neutrophils. Therefore, it is likely that genetic polymorphisms associated with lower *TLR1* expression and therefore smaller TLR1 protein abundance will lead to a weaker cytokine and chemokine responses to *M. tb* infection. This may delay granuloma formation leading to insufficient restriction of bacterial growth, thus predisposing to TB. The contribution of the rest of the *TLR1*-controlled genes in TB pathogenesis is yet to be determined. Some of these genes have been previously linked with TB. Thus, adenosine deaminase encoded by the *ADA* gene is a very sensitive biomarker used to diagnose patients with pleural tuberculosis (Banales *et al.*, 1991). Likewise, PTX3 (pentraxin 3, long) was found to be elevated in plasma of TB patients compared to healthy controls. The success of TB treatment leads to the reduction of the PTX3 levels, whilst the failure of the treatment results in a further increase in its levels (Azzurri *et al.*, 2005). Another gene, *ZC3H12A* (Zinc Finger CCCH-type containing 12A), is involved in post-transcriptional regulation of pro-inflammatory cytokine production and has been described in host defense mechanisms in TB pathogenesis (Lim *et al.*, 2015).

In summary, this finding suggests that expression of multiple immune genes in the *M. tb*-infected macrophages depends on the level of expression of *TLR1*, which itself is affected by polymorphisms in the *TLR1* gene. This functional effect explains the association of the TLR1 polymorphisms with TB and highlights downstream *TLR1*-regulated genes as important components of anti-TB immune response. The discovery of this *TLR1*-driven network will help better understand mechanisms of macrophage responses to mycobacterial infection. Proteins encoded by some of these genes may be useful as biomarkers or might become targets for new therapeutic approaches.

Table 3.2-2: GO enrichment of significantly up-regulated genes in *M. tb* infected macrophages.

ID	Gene Ontology terms	Genes	Benjamini corrected P-value
GO:0005515	protein binding	1618	2.2E-30
GO:0006954	inflammatory response	143	2.5E-23
GO:0005829	cytosol	687	8.9E-22
GO:0016020	membrane	494	4.6E-22
GO:0005654	nucleoplasm	576	1.1E-17
GO:0070062	extracellular exosome	559	4.7E-13
GO:0005737	cytoplasm	938	1.3E-11
GO:0005925	focal adhesion	110	1.8E-09
GO:0071222	cellular response to lipopolysaccharide	44	6.3E-07
GO:0009986	cell surface	132	4.4E-07
GO:0034097	response to cytokine	27	9.7E-07
GO:0006955	immune response	109	2.7E-06
GO:0042127	regulation of cell proliferation	59	4.4E-06
GO:0032496	response to lipopolysaccharide	53	1.5E-05
GO:0006928	movement of cell or subcellular component	34	2.4E-05
GO:0008360	regulation of cell shape	46	6.4E-05
GO:0051092	positive regulation of NF-kappaB transcription factor activity	44	8.8E-05
GO:0050900	leukocyte migration	41	1.4E-04
GO:0031625	ubiquitin protein ligase binding	75	1.0E-03
GO:0032587	ruffle membrane	30	2.4E-04
GO:0005524	ATP binding	291	1.1E-03
GO:0048661	positive regulation of smooth muscle cell proliferation	25	4.1E-04
GO:0005794	Golgi apparatus	177	2.7E-04
GO:0016607	nuclear speck	55	4.2E-04
GO:0006915	apoptotic process	126	9.8E-04
GO:0051082	unfolded protein binding	36	2.6E-03
GO:0044822	poly(A) RNA binding	225	2.4E-03
GO:0030433	ER-associated ubiquitin-dependent protein catabolic process	24	1.4E-03
GO:0048870	cell motility	14	1.4E-03
GO:0045121	membrane raft	55	7.5E-04
GO:0008285	negative regulation of cell proliferation	93	1.7E-03
GO:0000139	Golgi membrane	126	8.8E-04
GO:0019221	cytokine-mediated signaling pathway	40	2.1E-03
GO:0007267	cell-cell signaling	65	2.5E-03
GO:0002230	positive regulation of defense response to virus by host	13	2.6E-03
GO:0031663	lipopolysaccharide-mediated signaling pathway	16	2.6E-03
GO:0008380	RNA splicing	47	2.8E-03

GO:0043547	positive regulation of GTPase activity	123	2.8E-03
GO:0048471	perinuclear region of cytoplasm	130	1.4E-03
GO:0071407	cellular response to organic cyclic compound	23	3.0E-03
GO:0005856	cytoskeleton	85	1.5E-03
GO:0010628	positive regulation of gene expression	66	3.3E-03
GO:0030036	actin cytoskeleton organization	39	3.6E-03
GO:0014911	positive regulation of smooth muscle cell migration	12	4.5E-03
GO:0001618	virus receptor activity	25	1.2E-02
GO:0007155	cell adhesion	102	5.7E-03
GO:0007265	Ras protein signal transduction	25	5.9E-03
GO:0060333	interferon-gamma-mediated signaling pathway	25	7.4E-03
GO:0051897	positive regulation of protein kinase B signaling	28	7.4E-03
GO:0050727	regulation of inflammatory response	23	8.2E-03
GO:0032570	response to progesterone	17	8.4E-03
GO:0051607	defense response to virus	45	8.8E-03
GO:0043123	positive regulation of I-kappaB kinase/NF-kappaB signaling	44	1.0E-02
GO:0004872	receptor activity	55	2.1E-02
GO:0007249	I-kappaB kinase/NF-kappaB signaling	22	1.1E-02
GO:0005911	cell-cell junction	45	6.1E-03
GO:0005813	centrosome	92	6.2E-03
GO:0019901	protein kinase binding	85	2.2E-02
GO:0031410	cytoplasmic vesicle	57	6.2E-03
GO:0009615	response to virus	33	1.3E-02
GO:0042802	identical protein binding	151	2.5E-02
GO:0030335	positive regulation of cell migration	48	1.5E-02
GO:0035994	response to muscle stretch	10	1.5E-02
GO:0007165	signal transduction	221	1.6E-02
GO:0000982	transcription factor activity, RNA polymerase II core promoter proximal region sequence-specific binding	12	2.9E-02
GO:0045335	phagocytic vesicle	16	9.3E-03
GO:0071260	cellular response to mechanical stimulus	24	1.8E-02
GO:0046718	viral entry into host cell	26	1.8E-02
GO:0008283	cell proliferation	82	1.9E-02
GO:0005838	proteasome regulatory particle	8	1.0E-02
GO:0006986	response to unfolded protein	17	1.9E-02
GO:0043234	protein complex	88	1.1E-02
GO:0005525	GTP binding	85	3.4E-02
GO:0005887	integral component of plasma membrane	256	1.1E-02
GO:0030336	negative regulation of cell migration	29	2.3E-02
GO:0030168	platelet activation	33	2.7E-02
GO:0045944	positive regulation of transcription from RNA polymerase II promoter	188	3.1E-02

GO:0050728	negative regulation of inflammatory response	25	3.4E-02
GO:0000187	activation of MAPK activity	31	3.4E-02
GO:1901998	toxin transport	15	3.5E-02
GO:0001666	response to hypoxia	44	3.7E-02
GO:0045893	positive regulation of transcription, DNA-templated	107	3.8E-02
GO:0043209	myelin sheath	39	2.0E-02
GO:0016032	viral process	68	3.9E-02
GO:0005770	late endosome	33	2.1E-02
GO:0046627	negative regulation of insulin receptor signaling pathway	13	4.2E-02
GO:0010634	positive regulation of epithelial cell migration	14	4.4E-02
GO:0009611	response to wounding	21	4.8E-02
GO:0032693	negative regulation of interleukin-10 production	8	4.9E-02
GO:0048010	vascular endothelial growth factor receptor signaling pathway	23	4.9E-02
GO:0048013	ephrin receptor signaling pathway	26	4.9E-02
GO:0030659	cytoplasmic vesicle membrane	33	3.6E-02
GO:0005789	endoplasmic reticulum membrane	160	4.5E-02
GO:0000932	cytoplasmic mRNA processing body	23	4.4E-02
GO:0042629	mast cell granule	10	4.7E-02

ID	KEGG pathways	Genes	Benjamini corrected P-value
hsa05169	Epstein-Barr virus infection	74	2.3E-09
hsa04668	TNF signaling pathway	50	3.5E-09
hsa04380	Osteoclast differentiation	53	3.0E-07
hsa04060	Cytokine-cytokine receptor interaction	78	5.8E-07
hsa05132	Salmonella infection	38	9.5E-07
hsa04620	Toll-like receptor signaling pathway	42	1.4E-05
hsa05134	Legionellosis	27	1.4E-05
hsa04666	Fc gamma R-mediated phagocytosis	36	1.5E-05
hsa05152	Tuberculosis	59	4.2E-05
hsa05164	Influenza A	58	4.8E-05
hsa04621	NOD-like receptor signaling pathway	25	2.2E-04
hsa05145	Toxoplasmosis	42	2.3E-04
hsa05140	Leishmaniasis	29	3.8E-04
hsa05142	Chagas disease (American trypanosomiasis)	37	7.4E-04
hsa05131	Shigellosis	26	1.1E-03
hsa04630	Jak-STAT signaling pathway	46	1.7E-03
hsa05168	Herpes simplex infection	54	3.0E-03
hsa05205	Proteoglycans in cancer	57	5.0E-03
hsa05203	Viral carcinogenesis	58	5.2E-03
hsa04064	NF-kappa B signaling pathway	30	5.8E-03

hsa04010	MAPK signaling pathway	68	8.3E-03
hsa05133	Pertussis	26	1.3E-02
hsa05321	Inflammatory bowel disease (IBD)	23	1.5E-02
hsa04144	Endocytosis	67	1.7E-02
hsa05162	Measles	39	2.0E-02
hsa05230	Central carbon metabolism in cancer	22	3.3E-02
hsa04623	Cytosolic DNA-sensing pathway	22	3.3E-02
hsa04145	Phagosome	42	4.6E-02

Table 3.2-3: GO enrichment of significantly down-regulated genes in *M. tb*-infected macrophages.

ID	Gene Ontology terms	Genes	Benjamini corrected P-value
GO:0046872	metal ion binding	445	4.2E-13
GO:0005829	cytosol	626	1.1E-10
GO:0005634	nucleus	950	6.8E-10
GO:0005622	intracellular	282	9.0E-09
GO:0005737	cytoplasm	905	3.5E-08
GO:0005739	mitochondrion	265	1.1E-05
GO:0005515	protein binding	1454	7.5E-05
GO:0003700	transcription factor activity, sequence-specific DNA binding	193	8.0E-03
GO:0016020	membrane	384	9.8E-03
GO:0005764	lysosome	55	1.4E-02
GO:0043231	intracellular membrane-bounded organelle	114	1.5E-02
GO:0005759	mitochondrial matrix	73	1.6E-02

ID	KEGG pathways	Genes	Benjamini corrected P-value
hsa01100	Metabolic pathways	226	1.21E-03

Table 3.2-4: GO enrichment of TLR1-regulated network genes

ID	Gene Ontology terms	Genes	Benjamini corrected P-value
GO:0006954	inflammatory response	10	6.73E-06
GO:0070098	chemokine-mediated signaling pathway	6	3.97E-05
GO:0008009	chemokine activity	5	2.55E-04
GO:0045236	CXCR chemokine receptor binding	3	7.43E-03
GO:0006935	chemotaxis	5	1.08E-02
GO:0006955	immune response	7	1.10E-02
GO:0071347	cellular response to interleukin-1	4	2.76E-02

ID	KEGG pathways	Genes	Benjamini corrected P-value
hsa04062	Chemokine signaling pathway	7	8.70E-04
hsa04668	TNF signaling pathway	5	8.16E-03
hsa05134	Legionellosis	4	1.15E-02
hsa05132	Salmonella infection	4	3.00E-02

3.2.3 Identification of the TB-associated *cis*-eQTL variant in the *ARHGAP27* gene that encodes a Rho-GAP protein

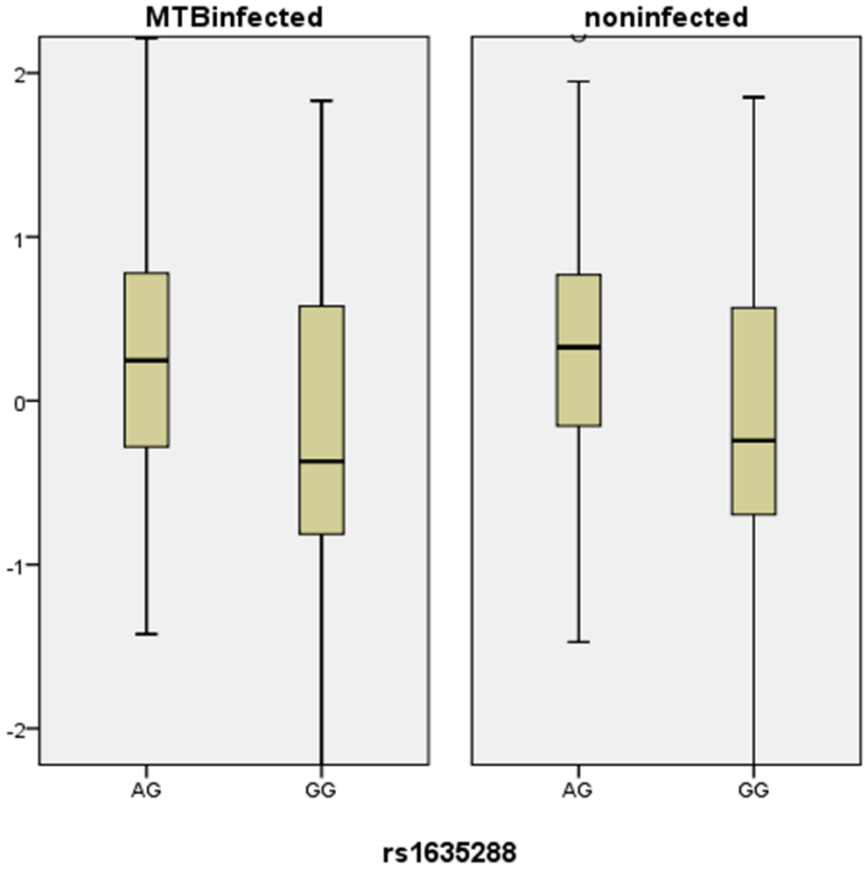

Figure 3.2-4: Box-whisker plot shows the DNA variant (rs1635288) act as *cis*-eQTL for ARHGAP27 in non-infected human macrophages or infected with *M. tb*.

Another finding that emerged from our study of gene expression in macrophages was the discovery of a new *cis*-eQTL for the *ARHGAP27* gene. We found that DNA polymorphism rs1635288 located 245 kb upstream of the *ARHGAP27* gene, is highly associated with its expression in both *M. tb*-infected and non-infected macrophages ($P = 2.4 \times 10^{-18}$, **Figure 3.2-4**). In addition, the same variant is associated with TB risk in our GWAS (Curtis *et al.*, 2015). Its allele A is associated with the increased level of the *ARHGAP27*

expression and protects from TB in our GWAS (OR = 0.86, P = 8.3 x 10^{-5}). This level of association did not reach genome-wide significance, and hence the association of this SNP with TB was not recognized. However, our finding that this SNP is a strong eQTL affecting gene expression in macrophages, a cell type that is particularly important in TB pathogenesis, made this SNP a strong candidate, suggesting that its association with TB is genuine rather than a statistical artifact. Our data also showed that the level of expression of *ARHGAP27* was reduced after *M. tb* infection (-0.15 log 2-fold change and FDR < 0.05). Overall, these findings linked ARHGAP27 with TB pathogenesis. Therefore, I decided to study the role of ARHGAP27 using macrophage models of mycobacterial infection that I established previously while studying the role of ASAP1.

ARHGAP27 is a Rho-GAP that regulates the activity of Rho GTPases. The cycling of Rho GTPase is tightly controlled by Rho GEFs, Rho GAPs, and guanine nucleotide dissociation inhibitors (GDIs) (Heasman and Ridley, 2008). Since their discovery in the 1980s, around 80 members of Rho-GAP family have been recognized in *Homo sapiens*. In fact, Rho GAPs far outnumber the 20 Rho GTPases, indicating that some GAPs play specific function for each Rho GTPase or have tissue-specific functions (Peck *et al.*, 2002; Tcherkezian and Lamarche-Vane, 2007; Hodge and Ridley, 2016). Few Rho GAPs have been investigated in mammalian cells for their role in cellular functions. ARHGAP27 is multidomain Rho-GAP that contains an N-terminus Src homology 3 (SH3) domain followed by WW domain, a PH domain, and a C-terminus Rho-GAP domain. ARHGAP27 exerts GTPase activity towards Cdc42 and Rac1, but not RhoA (Sakakibara *et al.*, 2004). ARHGAP27 was identified as an interacting partner for CIN85 (Cbl-interacting protein of 85kDa). It was shown that overexpression of truncated form of ArhGAP27, lacking the three

WW domains, inhibited internalization of transferrin receptor significantly, suggesting that ARHGAP27 may be implicated in clathrin-mediated endocytosis (Sakakibara *et al.*, 2004).

3.2.4 Expression of ARHGAP27 is reduced after BCG infection

Initially, I tested the level of *ARHGAP27* expression in THP-1 cells and its change after mycobacterial infection. PMA-differentiated THP-1 cells were infected with BCG at an MOI of 10. RNA was collected at 1, 4, and 24 hours. The qPCR results demonstrated that the level of *ARHGAP27* was significantly reduced upon infection with BCG at 1 hour to 24 hours (**Figure 3.2-5**).

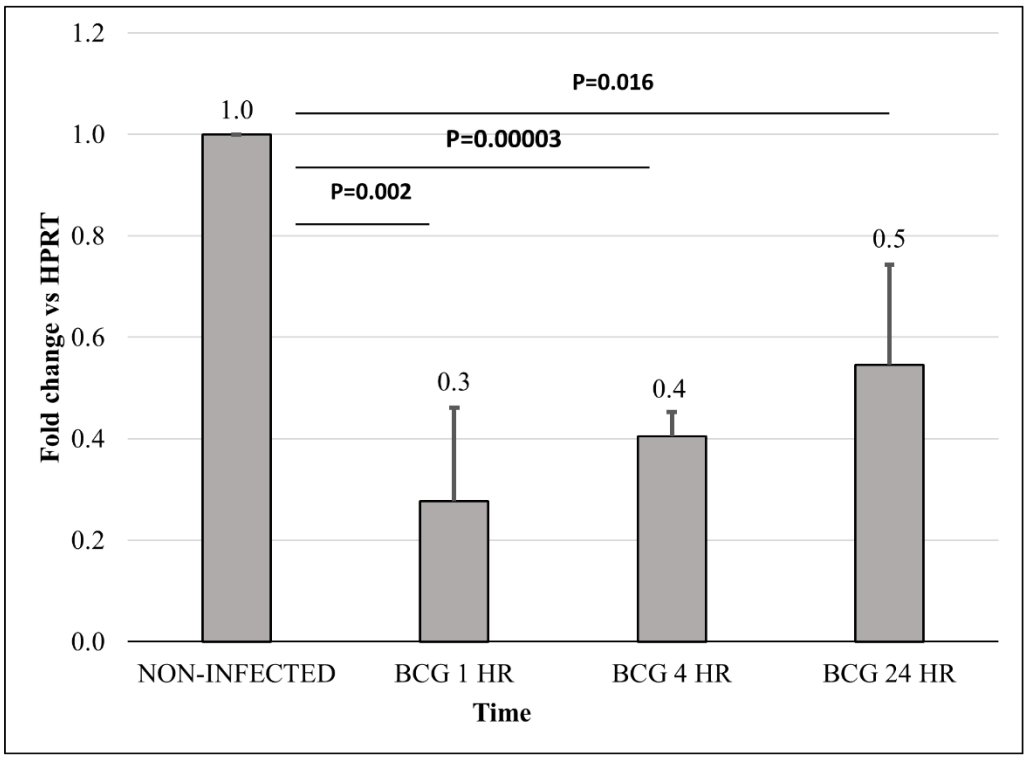

Figure 3.2-5: ARHGAP27 expression in macrophages

The qPCR result shows that *ARHGAP27* expression level in THP-1 macrophages infected with BCG at MOI of 10. The data are expressed as fold change normalized to the housekeeping gene HPRT Data indicate mean ± SD from three independent experiments performed in duplicates. Two-tailed Student's t-test was used.

3.2.5 Making the ARHGAP27 knockout THP-1 cell line

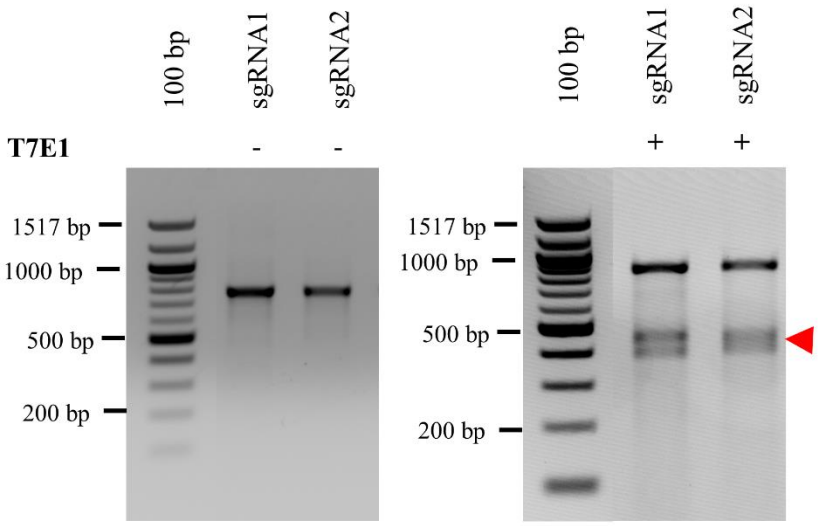

Figure 3.2-6: T7E1 assay validates the efficiency for sgRNAs targeting ARHGAP27.

PCR products flanking exon 3 of *ARHGAP27* were amplified from DNA extracted from a pool of CRISPR-Cas9 edited cells transduced with lentiGuide-Puro-*ARHGAP27* guides. Heteroduplexes products were subjected to T7E1 nuclease to induce mismatch bands where indels found. The PCR products were visualized using 2% of agarose gel before T7E1 treatment (left) or after T7E1 treatment (right). Mismatched bands were not observed in PCR amplicons that were not incubated with the T7E1 enzyme. Mismatched bands were displayed after the T7E1 treatment in transduced cells as indicated by red arrows.

The ARHGAP27 protein is a regulator of Rho GTPases. The Rho GTPase activities are known to be essential for various processes in cells, such as cytoskeletal dynamics, phagocytosis, motility and other cell functions. However, the role of ARHGAP27 in macrophages and during mycobacteria infection has not been explored. To characterize its functions, I took a similar approach to that used for the characterization of *ASAP1* in the macrophage-like THP-1 cell line. I set to generate the *ARHGAP27*- knockout in THP-1 cells using CRISPR-Cas9. First, I designed two sgRNAs recognizing exon 3 of *ARHGAP27* (ENST00000376922.6) using an online tool and cloned them into the lentiGuide-Puro vector.

LentiGuide-Puro-*ARHGAP27* guides were transduced into Hela cells expressing Cas9 to validate their efficiency in genome editing. Two days after transduction, genomic DNA was extracted, amplified, and incubated with the T7E1 enzyme. The enzyme induced cleavage of the ARHGAP27 amplicons containing mutations (**Figure 3.2-6**).

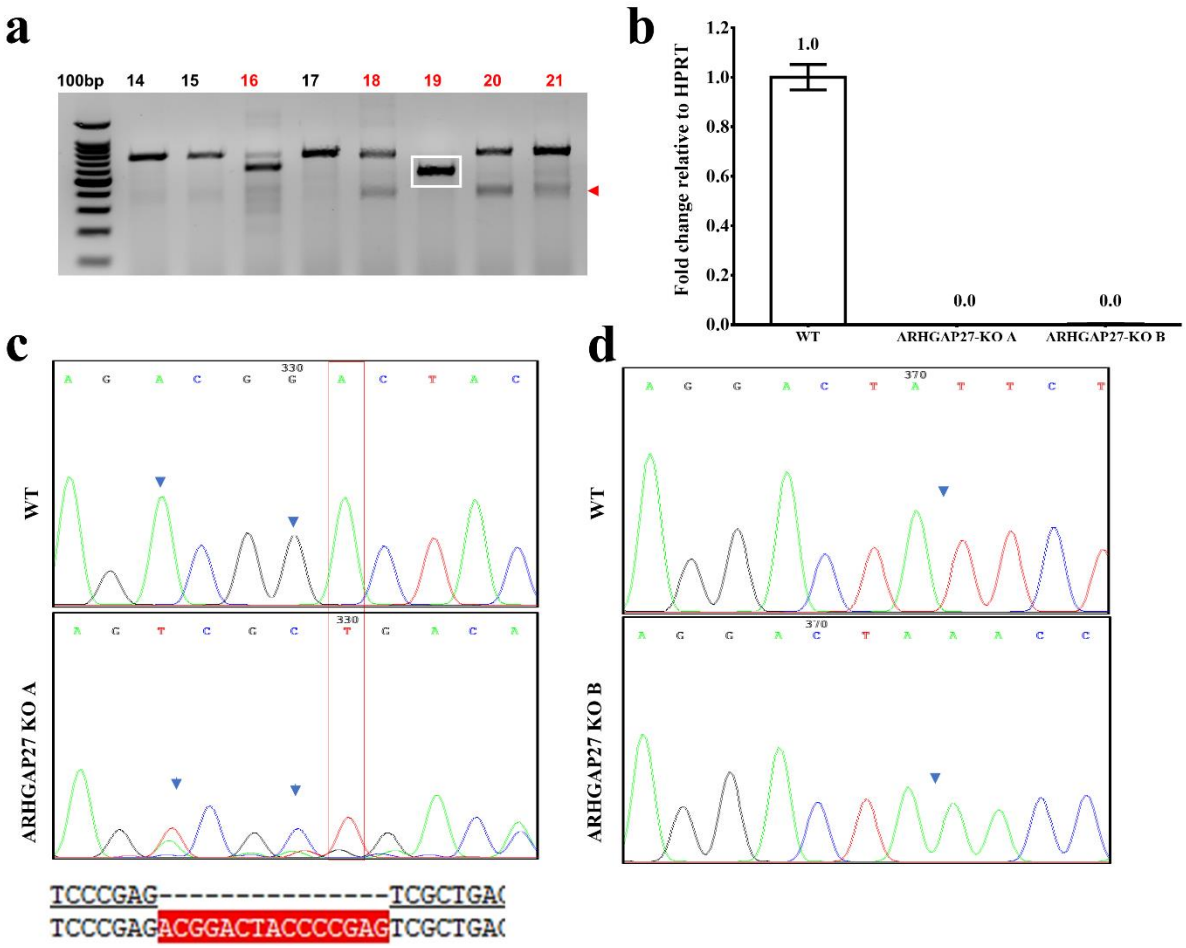

Figure 3.2-7: Generation and validation of the ARHGAP27-KO THP-1 single cell clones.

(**a**) Representative image of the T7E1 assay showing PCR amplicons from individual clones as indicated by numbers on the top. Single cell clones that were sensitive to the T7E1 enzyme are indicated by red numbers; unedited are labeled with black numbers. The band from the single cell clone #19, ARHGAP27-KO clone B shown in white rectangle migrated faster than other clones, indicating a large deletion. (**b**) Quantitative PCR was performed with the ARHGAP27 primers flanking the targeted exon to confirm CRISPR-Cas9 editing in the ARHGAP27-KO clones A and B. (**c**) Sanger sequencing of the ARHGAP27-KO clone A showed a deletion of 15 nucleotides. Arrows indicate sites of multiple editing and red rectangle shows a missing A in both alleles. (**d**) Sanger sequencing of the ARHGAP27-KO clone B showed a deletion of 234 nucleotides from the genomic DNA including 125 nucleotides located within the ARHGAP27 exon. Arrow indicates the editing site.

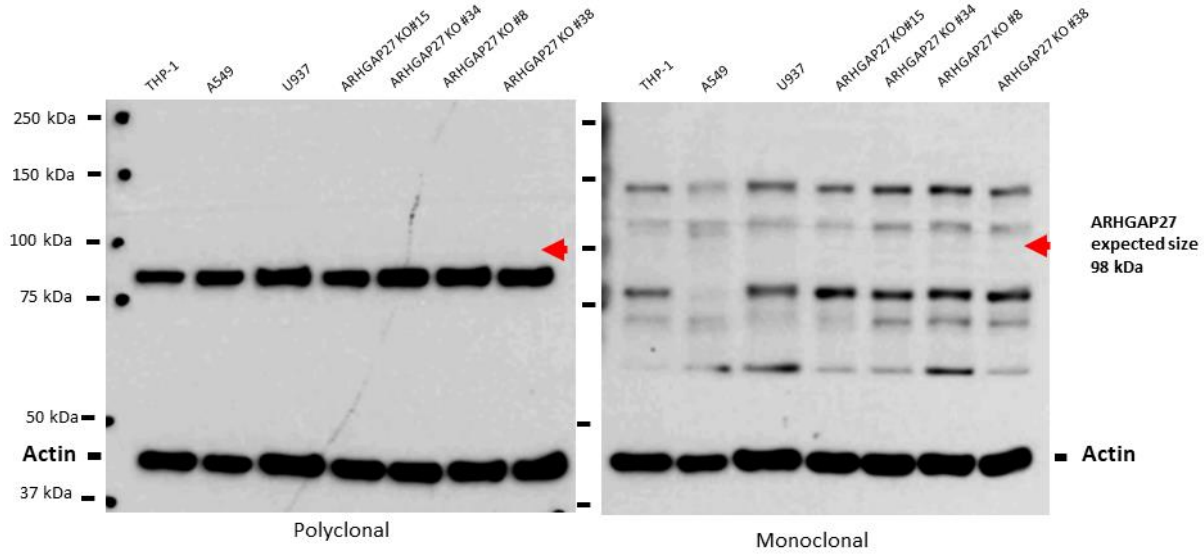

Figure 3.2-8: Western blotting for ARHGAP27.

Cell lysates of the wild-type cells (THP-1, A579, and U937) and the ARHGAP27 KO single-cells (KO#18, KO#34, KO#8, and KO#38) were probed with ARHGAP27 polyclonal (left plot) and monoclonal (right plot) antibody and Actin antibody as a loading control. Red arrows show the expected size of the ARHGAP27 protein (98 kDa).

To generate the ARHGAP27-KO THP-1 cells, I transduced THP-1 cells that stably express Cas9 with the lentiviral vector LentiGuide-Puro-*ARHGAP27* harboring either sgRNA1 or sgRNA2. Transduced cells were selected with puromycin and subjected to limiting dilution for clonal expansion. Single cell clones were then screened for genome editing using T7E1 assay (**Figure 3.2-7a**). All single cell clones that were suggestive of a mutation in the T7E1 assay were then subjected to further inspection to confirm genome editing. To confirm the knockout of the *ARHGAP27* gene, I tested several antibodies against ARHGAP27 for western blotting (**Figure 3.2-8**) and immunochemistry staining. Unfortunately, none of the tested antibodies showed specificity to the ARHGAP27 protein, so

they were not suitable for western blotting. Consequently, two potential ARHGAP27-KO THP-1 clones (A from sgRNA1 and B from sgRNA2) were examined for the *ARHGAP27* expression using qPCR with a set of primers flanking the sgRNAs target sites. Results showed that the ARHGAP27 expression was absent in both clones (**Figure 3.2-7b**). Sanger sequencing showed that clone A had a deletion of 15 nucleotides (**Figure 3.2-7c**) and clone B had a deletion of 234 nucleotides from the genomic DNA, including 125 nucleotides within the ARHGAP27 exon 3 (**Figure 3.2-7d**).

3.2.5.1 Knockout of the ARHGAP27 gene reduces the uptake of mycobacteria by macrophages

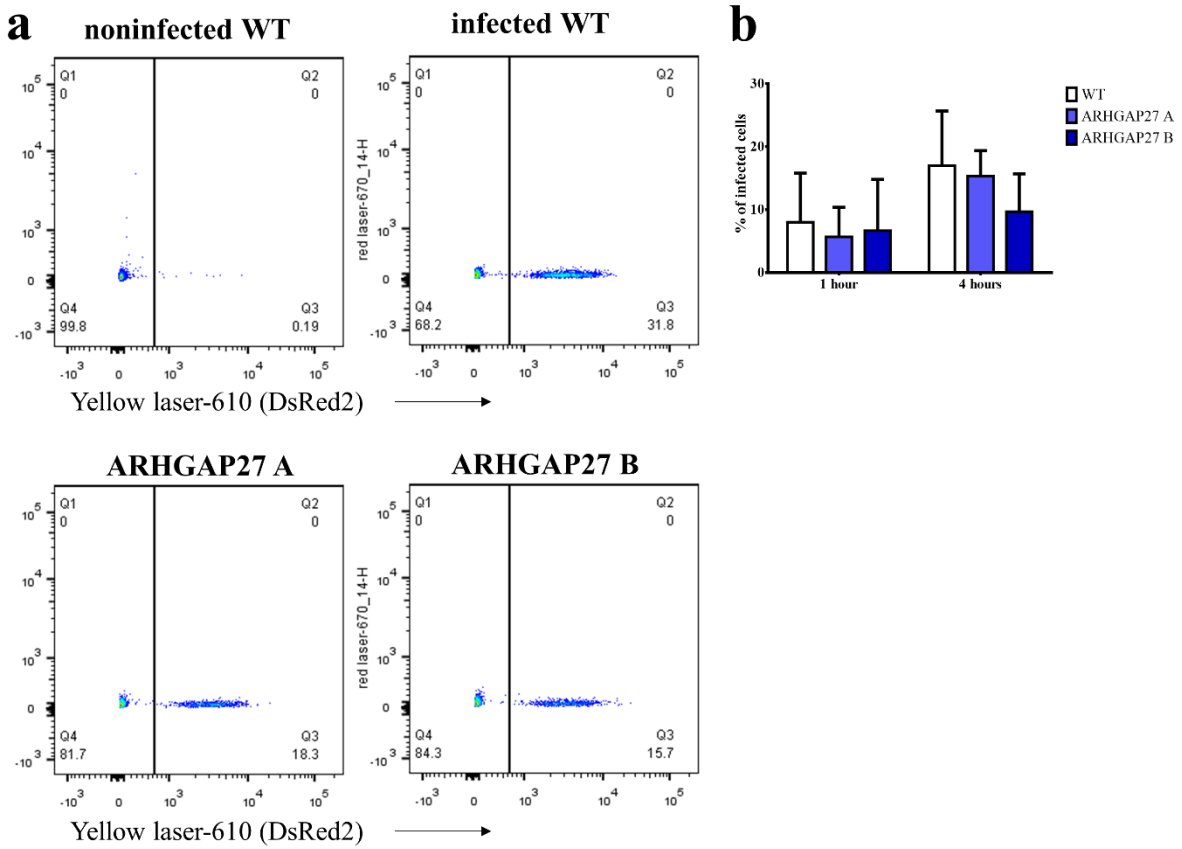

Figure 3.2-9: Flow cytometry assessment of the phagocytosis of mycobacteria in THP-1 cells lacking ARHGAP27

Differentiated wild-type THP-1 cells and ARHGAP27-KO clones A and B were infected with the DsRed2-expressing BCG at MOI of 10 for 1 and 4 hours. Phagocytosis was assessed using flow cytometry. (**a**) Representative images of flow cytometry. The DsRed2-expressing BCG was detected by yellow laser channel. (**b**) Graph representing data as means ± SD from three independent experiments. Two-tailed Student's t-test was used.

Despite the fact that little is known about ARHGAP27, one study has linked it to the receptor-mediated endocytosis (Sakakibara *et al.*, 2004). To study the role of ARHGAP27 in the macrophage engulfment of mycobacteria, I analyzed THP-1 clonal cell lines, in which ARHGAP27 was knocked out. The differentiated control THP-1 cells and the ARHGAP27-KO clones were infected with fluorescent BCG at MOI of 10 and analyzed for infection using flow cytometry. Initial data show reduced uptake in clonal cell lines lacking ARHGAP27 at 4 hours after infection (**Figure 3.2-9a**). However, further quantitative analysis of flow cytometry results from three experiments indicated that the reduction in macrophage uptake of mycobacteria was not significant at 1 and 4 hours following infection (**Figure 3.2-9b**). Nevertheless, the flow cytometry method has limited power to detect fluorescent signal from macrophages infected with DsRed2-BCG, as discussed earlier and shown in **Figure 3.1-21** and **Figure 3.1-22**.

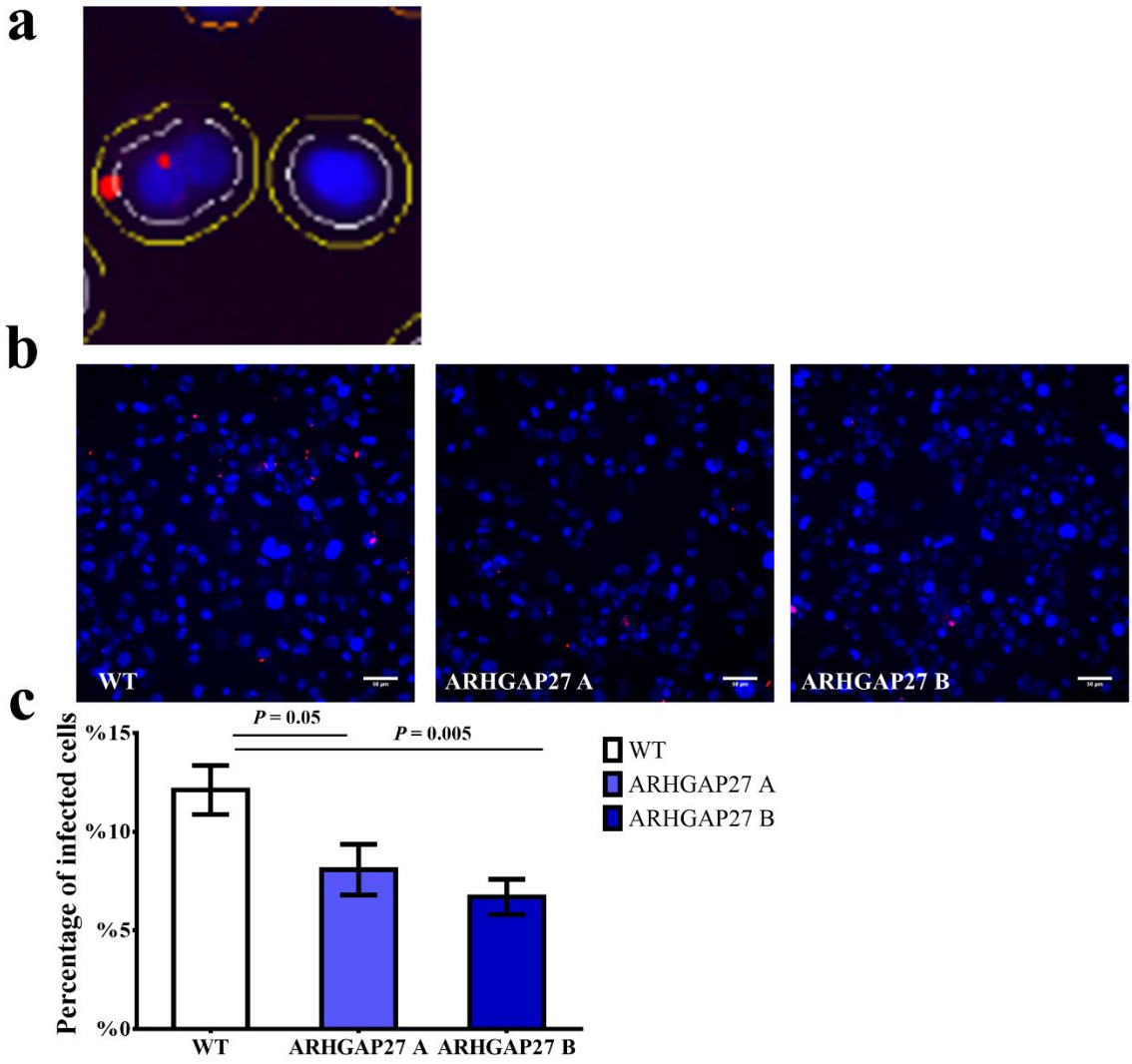

Figure 3.2-10: Assessment of the phagocytosis of mycobacteria in THP-1 cells lacking ARHGAP27 using automated fluorescence microscope.

Differentiated wild-type THP-1 cells and ARHGAP27-KO clones A and B were infected with the DsRed2-expressing BCG at MOI of 10 for 4 hours. Cells were fixed and stained for nuclei using the Hoechst dye. Images were obtained using Thermo Fischer Scientific ArrayScan XTI automated fluorescence microscope with 20x magnification Zeiss objective. (**a**) Representative image shows gate around the nucleus (white) and another gate (yellow) highlight the extended area to be included in spot detection. (**b**) Representative images for the wild-type THP-1 cells and ARHGAP27-KO clones A and clone B infected with the BCG-expressing DeRed2. Scale bar, 50µm. (**c**) Data expressed as mean ± s.e.m from two experiments (7000-9000 cells per line). Two-tailed Student's t-test was used.

To overcome the limitations encountered in the previous experiment, I assessed the impact of the ARHGAP27 knockout on macrophage uptake of mycobacteria using a high-throughput microscopy imaging system. The wild-type THP-1 cells and the ARHGAP27-KO THP-1 clones were differentiated in 24-well plates, infected with DsRed2-BCG at MOI of 10, and incubated for 4 hours. Images were acquired using Cellomics Arrayscan XTI automated fluorescence machine using parameters and settings as in (**Figure 3.1-24**). As shown in (**Figure 3.2-10b**), mycobacteria infection was reduced in the THP-1 clones lacking ARHGAP27. Quantitative data analysis shows that 8% of the ARHGAP27-KO clone A and 6.7% of the ARHGAP27-KO clone B were infected with DsRed2-BCG compared to 12% observed in control cells (**Figure 3.2-10c**). Thus, the absence of ARHGAP27 in macrophages led to a significant reduction of mycobacteria uptake ($P < 0.05$, **Figure 3.2-10c**).

3.2.5.2 ARHGAP27-knockout macrophages have impaired capacity for matrix degradation

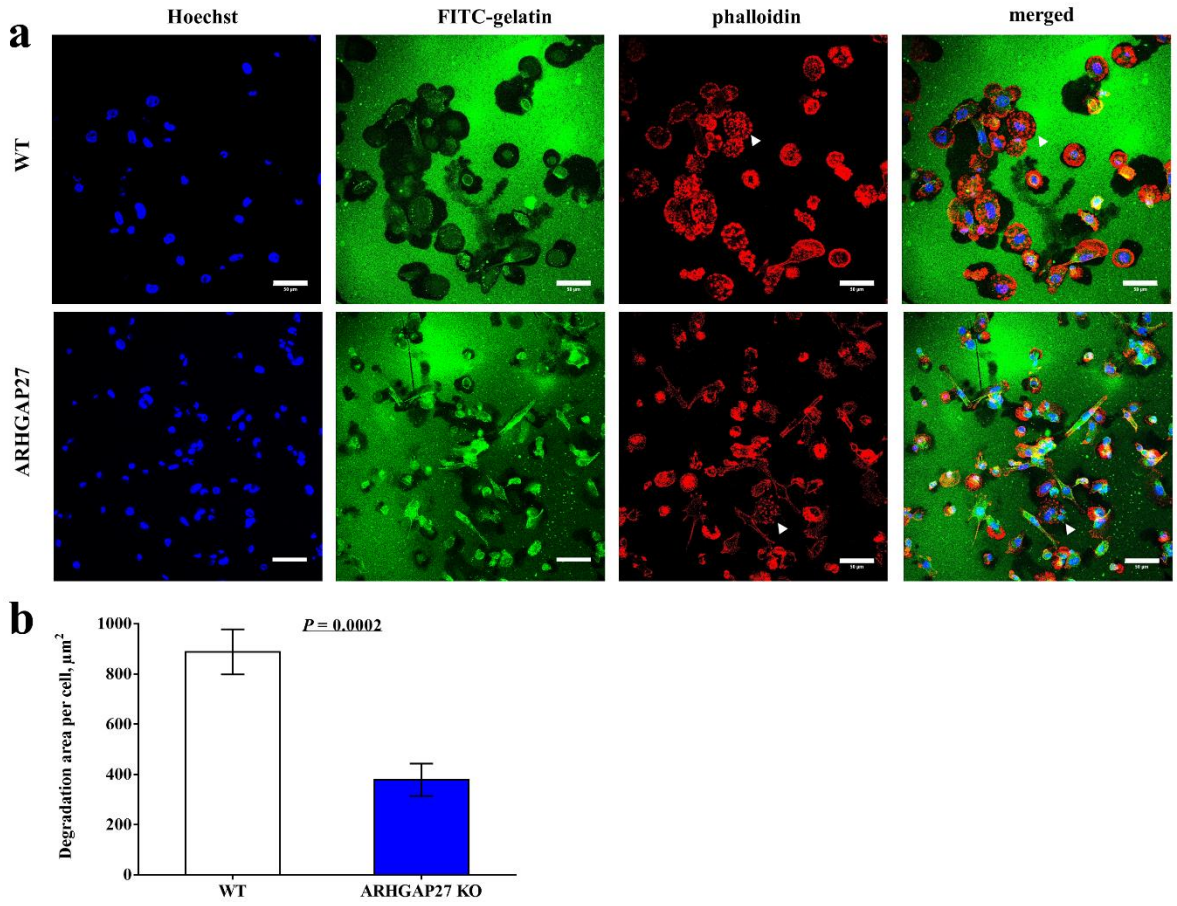

Figure 3.2-11: Matrix degradation is affected by the ARHGAP27-KO THP-1 cells is reduced.

Confocal immunofluorescence microscopy analysis of gelatin degradation by wild-type THP-1 cells and ARHGAP27-KO THP-1 cells. Cells were differentiated with PMA for 3 days and plated on the FITC-conjugated gelatin (green) for 24 hours (5 x 10^4). (**a**) The cells were stained with Phalloidin for actin (red) and the Hoechst dye for the nucleus (blue). Dark regions in the fluorescent gelatin matrix (green) show matrix degradation; white arrowheads indicate invadosomes. The pictures were acquired with a confocal laser scanning microscope and are representative of three independent experiments. Scale bar, 50µm. (**b**) The graph represents quantification of matrix area degraded per cell (~450 cells were analyzed per condition). Data indicate means ± s.e.m from three independent experiments. Two-tailed Student's t-test was used.

Next, I assessed whether the ability of the ARHGAP27-KO THP-1 cells to degrade matrix is affected. Briefly, differentiated cells were laid out on FITC-labelled gelatin matrix for 24 hours. Cells then were fixed and stained for nuclei and F-actin. The cells were able to form invadosomes; this function was not affected in THP-1 cells lacking ARHGAP27 (**Figure 3.2-11a**, white arrow). Nonetheless, the wild-type cells demonstrated a noticeably larger area of matrix degradation compared with the ARHGAP27-KO cells (888 μm^2 vs 379 μm^2 $P = 0.0002$). Thus, although the formation of invadosomes was not disrupted by the absence of ARHGAP27, matrix degradation was significantly impaired.

3.2.5.3 Macrophage migration is reduced in THP-1 cells lacking ARHGAP27

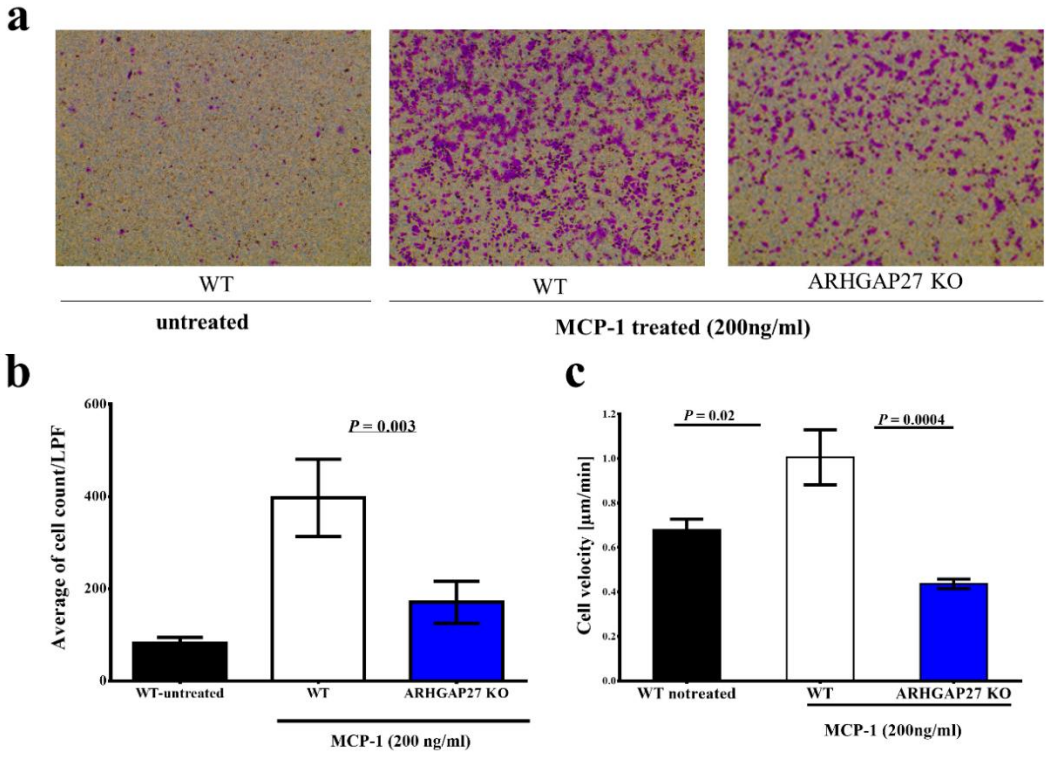

Figure 3.2-12: Macrophage migration is impaired in the ARHGAP27-KO THP-1 cells.

(**a**) Representative images showing THP-1 cell transwell migration. The lower chamber of the transwell apparatus was filled with tissue culture medium (untreated) or tissue culture medium supplemented with chemokine MCP-1. Migratory cells at the underside of the porous membrane were stained with crystal violet, pictures of the migrated cells (purple stained) were taken using a microscope with a 20x objective. (**b**) Quantification of cells was done using ImageJ software and expressed as the average of cell number per LPF from three independent experiments (average of 3-5 field per experiment). Error bar, mean ± s.e.m. Two-tailed Student's t-test was used. (**c**) Differentiated wild-type THP-1 cells and the ARHGAP27-KO cells were seeded on the fibronectin-coated coverslips for 24 hours. Coverslips were then inverted onto Dunn chambers containing tissue culture medium (non-treated), or medium supplemented with 200 ng/ml of MCP-1 and imaged every 4 mins for up to 5 hours. Cells were tracked using Manual tracking plugin of ImageJ and velocity was calculated. The graph represents one experiment with ~ 20 cells tracked. Error bars, mean ± s.e.m. Two-tailed Student's t-test was used.

The previous experiment demonstrated the effect of ARHGAP27 on matrix degradation by macrophages. To further investigate whether the lack of ARHGAP27 influence migration of macrophages, I used a transwell migration assay. As previously described (**Figure 3.1-15**), a total of 1 x 10^5 differentiated wild-type THP-1 cells and cells lacking ARHGAP27 were seeded onto the insert and allowed to migrate towards MCP-1 added to the bottom compartment at a concentration of 200 ng/ml, which was empirically determined (**Figure 3.1-14b**). The quantitative analysis showed that the average number of migrating wild-type cells was higher than that observed for the ARHGAP27-KO cells (397 cells/LPF vs 170 cells/LPF, P = 0.003, **Figure 3.2-12a** and **b**). To further confirm this result and to precisely estimate cell velocity, I use Dunn chamber. Briefly, differentiated wild-type and ARHGAP27-KO THP-1 cells were plated on the fibronectin-coated glass that was then inverted onto Dunn chambers containing either tissue culture growth medium or medium supplemented with the chemoattractant, MCP-1. Recorded time-lapse analysis showed that velocity of the ARHGAP27-KO cells was substantially reduced compared to the wild-type cells, 0.44 ± 0.1 μm/min vs. 1.005 ± 0.5(±s.e.m) μm/min (P = 0.0004, **Figure 3.2-12c**). Taken together, these results show that the ARHGAP27 protein is crucial for cell motility, and its absence resulted in significant reduction of macrophage migration.

3.2.5.4 Intracellular bacterial growth is not affected by ARHGAP27

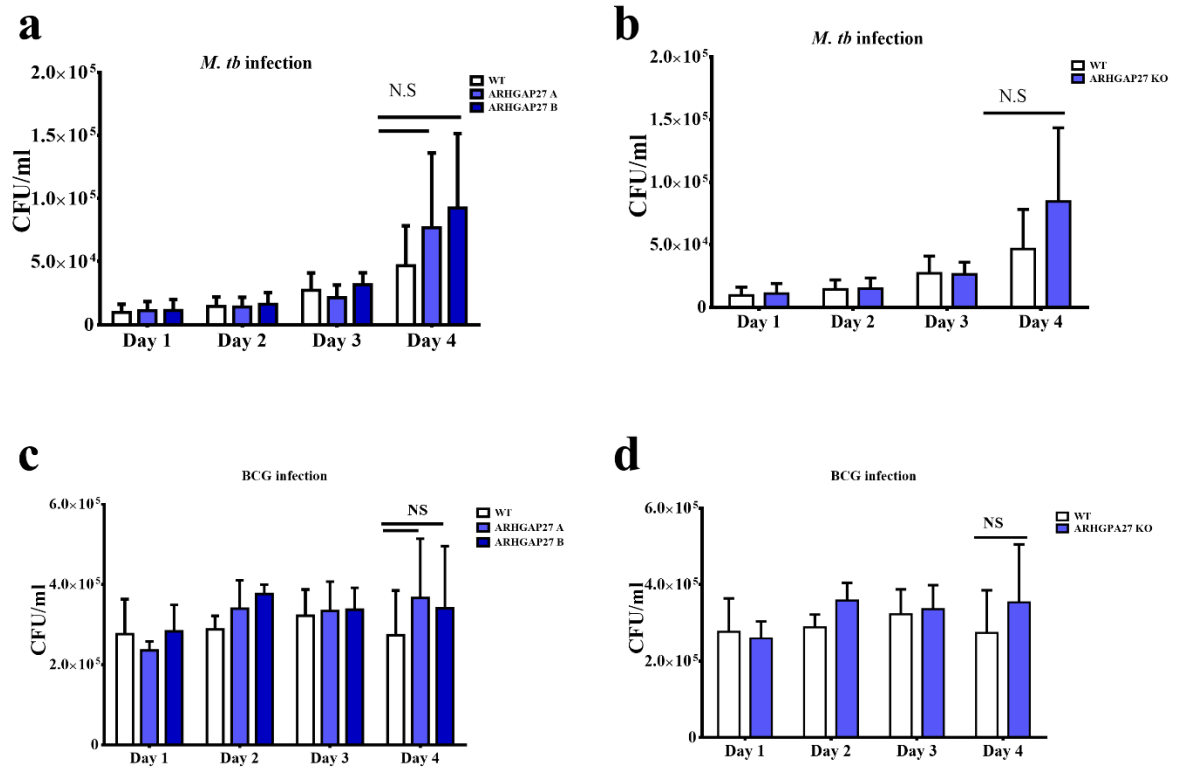

Figure 3.2-13: ARHGAP27 knockout does not affect the intracellular growth of mycobacteria in macrophages.

PMA differentiated wild-type THP-1 cells and two ARHGAP27-KO clones were infected with *M. tb* or BCG at MOI of ~2 and monitored for 96 h. (**a**) CFU assay of ARHGAP27-KO clones A and B and wild-type THP-1 cells at day 1, 2, 3, and 4 post-infection with *M. tb* (H37Rv). (**b**) As in (a) with two ARHGAP27-KO clones combined. (**c**) CFU assay of ARHGAP27-KO clones A and B and wild-type THP-1 cells at day 1, 2, 3, and 4 post-infection with BCG. (**d**) As in (**c**) with two ARHGAP27-KO clones combined. Data indicate means ± SD from three independent experiments. Two-tailed Student's t-test was used, not significant (NS).

I, next, assessed the ability of cells lacking ARHGAP27 to restrict intracellular mycobacterial multiplication using CFU, as previously described (**Figure 3.1-18**). Briefly, after *M. tb* or BCG infection, wild-type THP-1 cells and ARHGAP27-KO clones were

monitored for 96 hours. Then, cells were lysed and plated in duplicates for CFU. Data showed that the two ARHGAP27-KO clones had similar ability to restrict the intracellular growth of *M. tb* (**Figure 3.2-13a**) or BCG (**Figure 3.2-13c**) as the wild-type THP1 cells.The combined analysis of both ARHGAP27-KO clones showed similar results (**Figure 3.2-13b**) and (**Figure 3.2-13d**). I also extended this experiment to 10 days post infection, but the results were not informative after day 4 (**S 3**) due to the large variation observed between technical replicates in this experiment. Collectively, CFU counting showed that ARHGAP27 did not influence the intracellular *M. tb* or BCG growth in THP-1 macrophages, at least up to 4 days post-infection.

3.2.5.5 No effect of ARHGAP27 on the viability of the THP-1 macrophages infected with mycobacteria

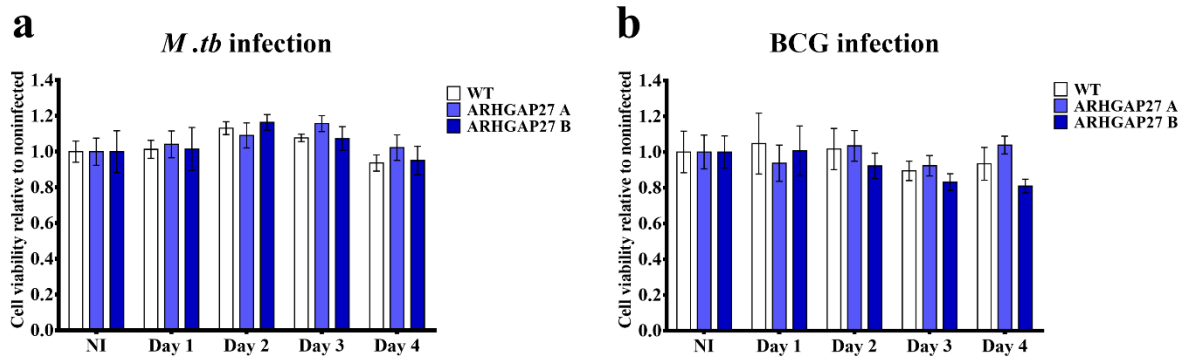

Figure 3.2-14: Evaluation of the viability of wild-type and ARHGAP27-KO THP-1 cells infected with *M. tb* or BCG.

The wild-type THP-1 cells (white) and ARHGAP27KO clones A, (blue) and B (dark blue) were infected with (**a**) *M. tb* or (**b**) BCG and monitored for 4 days. Cell viability was determined by CellTiter 96 One Solution Reagent. Data were expressed as a relative ratio to non-infected cells. Data indicate means ± s.e.m from three independent experiments performed in duplicates. Two-tailed Student's t-test was used.

Next, I used MTS assay to evaluate cell viability in the ARHGAP27-KO THP-1 macrophages infected with mycobacteria. Differentiated wild-type and ARHGAP27-KO cells were infected with *M. tb* or BCG strains at MOI of 2 and studied for cell viability for up to 4 days. The results of the viability assay showed that cells lacking ARHGAP27 were as viable as the wild-type cells infected with either *M. tb* or BCG (**Figure 3.2-14a** and **b**, respectively). Thus, ARHGAP27 did not affect macrophage viability in the context of mycobacterial infection.

3.2.6 Gene tagging using homology-directed repair

The CRISPR-Cas9 technology allows targeted genome editing and has been used for tagging genes of interest. The insertion of specific tag sequences in precise locations leads to the expression of the target protein fused to a tag, e.g., a fluorescent protein. Importantly, the targeted gene is expressed from its native chromosomal locus under endogenous regulation. This approach also provides a tool for studying proteins that have no commercially available antibodies, such as ARHGAP27. My goal here was to test the feasibility of this strategy. Specifically, I aimed to insert coding sequences of the fluorescent protein in the *ASAP1* and *ARHGAP27* genes, so that fused proteins are expressed from their native genomic locations. This would allow us to study endogenously expressed ASAP1 and ARHGAP27 proteins, analyzing their intracellular localization in the context of mycobacterial infection using a live-imaging microscopy system. Previously Lackner et al. used a generic strategy to tag an endogenous gene with the help of CRISPR-Cas9. Briefly, a universal donor plasmid (pMA - Universal *tia1l* vector) was constructed where *tai1l* sgRNAs, recognizing a zebrafish gene, were used to excise the tag flanked by two *tai1l* recognition sites (**Figure 3.2-15a**). Thereafter, the released tag sequence is incorporated into the gene of interest where Cas9 makes a cut guided by a gene-specific sgRNA (Lackner *et al.*, 2015).

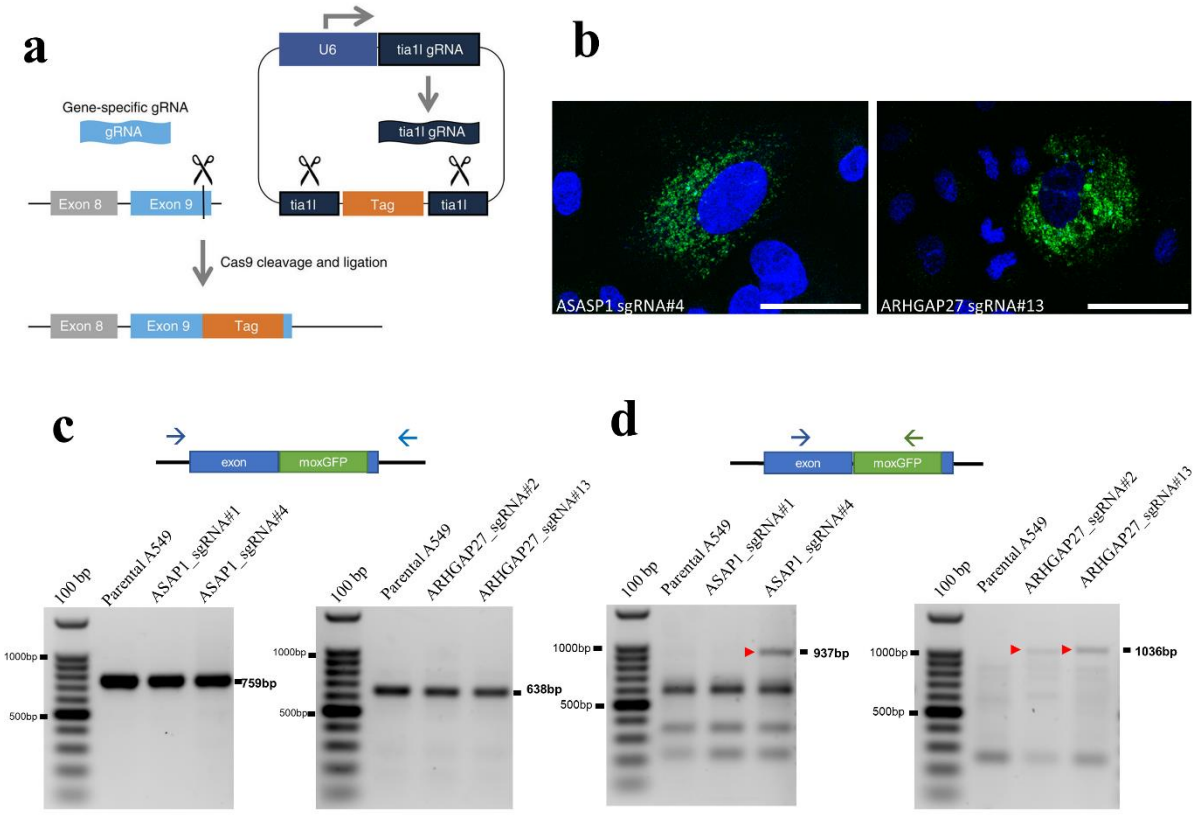

Figure 3.2-15: CRISPR-Cas9-mediated gene tagging

(**a**) Schematic representation: A549 stably expressing Cas9 were co-transfected with sgRNAs targeting a locus of interest (exon 30 of *ASAP1* and exon 17 of *ARHGAP27*) and a universal plasmid adapted from (Lackner *et al.*, 2015). (**b**) Representative images of confocal microscopy for *ASAP1*_sgRNA#4 (left) and *ARHGAP27*#13 (right) tagged with moxGFP under endogenous expression. (**c**) Screening of transfected A549 for tag incorporation using primers flanking the fused moxGFP. (**d**) Screening of transfected A549 for tag incorporation using a forward primer that binds genomic DNA and a reverse primer that binds moxGFP.

Initially, I designed two sgRNAs targeting 3'-coding region of the *ASAP1* and *ARHGAP27* genes (**Figure 3.2-16a** and **b**, respectively). I also constructed three versions of the donor plasmid taking into account each possible reading frame induced by a Cas9 cut as previously described (Lackner *et al.*, 2015). As a fluorescent protein tag, I used moxGFP,

which was optimized for the use in multiple cellular compartments, especially oxidizing environments and biological membranes (Costantini *et al.*, 2015). The stop and start codons were not included in donor cassettes so that they can be fused with the coding sequence of a gene, and their expressions would be driven by the endogenous machinery. I tested this system using A549 cells that we previously engineered to stably express Cas9. These cells are easier to transfect than THP-1 cells. Furthermore, A549 are alveolar epithelial cells that can be infected with *M. tb* and provide another model for the studies of mycobacterial infection. I co-transfected these A549 cells with the corresponding pMA-universal *tai1l* vector and the vector encoding a sgRNA targeting either exon 30 of *ASAP1* or exon 17 of *ARHGAP27*. Puromycin was introduced for 48 hours to enrich for cells transfected with a sgRNA plasmid. Thereafter, I checked for the moxGFP-positive cells using fluorescent microscopy. I found few cells that were positive for the green fluorescent signal (**Figure 3.2-15b**). Then, I genotyped the transfected cell mixtures using either primers flanking moxGFP, or one primer located in the flanking region and another one located in the moxGFP sequence. Genotyping using two flanking primers was not enough to detect a very small number of cells with the integrated moxGFP tag (**Figure 3.2-15c**). However, when using a primer that binds to the moxGFP sequence and another one that binds to the flanking genomic sequence, I detected cells where the integration of moxGFP occurred when transfected with either *ASAP1* sgRNA#4 or with the *ARHGAP27* sgRNA #2 or #13 (**Figure 3.2-15d**). I detected specific PCR products in the transfected cells that were not amplified in the parental A549 cells (**Figure 3.2-15d**).

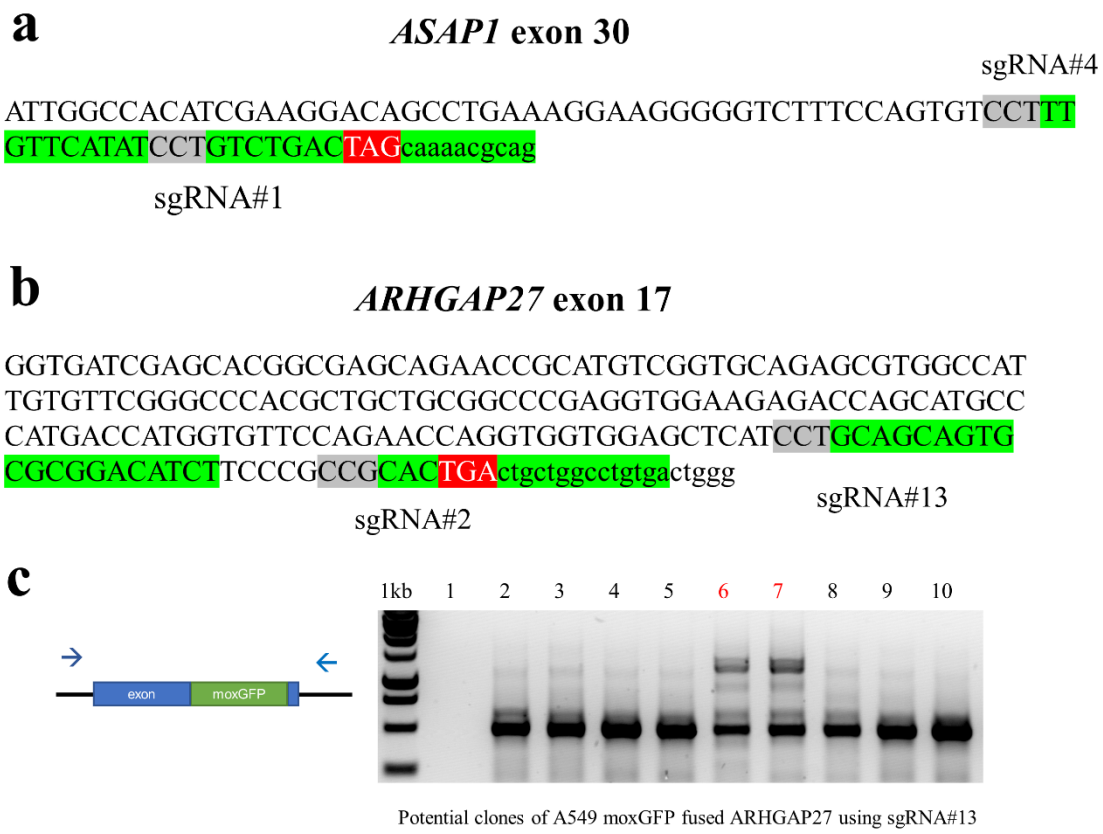

Figure 3.2-16: sgRNAs targeting genes of interest to be tagged with moxGFP.

(**a**) The sequence of exon 30 of *ASAP1* showing sgRNAs (green), PAM sequence (Gray), stop codon (red), and noncoding sequence (small letters). (**b**) The sequence of exon 17 of *ARHGAP27* showing sgRNAs (green), PAM sequence (Gray), stop codon (red), and the noncoding sequence (small letters) (**c**) (Left) schematic diagram shows primers binding the genomic DNA that used for screening. (Right) PCR screening using primers flanking the fused moxGFP was used to identify single cell clones for ARHGAP27 tagged with moxGFP at sgRNA#13 recognition site

Next, the pool of transfected cells was subjected to limiting dilution to isolate single cell clones with the correct incorporation within the gene reading frame, as shown in (**Figure 3.2-15b**). I screened the isolated single cell clones using PCR primers flanking the fused moxGFP (left panel, **Figure 3.2-16c**). PCR showed clones with the potential insert of

moxGFP in the ARHGAP*27* gene (Right panel, **Figure 3.2-16c**). Then, I also screened all possible tagged clones using two sets of primers (forward primer binds the flanking genome sequence and the reverse primer binds moxGFP sequence, or the forward primer binds moxGFP sequence, and the reverse primer binds the flanking genome sequence). PCR products showed that moxGFP was integrated into one clone in the ASAP1 gene and in 7 clones in the ARHGAP27 gene (**Figure 3.2-17a**). If moxGFP was inserted within the open reading frame, such a fused protein could be detected using anti-GFP antibody. However, immunoblotting showed that none of the clones expressed moxGFP at the protein level, suggesting that the moxGFP sequence was not inserted within an open reading frame (**Figure 3.2-17b**). In addition, Sanger sequencing of clone 6 for the *ARHGAP27* gene showed that moxGFP DNA was integrated, but the sequence had multiple mutations introduced by Cas9, which prevented the expression of the correct ARHGAP27–moxGFP protein (**Figure 3.2-17c**). Overall, I could not isolate any single clones bearing moxGFP precisely incorporated into the *ASAP1* or *ARHGAP27* genes. Therefore, the strategy for the insertion of tag sequences into genes of interest has not had enough success rate and needs further improvement.

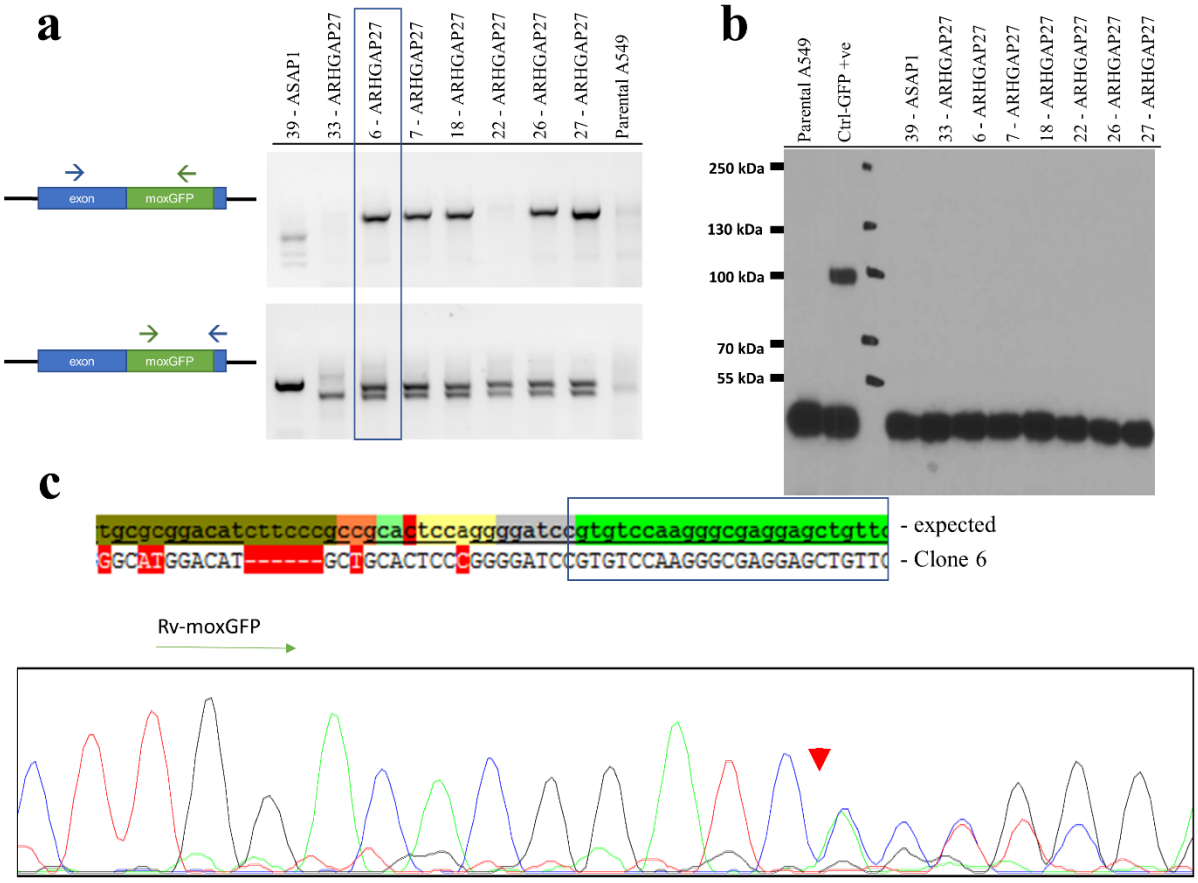

Figure 3.2-17: Confirming genome integration of moxGFP in the target genes

(a) PCR screening using two sets of primers (forward primer binds genome and reverse primer binds moxGFP (top panel); forward primer binds moxGFP, and reverse primer binds genome). (**b**) WB was probed for GFP to identified clones with moxGFP protein. (**c**) Sanger sequences show the presence of integrated moxGFP in ARHGAP27 (highlighted-green is moxGFP sequence) (clone 6).

Chapter 4 Discussion and conclusion

4.1 Genome-wide studies decipher genetic susceptibility to TB

Host genetic factors are known to predispose to TB. Identification of genetic variants associated with TB susceptibility can highlight specific genes that contribute to TB pathogenesis. Understanding biological mechanisms that implicate such genes will help to better understand host-pathogen interaction during *M. tb* infection and reveal its critical mechanisms that are essential for the progression to active TB. Furthermore, it may help to develop new host-directed therapies for TB treatment that are essential given the global spread of multi-drug resistant TB (Zumla *et al.*, 2015)

Genome-wide studies proved to be an efficient approach for the discovery of disease-associated genes in various disorders. Our group conducted two unbiased genome-wide studies to identify novel genes involved in TB, a GWAS of susceptibility to TB and a study of genetic regulation of gene expression in *M.tb*-infected macrophages. Initially, our laboratory conducted a GWAS of which 5,914 patients with active pulmonary TB and 6,022 healthy volunteers from Russia were studied. Association analysis of more than 7 million SNPs across the genome identified a novel locus on chromosome 8q24 associated with TB. Seven polymorphisms located in introns of the *ASAP1* gene within this locus were significantly associated with susceptibility to TB ($P = 2.6 \times 10^{-11}$). Moreover, we have shown that one of these TB-associated SNPs was also associated with the level of ASAP1

expression in *M.tb*-infected dendritic cells. Generally, it should be noted that identifying an eQTL indirectly provides only evidence of an association between genotype and gene transcription (Edwards *et al.*, 2013). It is yet to be established how this SNP or other co-inherited with it regulate ASAP1 expression in DCs. However, this finding firmly linked the ASAP1 gene with TB, suggesting that the ASAP1 protein is involved in its pathogenesis.

Some important limitations in our genome-wide studies must be discussed. In GWAS, one of the aims of the analysis is to tease apart the putative genetic variant from other SNPs in a given locus, which is often not straightforward. Using A Bayesian approach and GWAS-eQTL link highlighted rs10956514 SNP as the potential candidate variant. It is important to restate that the main reason as to why GWAS experiments are performed is the desire to have a better understanding of the set of genes that are associated with susceptibility to a particular trait. Thus, it is important to identify the target genes through which associated variants influence the phenotypes, leading to the discovery of new genes or/and pathways involved in biological processes. Equally important, a gene whose expression is indirectly influenced by a non-coding SNP could be a more important diagnostic or therapeutic target than the direct target gene. Consequently, it is critical to recognize both the direct targets of a trait-associated regulatory element and other genes affected by the reduced levels of the direct targets.

Another limitation of our GWAS is that *M. tb* infection status of our controls was unknown. Our control cohort is likely to include healthy individuals who were previously not exposed to *M. tb* and those who were exposed but were not infected or did not progress to active TB. Therefore, we could not answer if ASAP1 is associated with primary infection or with reactivation from latent to active TB.

Next, we studied transcriptional responses to *M. tb* infection in macrophages. We chose macrophages for this study because of the essential role they play in TB pathogenesis. Alveolar macrophages are the first immune cells to encounter *M. tb* bacilli contained within inhaled aerosol particles (Philips and Ernst, 2012). In addition, macrophages shape the outcome of TB infection by transforming into various macrophage forms that orchestrate the formation of granulomas (Flynn, Chan and Lin, 2011; Ramakrishnan, 2012). First, our results provided an extensive characterization of transcriptional programmes with which macrophages respond to live *M. tb*. Second, our analyses revealed genetic variants (eQTLs) that regulate gene expression in macrophages.

Importantly, we identified an eQTL SNP located upstream of the *ARHGAP27* gene that regulates its expression in non-infected and *M. tb*-infected macrophages ($P = 2.4 \times 10^{-18}$). Individuals carrying rs1635288 allele A showed an increased level of *ARHGAP27* expression and reduced TB risk in our GWAS (OR = 0.86, $P = 8.3 \times 10^{-5}$). This finding provided important additional evidence suggesting that rs1635288 is a functional SNP, which increases prior probability of it being functionally relevant. Therefore, we considered it being associated with TB, despite that its association in our GWAS was nominally below the genome-wide significance level. This association linked the ARHGAP27 protein with TB pathogenesis.

One of the limitations in our preliminary results of gene expression analysis of the 144 donors, is that we did not adjust for the age and gender of the participating subjects. It also did not consider seasonal variation. Future analyses should address these factors to eliminate their potentially confounding effects on gene expression (Ranz, Castillo-Davis, Meiklejohn, & Hartl, 2003). It is necessary to note that our study design of gene expression

analysis does not allow us to separate *M. tb*-specific response eQTL from those commonly shared with other infectious agents or stimuli. This question should be addressed in experimental models using other pathogens and specific stimuli.

Interestingly, ARHGAP27 and ASAP1 are GTPases Activating Proteins that control the activity of small GTPases and regulate actin cytoskeleton rearrangements. Thus, our findings suggested an important role of GAPs in mycobacterial infection and susceptibility to TB. Then, I used several approaches trying to understand functional mechanisms implicating ASAP1 and ARHGAP27 in TB.

4.2 Reduced level of ASAP1 and ARHGAP27 expression leads to defects in cell migration

The ASAP1 protein has been known to be involved in cytoskeleton regulation, membrane remodelling and invadosome formation particularly in cancer cells, where its expression was associated with the increased invasiveness and metastasis (Ehlers *et al.*, 2005; Onodera *et al.*, 2005; Bharti *et al.*, 2007; Lin *et al.*, 2008; Müller *et al.*, 2010). However, the mechanisms implicating ASAP1 in TB pathogenesis were unknown and were the main focus of my Ph.D. work. Initially, we studied its expression in immune cells and demonstrated that the levels of *ASAP1* expression were significantly increased in macrophages and DCs compared to monocytes and other immune cells.

Then, I studied roles of ASAP1 and ARHGAP27 using myeloid cell models, including primary monocyte-derived macrophages and DCs and THP-1 macrophages. I found that ASAP1 and ARHGAP27 significantly affected the motility of such cells. Thus, depletion

of ASAP1 in human monocyte-derived DCs and macrophages impaired their capacity to degrade extracellular matrix and migrate towards chemoattractant. Existing podosomes were not affected in the ASAP1-depleted DCs or macrophages as indicated by the presence of actin core in these cells. However, podosome turnover and re-assembly were delayed in the ASAP1-depleted DCs compared to the normal cells. In fact, invadosomes are dynamic structures that have half-lives of actin turnover from minutes to hours, but little is known about how their turnover is regulated (Murphy and Courtneidge, 2011). Furthermore, matrix degradation ability and cell motility in THP-1 cells, in which ASAP1 was knocked out, were significantly impaired, confirming the previous findings in primary cells. Similar to ASAP1, the ARHGAP27-knockout THP-1 cells showed a defect in their ability to degrade matrix and to migrate towards the chemokine gradient, CCL2, even though they were able to form invadopodia.

We studied changes in the level of expression of ASAP1 and ARHGAP27 in DCs and macrophages after mycobacterial infection and found that they were reduced. Furthermore, alleles of eQTL SNPs in the *ASAP1* and *ARHGAP27* genes that were associated with a stronger reduction of gene expression were also associated with the increased risk of TB in our GWAS, suggesting that low levels of expression of these genes predispose to TB. During early stages of *M. tb* infection, DCs engulf mycobacteria and migrate to the lung-draining lymph nodes to activate T cells and initiate the adaptive immune response. *M. tb* is known to inhibit migration as well as other functions of DCs, and the adaptive immunity in TB is delayed compared with other microbial infections (Wolf *et al.*, 2007, 2008; Roberts and Robinson, 2014). Thus, inhibition of expression of the key cytoskeleton regulators, such as

ASAP1 and ARHGAP27, may be one of the immune evasion mechanism used by *M. tb* bacilli to delay the onset of the adaptive immune response, giving it time to propagate. In such a model, subjects with the genetically determined low levels of expression of these genes would be at the increased risk of TB, as was detected by our GWAS. Furthermore, given that latent TB is a state of dynamic equilibrium, it is likely that trafficking of immune cells in granulomas has to be constantly maintained. Therefore, impaired migration of DCs and/or macrophages due to the reduced expression of the cytoskeleton regulator genes may also contribute at late stages of infection leading to reactivation of latent TB.

4.3 ASAP1 and ARHGAP27 are involved in phagocytosis of mycobacteria

Proteins that control cytoskeleton rearrangements, such as ASAP1 and ARHGAP27, may be involved in a variety of intracellular processes and their effects on susceptibility to TB may be pleiotropic. Therefore, I did not limit my analysis to cell migration, but studied other essential aspects of host-pathogen interactions, in particular uptake of mycobacteria, the viability of the infected cells and the killing of mycobacteria by macrophages. My experiments showed that ASAP1 and ARHGAP27 influence the macrophage uptake of mycobacteria at an early time point. Macrophages lacking ASAP1 or ARHGAP27 that were exposed to mycobacteria at MOI of 10 for 4 hours showed reduced engulfment of mycobacteria compared to control cells. Although the reduced phagocytosis seen in flow cytometry results was not significant, it was on the same trend with the data obtained by the high-throughput imaging system. Macrophages and other professional phagocytes are capable of and equipped for engulfing foreign particles contributing to the elimination of infection

and the clearance of damaged cells. Consistent with these findings, ASAP1 knockdown has been implicated in reduced macropinocytosis of *Salmonella* (Davidson *et al.*, 2015). Also, overexpression of the mutant form of ARHGAP27 impaired receptor-mediated endocytosis (Sakakibara *et al.,* 2004). TB infection is initiated when aerosol particles containing one to three bacilli reach lung alveolus (Rajaram *et al.*, 2014) and alveolar macrophages encounter and engulf the pathogen. In addition to their impaired migration, the reduced phagocytic activity that is genetically controlled by the reduced expression of *ASAP1* and *ARHGAP27* may result in the reduced engulfment of the bacilli by macrophage at the early stages of the infection. That will allow *M. tb* to replicate in the extracellular milieu for a longer period and increase in number, which will consequently increase the chances for *M. tb* to be engulfed by a larger number of alveolar macrophages. Macrophages are also essential cells within granulomas. The defect in the macrophage phagocytosis machinery may lead to the increased burden of extracellular *M. tb* bacilli that were released from bursting necrotic cells and not engulfed by other macrophages, resulting in the caseating granuloma at later stages of pulmonary TB.

4.4 ASAP1 and ARHGAP27 do not affect viability of macrophages and intracellular replication of mycobacteria

Both ASAP1 and ARHGAP27 proteins have been shown to be involved in endocytic machinery (Sakakibara *et al.*, 2004; Inoue *et al.*, 2008). Mycobacteria are known to arrest phagosomal maturation and replicate inside phagosome (Armstrong and Hart, 1971, 1975; Via *et al.,* 1997). Mycobacteria evolve to inhibit phagosomal fusion and use macrophages as

their expansion niche. Therefore, we tested impacts of ASAP1 and ARHGAP27 on the intracellular growth of mycobacteria. Our results show that knockout of ASAP1 and ARHGAP27 does not influence *M. tb* or BCG replication and viability inside THP-1 macrophages.

One can argue that the reduced phagocytic activity observed in the ASAP1- and ARHGAP27-knockout THP-1 cells may mask their effects on bacterial replication. Even if fewer gene knockout cells were infected compared to control cells, the deficient cells might provide a supportive environment for intracellular replication. First, there are some differences in the experimental settings. For the phagocytosis assay, cells were infected with MOI of 10 and were washed to remove extracellular bacteria. On the other hand, for bacterial viability and cell viability, macrophages were infected with MOI of 2 and were not washed, allowing for more contact between cells and mycobacteria. Reduced phagocytosis activity was observed in the first experiment after 4 hours of mycobacteria infection. However, in the second experimental setting, we observed no difference between knockout cells and control cells.

Moreover, mycobacteria have evolved to inhibit apoptosis, which leads to the eradication of infection by efferocytosis. Necrosis of infected cells is believed to help bacterial dissemination. *M. tb* has been shown to escape from phagosomes to cytosol proceeding to cell death (Simeone *et al.*, 2012). This was not the case in our knockout models. Cell viability in ASAP1 and ARHGAP27 deficient cells was not affected following *M. tb* infection. MTS assay estimates viable cells based on their metabolic activity. Reduced viability may be considered as a sign of increased bacterial burden in infected cells leading to cell death, which can be seen in MTS assay. We did not observe any variation in cell viability

between THP-1 cell lacking ASAP1 or ARHGAP27 compared to the wild-type THP-1 cells. Recent studies using live-imaging demonstrated that *M. tb* started to replicate better in infected cells that were losing their plasma membrane integrity (Lerner *et al.*, 2017; Mahamed *et al.*, 2017), leading to cascades of cell death (Mahamed *et al.*, 2017). In vitro study demonstrated virulent *M. tb* lyse the infected cell when the cellular niche is no longer needed. Macrophages infected with *M. tb* at low MOI die when the intracellular bacterial load passes a threshold of approximately 20 bacilli per macrophages (Lee *et al.*, 2006). Taken together, we can infer that there is no difference in the bacterial replication that might be masked by the reduced cell phagocytic activity.

It is important to recognize that designing sgRNAs with strict criteria that used in this project was not going to completely abolish off-target sequences. The major limitation is that using a lentiviral system to generate cell lines stably expressing both Cas9 protein and sgRNA might increase the chance of having off-target effects when knockout cell lines intended to be used for long period of time. Tight regulation of Cas9 activity or transient transfection of Cas9 protein or/and sgRNA may potentially minimize that off-target cleavage (Wang, La Russa and Qi, 2016). Another limitation when using cancer cell lines is that any functional roles could be obscured or falsely elevated by cellular genome instability and variability due to extensive passaging and different culture conditions (Edwards *et al.*, 2013).

4.5 ASAP1 interactomes

Both ASAP1 and ARHGAP27 are GTPase Activating Proteins (GAPs), and we have observed that they are involved in similar functions, matrix degradation, cell migration, and phagocytosis, during mycobacterial infection. We hypothesized that these two TB-associated proteins might directly or indirectly interact in the same compartment or signaling pathway. We used the newly developed technique to study protein interactomes, known as Rapid immunoprecipitation mass spectrometry of endogenous protein (RIME) (Mohammed *et al.*, 2013, 2016). In RIME, proteins interacting with the target protein are crosslinked and then pulled down using an antibody against the target protein. We had an excellent commercial antibody against ASAP1. I tested multiple commercial antibodies against the ARHGAP27 protein, but unfortunately did not find any of that worked well in western blotting, so they were not useful for RIME either. Therefore, I studied the ASAP1 interactome only. I compared proteins interacting with ASAP1 in non-infected and BCG-infected THP-1 macrophages. In non-infected cells, the ASAP1 partners were known to be involved in cytoskeleton remodeling. Some of the interactors have been involved in phagocytosis and/or cell migration such as PTPN12, TNS3, IQGAP1, and INPP5D. Interestingly, one of the frequently detected ASAP1-interacting partners was ITGB2, a β2 integrin, which is leukocyte-specific and binds to plasminogen, intracellular adhesion molecule 2 and vascular cell adhesion molecule (Schachtner *et al.*, 2013). It has been shown that β2 integrins are essential for podosome formation in DCs (Gawden-Bone *et al.*, 2014), and we and others demonstrated that ASAP1 localized to podosomes (**Figure 3.1-2**) (Shiba and Randazzo, 2011; Curtis *et al.*, 2015)

Following BCG infection I found additional proteins interacting with ASAP1. Thus, ATP6V1B2 is known to be involved in the endocytic pathways, particularly, in the phagosomal compartments. Some of the ASAP1 interactors have been implicated in mitochondrial morphology (e.g., SH3GLB1 and FIS1). Interestingly, our results show that ASAP1 may interact with EVL in resting cells and with αII-spectrin after infection with mycobacteria. EVL has been reported to interact with the αII-spectrin SH3 domain, which makes it as a potential link between the spectrin-based skeleton and actin dynamics (Bournier *et al.,* 2006). These findings indicate that ASAP1 might link actin cytoskeleton with spectrins.

Unexpectedly, our result demonstrated two distinct interactomes for ASAP1 in non-infected cells and following mycobacterial infection. Of particular interest was the interaction between ASAP1 and the BASP1 protein induced in the BCG-infected macrophages. BASP1 is known to interact with the WT1 protein, which gene was associated with TB risk in previous GWAS (Thye *et al.*, 2012; Chimusa *et al.*, 2014; Curtis *et al.*, 2015). Therefore, BASP1 physically interacts with two TB-associated proteins, ASAP1 and WT1, linking them in one pathway. The WT1 protein is a zinc finger transcription factor (Carpenter *et al.*, 2004). Therefore, ASAP1 via the BASP1-WT1 pathway may regulate a transcription programme that may be particularly relevant to TB.

There are well-recognized limitations for RIME such as the necessity of using high-affinity and high-specificity antibodies. A more relevant limitation is the inability to separate multiple complexes. Some proteins have many partners in different compartments. RIME purifies all of these partners in a single experiment, indicating a reduced resolution of the subtle differences in complexes at each site and leading to a failure to distinguish direct from

indirect interactions (Mohammed *et al.*, 2016). Therefore, further experiments using co-immunoprecipitation will be needed to better understand the ASAP1 interactome. Moreover, given that the BCG infection in my experiments was for 4 hours, only a fraction of the cells were infected. In such circumstances, some of the ASAP1 interactions were induced not directly by the infection, but indirectly by the secreted bacterial proteins or host cytokines.

4.6 ASAP1 is involved in regulation of gene expression

I studied the role of ASAP1 in regulation of gene expression in non-infected and BCG-infected THP-1 macrophages, comparing the wild-type and the ASAP1-knockout cells, and found a large number of differentially expressed genes. The GO terms and KEGG functional annotation analysis of genes whose expression was significantly different between the wild-type and the ASAP1-knockout cells indicated that ASAP1 plays a role in immune response. This finding is in agreement with previous studies describing ASAP1 as a negative regulator of the NF-κB pathway (Haque *et al.*, 2011; Tien *et al.*, 2015). Moreover, the comparison between the wild-type THP-1 cells and cells lacking ASAP1 in the context of mycobacterial infection suggested that ASAP1 is essential for the regulation of genes important for phagocytosis and other actin cytoskeleton remodeling. Importantly, some of the differentially expressed genes were annotated to phagosomes such as v-ATPase subunits and coronin 1 that are known for their inhibitory role in the fusion of lysosomes with phagosomes containing mycobacteria. Additionally, some genes, such as *TLR2* and *SLC11A1,* have been previously identified to be associated with susceptibility to TB (Vidal *et al.*, 1993; Ben-Ali *et al.*, 2004) .

4.7 Proposed model of implicating ASAP1 and ARHGAP27 in TB.

We propose a model showing how ASAP1 and ARHGAP27 are involved in TB pathogenesis and how their reduced expressions predispose individuals to TB. First, genetically regulated reduced ASAP1 in macrophages and DCs may contribute initially to the delayed and reduced phagocytosis that will allow for invading pathogens to multiply extracellularly, which increases the possibility of a larger number of cells to be infected. DCs that engulf *M. tb* migrate to lymph nodes, but their migration will be slowed down by the reduced expression of ASAP1, particularly in genetically predisposed subjects. This will lead to the delay in T cell responses at an early stage of TB infection. At a later stage of infection, the trafficking of myeloid cells is required to constantly maintain granuloma structure. The impaired migration caused by the low expression of *ASAP1* as well as the reduced phagocytic engulfment of the necrotic cells may contribute eventually to the breakdown of granulomas and dissemination of *M. tb*. Similar to *ASAP1*, genetically-determined low expression of *ARHGAP27* may lead to reduced phagocytosis in alveolar macrophages, allowing for the extracellular growth of the pathogen. Moreover, reduced migration and phagocytic activity associated with low ARHGAP27 expression may result in the disruption of the immune balance in granuloma at later stages of infection and TB reactivation.

4.8 Discovery of the TLR1-mediated transcriptional network in *M. tb*-infected macrophages.

The identification of response eQTLs that influence gene expression following *M. tb* infection in macrophages led us to the discovery of the TLR1-driven transcriptional network. Most of known TLRs recognize distinct PAMPs that trigger the activation of downstream signaling pathways, leading ultimately to the production of proinflammatory cytokines and activation of host immune responses via the NF-κB signaling pathway (Basu, Shin and Jo, 2012). It is not new that TLR1 is linked to TB pathogenesis. TLR1 and TLR6 recognize lipopeptides as heterodimers with TLR2. TLR2-deficient mice are very susceptible to TB, indicating the importance of TLR2 in immunity to TB (Drennan *et al.*, 2004). Upon stimulation with TLR agonists including LPS, peptidoglycan, 19-kDa lipoprotein, and Pam3CDK4, proinflammatory cytokines production in $TLR1^{-/-}$ deficient macrophages was noticeably impaired when challenged with native purified *M. tb* lipoprotein or synthetic triacylated lipopeptide Pam3CSK4. In addition, challenging of the TLR1-deficient macrophages with the whole mycobacteria led to partially reduced production of TNF-α, indicating that TLR1 is involved in recognition of mycobacteria components (Takeuchi *et al.*, 2002). Later, Jin et al. revealed the crystal structure of the lipopeptide-induced association of TLR1 and TLR2 (Jin *et al.*, 2007). Nonetheless, it has not been determined whether TLR1 or TLR6 plays a dominant role in TB pathogenesis in humans.

Genetic variants located in the TLR1 gene have been associated with susceptibility to TB. For example, rs3923647 was reported to be strongly protective for pulmonary TB in the Ghanaian population. PMBC from carriers of rs3923647 TT genotype showed augmented

production of IFN-γ upon mycobacteria challenge compared to its levels in people with the AT and AA genotypes (Meyer *et al.*, 2016). Another TLR1 variant (rs4833095) found in meta-analysis associated with protection from TB in individuals from different genetic backgrounds (Asia, Africa, and Europe) (Schurz *et al.*, 2015). Consistently, we also found this SNP associated with resistance to TB in our Russian GWAS. Interestingly, the same variant was one of the eQTL found in our macrophages study. In addition, TLR1 SNP rs5743618, in strong LD with rs4833095 (Schurz *et al.*, 2015), has been reported to be associated with resistance to TB (Hart and Tapping, 2012).

A recent study in monocytes described TLR1-induced gene network after stimulation with Pam3CSK4 (Quach *et al.*, 2016). In this study, the missense variant rs5743618 (I602S) trans-regulated expression of a large number of genes (432 genes). However, Quach et al. did not find any *cis*-QTLs that affect TLR1 expression. With further inspection, we found only 3 genes (*CXCL2*, *ADA*, and *IL6*) that overlap with the Quach et al. network. The discrepancy between the TLR1 genes network, in part, can be explained by the use of the different cellular models, monocytes versus macrophages, since some eQTLs might be identified in a cell-specific manner (Fairfax and Knight, 2014). Another reason is that in our study, we used live *M. tb* that is likely to be recognized by multiple receptors leading to triggering more downstream pathways than that stimulated by the synthetic triacylated TLR1 ligand, Pam3CSK4. The cooperation between several pathways stimulated by the whole organism is likely to orchestrate the TLR1-related response and affect the gene expression and eventually the eQTL network. Currently, other members of our laboratory continue to work on characterization and validation of the newly discovered TLR1-regulated network using the

TLR1-knockout THP-1 cells, established using CRISPR-Cas9 technology, similarly to the approach that I used here.

Chapter 5 Future direction

Currently, our lab is analyzing data for the transcriptional responses in *M. tb*-infected macrophages obtained from 591 healthy volunteers. Such a large sample size will increase the statistical power to identify novel *cis*-eQTLs, *trans*-eQTLs, and perhaps *trans*-eQTL-regulated gene networks. We are also mapping eQTLs affecting alternative splicing of transcripts. Alternative splicing can influence protein functions, by affecting transcript stability, structure, function, and subcellular localization (Kalam, Fontana and Kumar, 2017). This may lead to the identification of new regulatory eQTLs.

In addition to virulent *M. tb* infection, the expanded dataset will include transcriptomes from macrophages infected with either attenuated BCG or a highly virulent Beijing strain of M. tb. Studying transcriptional responses in macrophages induced by different mycobacterial strains may lead to the identification of strain-specific eQTLs.

To follow up analysis of the *TLR1*-mediated transcriptional network, our lab has now generated TLR1-knockout THP-1 cell line. The aim of this project is to study transcriptional responses after *M. tb* infection in the knockout and wild-type cell in order to validate our newly identified TLR1-regulated gene network. We hypothesize that loss-of-function mutations in the *TLR1* gene should affect expressions of genes induced by the TLR1-mediated signaling and essentially point to the same gene network as in our eQTL analysis. We will then perform infection experiments analyzing *M.tb*-induced death of macrophages

and their ability to control intracellular *M. tb* replication. This will allow establishing if the TLR1-mediated transcriptional program has mostly intrinsic effect on macrophages or if it mainly affects cytokine secretion, recruiting and activating other immune cells.

It would be of keen interest to extend analysis of the genetics of gene expression in additional relevant cell types, such as neutrophils and DCs, at different time points (e.g., 4 hours and 48 hours) that will help better understanding of the genetic architecture of TB pathogenesis, with the ultimate aim of deciphering the genetic factors controlling human susceptibility to TB. For illustration, neutrophils are a less studied cellular model in *M. tb* infection than other immune components. They are difficult to work with due to their short lifespan (Lowe *et al.*, 2012). However, it has been observed that neutrophils are a frequently infected cell type in the sputum of TB patients, indicating their role in transporting bacilli to the airway (Eum *et al.*, 2010).

My current work demonstrated that ASAP1 and ARHGAP27 are implicated in TB pathogenesis, affecting phagocytosis of mycobacteria and migration of macrophages and DCs. We did not find evidence that reduced expression of these proteins impairs the capacity of macrophages to control the growth of the intracellular mycobacteria. However, our analysis was restricted to 4 days only, due to technical difficulties with the CFU assay beyond this time point. Now, live imaging experiments should be used to extend these analyses. Using live imaging for evaluating macrophage ability in restricting intracellular growth in cells with gene knockouts can overcome the variation observed in the CFU assay. Live imaging-based assay also can track and analyze infection in a single cell for a longer period (more than 4 days), which will increase the statistical power when analyzing hundreds of macrophages. Moreover, it facilitates the quantification of the initial infection and

distinguishes it from bacilli replicated within macrophage after the initial entry. New high-throughput confocal microscopy imaging system Opera Phenix from Perkin Elmer is now available at our Department. It will facilitate large-scale analyses of *M. tb* infection in various cell models.

The engulfment of particles or pathogens is a complicated process, which might be achieved either by receptor-mediated phagocytosis or macropinocytosis. In our uptake assays (flow cytometry, CFU counting, imaging), we could not discriminate if the defect observed in the ASAP1- and ARHGAP27-knockout cells was related to phagocytosis or macropinocytosis. It has been reported that activation of macrophages with TNF-α and IFN-γ reprogrammed endocytic machinery from phagocytosis to macropinocytosis allowing the transfer of internalized cargo to lysosomes in a receptor-independent manner for the rapid elimination of pathogens (Bosedasgupta and Pieters, 2014). Therefore, the defect observed in our knockout models should be scrutinized to highlight which of these mechanisms is affected by knocking out ASAP1 or ARHGAP27. The A549 cells are type II alveolar epithelial cells that cover the alveoli. It has been reported that *M. tb* induces its entry into nonphagocytic cells via macropinocytosis (García-Pérez, Mondragón-Flores and Luna-Herrera, 2003; Garcia-Perez, Castrejon-Jimenez and Luna-Herrera, 2012). A549 could be used to interrogate whether macropinocytosis is affected by knocking out ASAP1 or ARHGAP27. In addition to A549, TNF-α- or IFN-γ-activated macrophage can be used to study macropinocytosis. Furthermore, the study of ASAP1 and ARHGAP27 roles in TB should be extended to other cellular functions that are important in TB pathogenesis such as autophagy and antigen presentation.

Finally, the mouse model has been used for decades to study TB *in vivo*. Knockout mice for ASAP1 or/and ARHGAP27 will help better understand their involvement in more complex organism systems. In addition, zebrafish can be used to assess early formation of granulomas, which mainly depend on the presence of macrophages and neutrophils in this model. Taken together these experiments will help to further dissect the role of cytoskeleton regulators in TB pathogenesis.

Given the current spreading of multi-drug resistant *M. tb* strains and long duration of the complex drug regimen, causing problems with toxicity, new therapies are urgently required for TB treatment (Zumla *et al.*, 2015). Host-directed therapies (HDTs) aim to improve immune mechanisms by augmenting the ability of host cells to kill *M. tb* or by modulating the immune response to prevent excessive inflammation, cell death, and tissue damage. Moreover, since HDT approach targets the host, it is likely to lower the risk of developing further drug resistance compared to conventional antibiotics and may work synergistically with antibiotics to shorten the treatment course.

The host tyrosine kinases are known to be implicated in the engulfment of mycobacteria. Imatinib, the commercial tyrosine kinase inhibitor developed for the treatment of chronic myelogenous leukemia, was shown to reduce the uptake of mycobacteria in macrophages. (Napier *et al.*, 2011). Another clinically used EGFR inhibitor, gefitinib, has efficacy for preventing bacterial replication in both infected macrophages and mice (Stanley *et al.*, 2014). Lastly, Src tyrosine kinase inhibitor, AZD0530, led to lower burden of *M. tb* and reduced disease pathology in guinea pigs as well as reduced survival of *M. tb* in THP-1 macrophages (Chandra *et al.*, 2013). ASAP1 has been found to bind to and be phosphorylated

by FA kinase (FAK) protein, which in turn is regulated by Src (Parsons, 2003; Zhao *et al.*, 2016).

The discovery of the ASAP1 and ARHGAP27 as essential TB-associated proteins point at them as potential targets for HDTs. Although at present no existing drugs target these proteins, further analysis of the ASAP1 and ARHGAP27 signaling pathways may help to identify partner proteins that already have existing compounds modulating their activity. Of note, small molecules targeting cytoskeleton regulation pathways have been extensively developed by the pharmaceutic industry as potential anti-cancer drugs. In light of our findings emphasizing important roles of cytoskeleton regulators in TB pathogenesis, this pool of available compounds may now facilitate discovery of novel host-directed therapies for TB.

References

Albert, F. W. and Kruglyak, L. (2015) 'The role of regulatory variation in complex traits and disease.', *Nature reviews. Genetics*. Nature Publishing Group, 16(4), pp. 197–212. doi: 10.1038/nrg3891.

Angers-Loustau, A. *et al.* (1999) 'Protein tyrosine phosphatase-PEST regulates focal adhesion disassembly, migration, and cytokinesis in fibroblasts.', *The Journal of cell biology*, 144(5), pp. 1019–31. doi: 10.1083/jcb.144.5.1019.

Armstrong, J. A. and Hart, P. D. (1971) 'Response of cultured macrophages to Mycobacterium tuberculosis, with observations on fusion of lysosomes with phagosomes.', *The Journal of experimental medicine*, 134(3 Pt 1), pp. 713–40. Available at: http://www.ncbi.nlm.nih.gov/pubmed/15776571.

Armstrong, J. A. and Hart, P. D. (1975) 'Phagosome-lysosome interactions in cultured macrophages infected with virulent tubercle bacilli. Reversal of the usual nonfusion pattern and observations on bacterial survival.', *The Journal of experimental medicine*, 142(1), pp. 1–16. Available at: http://www.ncbi.nlm.nih.gov/pubmed/807671.

Awuh, J. A. and Flo, T. H. (2016) 'Molecular basis of mycobacterial survival in macrophages', *Cellular and Molecular Life Sciences*. Springer International Publishing, (1), pp. 1–24. doi: 10.1007/s00018-016-2422-8.

Azzurri, A. *et al.* (2005) 'IFN-gamma-inducible protein 10 and pentraxin 3 plasma levels are tools for monitoring inflammation and disease activity in Mycobacterium tuberculosis infection.', *Microbes and infection*, 7(1), pp. 1–8. doi: 10.1016/j.micinf.2004.09.004.

Bach, H. *et al.* (2008) 'Mycobacterium tuberculosis Virulence Is Mediated by PtpA Dephosphorylation of Human Vacuolar Protein Sorting 33B', *Cell Host and Microbe*, 3(5), pp. 316–322. doi: 10.1016/j.chom.2008.03.008.

Banales, J. L. *et al.* (1991) 'Adenosine deaminase in the diagnosis of tuberculous pleural effusions: A report of 218 patients and review of the literature', *Chest*, 99(2), pp. 355–357. doi: 10.1378/chest.99.2.355.

Bar-Sagi, D. and Hall, A. (2000) 'Ras and Rho GTPases: a family reunion.', *Cell*, 103(2), pp. 227–38. doi: S0092-8674(00)00115-X [pii].

Barreiro, L. B. *et al.* (2012) 'Deciphering the genetic architecture of variation in the immune response to Mycobacterium tuberculosis infection.', *Proceedings of the National Academy of Sciences of the United States of America*, 109(4), pp. 1204–9. doi: 10.1073/pnas.1115761109.

Basu, J., Shin, D.-M. and Jo, E.-K. (2012) 'Mycobacterial signaling through toll-like receptors.', *Frontiers in cellular and infection microbiology*, 2(November), p. 145. doi: 10.3389/fcimb.2012.00145.

Behr, M. A. (2002) 'BCG — different strains, different vaccines?', *The Lancet Infectious Diseases*. Elsevier, 2(2), pp. 86–92. doi: 10.1016/S1473-3099(02)00182-2.

Bellamy, R. (1998) 'Genetics and pulmonary medicine. 3. Genetic susceptibility to tuberculosis in human populations.', *Thorax*, 53(7), pp. 588–93. Available at: http://www.pubmedcentral.nih.gov/articlerender.fcgi?artid=1745258&tool=pmcentrez&rendertype=abstract (Accessed: 16 October 2014).

Ben-Ali, M. *et al.* (2004) 'Toll-like receptor 2 Arg677Trp polymorphism is associated with susceptibility to tuberculosis in Tunisian patients.', *Clinical and diagnostic laboratory immunology*, 11(3), pp. 625–6. doi: 10.1128/CDLI.11.3.625-626.2004.

Bharti, S. *et al.* (2007) 'Src-dependent phosphorylation of ASAP1 regulates podosomes.', *Molecular and cellular biology*, 27(23), pp. 8271–83. doi: 10.1128/MCB.01781-06.

Bindea, G. *et al.* (2009) 'ClueGO: A Cytoscape plug-in to decipher functionally grouped gene ontology and pathway annotation networks', *Bioinformatics*, 25(8), pp. 1091–1093. doi: 10.1093/bioinformatics/btp101.

Bloch, D. B. *et al.* (2000) 'Sp110 localizes to the PML-Sp100 nuclear body and may function as a nuclear hormone receptor transcriptional coactivator.', *Molecular and cellular biology*, 20(16), pp. 6138–46. Available at: http://www.ncbi.nlm.nih.gov/pubmed?cmd=search&term=10913195&dopt=b (Accessed: 17 October 2014).

Boisson-Dupuis, S. *et al.* (2015) 'Inherited and acquired immunodeficiencies underlying tuberculosis in childhood.', *Immunological reviews*, 264(1), pp. 103–20. doi: 10.1111/imr.12272.

Bompard, G. *et al.* (2005) 'Involvement of Rac in actin cytoskeleton rearrangements induced by MIM-B.', *Journal of cell science*, 118(Pt 22), pp. 5393–403. doi: 10.1242/jcs.02640.

Bonilla, D. L. *et al.* (2013) 'Autophagy regulates phagocytosis by modulating the expression of scavenger receptors.', *Immunity*, 39(3), pp. 537–47. doi: 10.1016/j.immuni.2013.08.026.

Bosedasgupta, S. and Pieters, J. (2014) 'Inflammatory stimuli reprogram macrophage phagocytosis to macropinocytosis for the rapid elimination of pathogens.', *PLoS pathogens*. Edited by S. Ehrt, 10(1), p. e1003879. doi: 10.1371/journal.ppat.1003879.

Botelho, R. J. and Grinstein, S. (2011) 'Phagocytosis.', *Current biology : CB*, 21(14), pp. R533-8. doi: 10.1016/j.cub.2011.05.053.

Bournier, O. *et al.* (2006) 'Spectrin interacts with EVL (Enabled/vasodilator-stimulated phosphoprotein-like protein), a protein involved in actin polymerization.', *Biology of the cell*, 98(5), pp. 279–93. doi: 10.1042/BC20050024.

Boyden, S. (1962) 'The chemotactic effect of mixtures of antibody and antigen on polymorphonuclear leucocytes.', *The Journal of experimental medicine*, 115(3), pp. 453–66. doi: 10.1084/jem.115.3.453.

BOYUM, A. (1964) 'SEPARATION OF WHITE BLOOD CELLS.', *Nature*, 204(4960), pp. 793–4. doi: 10.1038/204793a0.

Brandt, D. T. *et al.* (2007) 'Dia1 and IQGAP1 interact in cell migration and phagocytic cup formation.', *The Journal of cell biology*, 178(2), pp. 193–200. doi: 10.1083/jcb.200612071.

Brewer, T. F. (2000) 'Preventing tuberculosis with bacillus Calmette-Guérin vaccine: a meta-analysis of the literature.', *Clinical infectious diseases : an official publication of the Infectious Diseases Society of America*, 31 Suppl 3, pp. S64-7. doi: 10.1086/314072.

Brielmeier, M. *et al.* (1998) 'Improving stable transfection efficiency: Antioxidants dramatically improve the outgrowth of clones under dominant marker selection', *Nucleic Acids Research*, 26(9), pp. 2082–2085. doi: 10.1093/nar/26.9.2082.

Carpenter, B. *et al.* (2004) 'BASP1 is a transcriptional cosuppressor for the Wilms' tumor suppressor protein WT1.', *Molecular and cellular biology*, 24(2), pp. 537–49. doi: 10.1128/MCB.24.2.537.

CDC (2008) *Guideline for Disinfection and Sterilization in Healthcare Facilities*, *Centers for Disease Control and Prevention*. CDC. Available at: http://www.cdc.gov/hicpac/Disinfection_Sterilization/6_0disinfection.html (Accessed: 6 October 2014).

Cervero, P., Panzer, L. and Linder, S. (2013) 'Podosome Reformation in Macrophages: Assays and Analysis', in Coutts, A. S. (ed.) *Adhesion Protein Protocols*. Totowa, NJ: Humana Press, pp. 97–121. doi: 10.1007/978-1-62703-538-5_6.

Chandra, P. *et al.* (2013) 'Targeting Drug-Sensitive and -Resistant Strains of Mycobacterium tuberculosis by Inhibition of Src Family Kinases Lowers Disease Burden and Pathology.', *mSphere*, 1(2). doi: 10.1128/mSphere.00043-15.

Chapuis, F. *et al.* (1997) 'Differentiation of human dendritic cells from monocytes in vitro.', *European journal of immunology*, 27(2), pp. 431–41. doi: 10.1002/eji.1830270213.

Chen, M. *et al.* (2014) 'Direct interaction of 14-3-3ζ with ezrin promotes cell migration by regulating the formation of membrane ruffle.', *Journal of molecular biology*. Elsevier Ltd, 426(18), pp. 3118–3133. doi: 10.1016/j.jmb.2014.06.021.

Chen, P. W. *et al.* (2016) 'The Arf GTPase-activating protein, ASAP1, binds nonmuscle myosin 2A to control remodeling of the actomyosin network', *Journal of Biological Chemistry*, 291(14), pp. 7517–7526. doi: 10.1074/jbc.M115.701292.

Cherfils, J. and Zeghouf, M. (2013) 'Regulation of small GTPases by GEFs, GAPs, and GDIs.', *Physiological reviews*, 93(1), pp. 269–309. doi: 10.1152/physrev.00003.2012.

Cheung, V. G. and Spielman, R. S. (2009) 'Genetics of human gene expression: mapping DNA variants that influence gene expression.', *Nature reviews. Genetics*, 10(9), pp. 595–604. doi: 10.1038/nrg2630.

Chimusa, E. R. *et al.* (2014) 'Genome-wide association study of ancestry-specific TB risk in the South African Coloured population.', *Human molecular genetics*, 23(3), pp. 796–809. doi: 10.1093/hmg/ddt462.

Chira, S. *et al.* (2017) 'CRISPR/Cas9: Transcending the Reality of Genome Editing', *Molecular Therapy - Nucleic Acids*. Elsevier Ltd., 7(3), pp. 211–222. doi: 10.1016/j.omtn.2017.04.001.

Colditz, G. A. *et al.* (1994) 'Efficacy of BCG vaccine in the prevention of tuberculosis. Meta-analysis of the published literature', *JAMA*, 271(9), pp. 698–702. doi: 10.1001/jama.1994.03510330076038.

Comstock, G. W. (1978) 'Tuberculosis in Twins: A Re-Analysis of the Prophit Survey 1-3', *American Review of Respiratory Disease*, 117(4), p. 621.

Conesa, A. *et al.* (2016) 'A survey of best practices for RNA-seq data analysis', *Genome Biology*, 17(1), p. 13. doi: 10.1186/s13059-016-0881-8.

Cong, L. *et al.* (2013) 'Multiplex Genome Engineering Using CRISPR/Cas Systems', *Science*, 339(6121), pp. 819–823. doi: 10.1126/science.1231143.

Cookson, W. *et al.* (2009) 'Mapping complex disease traits with global gene expression.', *Nature reviews. Genetics*, 10(3), pp. 184–94. doi: 10.1038/nrg2537.

Costantini, L. M. *et al.* (2015) 'A palette of fluorescent proteins optimized for diverse cellular environments.', *Nature communications*. Nature Publishing Group, 6(May), p. 7670. doi: 10.1038/ncomms8670.

Curtis, J. *et al.* (2015) 'Susceptibility to tuberculosis is associated with variants in the ASAP1 gene encoding a regulator of dendritic cell migration.', *Nature genetics*, 47(5), pp. 523–527. doi: 10.1038/ng.3248.

Davidson, A. C. *et al.* (2015) 'The Arf GTPase-Activating Protein Family Is Exploited by Salmonella enterica Serovar Typhimurium To Invade Nonphagocytic Host Cells.', *mBio*, 6(1), pp. 1–11. doi: 10.1128/mBio.02253-

14.Editor.

Draw Venn Diagram (no date). Available at: http://bioinformatics.psb.ugent.be/webtools/Venn/ (Accessed: 4 September 2017).

Drennan, M. B. *et al.* (2004) 'Toll-Like Receptor 2-Deficient Mice Succumb to Mycobacterium tuberculosis Infection', *American Journal of Pathology*, 164(1), pp. 49–57. doi: 10.1016/S0002-9440(10)63095-7.

Edwards, S. L. *et al.* (2013) 'Beyond GWASs: illuminating the dark road from association to function.', *American journal of human genetics*. The American Society of Human Genetics, 93(5), pp. 779–97. doi: 10.1016/j.ajhg.2013.10.012.

Egami, Y., Fukuda, M. and Araki, N. (2011) 'Rab35 regulates phagosome formation through recruitment of ACAP2 in macrophages during FcγR-mediated phagocytosis.', *Journal of cell science*, 124(Pt 21), pp. 3557–67. doi: 10.1242/jcs.083881.

Ehlers, J. P. *et al.* (2005) 'DDEF1 is located in an amplified region of chromosome 8q and is overexpressed in uveal melanoma', *Clinical Cancer Research*, 11(10), pp. 3609–3613. doi: 10.1158/1078-0432.CCR-04-1941.

Ehrt, S. and Schnappinger, D. (2009) 'Mycobacterial survival strategies in the phagosome: Defence against host stresses', *Cellular Microbiology*, 11(8), pp. 1170–1178. doi: 10.1111/j.1462-5822.2009.01335.x.

Ellner, J. J. (2012) 'Tuberculosis', in *Goldman's Cecil Medicine*. Elsevier, pp. 1939–1948. doi: 10.1016/B978-1-4377-1604-7.00332-8.

Ernst, J. D. (2012) 'The immunological life cycle of tuberculosis.', *Nature reviews. Immunology*. Nature Publishing Group, 12(8), pp. 581–91. doi: 10.1038/nri3259.

Eum, S.-Y. *et al.* (2010) 'Neutrophils are the predominant infected phagocytic cells in the airways of patients with active pulmonary TB.', *Chest*, 137(1), pp. 122–8. doi: 10.1378/chest.09-0903.

Fairfax, B. P. *et al.* (2014) 'Innate immune activity conditions the effect of regulatory variants upon monocyte gene expression.', *Science (New York, N.Y.)*, 343(6175), p. 1246949. doi: 10.1126/science.1246949.

Fairfax, B. P. and Knight, J. C. (2014) 'Genetics of gene expression in immunity to infection.', *Current opinion in immunology*. Elsevier Ltd, 30(1), pp. 63–71. doi: 10.1016/j.coi.2014.07.001.

Farh, K. K.-H. *et al.* (2015) 'Genetic and epigenetic fine mapping of causal autoimmune disease variants.', *Nature*. Nature Publishing Group, 518(7539), pp. 337–43. doi: 10.1038/nature13835.

Fine, P. E. (1995) 'Variation in protection by BCG: implications of and for heterologous immunity.', *Lancet*, 346(8986), pp. 1339–45. Available at: http://www.ncbi.nlm.nih.gov/pubmed/7475776 (Accessed: 13 August 2014).

Flannagan, R. S., Jaumouillé, V. and Grinstein, S. (2012) 'The cell biology of phagocytosis.', *Annual review of pathology*, 7, pp. 61–98. doi: 10.1146/annurev-pathol-011811-132445.

Flynn, J. L., Chan, J. and Lin, P. L. (2011) 'Macrophages and control of granulomatous inflammation in tuberculosis.', *Mucosal immunology*. Nature Publishing Group, 4(3), pp. 271–8. doi: 10.1038/mi.2011.14.

Fortin, a *et al.* (2007) 'Host genetics of mycobacterial diseases in mice and men: forward genetic studies of BCG-osis and tuberculosis.', *Annual review of genomics and human genetics*, 8, pp. 163–92. doi: 10.1146/annurev.genom.8.080706.092315.

Fox, G. J., Orlova, M. and Schurr, E. (2016) 'Tuberculosis in Newborns: The Lessons of the "Lübeck Disaster" (1929–1933)', *PLoS Pathogens*, 12(1), p. e1005271. doi: 10.1371/journal.ppat.1005271.

Frigerio, G. *et al.* (2007) 'Two human ARFGAPs associated with COP-I-coated vesicles.', *Traffic (Copenhagen, Denmark)*, 8(11), pp. 1644–55. doi: 10.1111/j.1600-0854.2007.00631.x.

Galagan, J. E. (2014) 'Genomic insights into tuberculosis', *Nature Reviews Genetics*. Nature Publishing Group, (March). doi: 10.1038/nrg3664.

Gao, K. *et al.* (2015) 'Front-signal-dependent accumulation of the RHOA inhibitor FAM65B at leading edges polarizes neutrophils.', *Journal of cell science*, 128(5), pp. 992–1000. doi: 10.1242/jcs.161497.

García-Pérez, B. E. *et al.* (2008) 'Internalization of a non-pathogenic mycobacteria by macropinocytosis in human alveolar epithelial A549 cells', *Microbial Pathogenesis*, 45(1), pp. 1–6. doi: 10.1016/j.micpath.2008.01.009.

Garcia-Perez, B. E., Castrejon-Jimenez, N. S. and Luna-Herrera, J. (2012) 'The Role of Non-Phagocytic Cells in Mycobacterial Infections', *Understanding Tuberculosis - Analyzing the Origin of Mycobacterium Tuberculosis Pathogenicity*, pp. 1–31. doi: 10.5772/30335.

García-Pérez, B. E., Mondragón-Flores, R. and Luna-Herrera, J. (2003) 'Internalization of Mycobacterium tuberculosis by macropinocytosis in non-phagocytic cells', *Microbial Pathogenesis*, 35, pp. 49–55. doi: 10.1016/S0882-4010(03)00089-5.

Gawden-Bone, C. *et al.* (2010) 'Dendritic cell podosomes are protrusive and invade the extracellular matrix using metalloproteinase MMP-14.', *Journal of cell science*, 123(Pt 9), pp. 1427–37. doi: 10.1242/jcs.056515.

Gawden-Bone, C. *et al.* (2014) 'A crucial role for β2 integrins in podosome formation, dynamics and Toll-like-receptor-signaled disassembly in dendritic cells.', *Journal of cell science*, 127(Pt 19), pp. 4213–24. doi: 10.1242/jcs.151167.

Geijtenbeek, T. B. H. *et al.* (2002) 'Mycobacteria Target DC-SIGN to Suppress Dendritic Cell Function',

Journal of Experimental Medicine, 197(1), pp. 7–17. doi: 10.1084/jem.20021229.

Gillespie, S. H. (2006) *Principles and Practice of Clinical Bacteriology Editors*. Second. Edited by S. H. Gillespie and P. M. Hawkey. West Sussex: John Wiley & Sons Ltd.

Goc, A. *et al.* (2012) 'Rac1 activation driven by 14-3-3ζ dimerization promotes prostate cancer cell-matrix interactions, motility and transendothelial migration.', *PloS one*, 7(7), p. e40594. doi: 10.1371/journal.pone.0040594.

Götz, A. and Jessberger, R. (2013) 'Dendritic cell podosome dynamics does not depend on the F-actin regulator SWAP-70.', *PloS one*, 8(3), p. e60642. doi: 10.1371/journal.pone.0060642.

Gupta, A. *et al.* (2012) 'Mycobacterium tuberculosis: immune evasion, latency and reactivation.', *Immunobiology*. Elsevier GmbH., 217(3), pp. 363–74. doi: 10.1016/j.imbio.2011.07.008.

Haque, A. *et al.* (2011) 'An ADP ribosylation factor-GTPase activating protein negatively regulates the production of proinflammatory mediators in response to lipopolysaccharide.', *Cancer immunology, immunotherapy : CII*, 60(10), pp. 1439–46. doi: 10.1007/s00262-011-1048-9.

Harding, C. V and Boom, W. H. (2010) 'Regulation of antigen presentation by Mycobacterium tuberculosis: a role for Toll-like receptors.', *Nature reviews. Microbiology*. Nature Publishing Group, 8(4), pp. 296–307. doi: 10.1038/nrmicro2321.

Hart, B. E. and Tapping, R. I. (2012) 'Differential trafficking of TLR1 I602S underlies host protection against pathogenic mycobacteria.', *Journal of immunology (Baltimore, Md. : 1950)*, 189(11), pp. 5347–55. doi: 10.4049/jimmunol.1201545.

Harvey, R. A. (2008) *Lippincott's Illustrated Reviews: Microbiology Third Edition*. 3rd edn, *Lippincott Williams & Wilkins*. 3rd edn. Edited by R. A. Harvey, P. C. Champe, and B. D. Fisher. Lippincott Williams & Wilkins.

Heasman, S. J. and Ridley, A. J. (2008) 'Mammalian Rho GTPases: new insights into their functions from in vivo studies.', *Nature reviews. Molecular cell biology*, 9(9), pp. 690–701. doi: 10.1038/nrm2476.

Hmama, Z. *et al.* (2015) 'Immunoevasion and immunosuppression of the macrophage by Mycobacterium tuberculosis', *Immunological Reviews*, 264(1), pp. 220–232. doi: 10.1111/imr.12268.

Hodge, R. G. and Ridley, A. J. (2016) 'Regulating Rho GTPases and their regulators', *Nature Reviews Molecular Cell Biology*. Nature Publishing Group. doi: 10.1038/nrm.2016.67.

Hossain, M. M. and Norazmi, M. N. (2013) 'Pattern Recognition Receptors and Cytokines in Infection-The Double-Edged Sword?', *Biomed Res Int*, 2013, p. 179174. doi: 10.1155/2013/179174.

Humphreys, D. *et al.* (2012) 'Salmonella virulence effector SopE and Host GEF ARNO cooperate to recruit and activate WAVE to trigger bacterial invasion.', *Cell host & microbe*. Elsevier Inc., 11(2), pp. 129–39. doi: 10.1016/j.chom.2012.01.006.

Inoue, H. *et al.* (2008) 'Arf GTPase-activating protein ASAP1 interacts with Rab11 effector FIP3 and regulates pericentrosomal localization of transferrin receptor-positive recycling endosome.', *Molecular biology of the cell*, 19(10), pp. 4224–37. doi: 10.1091/mbc.E08-03-0290.

Inoue, H. and Randazzo, P. a (2007) 'Arf GAPs and their interacting proteins.', *Traffic (Copenhagen, Denmark)*, 8(11), pp. 1465–75. doi: 10.1111/j.1600-0854.2007.00624.x.

Ishikawa, E., Mori, D. and Yamasaki, S. (2016) 'Recognition of Mycobacterial Lipids by Immune Receptors', *Trends in Immunology*. Elsevier Ltd, xx(1), pp. 1–11. doi: 10.1016/j.it.2016.10.009.

Ishino, Y. *et al.* (1987) 'Nucleotide sequence of the iap gene, responsible for alkaline phosphatase isozyme conversion in Escherichia coli, and identification of the gene product.', *Journal of Bacteriology*, 169(12), pp. 5429–5433. doi: 10.1128/jb.169.12.5429-5433.1987.

Jaguin, M. *et al.* (2013) 'Polarization profiles of human M-CSF-generated macrophages and comparison of M1-markers in classically activated macrophages from GM-CSF and M-CSF origin', *Cellular Immunology*. Academic Press, 281(1), pp. 51–61. doi: 10.1016/J.CELLIMM.2013.01.010.

Jaumouillé, V. and Grinstein, S. (2011) 'Receptor mobility, the cytoskeleton, and particle binding during phagocytosis.', *Current opinion in cell biology*, 23(1), pp. 22–9. doi: 10.1016/j.ceb.2010.10.006.

Jayachandran, R. *et al.* (2007) 'Survival of mycobacteria in macrophages is mediated by coronin 1-dependent activation of calcineurin.', *Cell*, 130(1), pp. 37–50. doi: 10.1016/j.cell.2007.04.043.

Jepson, A. (1998) 'Twin studies for the analysis of heritability of infectious diseases', *Bulletin de l'Institut Pasteur*, 96(2), pp. 71–81. doi: 10.1016/S0020-2452(98)80001-8.

Jepson, A. *et al.* (2001) 'Genetic regulation of acquired immune responses to antigens of Mycobacterium tuberculosis: a study of twins in West Africa.', *Infection and immunity*, 69(6), pp. 3989–94. doi: 10.1128/IAI.69.6.3989-3994.2001.

Jiang, W. *et al.* (2013) 'RNA-guided editing of bacterial genomes using CRISPR-Cas systems', *Nature Biotechnology*. Nature Publishing Group, 31(3), pp. 233–239. doi: 10.1038/nbt.2508.

Jin, M. S. *et al.* (2007) 'Crystal Structure of the TLR1-TLR2 Heterodimer Induced by Binding of a Tri-Acylated Lipopeptide', *Cell*, 130(6), pp. 1071–1082. doi: 10.1016/j.cell.2007.09.008.

Kalam, H., Fontana, M. F. and Kumar, D. (2017) *Alternate splicing of transcripts shape macrophage response*

to Mycobacterium tuberculosis infection, *PLOS Pathogens*. doi: 10.1371/journal.ppat.1006236.

Kallmann, F. J. and Reisner, D. (1942) 'TWIN STUDIES ON GENETIC VARIATIONS IN RESISTANCE TO TUBERCULOSIS', *Journal of Heredity*, 47, pp. 269–276. doi: https://doi.org/10.1093/oxfordjournals.jhered.a105302.

Kang, P. B. *et al.* (2005) 'The human macrophage mannose receptor directs Mycobacterium tuberculosis lipoarabinomannan-mediated phagosome biogenesis.', *The Journal of experimental medicine*, 202(7), pp. 987–99. doi: 10.1084/jem.20051239.

Karbowski, M., Jeong, S.-Y. and Youle, R. J. (2004) 'Endophilin B1 is required for the maintenance of mitochondrial morphology.', *The Journal of cell biology*, 166(7), pp. 1027–39. doi: 10.1083/jcb.200407046.

Kartberg, F. *et al.* (2010) 'ARFGAP2 and ARFGAP3 are essential for COPI coat assembly on the Golgi membrane of living cells.', *The Journal of biological chemistry*, 285(47), pp. 36709–20. doi: 10.1074/jbc.M110.180380.

Katt, M. E. *et al.* (2016) 'In Vitro Tumor Models: Advantages, Disadvantages, Variables, and Selecting the Right Platform.', *Frontiers in bioengineering and biotechnology*, 4(February), p. 12. doi: 10.3389/fbioe.2016.00012.

Katz, M. *et al.* (2007) 'A reciprocal tensin-3-cten switch mediates EGF-driven mammary cell migration.', *Nature cell biology*, 9(8), pp. 961–9. doi: 10.1038/ncb1622.

Keane, J. *et al.* (2001) 'Tuberculosis Associated with Infliximab, a Tumor Necrosis Factor α–Neutralizing Agent', *New England Journal of Medicine*, 345(15), pp. 1098–1104. doi: 10.1056/NEJMoa011110.

Kerr, M. C. and Teasdale, R. D. (2009) 'Defining macropinocytosis.', *Traffic (Copenhagen, Denmark)*, 10(4), pp. 364–71. doi: 10.1111/j.1600-0854.2009.00878.x.

Killick, K. E. *et al.* (2013) 'Receptor-mediated recognition of mycobacterial pathogens.', *Cellular microbiology*, 15(9), pp. 1484–95. doi: 10.1111/cmi.12161.

Kramer, N. *et al.* (2013) 'In vitro cell migration and invasion assays.', *Mutation research*, 752(1), pp. 10–24. doi: 10.1016/j.mrrev.2012.08.001.

Kumar, D. *et al.* (2010) 'Genome-wide analysis of the host intracellular network that regulates survival of Mycobacterium tuberculosis.', *Cell*. Elsevier Ltd, 140(5), pp. 731–43. doi: 10.1016/j.cell.2010.02.012.

Lackner, D. H. *et al.* (2015) 'A generic strategy for CRISPR-Cas9-mediated gene tagging', *Nature Communications*, 6, p. 10237. doi: 10.1038/ncomms10237.

Lambrechts, A. *et al.* (2000) 'cAMP-dependent protein kinase phosphorylation of EVL, a Mena/VASP relative,

regulates its interaction with actin and SH3 domains.', *The Journal of biological chemistry*, 275(46), pp. 36143–51. doi: 10.1074/jbc.M006274200.

Lee, B.-Y. *et al.* (2010) 'The Mycobacterium bovis bacille Calmette-Guerin phagosome proteome.', *Molecular & cellular proteomics : MCP*, 9(1), pp. 32–53. doi: 10.1074/mcp.M900396-MCP200.

Lee, J. *et al.* (2006) 'Macrophage apoptosis in response to high intracellular burden of Mycobacterium tuberculosis is mediated by a novel caspase-independent pathway.', *Journal of immunology (Baltimore, Md. : 1950)*, 176(7), pp. 4267–74. doi: 10.4049/jimmunol.176.7.4267.

Lee, M. N. *et al.* (2014) 'Common genetic variants modulate pathogen-sensing responses in human dendritic cells.', *Science (New York, N.Y.)*, 343(6175), p. 1246980. doi: 10.1126/science.1246980.

Lerner, T. R. *et al.* (2017) 'Mycobacterium tuberculosis replicates within necrotic human macrophages.', *The Journal of cell biology*, 216(3), pp. 583–594. doi: 10.1083/jcb.201603040.

Levin, R., Grinstein, S. and Schlam, D. (2014) 'Phosphoinositides in phagocytosis and macropinocytosis.', *Biochimica et biophysica acta*. Elsevier B.V. doi: 10.1016/j.bbalip.2014.09.005.

Lim, Y.-J. *et al.* (2015) 'Mycobacterium tuberculosis 38-kDa antigen induces endoplasmic reticulum stress-mediated apoptosis via toll-like receptor 2/4.', *Apoptosis : an international journal on programmed cell death*, 20(3), pp. 358–70. doi: 10.1007/s10495-014-1080-2.

Lin, D. *et al.* (2008) 'ASAP1, a gene at 8q24, is associated with prostate cancer metastasis', *Cancer Research*, 68(11), pp. 4352–4359. doi: 10.1158/0008-5472.CAN-07-5237.

Lin, Y. *et al.* (1998) 'Production of Monocyte Chemoattractant Protein 1 in Tuberculosis Patients', *Infection and immunity*, 66(5), pp. 2319–2322.

Linder, S. (2009) 'Invadosomes at a glance.', *Journal of cell science*, 122(Pt 17), pp. 3009–13. doi: 10.1242/jcs.032631.

Liu, Y. *et al.* (2002) 'The association of ASAP1, an ADP ribosylation factor-GTPase activating protein, with focal adhesion kinase contributes to the process of focal adhesion assembly.', *Molecular biology of the cell*, 13(6), pp. 2147–56. doi: 10.1091/mbc.E02-01-0018.

Lowe, D. M. *et al.* (2012) 'Neutrophils in tuberculosis: friend or foe?', *Trends in immunology*. Elsevier Ltd, 33(1), pp. 14–25. doi: 10.1016/j.it.2011.10.003.

Lurie, M. B., Abramson, S. and Heppleston, A. G. (1952) 'On the response of genetically resistant and susceptible rabbits to the quantitative inhalation of human type tubercle bacilli and the nature of resistance to tuberculosis.', *The Journal of experimental medicine*, 95(2), pp. 119–34. Available at:

http://www.ncbi.nlm.nih.gov/pubmed/2212059 (Accessed: 18 October 2014).

Machnicka, B. *et al.* (2012) 'Spectrin-based skeleton as an actor in cell signaling.', *Cellular and molecular life sciences : CMLS*, 69(2), pp. 191–201. doi: 10.1007/s00018-011-0804-5.

Mahamed, D. *et al.* (2017) 'Intracellular growth of Mycobacterium tuberculosis after macrophage cell death leads to serial killing of host cells.', *eLife*, 6. doi: 10.7554/eLife.22028.

Mali, P. *et al.* (2013) 'RNA-Guided Human Genome Engineering via Cas9', *Science*, 339(6121), pp. 823–826. doi: 10.1126/science.1232033.

Manolio, T. a *et al.* (2009) 'Finding the missing heritability of complex diseases.', *Nature*. Nature Publishing Group, 461(7265), pp. 747–53. doi: 10.1038/nature08494.

Martinson, N. a, Hoffmann, C. J. and Chaisson, R. E. (2011) 'Epidemiology of Tuberculosis and HIV: Recent Advances in Understanding and Responses', *Proceedings of the American Thoracic Society*, 8(3), pp. 288–293. doi: 10.1513/pats.201010-064WR.

Martinu, L. *et al.* (2002) 'Endocytosis of epidermal growth factor receptor regulated by Grb2-mediated recruitment of the Rab5 GTPase-activating protein RN-tre.', *The Journal of biological chemistry*, 277(52), pp. 50996–1002. doi: 10.1074/jbc.M204869200.

May, R. C. and Machesky, L. M. (2001) 'Phagocytosis and the actin cytoskeleton.', *Journal of cell science*, 114(Pt 6), pp. 1061–1077.

McKinney, J. D. *et al.* (2000) 'Persistence of Mycobacterium tuberculosis in macrophages and mice requires the glyoxylate shunt enzyme isocitrate lyase.', *Nature*, 406(6797), pp. 735–8. doi: 10.1038/35021074.

Meena, L. S. and Rajni, T. (2010) 'Survival mechanisms of pathogenic Mycobacterium tuberculosis H37Rv', *FEBS Journal*, 277(11), pp. 2416–2427. doi: 10.1111/j.1742-4658.2010.07666.x.

Meyer, C. G. *et al.* (2016) 'TLR1 Variant H305L Associated with Protection from Pulmonary Tuberculosis.', *PloS one*, 11(5), p. e0156046. doi: 10.1371/journal.pone.0156046.

Meyer, C. G. and Thye, T. (2014) 'Seminars in Immunology Host genetic studies in adult pulmonary tuberculosis', *Seminars in Immunology*. Elsevier Ltd, 26(6), pp. 445–453. doi: 10.1016/j.smim.2014.09.005.

Miltenyi, S. *et al.* (1990) 'High gradient magnetic cell separation with MACS.', *Cytometry*, 11(2), pp. 231–8. doi: 10.1002/cyto.990110203.

Mohammed, H. *et al.* (2013) 'Endogenous Purification Reveals GREB1 as a Key Estrogen Receptor Regulatory Factor', *Cell Reports*. The Authors, 3(2), pp. 342–349. doi: 10.1016/j.celrep.2013.01.010.

Mohammed, H. *et al.* (2016) 'Rapid immunoprecipitation mass spectrometry of endogenous proteins (RIME) for analysis of chromatin complexes', *Nature Protocols*, 11(2), pp. 316–326. doi: 10.1038/nprot.2016.020.

Mohammed, H. and Carroll, J. S. (2013) 'Approaches for assessing and discovering protein interactions in cancer', *Mol Cancer Res*, 11(11), pp. 1295–302. doi: 10.1158/1541-7786.MCR-13-0454.

Mojica, F. J. M. *et al.* (2005) 'Intervening sequences of regularly spaced prokaryotic repeats derive from foreign genetic elements.', *Journal of molecular evolution*, 60(2), pp. 174–82. doi: 10.1007/s00239-004-0046-3.

Möller, M. and Hoal, E. G. (2010) 'Current findings, challenges and novel approaches in human genetic susceptibility to tuberculosis.', *Tuberculosis (Edinburgh, Scotland)*, 90(2), pp. 71–83. doi: 10.1016/j.tube.2010.02.002.

Morley, M. *et al.* (2004) 'Genetic analysis of genome-wide variation in human gene expression.', *Nature*, 430(7001), pp. 743–7. doi: 10.1038/nature02797.

Müller, T. *et al.* (2010) 'ASAP1 promotes tumor cell motility and invasiveness, stimulates metastasis formation in vivo, and correlates with poor survival in colorectal cancer patients', *Oncogene*, 29(16), pp. 2393–2403. doi: 10.1038/onc.2010.6.

Murphy, D. a and Courtneidge, S. a (2011) 'The "ins" and "outs" of podosomes and invadopodia: characteristics, formation and function.', *Nature reviews. Molecular cell biology*. Nature Publishing Group, 12(7), pp. 413–26. doi: 10.1038/nrm3141.

Napier, R. J. *et al.* (2011) 'Imatinib-sensitive tyrosine kinases regulate mycobacterial pathogenesis and represent therapeutic targets against tuberculosis.', *Cell host & microbe*. Elsevier Inc., 10(5), pp. 475–85. doi: 10.1016/j.chom.2011.09.010.

Newport, M. J. *et al.* (1996) 'A mutation in the interferon-gamma-receptor gene and susceptibility to mycobacterial infection.', *The New England journal of medicine*, 335(26), pp. 1941–9. doi: 10.1056/NEJM199612263352602.

Newport, M. and Levin, M. (1999) 'Genetic susceptibility to tuberculosis', *Journal of Infection*, 39(2), pp. 117–121. doi: 10.1016/S0163-4453(99)90002-6.

Niedergang, F. and Chavrier, P. (2005) 'Regulation of phagocytosis by Rho GTPases.', *Current topics in microbiology and immunology*, 291, pp. 43–60. Available at: http://www.ncbi.nlm.nih.gov/pubmed/15981459.

Nishi, T. and Forgac, M. (2002) 'THE VACUOLAR (H+)-ATPASES — NATURE'S MOST VERSATILE PROTON PUMPS', *Nature Reviews Molecular Cell Biology*, 3(2), pp. 94–103. doi: 10.1038/nrm729.

Nishio, M. *et al.* (2007) 'Control of cell polarity and motility by the PtdIns(3,4,5)P3 phosphatase SHIP1.',

Nature cell biology, 9(1), pp. 36–44. doi: 10.1038/ncb1515.

O'Garra, A. *et al.* (2013) *The immune response in tuberculosis.*, *Annual review of immunology*. doi: 10.1146/annurev-immunol-032712-095939.

Onodera, Y. *et al.* (2005) 'Expression of AMAP1, an ArfGAP, provides novel targets to inhibit breast cancer invasive activities.', *The EMBO journal*, 24(5), pp. 963–73. doi: 10.1038/sj.emboj.7600588.

Ottenhoff, T. H. M. *et al.* (2002) 'Genetics, cytokines and human infectious disease: lessons from weakly pathogenic mycobacteria and salmonellae.', *Nature genetics*, 32(1), pp. 97–105. doi: 10.1038/ng0902-97.

Pacis, A., Nédélec, Y. and Barreiro, L. B. (2014) 'When genetics meets epigenetics: deciphering the mechanisms controlling inter-individual variation in immune responses to infection.', *Current opinion in immunology*, 29(1), pp. 119–26. doi: 10.1016/j.coi.2014.06.002.

Pai, M. *et al.* (2016) 'Tuberculosis.', *Nature reviews. Disease primers*, 2, p. 16076. doi: 10.1038/nrdp.2016.76.

Pan, H. *et al.* (2005) 'Ipr1 gene mediates innate immunity to tuberculosis.', *Nature*, 434(7034), pp. 767–72. doi: 10.1038/nature03419.

Parrish, N. M., Dick, J. D. and Bishai, W. R. (1998) 'Mechanisms of latency in Mycobacterium tuberculosis', *Trends in Microbiology*, 6(3), pp. 107–112. doi: 10.1016/S0966-842X(98)01216-5.

Parsons, J. T. (2003) 'Focal adhesion kinase: the first ten years.', *Journal of cell science*, 116(Pt 8), pp. 1409–16. doi: 10.1242/jcs.00373.

Peck, J. *et al.* (2002) 'Human RhoGAP domain-containing proteins : structure , function and evolutionary relationships', 528, pp. 27–34.

Philips, J. a and Ernst, J. D. (2012) 'Tuberculosis pathogenesis and immunity.', *Annual review of pathology*, 7, pp. 353–84. doi: 10.1146/annurev-pathol-011811-132458.

Pickrell, J. K. *et al.* (2010) 'Understanding mechanisms underlying human gene expression variation with RNA sequencing.', *Nature*. Nature Publishing Group, 464(7289), pp. 768–72. doi: 10.1038/nature08872.

Pieters, J. (2008) 'Mycobacterium tuberculosis and the macrophage: maintaining a balance.', *Cell host & microbe*, 3(6), pp. 399–407. doi: 10.1016/j.chom.2008.05.006.

Pittis, M. G. and Garcia, R. C. (1999) 'Annexins VII and XI are present in a human macrophage-like cell line. Differential translocation on FcR-mediated phagocytosis.', *Journal of leukocyte biology*, 66(5), pp. 845–50. Available at: http://www.ncbi.nlm.nih.gov/pubmed/10577518 (Accessed: 21 September 2017).

Podinovskaia, M. *et al.* (2013) 'Infection of macrophages with Mycobacterium tuberculosis induces global

modifications to phagosomal function', *Cellular Microbiology*, 15(6), pp. 843–859. doi: 10.1111/cmi.12092.

Poirier, K. *et al.* (2013) 'Mutations in TUBG1, DYNC1H1, KIF5C and KIF2A cause malformations of cortical development and microcephaly.', *Nature genetics*, 45(6), pp. 639–47. doi: 10.1038/ng.2613.

Pomatto, L. C. D., Raynes, R. and Davies, K. J. A. (2016) 'The peroxisomal Lon protease LonP2 in aging and disease: Functions and comparisons with mitochondrial Lon protease LonP1', *Biological Reviews*, 92, pp. 739–753. doi: 10.1111/brv.12253.

Quach, H. *et al.* (2016) 'Genetic Adaptation and Neandertal Admixture Shaped the Immune System of Human Populations.', *Cell*, 167(3), p. 643–656.e17. doi: 10.1016/j.cell.2016.09.024.

Rajaram, M. V. S. *et al.* (2014) 'Macrophage immunoregulatory pathways in tuberculosis.', *Seminars in immunology*. Elsevier Ltd, 26(6), pp. 471–85. doi: 10.1016/j.smim.2014.09.010.

Ramakrishnan, L. (2012) 'Revisiting the role of the granuloma in tuberculosis.', *Nature reviews. Immunology*. Nature Publishing Group, 12(5), pp. 352–66. doi: 10.1038/nri3211.

Ran, F. A. *et al.* (2013) 'Genome engineering using the CRISPR-Cas9 system.', *Nature protocols*, 8(11), pp. 2281–2308. doi: 10.1038/nprot.2013.143.

Randazzo, P. a *et al.* (2000) 'The Arf GTPase-activating protein ASAP1 regulates the actin cytoskeleton.', *Proceedings of the National Academy of Sciences of the United States of America*, 97(8), pp. 4011–6. doi: 10.1073/pnas.070552297.

Ricaño-Ponce, I. and Wijmenga, C. (2013) 'Mapping of immune-mediated disease genes.', *Annual review of genomics and human genetics*, 14, pp. 325–53. doi: 10.1146/annurev-genom-091212-153450.

Roberts, L. L. and Robinson, C. M. (2014) 'Mycobacterium tuberculosis infection of human dendritic cells decreases integrin expression, adhesion and migration to chemokines.', *Immunology*, 141(1), pp. 39–51. doi: 10.1111/imm.12164.

Rougerie, P. *et al.* (2013) 'Fam65b is a new transcriptional target of FOXO1 that regulates RhoA signaling for T lymphocyte migration.', *Journal of immunology (Baltimore, Md. : 1950)*, 190(2), pp. 748–55. doi: 10.4049/jimmunol.1201174.

Roy, A. *et al.* (2014) 'Effect of BCG vaccination against Mycobacterium tuberculosis infection in children: systematic review and meta-analysis.', *BMJ (Clinical research ed.)*, 349(August), p. g4643. doi: 10.1136/bmj.g4643.

Ruetz, T., Cornick, S. and Guttman, J. A. (2011) 'The spectrin cytoskeleton is crucial for adherent and invasive bacterial pathogenesis.', *PloS one*, 6(5), p. e19940. doi: 10.1371/journal.pone.0019940.

Ruetz, T. J., Lin, A. E. and Guttman, J. A. (2012) 'Shigella flexneri utilize the spectrin cytoskeleton during invasion and comet tail generation.', *BMC microbiology*, 12(1), p. 36. doi: 10.1186/1471-2180-12-36.

Russell, D. G. (2001) 'Mycobacterium tuberculosis: here today, and here tomorrow', *Nat. Rev. Mol. Cell Biol*, 2(8), p. 569–577. doi: 10.1038/35085034.

Sakakibara, T. *et al.* (2004) 'Identification and characterization of a novel Rho GTPase activating protein implicated in receptor-mediated endocytosis', *FEBS Letters*, 566(1–3), pp. 294–300. doi: 10.1016/j.febslet.2004.03.101.

Sanjana, N. E., Shalem, O. and Zhang, F. (2014) 'Improved vectors and genome-wide libraries for CRISPR screening.', *Nature methods*. Nature Publishing Group, 11(8), pp. 783–784. doi: 10.1038/nmeth.3047.

Santy, L. C. and Casanova, J. E. (2002) 'GTPase signaling: bridging the GAP between ARF and Rho.', *Current biology : CB*, 12(10), pp. R360-2. doi: 10.1016/S0960-9822(02)00860-6.

Schachtner, H. *et al.* (2013) 'Podosomes in adhesion, migration, mechanosensing and matrix remodeling.', *Cytoskeleton (Hoboken, N.J.)*, 70(10), pp. 572–89. doi: 10.1002/cm.21119.

Schäfer, G. *et al.* (2009) 'Non-opsonic recognition of mycobacterium tuberculosis by phagocytes', *Journal of Innate Immunity*, 1(3), pp. 231–243. doi: 10.1159/000173703.

Schindelin, J. *et al.* (2012) 'Fiji: an open-source platform for biological-image analysis', *Nature Methods*, 9(7), pp. 676–682. doi: 10.1038/nmeth.2019.

Schurr, E. (2011) 'The contribution of host genetics to tuberculosis pathogenesis.', *Kekkaku : [Tuberculosis]*, 86(1), pp. 17–28. Available at: http://www.ncbi.nlm.nih.gov/pubmed/21401002.

Schurz, H. *et al.* (2015) 'TLR1, 2, 4, 6 and 9 Variants Associated with Tuberculosis Susceptibility: A Systematic Review and Meta-Analysis.', *PloS one*. Edited by G. R. Wallace, 10(10), p. e0139711. doi: 10.1371/journal.pone.0139711.

Schymeinsky, J. *et al.* (2009) 'A fundamental role of mAbp1 in neutrophils: impact on beta(2) integrin-mediated phagocytosis and adhesion in vivo.', *Blood*, 114(19), pp. 4209–20. doi: 10.1182/blood-2009-02-206169.

Shenoi, S. and Friedland, G. (2009) 'Extensively drug-resistant tuberculosis: a new face to an old pathogen.', *Annual review of medicine*, 60, pp. 307–20. doi: 10.1146/annurev.med.60.053107.103955.

Shiba, Y. and Randazzo, P. a (2011) 'GEFH1 binds ASAP1 and regulates podosome formation.', *Biochemical and biophysical research communications*. Elsevier Inc., 406(4), pp. 574–9. doi: 10.1016/j.bbrc.2011.02.093.

Simeone, R. *et al.* (2012) 'Phagosomal rupture by Mycobacterium tuberculosis results in toxicity and host cell death.', *PLoS pathogens*, 8(2), p. e1002507. doi: 10.1371/journal.ppat.1002507.

Skeiky, Y. A. W. and Sadoff, J. C. (2006) 'Advances in tuberculosis vaccine strategies.', *Nature reviews. Microbiology*, 4(6), pp. 469–76. doi: 10.1038/nrmicro1419.

Sloggett, C., Goonasekera, N. and Afgan, E. (2013) 'BioBlend: automating pipeline analyses within Galaxy and CloudMan.', *Bioinformatics (Oxford, England)*, 29(13), pp. 1685–6. doi: 10.1093/bioinformatics/btt199.

Soldati, T. and Neyrolles, O. (2012) 'Mycobacteria and the intraphagosomal environment: take it with a pinch of salt(s)!', *Traffic (Copenhagen, Denmark)*, 13(8), pp. 1042–52. doi: 10.1111/j.1600-0854.2012.01358.x.

Stanley, S. A. *et al.* (2014) 'Identification of host-targeted small molecules that restrict intracellular Mycobacterium tuberculosis growth.', *PLoS pathogens*, 10(2), p. e1003946. doi: 10.1371/journal.ppat.1003946.

Stein, C. M. and Western, C. (2012) *Genetics of Susceptibility to Tuberculosis. In: eLS*. Chichester, UK: John Wiley & Sons, Ltd. doi: 10.1002/9780470015902.a0023886.

Sterne, J. A. C., Rodrigues, L. C. and Guedes, I. N. (1998) 'Does the efficacy of BCG decline with time since vaccination?', *International Journal of Tuberculosis and Lung Disease*, pp. 200–207.

Stojanovski, D. *et al.* (2004) 'Levels of human Fis1 at the mitochondrial outer membrane regulate mitochondrial morphology.', *Journal of cell science*, 117(Pt 7), pp. 1201–10. doi: 10.1242/jcs.01058.

Sun, J. *et al.* (2010) 'Mycobacterial Nucleoside Diphosphate Kinase Blocks Phagosome Maturation in Murine Raw 264.7 Macrophages', *PLoS ONE*. Edited by A. K. Tyagi, 5(1), p. e8769. doi: 10.1371/journal.pone.0008769.

Swanson, J. a (2008) 'Shaping cups into phagosomes and macropinosomes.', *Nature reviews. Molecular cell biology*, 9(August), pp. 639–649. doi: 10.1038/nrm2447.

Tailleux, L. *et al.* (2008) 'Probing host pathogen cross-talk by transcriptional profiling of both Mycobacterium tuberculosis and infected human dendritic cells and macrophages.', *PloS one*, 3(1), p. e1403. doi: 10.1371/journal.pone.0001403.

Takeuchi, O. *et al.* (2002) 'Cutting edge: role of Toll-like receptor 1 in mediating immune response to microbial lipoproteins.', *Journal of immunology (Baltimore, Md. : 1950)*, 169(1), pp. 10–14. doi: 10.4049/jimmunol.169.1.10.

Tcherkezian, J. and Lamarche-Vane, N. (2007) 'Current knowledge of the large RhoGAP family of proteins', *Biology of the Cell*, 99(2), pp. 67–86. doi: 10.1042/BC20060086.

Thye, T. *et al.* (2010) 'Genome-wide association analyses identifies a susceptibility locus for tuberculosis on chromosome 18q11.2.', *Nature genetics*, 42(9), pp. 739–41. doi: 10.1038/ng.639.

Thye, T. *et al.* (2012) 'Common variants at 11p13 are associated with susceptibility to tuberculosis.', *Nature*

genetics. Nature Publishing Group, 44(3), pp. 257–9. doi: 10.1038/ng.1080.

Tien, D. N. *et al.* (2015) 'AMAP1 as a negative-feedback regulator of nuclear factor-κB under inflammatory conditions', *Scientific Reports*, 4(1), p. 5094. doi: 10.1038/srep05094.

Tomlinson, M. G. *et al.* (2004) 'SHIP family inositol phosphatases interact with and negatively regulate the Tec tyrosine kinase.', *The Journal of biological chemistry*, 279(53), pp. 55089–96. doi: 10.1074/jbc.M408141200.

Tyagi, A. K., Nangpal, P. and Satchidanandam, V. (2011) 'Development of vaccines against tuberculosis.', *Tuberculosis (Edinburgh, Scotland)*. Elsevier Ltd, 91(5), pp. 469–78. doi: 10.1016/j.tube.2011.01.003.

Unniyampurath, U., Pilankatta, R. and Krishnan, M. N. (2016) 'RNA interference in the age of CRISPR: Will CRISPR interfere with RNAI?', *International Journal of Molecular Sciences*, 17(3). doi: 10.3390/ijms17030291.

Urdahl, K. B., Shafiani, S. and Ernst, J. D. (2011) 'Initiation and regulation of T-cell responses in tuberculosis', *Mucosal Immunology*. Nature Publishing Group, 4(3), pp. 288–293. doi: 10.1038/mi.2011.10.

Valentin-Weigand, P. and Goethe, R. (1999) 'Pathogenesis of Mycobacterium avium subspecies paratuberculosis infections in ruminants: Still more questions than answers', *Microbes and Infection*, 1(13), pp. 1121–1127. doi: 10.1016/S1286-4579(99)00203-8.

Vasquez, L. J. *et al.* (2016) 'From GWAS to function: lessons from blood cells', *ISBT Science Series*, 11(S1), pp. 211–219. doi: 10.1111/voxs.12217.

Verreck, F. A. W. *et al.* (2004) 'Human IL-23-producing type 1 macrophages promote but IL-10-producing type 2 macrophages subvert immunity to (myco)bacteria.', *Proceedings of the National Academy of Sciences of the United States of America*, 101(13), pp. 4560–4565.

Via, L. E. *et al.* (1997) 'Arrest of mycobacterial phagosome maturation is caused by a block in vesicle fusion between stages controlled by rab5 and rab7.', *The Journal of biological chemistry*, 272(20), pp. 13326–31. doi: 10.1074/jbc.272.20.13326.

Vidal, S. M. *et al.* (1993) 'Natural resistance to infection with intracellular parasites: isolation of a candidate for Bcg.', *Cell*, 73(3), pp. 469–85. doi: 10.1016/0092-8674(93)90135-D.

Wang, H., La Russa, M. and Qi, L. S. (2016) 'CRISPR/Cas9 in Genome Editing and Beyond', *Annual Review of Biochemistry*, 85(1), pp. 227–264. doi: 10.1146/annurev-biochem-060815-014607.

Wang, Z., Gerstein, M. and Snyder, M. (2009) 'RNA-Seq: a revolutionary tool for transcriptomics.', *Nature reviews. Genetics*, 10(1), pp. 57–63. doi: 10.1038/nrg2484.

Welch, M. D. *et al.* (1997) 'The human Arp2/3 complex is composed of evolutionarily conserved subunits and

is localized to cellular regions of dynamic actin filament assembly.', *The Journal of cell biology*, 138(2), pp. 375–84. Available at: http://www.ncbi.nlm.nih.gov/pubmed/9230079 (Accessed: 1 September 2017).

WHO (2016) *Global Tuberculosis Report*, *World Health Organization*. doi: WHO/HTM/TB/2016.13.

WHO (2017) *GLOBAL TUBERCULOSIS PROGRAMME, & WORLD HEALTH ORGANIZATION*, *WHO*. doi: 10.1088/1751-8113/44/8/085201.

Wilson, R. C. and Doudna, J. A. (2013) 'Molecular mechanisms of RNA interference.', *Annual review of biophysics*, 42(1), pp. 217–39. doi: 10.1146/annurev-biophys-083012-130404.

Wolf, A. J. *et al.* (2007) 'Mycobacterium tuberculosis Infects Dendritic Cells with High Frequency and Impairs Their Function In Vivo', *The Journal of Immunology*, 179(4), pp. 2509–2519. doi: 10.4049/jimmunol.179.4.2509.

Wolf, A. J. *et al.* (2008) 'Initiation of the adaptive immune response to Mycobacterium tuberculosis depends on antigen production in the local lymph node, not the lungs.', *The Journal of experimental medicine*, 205(1), pp. 105–15. doi: 10.1084/jem.20071367.

Wurfel, M. M. *et al.* (2008) 'Toll-like Receptor 1 Polymorphisms Affect Innate Immune Responses and Outcomes in Sepsis', *American Journal of Respiratory and Critical Care Medicine*, 178(7), pp. 710–720. doi: 10.1164/rccm.200803-462OC.

Yoon, S. *et al.* (2007) 'C6ORF32 is upregulated during muscle cell differentiation and induces the formation of cellular filopodia', *Developmental Biology*, 301(1), pp. 70–81. doi: 10.1016/j.ydbio.2006.11.002.

Zhao, M. *et al.* (2016) 'Novel Role of Src in Priming Pyk2 Phosphorylation.', *PloS one*, 11(2), p. e0149231. doi: 10.1371/journal.pone.0149231.

Zhao, S. *et al.* (2014) 'Comparison of RNA-Seq and microarray in transcriptome profiling of activated T cells.', *PloS one*, 9(1), p. e78644. doi: 10.1371/journal.pone.0078644.

Zumla, A. *et al.* (2013) 'Tuberculosis.', *The New England journal of medicine*, 368(8), pp. 745–55. doi: 10.1056/NEJMra1200894.

Zumla, A. *et al.* (2015) 'Towards host-directed therapies for tuberculosis.', *Nature reviews. Drug discovery*, 14(8), pp. 511–2. doi: 10.1038/nrd469

A.1 Supplementary Documents

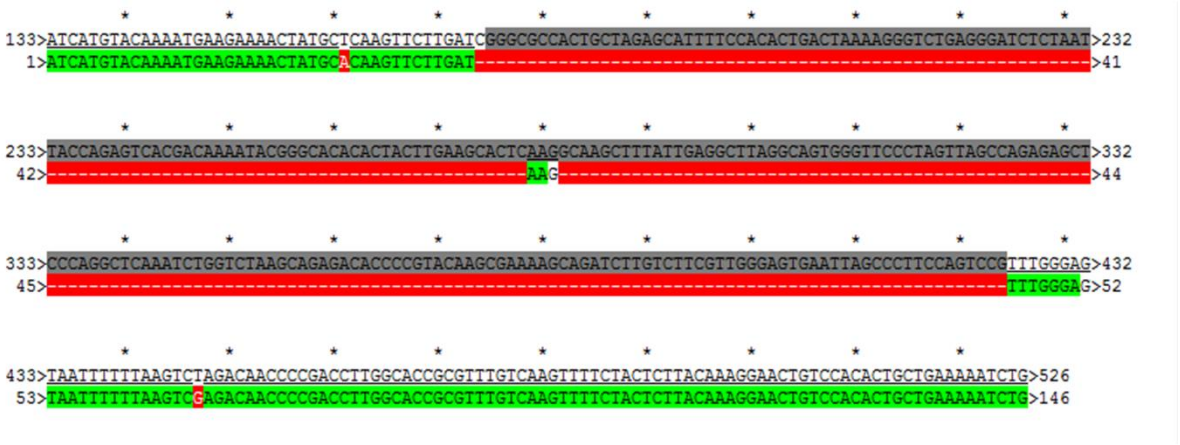

S 1: Sanger sequencing for THP-1 clone A related to Figure 3.1-13

THP-1 ASAP1 KO clone A showed an insertion of ~250 nucleotides as indicated by the gray color compared to the reference sequence ASAP1 exon 5 as shown by green color.

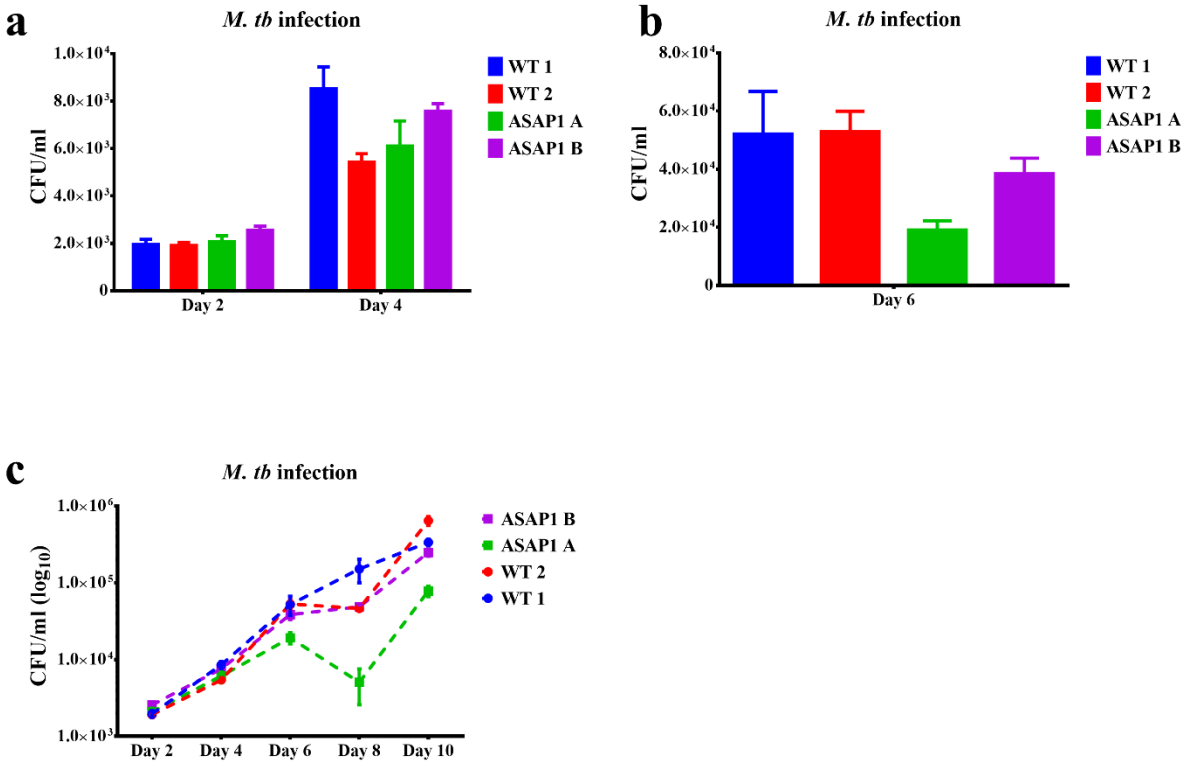

S 2: Intracellular mycobacterial growth in macrophage lacking ASAP1 related to Figure 3.1-18.

PMA differentiated THP-1 WT cells and two THP-1 ASAP1 knockout clonal cell lines were infected with *M. tb* or BCG expressing DsRed2 at MOI of ~2 and monitored for 96 h. CFU assay of ASAP1 knockout clonal cell lines (clone A and clone B) and WT at day (**a**) 2, 4, and (**b**) 6 post infection with *M. tb* (H37Rv). (**b**) CFU results of ASAP1 knockout clones were averaged and compared with WT. Data indicate means ± s.e.m from three independent experiments. T-test, Two-tailed Student's t.test was performed to highlight statistical significance in controlling mycobacterial growth between WT THP-1 cell and ASAP1 lacking cells. (**c**) CFU assay of ASAP1 knockout clonal cell lines (clone A and clone B) and WT in duplicate at day 2, 4, 6, 8 and 10 post-infection with *M. tb*. Data indicate $\log_{10}$ scale for means ± s.e.m from three independent experiments. T-test, Two-tailed Student's t.test was performed to highlight statistical significance in controlling mycobacterial growth between WT THP-1 cell and ASAP1 lacking cells.

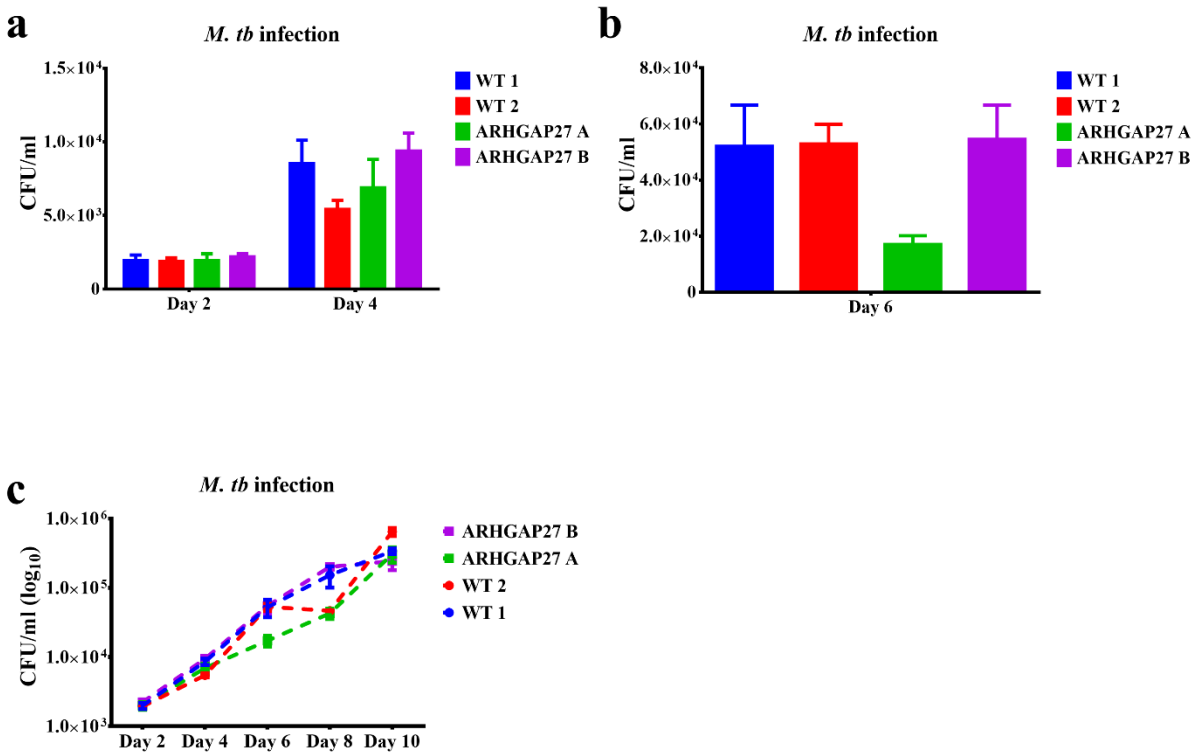

S 3: Intracellular mycobacterial growth in macrophage lacking *ARHGAP27* related to Figure 3.2-13.

PMA differentiated THP-1 WT cells and two THP-1 ARHGAP27 knockout clonal cell lines were infected with *M. tb* or BCG expressing DsRed2 at MOI of ~2 and monitored for 96 h. CFU assay of ASAP1 knockout clonal cell lines (clone A and clone B) and WT at day (**a)** 2, 4, and (**b**) 6 post infection *with M. tb* (H37Rv). (**b**) CFU assay of ARHGAP27 knockout clones were averaged and compared with WT. Data indicate means ± s.e.m from three independent experiments. T-test, Two-tailed Student's t.test was performed to highlight statistical significance in controlling mycobacterial growth between WT THP-1 cell and ASAP1 lacking cells. (**c**) CFU assay of ASAP1 knockout clonal cell lines (clone A and clone B) and WT in duplicate at day 2,4, 6, 8 and 10 post-infection with *M. tb*. Data indicate $\log_{10}$ scale for means ± s.e.m from three independent experiments. T-test, Two-tailed Student's t.test was performed to highlight statistical significance in controlling mycobacterial growth between WT THP-1 cell and ARHGAP27 lacking cells.